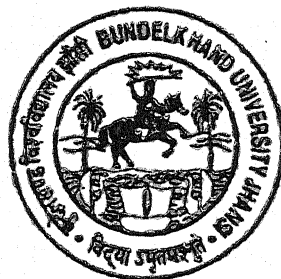
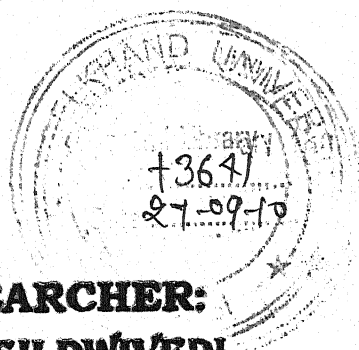


**EFFECTIVE ROLE OF THE ELECTRIC FIELD
IN CONDENSATION OF WATER AND
GLACIATION OF ICE IN CLOUDS**



**THESIS SUBMITTED TO
THE BUNDELKHAND UNIVERSITY
JHANSI**

**For the Degree of
DOCTOR OF PHILOSOPHY
In
PHYSICS**



SUPERVISOR:

DR. D.D. GUPTA

Reader

Department of Physics

Bipin Bihari P.G. College

Jhansi (U.P.)

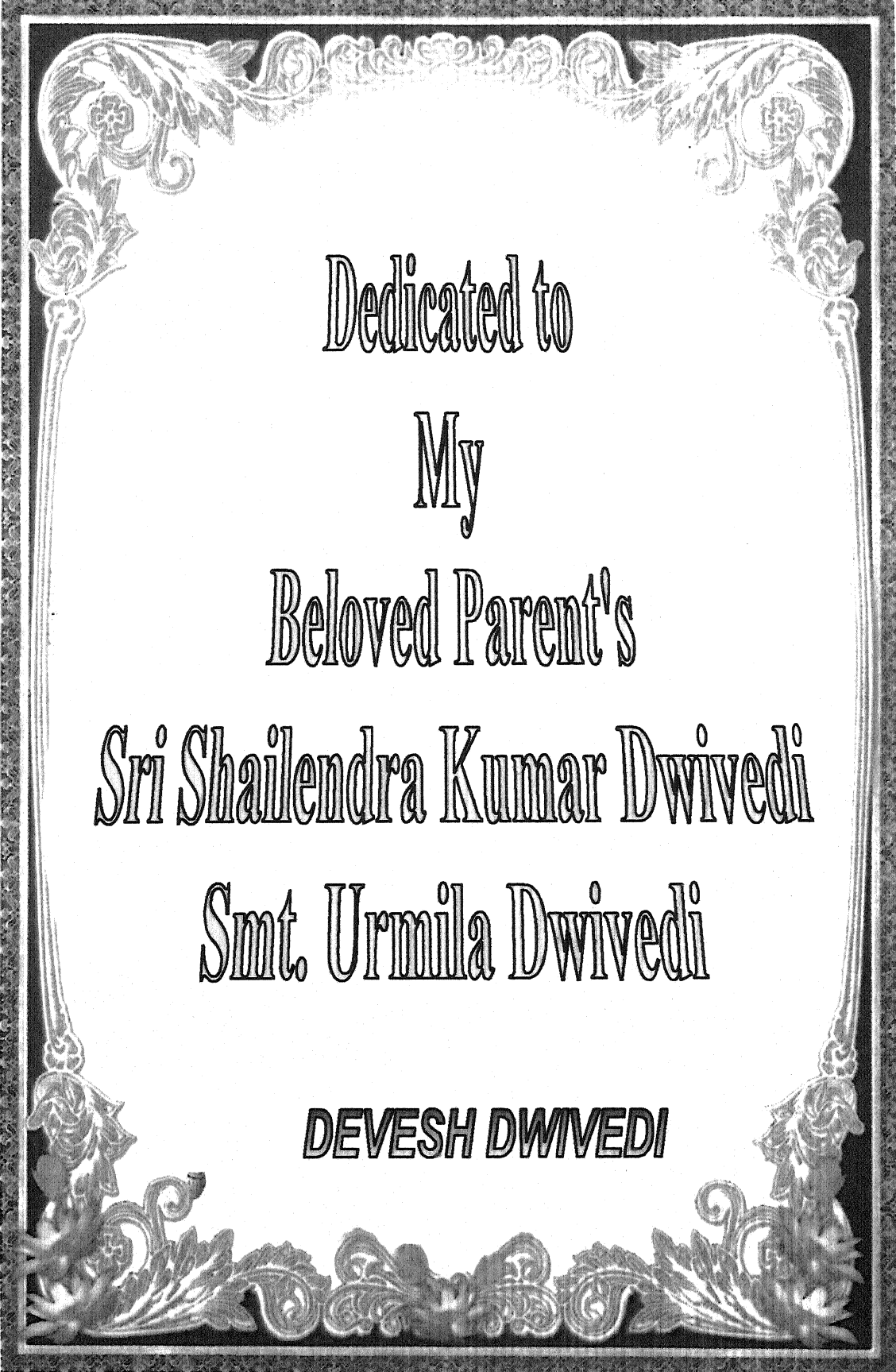
RESEARCHER:

DEVESH DWIVEDI

M.Sc. (Physics)

**DEPARTMENT OF PHYSICS
BIPIN BIHARI POST GRADUATE COLLEGE
JHANSI (U.P.), INDIA**

2009



Dedicated to
My
Beloved Parent's
Sri Shailendra Kumar Dwivedi
Smt. Urmila Dwivedi

DEVESH DWIVEDI

DEPARTMENT OF PHYSICS
BIPIN BIHARI P.G. COLLEGE JHANSI-284 001, U.P. (INDIA)
(AFFILIATED TO BUNDELKHAND UNIVERSITY, JHANSI)

Certificate

This is to certify that the present thesis entitled "Effective Role of the Electric Field in Condensation of Water and Glaciation of Ice in Clouds" embodies the unaided research work of Devesh Dwivedi. The thesis contains the result of his investigations conducted during the period worked as Ph.D. research scholar under my supervision, and fulfills the requirements for the submission for the degree. The candidate has put more than 200 days attendance in the department. The results of this thesis have not been submitted to any other university or institute for the award of any degree or diploma.

Date : 26.11.2009

Place: Jhansi



Dr. D.D. Gupta

(Supervisor)

Reader

Department of Physics

Bipin Bihari P.G. College

Jhansi (U.P.)

DECLARATION

I, Devesh Dwivedi, declare that the thesis entitled "Effective Role of the Electric Field in Condensation of Water and Glaciation of Ice in Clouds" under the Supervision of Dr. D.D. Gupta, Reader Department of Physics, Bipin Bihari Post Graduate College, Jhansi is being submitted for the degree of Doctor of Philosophy in Physics of Bundelkhand University, Jhansi is an innovative piece of work carried out with complete dedication by me, and to the best of my knowledge and belief. It has not been submitted elsewhere.

Date : 26.11.2009

Place: Jhansi

Devesh Dwivedi
(Devesh Dwivedi)
Researcher

CONTENTS

	Page No.
ACKNOWLEDGEMENT	i-vii
PREFACE	1-94
CHAPTER-1 INTRODUCTION	1
1.1 Chemical Potential	2
1.1 (i) Chemical Potential of water vapour in Humid Air	5
1.1 (ii) Chemical Potential of water in aqueous solutions.	6
1.2 Change in Chemical Potential	6
1.3 Gibbs phase Rule	7
1.4 Structure of an Isolated water molecule	12
1.5 Structure of Water Vapour	14
1.6 Structure of Ice	21
1.7 Structure of Water and Aqueous Solutions	26
1.8 Water Vapour Distribution in India	36
1.9 Surface properties of water substance	36
1.9 (i) Effect of Temperature on surface tension	36
1.9 (ii) Radius dependence of surface tension	40
1.9 (iii) Surface tension at vapour interface	40
1.9 (iv) Surface tension at ice-vapour interface and surface energy of ice	41
1.9 (v) Ice water interface (state between ice and water)	42
1.10 Nucleation	44
1.10 (i) Homogenous Nucleation of water	44
1.10 (ii) Heterogeneous Nucleation of water	45
1.11 Cloud condensation Nuclei (CCN)	47
1.12 Ice Forming Nuclei (IN)	47
1.13 Number concentration of CCN	54
1.14 A laboratory Study of Ice Nucleation due to electrical discharge	54
1.15 Experimental verification of Heterogeneous water drop nucleation	57
1.16 Electrical Inhomogeneties other than ions	58
1.16 (i) Ice forming nuclei	58
1.16 (ii) IN Concentration	61
1.17 Enhancement Ratio or Enhancement factor	65
1.17 (i) Ion Induced Nucleation	67
1.17 (ii) Electric field Induced Nucleation	68
1.18 Models of Nucleation	68
1.18 (i) Classical liquid drop model	73
1.18 (ii) Computer simulation and Monte Carlo Method	74
1.18 (iii) Molecular Model	80
1.18 (iv) Semi Molecular Model	80
1.18 (v) Extension of Molecular Model to Heterogeneous Nucleation.	80

1.19	Models for Heterogeneous water Nucleation	81
1.19 (i)	Nucleation on water in soluble, partially wettable CCN.	81
1.20	Electric field and electrification of clouds	83
1.20 (i)	Electrical state of cloudless atmosphere	83
1.20 (ii)	Electrical state of the atmospheric Aerosol	84
1.20 (iii)	Cloud electrification (Models for cloud electrification)	85
1.21	Effect of electric field of Microphysical Process.	91
1.21 (i)	Drop and Ice crystal nucleation	91
1.22	Conduction in the Atmosphere	92
1.23	Vertical Structure of Tropical precipitating cloud systems.	93
CHAPTER-2	MODIFICATION IN THE NUCLEATION OF WATER VAPOUR CONDENSATION AND ICE GLACIATION, DUE TO EXTERNAL ELECTRIC FIELD.	95-162
2.1	Introduction	95
2.2	Theoretical consideration	98
2.2.1	Homogeneous Nucleation Process	100
2.2.1 (i)	In the absence of an electric field	100
2.2.1 (ii)	In the presence of an external electric field	104
2.2.2	Ice Nucleation in the presence of an electric field.	109
2.3	Discussion of the Results	109
2.4	Conclusion	111
	Tables	113
	Graphs	119
CHAPTER-3	EQUIVALENCE OF THE EXTERNAL ELECTRIC FIELD WITH SUPERSATURATION RATIO DURING WATER VAPOUR CONDENSATION AND GLACIATIONS.	163-216
3.1	Introduction	163
3.2	Equilibrium between a pure water drop and pure water vapour or Humid Air	164
3.3	Equilibrium of Ice Crystal in Humid Air	171
3.4	Electrical state of atmosphere	171
3.5	Theoretical Consideration	176
3.5.1	Water Vapour Condensation	176
3.5.2	Nucleation rate	179
3.5.3	Water Vapour Ice Nucleation	180
3.6	Effect of external electrical field on nucleation during water vapour condensation and ice glaciations.	181
3.7	Equivalence between electric field and supersaturation ratio	182
3.8	Result and Discussion	184
3.9	Conclusion	185
	Tables	187
	Graphs	199

CHAPTER-4	EQUIVALENCE BETWEEN TEMPERATURE AND THE ELECTRIC FIELD DURING WATER VAPOUR CONDENSATION AND GLACIATION	217-237
4.1	Introduction	217
4.1.1	Water in the Atmosphere	217
4.1.2	The Standard Atmosphere	220
4.1.3	Thermal layers of the standard atmosphere	220
4.1.4	Water Vapour	223
4.1.5	Structure of Water Vapour	225
4.1.6	Vapour Pressure over pure droplets	227
4.1.7	Equation of state for water vapour	229
4.1.8	Equilibrium vapour pressure e_s and latent heat L over a range of temperatures	231
4.2	Theoretical Considerations	231
4.2.1	Equivalence between electric field and temperature	231
4.3	Results and Discussion	235
4.4	Conclusion	237
CHAPTER-5	EFFECT OF IONS ON ELECTRIC FIELD INDUCED NUCLEATION PHENOMENON AND STUDY OF THUNDERSTORMS	238-273
5.1	Introduction	238
5.2	Ions, the potential condensation nucleation centers	239
5.3	Ion Species in Troposphere	240
5.4	Ions in the atmosphere	243
5.5	Destruction of small ions in the atmosphere	244
5.6	An introduction on atmospheric electrical conductivity	245
5.6.1	Diurnal variation of the atmospheric electric field and conductivity at Maitri, Antarctica.	247
5.6.2	Variation in atmospheric electrical conductivity beneath a thundercloud.	248
5.7	Contribution of cloud and precipitation particles to the electrical conductivity and the relaxation time of the air in the thunderstorms.	252
5.8	Variation in atmospheric aerosols and electrical conductivity at Roorkee during the total solar eclipse of October 1995	254
5.8.1	Measurement of electrical conductivity	254
5.8.2	The observed variation in electrical conductivity	257
5.9	Using atmospheric electrical conductivity as an urban air pollution indicator.	260
5.10	Conductivity and ionic concentration	262
5.10.1	Sources of ions in the atmosphere	262
5.10.2	Conductivity in land and sea breeze	264
5.10.3	Atmospheric electric conductivity	264
5.10.4	Electrical conductivity in and above the thundercloud	264
5.11	Results and Discussion	267
5.12	Conclusion	273
	BIBLIOGRAPHY	274-294
	LIST OF PUBLICATIONS	

Acknowledgement

It gives me an immense pleasure to owe a debt of gratitude to my supervisor Dr. D.D. Gupta (Reader, Department of Physics, Bipin Bihari P.G. College, Jhansi) for his invaluable supervision and dedication that led me to give the present form to my research work.

I am thankful to Dr. S.N. Shrivastava (Principal, Bipin Bihari P.G. College, Jhansi), Dr. R.K. Shrivastava (Head, Dept. of Physics, Bipin Bihari P.G. College, Jhansi) and staff members of the Department of Physics for providing me necessary facilities and for their co-operation during this endeavour.

I shall equally indebted Dr. S.K. Mishra (Director, N.V.E.M.I. Gangaganj, Panki, Kanpur), for channellizing my dialecticism and guiding me at all points by throwing a flood of light over various aspects. His parental affection and ever flowing Kindness coupled with his undisminising scholarly touch has been all pervasive through out the period of scientific research.

I express my sincere thanks to Dr. U.P. Singh (Principal, T.D. College, Jaunpur) & Dr. Vikas Mishra (Reader, Department of Physics, D.B.S. College, Kanpur) for their keen interest and inspiring suggestions in the present work.

I take this opportunity to express my respects and regards to my parents, who had shown boundless affection and patience and have contributed a lot of my progress.

I can never forget the affection and hospitality, which I received from the family of Dr. D.D. Gupta during my stay at Jhansi. The cordial family atmosphere, which I found here, helped me in my work. Indeed I fail in words to express my gratitude for them. I feel pleasure to thank Smt. Neelam Gupta for her kind hospitality and courtesy.

Last, but no way least I should be failing in my duty if I do not extend my thanks to my friends Anand Kumar & Rajneesh Dwivedi for their co-operations.

Devesh Dwivedi
Devesh Dwivedi

PREFACE

The electric field which exists in the clouds is mainly responsible for enhanced ice crystal production within the supercooled fogs. Evans (1973) experimentally demonstrated that charged water molecules move to the crystal tips, thereby increasing the nucleation rates.

Singh et al. (1986) and Sharma et al. (1992) discussed the effect of external electric field on the relaxation time in the nucleation process of water vapour condensation and ice glaciations. The effect of electric field on condensation and further polarizability of water molecules have been discussed. (Singh, N., et. al. 2000, 2001).

Effect of orographic features on atmospheric electrical parameters of different cities of India was discussed by Kumar et al. (1998). Shaw (1998) has shown the effect of electrical discharge in the nucleation of water droplets.

Pinsky et al. (1999) showed that inertia of cloud droplets play a crucial role in the evolution of spectral during drop growth by diffusion. The change in electric field due to lightening in thunderstorm has been observed by Beasley and Eack (2000).

OBJECTIVE:

We have studied the effect of external electric field on the condensation of water and glaciations of ice in clouds. We have calculated the values of relaxation time by the help of Collins formula.

The equivalence between electric field with supersaturation ratio and Temperature has also been calculated for the present study in which spherical liquid drop model has been considered.

According to this model, an embryo of water molecule is formed. The embryo acquires a critical size (called nucleus). At a certain supersaturation ratio and temperature below this size, nucleus of water vapour molecules is formed. In presence of electric field, the Gibb's free energy is modified due to the polarization of water vapour molecules and hence the nucleus of smaller size is formed earlier and hence the nucleation rate enhanced.

THEORETICAL CONSIDERATION:

In chapter-1, we have reviewed the nucleation phenomenon in presence and absence of electric field due to workers. The nucleation rate and the relaxation time in the electric field induced cases have not been compared for temperature and supersaturation with the electric field. The models for the nucleation and electrification of clouds have also been studied.

Possible influence of cosmic rays on climate through thunderstorm clouds was studied by Lev. I. Dormana et al. (2005). Cosmic ray-induced Ionization in the atmosphere has been studied by I.G. Usoskin (2004). Gondot et al. (1988) developed a new type of sensor to measure ionic electrical conductivity and, convection conductivity both around and inside convection clouds. Vonnegut (1988) proposed the mechanism to explain thunderstorm electrification differ greatly in how they might affect or be affected by the cloud. Electric field changes of lightning observed in thunderstorms had been studied by William H. Beasley

(2000). During water vapour condensation the equivalence between supersaturation ratio and the external electric field has been established recently by Dwivedi, D. et al. (2008).

In chapter-2, we have estimated the effect of external electric field on Homogeneous nucleation phenomenon of water vapour condensation and ice glaciations under the variation of density and surface free energy with temperature at different values of electric field.

The frequency of growth of embryo beyond a critical size in the nucleation process corresponds to a free energy maximum, this energy is

$$\Delta G_w = -(\mu_v - \mu_l)n_w + \sigma_{w/v}S_n \quad (1)$$

Where μ_v , is the chemical potential of vapour and μ_l ; chemical potential of liquid. $\sigma_{w/v}$, the surface free energy of water vapour interface; and S_n , surface area of embryo; n_w , is the number of water molecules in the embryo.

Corresponding to the free energy maximum for a critical size nucleus, we have,

$$\frac{\partial \Delta G_w}{\partial n_w} = 0$$

and thus the eq. (1) becomes

$$\Delta G_w^* = \frac{2\sigma_{w/v}\mu_w'}{3n_w^{1/3}} n_w + \sigma_{w/v}\mu_w' n_w^{2/3} \quad (2)$$

$$\text{Where } \mu_w' = 4\pi \left(\frac{3m_w}{4\pi\rho_w} \right)^{2/3} \quad (3)$$

m_w , being the molecular mass and ρ_w the density of water.

In the absence of an electric field Collins (1955) evaluated the relaxation time.

$$\tau_0 = 9\pi kT(n_w^*)^{2/3} / \mu_w'^2 \beta_w \sigma_{w/v} \quad (4)$$

The number of water molecules in a critical nucleus is given by:

$$n_w^* = \left(\frac{r_w^*}{1.958 \times 10^{-8}} \right)^3 \quad (5)$$

Where r_w^* is the radius of the critical nucleus with

$$r_w^* = \frac{2\sigma_{w/v} M_w}{\rho_w RT \ln S_{v,w}} \quad (6)$$

In this expression $S_{v,w}$ is the supersaturation ratio of vapour over the plane water surface.

In eq. (4) putting the values from eq. (5), eq. (6) and than evaluating the values of τ_0 , putting the values of $m_w = 3 \times 10^{-23}$ gm.; $M_w = 18$; $N = 6.023 \times 10^{23}$; $k = 1.38 \times 10^{-16}$ erg K⁻¹; $R = 8.317 \times 10^7$ erg K⁻¹ mole⁻¹; $\mu_w' = 2.1792 \times 10^{-29}$. We have

$$\tau_0 = 3782.026 \times 10^{-9} \times \frac{\sigma_{w/v}}{\rho_w^2 T^{3/2} (\ln S_{v,w})^2} \quad (7)$$

Variation of density and surface free energies of water and ice with temperature has taken into account (Edward et al. 2003; Gupta et al. 2009).

In presence of an electric field we have

$$r_w^* = [3\rho_v (9 \propto \lambda E^2 / m_w)^{1/2} \tau_N / 2\rho_w]^{2/3} \quad (8)$$

In chapter-3, we have established equivalence between supersaturation ratio and the external electric field during water vapour condensation. Nucleus of a particular radius is obtained from eq. (6), whereas in presence of electric field the radius is given by eq. (8). If the size of the nucleus is obtained in two cases, than R.H.S. of these two equations may be equated to get.

$$\frac{2M_w\sigma_{w/v}}{\rho_w RT \ell n S_{v,w}} = \left[\frac{3\rho_v \tau E}{2\rho_w} \left(\frac{9\alpha\lambda}{m_w} \right)^{1/2} \right]^{2/3} \quad (9)$$

Which reduces to

$$E = \left[\frac{4}{9\rho_v \tau} \times \left(\frac{2m_w}{\rho_w \alpha \lambda} \right)^{1/2} \times \left(\frac{M_w \sigma_{w/v}}{RT \ell n S_{v,w}} \right)^{3/2} \right] \quad (10)$$

From eq. (10) we may write

$$E_{eq} = \left[\frac{4}{9\rho_v \tau} \times \left(\frac{2m_w}{\rho_w \alpha \lambda} \right)^{1/2} \times \left(\frac{M_w \sigma_{w/v}}{RT \ell n S_{v,w}} \right)^{3/2} \right] \quad (11)$$

Where $E = E_{eq}$, is equivalent electric field corresponding to supersaturation ratio $S_{v,w}$.

From eq. (11) we can write

$$E^{2/3} = \left(\frac{4}{9\rho_v \tau} \right)^{2/3} \times \left(\frac{2m_w}{\rho_w \alpha \lambda} \right)^{1/3} \times \left(\frac{M_w \sigma_{w/v}}{RT \ell n S_{v,w}} \right) \quad (12)$$

Which reduces to

$$\ell n(S_{v,w})_{eq} = \left(\frac{4}{9\rho_v \tau E} \right)^{2/3} \times \left(\frac{2m_w}{\rho_w \alpha \lambda} \right)^{1/3} \times \left(\frac{M_w \sigma_{w/v}}{RT} \right) \quad (13)$$

from eq. (11) and eq. (13) we have calculated the values of equivalent electric field and equivalent supersaturation ratios.

From the equations we came to know that the supersaturation ratio varies exponentially with equivalent electric field.

Also the nucleation rate J and Gibb's free energy for the formation of water and ice phase have been calculated.

In chapter-4, we have established an equivalence between temperature and the electric field during water vapour condensation and ice glaciations.

In presence of an external electric field, the rate of increase of radius with respect to time is given by Singh, N. (1986).

In absence of electric field the radius of the critical nucleus is given by

$$r_w^* = [2M_w \sigma_{w/v} / \rho_w RT \ln S_{v,w}] \quad (14)$$

But in presence of external electric field, the same critical radius is given by

$$r_w'^* = \left[\frac{3\rho_v \tau_N}{2\rho_w} \left(\frac{2\alpha \lambda E^2}{m_w} \right)^{1/2} \right]^{2/3} \quad (15)$$

In electric field induced nucleation, for a given size of the critical nucleus, we have described a relation between temperature and electric field, using eq. (14) and eq. (15) as

$$E = \left[\frac{2M_w \sigma_{w/v}}{\rho_w RT \ln S_{v,w}} \right]^{3/2} \left(\frac{2\rho_w}{3\rho_v} \right)^{1/2} \frac{1}{\tau_N T^{3/2}} \quad (16)$$

or $ET^{3/2} = K$ for a given supersaturation ratio and given relaxation time.

In chapter-5, we have described the effect of ions on the electric field nucleation phenomenon as well as the study of thunderstorms has been dealt with in atmospheric clouds. We have also discussed the electrical conductivity of air in thunderstorms, variation of diffusion coefficient of ions, attachment coefficient and studied the use of

atmospheric electrical conductivity as an air, pollution indicator through correlation analysis based on two year of daily averaged observations of the atmospheric electrical conductivity.

The chief ionizing agents in the lower atmosphere are the penetrating radiation from the radioactive substances in the earth's crust, radiation from the radioactive substances in the atmosphere and the cosmic rays.

In the Retezat Mountains concentrations of O_3 , NO_2 and SO_2 in summer season 2000-2002 were calculated and were low and below toxicity levels for forest trees. Ambient O_3 levels found in the Retezat did not affect crown condition of Norway spruce or European beech (Akula Venkatram, 2006).

Condensation of water vapour of ice germ formation in supercooled liquid, when ionizing radiations are passed (Varshney, 1969) is a milestone in the understanding of ions as centers of condensation. This basis has been confirmed theoretically (Vashneya, 1971). The pioneer worker (Castleman, 1979; Mohanen, 1970, 1974; Chan, 1980a, 1980b) has placed the belief on a firm footing.

IMPORTANCE OF PROPOSED STUDY:

The work proposed for investigation is very important as it may lead to air explanation of atmospheric problems related with nucleation. Thunderclouds have an electric field developed inside which causes nucleation. The several charging machines have been proposed. The present research work proposed would set up the effective role of external electric field in development of clouds and also set up a tool for artificial rain making.

CHAPTER-1

INTRODUCTION

CHAPTER-1

INTRODUCTION

In atmosphere there are a number of gases and water vapour are present in different proportion at different temperature and pressure. The amount of water vapour in the air determines how fast each molecule will return back to the surface. The amount of water vapour in an atmosphere is constrained by the restrictions of partial pressures and temperature. The water vapour exist in all three forms i.e. Gas (vapour), Liquid (water) and Solid (ice). The phase change of water vapour takes place the central role in cloud microphysics in the following manners-

1. Water vapour $\xrightleftharpoons[\text{Evaporation}]{\text{Condensation}}$ Liquid water.
2. Water vapour $\xrightarrow{\text{Condensation}}$ Liquid water $\xrightarrow{\text{Crystallization}}$ Solid water (ice).
3. Water vapour $\xrightarrow{\text{Glaciation}}$ Solid water (ice)

Approx. 99.99% of water vapour is contained in the troposphere.

1.1 CHEMICAL POTENTIAL:

To every phase certain energy in the form of latent heat is associated with it. This energy is called the chemical potential energy. When the phase change takes place there is a certain amount of energy given out or absorbed. According to "Willard Gibbs" an American physicist chemical potential ' μ ' is defined as follows - "If to any homogeneous mass in a state of hydrostatic stress we suppose an

infinitesimal quantity of any substance to be added, the mass remaining homogeneous and its entropy and volume remaining unchanged, the increase of the energy of the mass divided by the quantity of the substance added is the potential for that substance in the mass considered.”

Chemical potential is also referred to as partial molar Gibbs energy.

1.1 (i) Chemical Potential of water vapour in Humid Air: Let us derive chemical potential of water vapour and through the equilibrium the chemical potential of water in aqueous solutions. We have equation (Maxwell relations)

$$\left(\frac{\partial \mu_k}{\partial T}\right)_{p, n_j \neq K} = - \left(\frac{\partial S}{\partial n_k}\right)_{T, p, n_j \neq K} = S_K \quad (1.1)$$

From eq. (1.1) we have for an ideal gas K in mixture of ideal gases

$$\left(\frac{\partial \mu_k}{\partial T}\right)_{p, n_j \neq K} = v_k = \left(\frac{RT}{p_k}\right) \quad (1.2)$$

So that, upon integration

$$\mu_K = \mu_{K,0} + RT \ln p_k \quad (1.3)$$

Where the integration constant $\mu_{K,0}$ depends only on the temperature. For such a mixture the potential pressure is $p_k = X_k p$, so that also

$$\mu_k = \mu_{k,0} + RT \ln p + RT \ln X_k \quad (1.4)$$

Therefore if we assume pure water vapour at pressure e is an ideal gas, its chemical potential is

$$\mu_{v,o}(e, T) = \mu_{v,o}^+(T) + RT \ln e \quad (1.5)$$

Where $\mu_{v,o}^+(T)$ is the chemical potential at a standard state of unit pressure. Similarly the chemical potential $\mu_v(p, T)$ of water vapour in humid air at total pressure p is

$$\mu_v(p, T, X_v) = \mu_{v,o}^+(T) + RT \ln p + RT \ln X_v \quad (1.6)$$

From eq. (1.5) with $e = p$, we see that this last result may also be expressed as

$$\mu_v(p, T, X_v) = \mu_{v,o}(p, T) + RT \ln X_v \quad (1.7)$$

Which shows that $\mu_v \leq \mu_{v,o}$ since $X_v \leq 1$

In contrast to pure gases whose chemical potentials vary logarithmically with pressure, the chemical potential of a pure liquid is proportional to pressure, to an excellent approximation. This is obvious from.

$$\left(\frac{\partial \mu_k}{\partial p} \right)_{T, n_j \neq K} = \left(\frac{\partial v}{\partial n_k} \right)_{T, p, n_j \neq K} = v_k \quad (1.8)$$

On realizing that liquids are nearly incompressible thus for water we have

$$\left(\frac{\partial \mu_{w,o}}{\partial p} \right) = v_{w,o} \approx \text{Constant} \quad (1.9)$$

From which the chemical potential is found to be

$$\mu_{w,0}(p, T) \approx \mu_{w,0}(0, T) + v_{w,0}p \quad (1.10)$$

As we have seen, if a liquid and gas are in equilibrium the chemical potential of a given component will be the same in both phases, consequently, from eq. (1.3) the chemical potential of component K in a liquid solution, which is in equilibrium with its vapour at partial pressure p_k , is

$$\mu_{k,\ell} = \mu_{k,0} + RT \ln p_k \quad (1.11)$$

In addition, experiments show that for so-called 'ideal' solutions, for which there are no interactions between the solvent and solute molecules, the equilibrium vapour pressure of any component is proportional to its mole fraction in the solution. (This is known as Raoult's law).

Assuming Raoult's law then we have $p_k = X_{k,\ell} p_{k,0}$, where $X_{k,\ell}$ is the mole fraction of component K in the solution, and $p_{k,0}$ is the partial pressure of component K in equilibrium with the pure liquid phase of K at the same temperature. Then as a function of $X_{k,\ell}$, the chemical potential becomes

$$\mu_{k,\ell} = \mu_{k,\ell}^0 + RT \ln X_{k,\ell} \quad (1.12)$$

Where $\mu_{k,\ell}^0$ is a function of both temperature and total pressure, but is independent of the composition of the solution.

1.1 (ii) Chemical Potential of water in aqueous solutions: In clouds the liquid phase is rarely present in the form of pure water, but rather is generally a dilute aqueous salt solution.

Therefore, $\mu_{k,\ell} = \mu_{k,\ell}^0 + RT\ell nX_{k,\ell}$ is especially relevant to us, and we may use it to write the chemical potential for water in an ideal aqueous salt solution in the following form:

$$\mu_w(p, T, X_w) = \mu_w^+(p, T) + RT\ell nX_w \quad (1.13)$$

Where $X_w = \frac{n_w}{(n_w + n_s)} = 1 - X_s$ is the mole fraction of water, n_w and n_s being respectively the number of moles of water and salt in the solution. By analogy one would expect that the chemical potential of the salt component could be expressed in the same way, viz;

$$\mu_s(p, T, X_w) = \mu_s^+(p, T) + RT\ell nX \quad (1.14)$$

In passing, we may note that for

$$X_w = 1, \mu_w(p, T) = \mu_{w,o}(p, T) = \mu_w^+(p, T)$$

The chemical potential of pure water at (p, T) , there is no analogous simple physical interpretation for the quantity $\mu_s^+(p, T)$.

Experiments shows that most dilute solutions of non-electrolytes are in conformity with eq. (1.13) & eq. (1.14). In general, however, real aqueous solution depart from such ideal behaviour. It is customary to account for non-ideal solutions through the replacement of the mole fraction X by the activity $a \equiv fx$, where f is called the rational activity coefficient. Thus for real aqueous salt solutions we write

$$\mu_w(p, T, a_w) = \mu_{w,o}(p, T) + RT\ell na_w; a_w = f_w X_w \quad (1.15)$$

$$\mu_s(p, T, a_s) = \mu_s^+(p, T) + RT\ell na_s; a_s = f_s X_s \quad (1.16)$$

The importance of the activity to us is that it provides a direct measure of the equilibrium water vapour pressure over a real salt solution, or in other words, the generalization of Raoult's law to real solution we now turn to a demonstration of this property.

1.2 CHANGE IN CHEMICAL POTENTIAL:

Change in chemical potential of a system is given by

$$d\mu = -(\mu_v - \mu_\ell) \quad (1.17)$$

Where μ_v is the chemical potential of the vapour phase and μ_ℓ the chemical potential of liquid phase. This change in chemical potential appears as the energy of the formation of the liquid phase.

1.3 GIBBS PHASE RULE:

This rule enables us to determine the variance of a system i.e. the number of intensive variables, which may be freely specified without cause the system to depart from equilibrium. In equilibrium the system is characterized by a common T&p, and by a number of mole fractions in the various phases.

Let us denote the mole fraction of the k^{th} component in the j^{th} phase by

$$X_k^j = n_k^{(j)} / \sum_k n_k^{(j)}$$

Thus, for every phase we have the simple mass conservation constraint that $\sum_{k=1}^c X_k^{(j)} = 1$ for a total of ϕ constraints. In addition we have the condition –

$\mu'_k = \mu_k = \dots = \mu_k^{(a)}$, $K = 1, 2, 3, 4, \dots, c$. On the chemical potentials, which constitute another $(\phi-1)$ constraints for every k , for a total of $c(\phi-1)$ constraints. Therefore the number of thermodynamic degrees of freedom, is

$$w = 2 + \phi c - \phi - c(\phi - 1) = 2 + c - \phi \quad (1.18)$$

Which is the Gibb's phase rule for the bulk phases. As a simple application of above equation consider a homogeneous fluid, we have-

$$\phi = 1, c = 1 \text{ and so } w = 2.$$

For a mixture of two gases, $c=2$, $\phi = 1$ and hence $w=3$. For water in equilibrium with a vapour and ice, $c=1$, $\phi = 3$ and $w=0$, equilibrium is possible only for a single choice of temperature and pressure, which defines the triple point temp. T_t of this system. If this system is now exposed to the atmosphere, $c=2$ (water substance and air), $\phi = 3$ and so $w=1$.

1.4 STRUCTURE OF AN ISOLATED WATER MOLECULE:

Heat capacity of water vapour at constant volume near room temperature yield a value of approximately $3k$ per molecule, where k is the Boltzmann Constant. We must interpret the heat capacity measurements in terms of a contribution of $(\frac{1}{2}) k$ from each of the three translational degrees of freedom. This interpretation implies that the water molecule cannot have its three atoms arranged in a linear fashion, which is the same conclusion by investigating electrical properties of the water molecule. In water each hydrogen nucleus is bound to the central oxygen atom by a pair of electrons that are shared between them, these shared electron pair are called covalent chemical bond. Since such

measurements reveal a large electric dipole moment of $\mu = 1.83 \times 10^{-18}$ e.s.u. cm. (Hobb's, P.V., 1974; Eisenberg et al., 1969).

On the basis of such measurements, it has been concluded that the three atoms are situated at the vertices of a triangle, the geometry of which is given in fig. (1.1). Recent experiments show that the equilibrium O-H bond length is 0.95718 \AA and that the equilibrium H-O-H bond angle is 104.523° (Fletcher, N.H., 1970a; Hobb's, 1974).

In the structure of water molecule in its ground state, an oxygen atom has two electrons in the spherical 1s orbital, where they are bound tightly to the atomic nucleus, and two electrons, less tightly bound in the spherical 2s orbital (fig. 1.2). In addition, two electrons can be considered to occupy the 2P_x orbital, one electron in 2P_y orbital and one electron in 2P_z orbital. Since the 2P_y and 2P_z orbitals may contain two electrons each, these are incomplete. Therefore the electrons in these orbitals are free to couple with the 1s orbital of two hydrogen atoms, allowing them to form two O-H bonds. If these describe them to form two O-H bond of a water molecule one would expect water to have a bond angle of 90° . However experimentally, one find that the bond angle is some 15° larger. Since oxygen is more electronegative than hydrogen, oxygen exerts a greater force on the shared electron pair. Electrostatic repulsion between the two hydrogen atoms must, consequently, lead to an increase of the bond angle.

However, Heath and Linnet (1948) showed that this repulsion is insufficient to account for the experimentally, found bond angle. They suggested that the 'hybridization' of the 2s orbital of the oxygen atom;

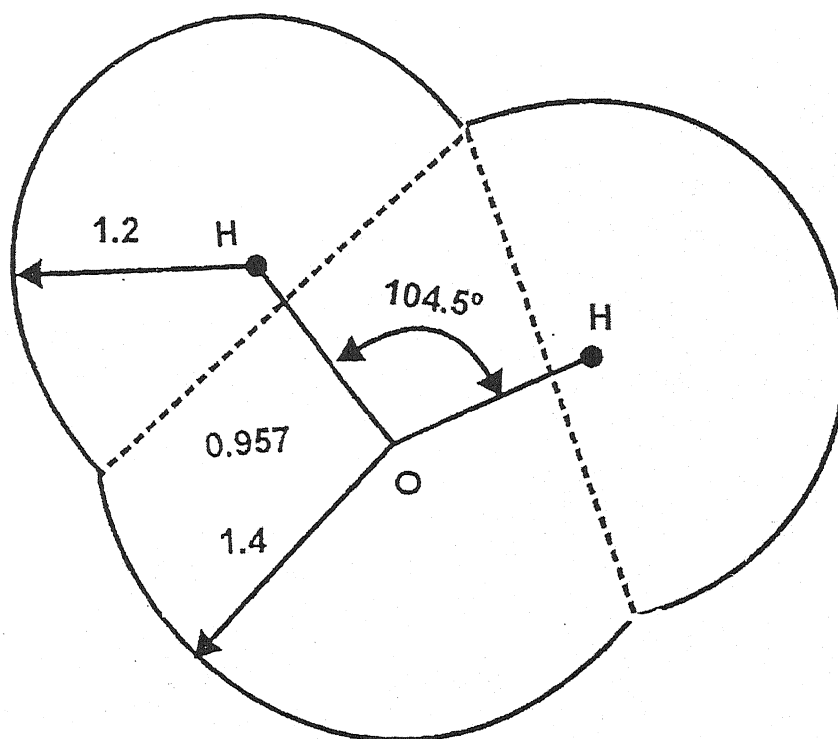


fig. 1.1 : Two dimensional geometry of a single water molecule. The O-H distance (in 10^{-4} cm) and the H-O-H angle are indicated, as the radii of the hydrogen and oxygen atoms.

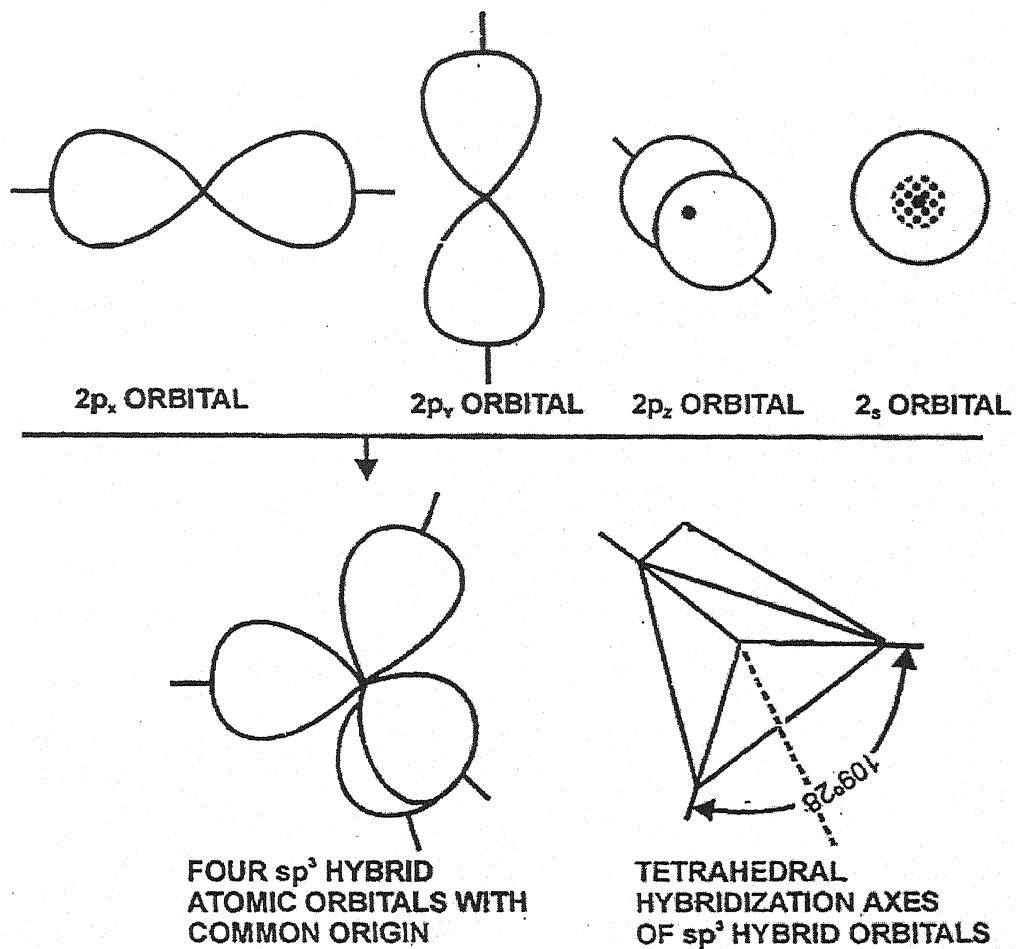


fig. 1.2 : Hybridization of orbitals of oxygen atom.

with its $2p_y$ and $2p_z$ orbitals, resulting in the formation of four Sp^3 -hybrid atomic orbitals. Two of these overlap with the hydrogen orbitals, while the two remaining orbitals form two lobes on the side of the Oxygen atom away from the Hydrogen atoms fig. (1.2). These lobes called lone-pair hybrids, are symmetrically located above and below the molecular plane and form roughly tetrahedral angles with the bond hybrids. (Exact 109.467°). It is this tetrahedral character of the water molecule which gives rise to a tetrahedral coordination of water molecules in water and ice.

Duncan and Pople (1953)& Bader and Jones (1963) have carried out quantum mechanical (molecular orbital theory) calculations of the electron density distribution shown in fig. (1.2), and show that there are four locations in the water molecules with high electron density; close to the Oxygen atom, close to each Hydrogen atom, and at the location of the lone pair orbitals, which appear as an electron density bulge behind the oxygen atom.

The charged distribution around a water molecule may also be approximated by 'electrostatic' or point charge models. In these models charges are assigned whose sign, magnitude, and location are such that the molecules as a whole is electrically neutral, and the electric dipole moment is equal to that experimentally measured. Such models have been worked out (Rowlinson, 1951; Bjerrum, 1951; Pople, 1951; Cambell, 1952; Cohen, 1962). Although such models are convenient in some cases, they generally do not correctly predict the higher electric moments. The current views of water structure is influenced greatly by molecular modeling simulations beginning in the 1980's, water is more like a 'gel' consisting of a single, huge hydrogen-bonded cluster. On a 10^{-12} - 10^{-9} sec

time scale, rotations and other thermal motions cause individual hydrogen bonds to break and re-form in new configurations, inducing ever-changing local discontinuities whose extent and influence depends on the temperature and pressure.

1.5 STRUCTURE OF WATER VAPOUR:

In contrast to ideal gas behaviour experiments show that water molecules in water vapour tend to interact & form clusters (Kell, 1972a). Though only in small concentration dimers as well as higher order polymers are considered to be present in water vapour. Recent experiments involving molecular beam techniques (Lin, 1973; Searcey, 1974) suggest that in highly supersaturated water vapour, clusters of up to 180 water molecules may be present. Clusters of 21 water molecules seemed to exhibit particularly large stability. It is interesting to note that 21 water molecules can be arranged in the form of a pentagonal dodecahedron with a molecules at each corner and a single molecule in the centre of the 'cage'.

At present however, no conclusive evidence of the actual geometric arrangement, if any, of water molecules in such clusters in vapour is available. Studies on the possible and more likely cluster types have been reviewed (Rao, 1972; Kell, 1972a). Recent theoretical studies of the formation of water clusters have been carried out (Kistenmacher et al., 1974a, 1974b; Abraham, 1974). Kistenmacher et al. found two possible stable configurations for the dimers, a cyclic form and an open form, which was more stable. For the large clusters the authors suggested not a single structure, but a statistical distribution of different configuration.

Between a pair of water molecules the potential energy of interaction U , has the general character of being strongly repulsive at very close separations and weakly attractive at longer range, so a simple expression for it is due to Stockmayer (1941).

$$U = -\frac{\mu^2 f}{r^3} - \frac{c}{r^6} + \frac{C\sigma^{18}}{r^{24}} \quad (1.19)$$

Where r is the separation of the molecules; μ is the dipole moment of an isolated water molecules; σ is the collision diameter (the molecular separation at which $U=0$ if $\mu=0$), c is an adjustable constant, and f is known function of the mutual orientation of the two molecules.

The first term on the right of eq. (1.19), is just the dipole-dipole contribution to the interaction energy, and may be attractive or repulsive. The second term represents contribution from-

1. The interaction energy between a permanent dipole of one molecule and the dipole it induces in the other (dipole polarization or induction interaction).
2. The net energy arising from momentary, fluctuating dipoles interacting with the corresponding induced dipoles (polarization-2 or dispersion interaction). Even though the time average of these dipole fluctuations may be zero, the energy contribution is proportional to their mean square, which is finite and positive.

Both (1) & (2) are usually referred to as Vander Wall's interaction, which by its nature can be seen to bring about an attractive force between the molecules. The third term in eq. (1.19), represents the short range repulsive forces, which loosely may be ascribed to the overlap of electronic orbitals, which are incompatible according to the Pauli exclusion principle.

There is little doubt that the Stockmayer potential or similar ones such as (Rowlinson, 1949, 1951), potential portray with fair accuracy the interaction between pairs of water molecules at large separations in dilute water vapour. This is evidenced by the fact that values for the second virial coefficient computed via. eq. (1.19), can be made to fit experimental values on the other hand, the same potential functions yields values for the third virial coefficient of water vapour, which disagree substantially with experiment. Partly, this is due to the approximate nature of eq. (1.19), and partly because three-body interactions should be included also, since other molecules in the system can significantly modify the interaction of a given pair. In particular the Stockmayer potential is insufficiently 'directional' in character to account for the geometry of cluster formation in water vapour.

1.6 STRUCTURE OF ICE:

At temperature between about -100°C & 0°C and at atmospheric pressure, water substance crystallizes from its gaseous or its liquid state to form a six fold symmetric or hexagonal solid called ice- I_h . At different pressure and temperatures ice assumes other crystalline modifications, which are discussed, for example in Fletcher (1970a) and Hobbs (1974), we shall concern ourselves here only ice- I_h , hence fourth referred to simply as 'Ice'.

X-ray diffraction studies demonstrate that in ice each oxygen atom is surrounded by four nearest neighbour oxygen atoms at a distance of about 2.76×10^{-8} cm. These four atoms form an almost regular tetrahedron. These tetrahedrons are joined together to form a hexagonal lattice fig. (1.3). These hexagonal space group is denoted by D_{6h}^4 or $P6_3/mmc$ and is characterized by 1 six-fold axis of rotation. Perpendicular to 1 mirror plane, (3+3) mirror planes, and a centre of symmetry.

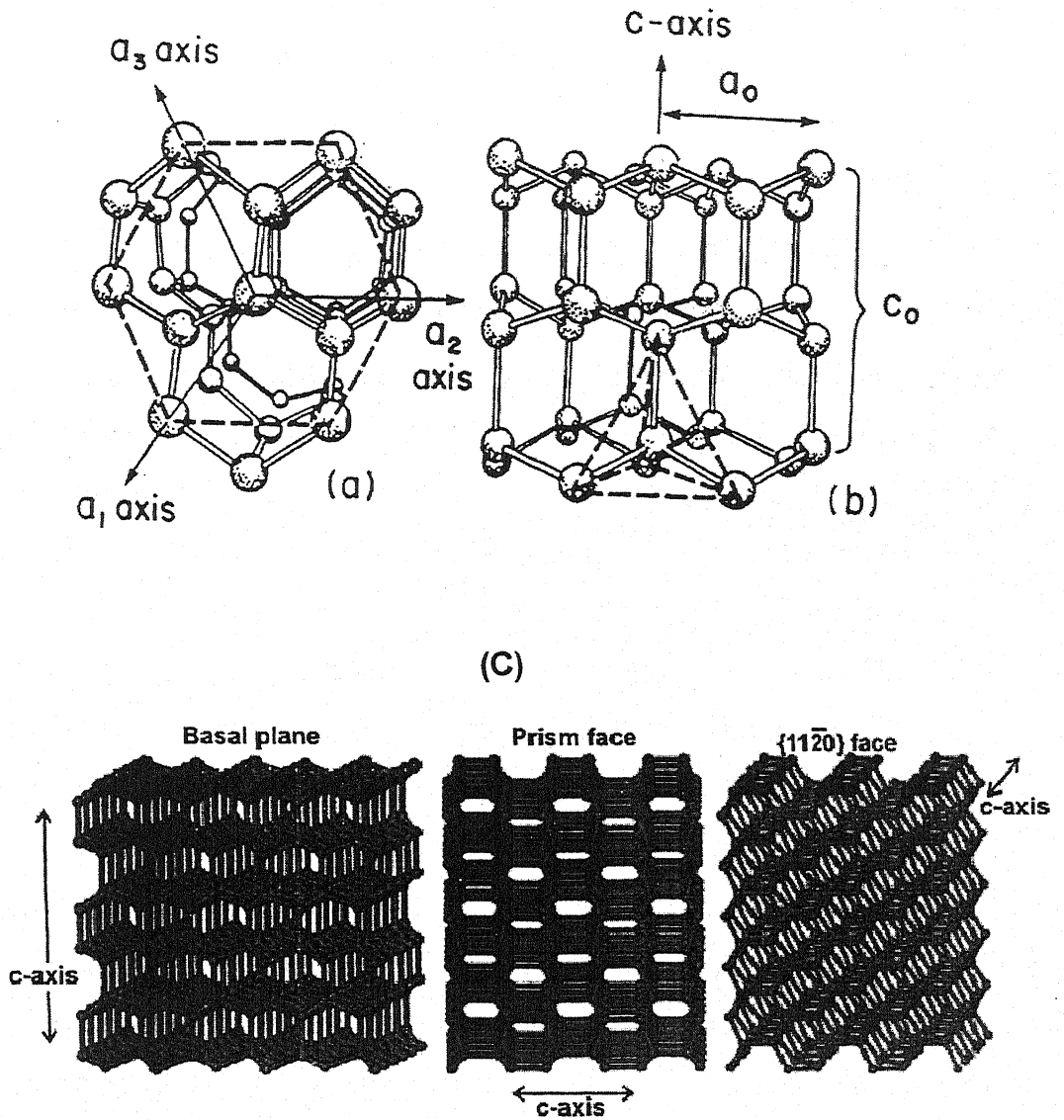


fig. 1.3 : Position of Oxygen atoms in ice- I_h : (a) view along c-axis, (b) view perpendicular to c-axis, (c) Hexagonal Ice-Structure.

Near 0°C , any given atom in ice also has 12 second nearest neighbours at a distance of about 4.52 \AA , 1 third nearest neighbour at 4.59 \AA , 6 fourth nearest neighbour at 5.26 \AA , 3 fifth nearest neighbour at 5.31 \AA , 6 sixth nearest neighbour at 6.36 \AA , 6 seventh nearest neighbour at 6.46 \AA , 9 eighth nearest neighbours at 6.69 \AA , 2 ninth nearest neighbours at 7.36 \AA and 18 tenth nearest neighbours at 7.81 \AA .

Each water molecule is hydrogen bonded to its four nearest neighbours. The hydrogen atoms in a water molecule are about 104 degrees apart, which is just about the right angle to build tetrahedral structures. The positively charged portion of one water molecule is attracted to the negatively, charged portion of a neighbour. This attraction, termed hydrogen bonding, gives water many of its unique properties. This is brought about through the formation of two hydrogen (O-H-O) bonds by each water molecule, each bond being directed towards a lone electron pair of a neighbouring water molecule. This manner of bonding leads to an open lattice structure, as illustrated in fig. (1.3). Perpendicular to the c-axis, the ice lattice consists of open-puckered hexagonal rings with oxygen atoms. Comparisons show that the arrangement of oxygen atoms in ice is isomorphous with the wurtzite structure of ZnS and the tridymite structure of SiO_2 .

Each unit cell of ice, a four sided prism set on a rhombic base, contains four water molecules and is characterized by the lattice constants a_0 and c_0 fig. (1.4). X-Ray data for a_0 and c_0 (Blackman,1957; Lonsdale,1958; Laplace,1960; Brill,1967 ; Kumai,1968) are summarized in fig.(1.5), as a function of temperature.

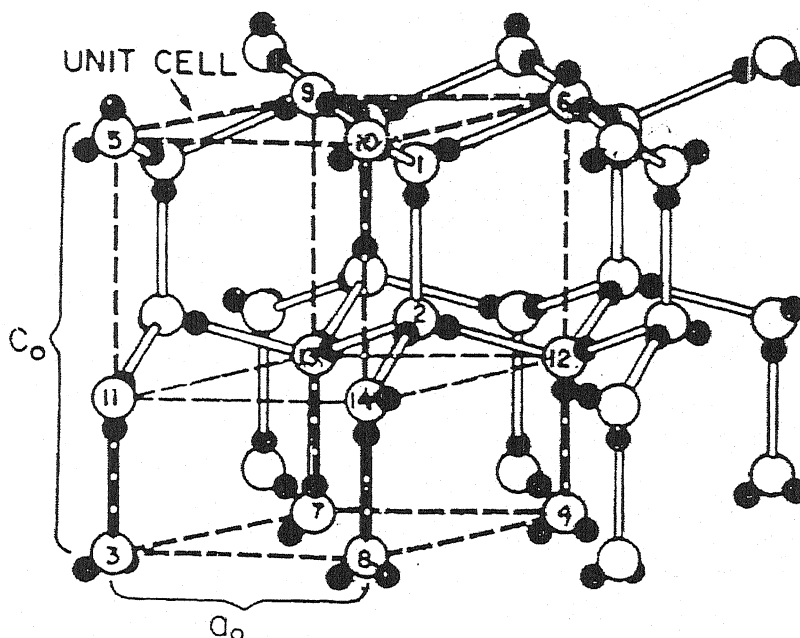


fig. 1.4: A typical disordered arrangement of protons in the ice-I_h structure; oxygens (1) and (2) contribute 12/12 each oxygen (3), (4), (5), (6) contribute 1/12 each, oxygens (7) to (12) contribute 2/12 each, and oxygens (13) and (14) contribute 4/2 each, for a total of $48/12 = 4$ oxygens.

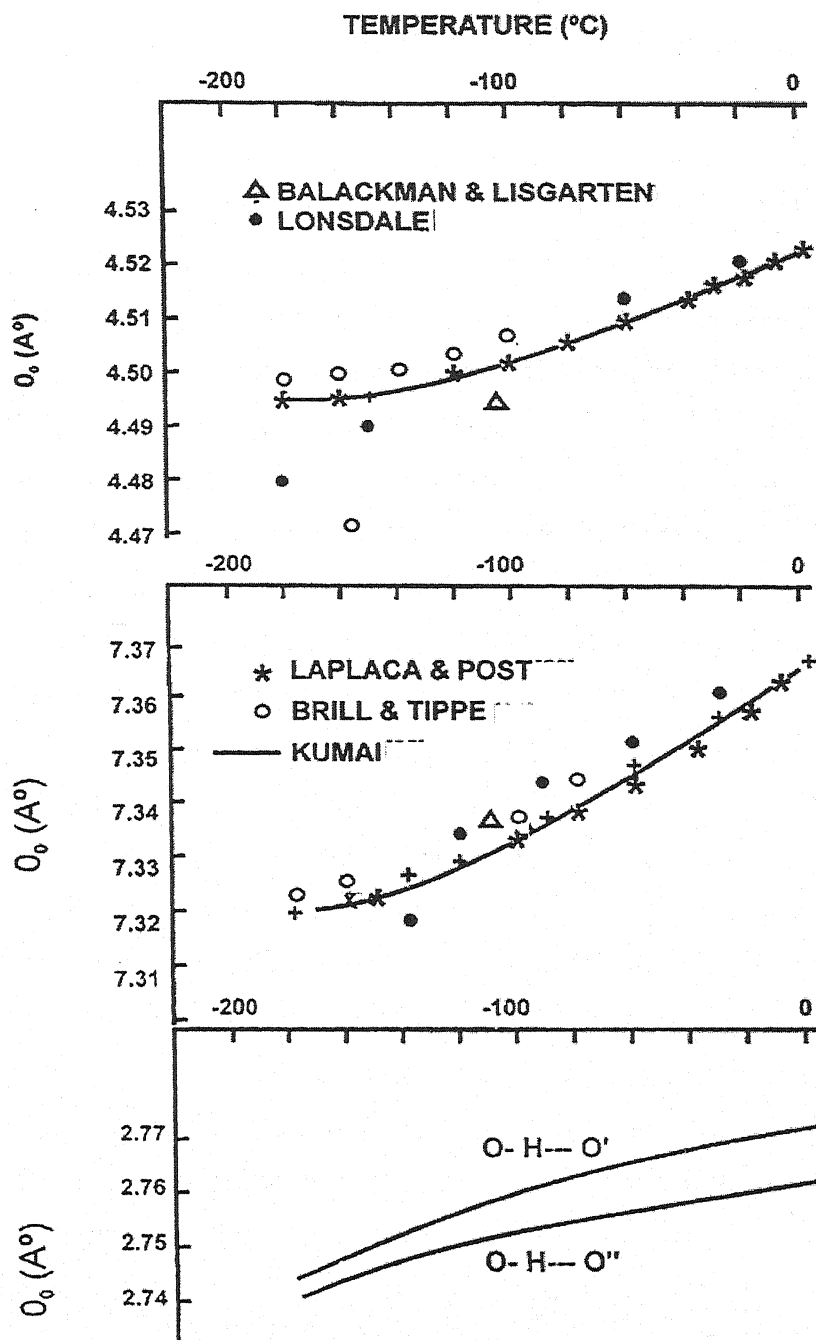


fig. 1.5: Temperature variation of the lattice parameters of ice- I_h according to Balackman et al. (1957); Lonsdale (1958); Laplaca (1960); Brill (1967) and Kumai (1968).

These measurements show that a_0 and c_0 decrease with decreasing temperature- the rate of decrease smaller, the lower the temperature-such that $(c_0/a_0) = 1.629$ for all temperatures. Using the values for a_0 and c_0 given in fig.(1.5), the volume of a unit cell of ice $V_{uc} = 2(a_0^2\sqrt{3/4}) c_0$, varies from $1.305 \times 10^{-22} \text{ cm}^3$ (0°C) to $1.281 \times 10^{-22} \text{ cm}^3$ (-180°C). Thus the number of water molecules cm^{-3} varies from 3.06×10^{22} (0°C) to 3.12×10^{22} (-180°C). According to Eisenberg and Kauzmann (1969), three points of view may be taken to define the hydrogen bond energy E_H in ice. First, one may assume that E_H is given by lattice energy E_L of one mole of ice (the difference in energy between one mole of isolated water molecules and one mole of ice, both at 0°K and with motionless atoms) divided by the number of hydrogen bonds in a mole.

Since both hydrogen atoms of a water molecule participate in one H-bond (excluding the molecules in the surface of ice), one may estimate E_H as $E_H = E_L/2 = 7.04 \text{ K cal mol}^{-1}$, based on the value for E_L found by Whalley et al. (1973). Second one may define E_H , possible more appropriately, in terms of sublimation enthalpy $(\Delta H)_s$ by writing $E_H = (\Delta H)_s/2$. Since $(\Delta H)_s$ is temperature dependent, so is E_H , and we find $E_H(0^\circ\text{K}) = 5.66 \text{ K cal mole}^{-1}$ and $E_H(0^\circ\text{C}) = 6.15 \text{ K cal mole}^{-1}$. In both of these definitions we ascribe the entire intermolecular energy in ice to hydrogen bonding we therefore include in E_H the effects of dispersion and short range repulsive forces which are present not only in the ice but also in crystals of non hydrogen bonded substance. The third definition of E_H is based on premise that the contribution to $(\Delta H)_s$ from the hydrogen bonds is distinct from that of other forces. One may therefore set $E_H = [(\Delta H)_s - E_{\text{other}}]/2$, where E_{other} represents the intermolecular energy associated with the other forces. This definition suffers from the fact that E_{other} is not an observed quantity and cannot presently be accurately calculated.

An accurate theoretical calculation of a single hydrogen bond in ice should include at least the effects of nearest neighbours. Generally the approach taken has been to assume the total hydrogen bond energy is given by the sum of the four component energies (dipole-dipole, dipole-polarization, polarization-polarization and short range inert-actions) and to evaluate each of these by approximate methods for two neighbouring water molecules at the relative positions found in ice. For this purpose various models for the charge distribution in a water molecule have been assumed.

The results of the most pertinent calculations on the subject have been summarized (Hobb's, 1974; Eisenberg, 1969). The values computed for E_H range from 4 to 8 k cal mole⁻¹. In all of these computations, the entire intermolecular energy has been attributed to hydrogen bonding.

The positions of hydrogen atoms in ice and subject to the Bernal-Fowler (BF) rules these require that-

1. Each water molecule is oriented such that its two hydrogen atoms are directed approximately towards two of four oxygen atoms which surround it tetrahedrally,
2. There is only one hydrogen atom on each O-O linkage and,
3. Each oxygen atoms has two nearest neighbouring hydrogen atoms.

Such that the water molecule as structural unit is preserved.

An ice structure, which obeys BF rules, is termed ideal. Natural ice, however, does not behave ideally. The following major aromatic defects are found in natural ice (stacking faults), chemical defects; molecular vacancies (Schottky defects), interstitial molecules (Frenkel defects), ionized states and orientational defects (Bjerrum defects).

1.7 STRUCTURE OF WATER AND AQUEOUS SOLUTIONS:

In ascribing 'structure' to a fluid such as water the time periods τ_v and τ_D just mentioned becomes especially relevant. In fact, we must consider three different time scales times $t \ll \tau_v$ times intermediate to τ_v and τ_D , at $t \gg \tau_D$. Assuming we were equipped with a camera which had shutter speeds less than τ_v , we could obtain a relatively sharp picture of the actual position of a water molecules at any given instant.

This would reveal the instantaneous water structure called the I-structure. If the shutter speed were between τ_v and τ_D , each molecule would complete many oscillations while the shutter was open and the resulting somewhat blurred picture would provide information on the vibrationally averaged position of the water molecules in water, i.e. V-structure (Eisenberg and Kauzmann) of water, if the shutter speed were larger than τ_D , the diffusionally averaged arrangement of the water molecules of D-structure could be found. Experimental studies which employ infrared or Raman spectroscopy, or neutron scattering techniques lead to information on the V-structure, while X-ray studies determine the D-Structure.

Spectroscopic studies show that the frequency of oscillation for water molecules is slightly smaller in water than in ice, the period of vibration being $\tau_v \approx 10^{-13}$ second. Studies on self diffusion, viscosity, dielectric relaxation, and nuclear magnetic resonance relaxation show that a water molecule in water has a characteristic displacement period near 0°C of $\tau_D \approx 10^{-11}$ sec.

Information on the state of hydrogen bonds in water can also be obtained from infrared and Raman spectra (Walrafen, 1966, 1967, 1968a, 1968b, 1972). Such spectra confirm that water molecules exists as entities

in water. They also give evidence that some O-H groups in H_2O are hydrogen bonded and, therefore, point towards a free, lone electron pair of a neighbouring H_2O molecule, while other O-H groups are non-directionally bonded to the surrounding water molecules and hence are disoriented with respect to neighbouring lone electron pairs (Kell, 1972a; Eisenberg, 1974). The latter are referred to as non-hydrogen bonded or 'broken' O-H groups. Estimates of the percentage of broken H-bonds in water as function of temperature are summarized in fig. (1.6).

These experimental findings are supported by recent studies, which attempt to simulate the molecular structure of water by purely theoretical methods (Rahman, 1971; Stillinger, 1972; Popkie, 1973; Kistenmacher, 1974a, 1974b). Applied conventional molecular dynamics to a system of 216 water molecules, which interacted via a potential function developed (Ben Naim and Stillinger, 1972; Ben Naim, 1972). This pair potential function is considerably more complicated than the Stockmayer potential eq. (1.19). It is based on Bjerrum's four point charge model for a water molecule and incorporates the linear bonding tendency between neighbours in a tetrahedral pattern such as that found through out the ice lattice. It has been argued (Stillinger, 1970, 1972) that this potential function also incorporates the principal features of non-additivity; i.e. it takes into account the many body aspect of the problem.

Recently, another pair potential function was developed (Clementi, 1973; Fromm, 1975; Popkie, 1973; Kistenmacher, 1974a, 1974b; Abraham, 1974). This function is based on an analytically fitted Hartree-Fock potential (Kern, 1972), the point charge model and correlation energy corrections due to induced dipole interaction and short-range effects. It was used in conjunction with the Monte- Carlo simulation,

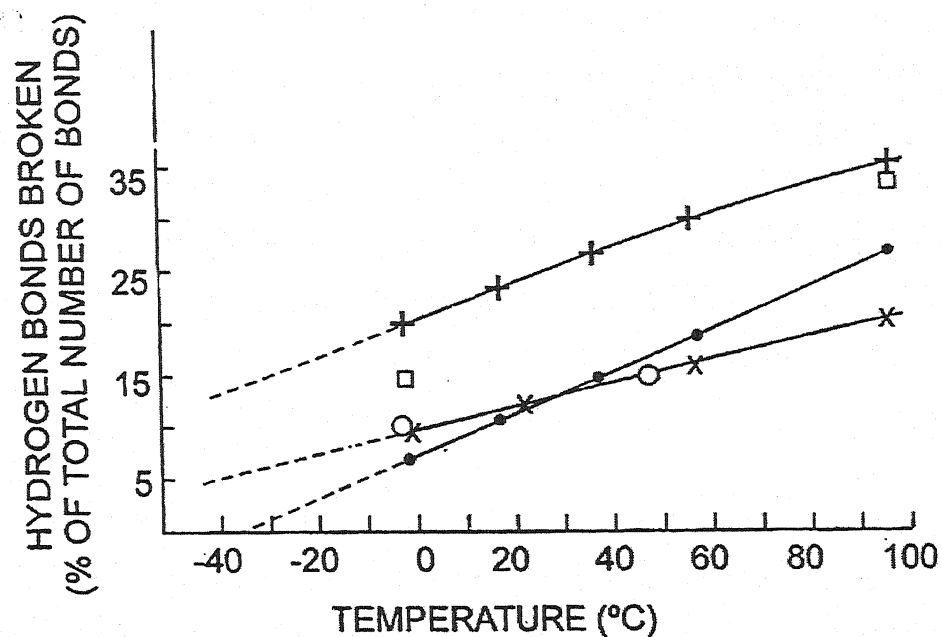


fig. 1.6 : Variation with temperature of number of hydrogen bonds broken in water.

method (Barker, 1969), to study a group of 125 water molecules. In addition, the molecular dynamic study (Stillinger, 1972), predicted that the hydrogen bond rupture mechanism in water is characterized by an excitation energy of about $2.5 \text{ K cal mol}^{-1}$. This is in good agreement with the Raman and infrared spectra experiments (Walrafen, 1966, 1967, 1968a, 1968b, 1972), who found that the energy necessary to rupture hydrogen bonds in water is about $2.55 \text{ Kcal Mole}^{-1}$. Infrared spectra taken (Worley, 1966), imply the comparable value of $2.4 \text{ Kcal mol}^{-1}$. Finally (Bucaro, 1971), inferred $2.5 \pm 0.1 \text{ Kcal mol}^{-1}$ from depolarized light scattering measurements.

Considerable uncertainties still exist as to how X-ray, infrared, and Raman Studies should be interpreted in terms of the arrangement of the water molecules in water. We shall now describe briefly just the main features of some of the more prominent models put forward for the water structure.

In the 'quasi-crystalline model' the water structure is assumed to resemble one of several possible forms; a broken-down ice. I_h structure, a quartz structure, a structure of octahedrally arranged, molecules (Van Eck, 1958), or a structural mixture of molecules arranged in a tridymite structure dispersed in a denser ice-III structure (John, 1966). In the 'interstitial model' the water is visualized as consisting of a highly hydrogen bonded structure inside of which non bonded or partially bonded molecules occupy interstitial structure position (Forslind, 1952; Danford, 1962; Krestov, 1964). In the 'Clathrate model' water is assumed to have a structure similar to the clathrate structure of gas hydrates except that instead of a gas molecule a water molecule is held inside each cavity of a cage like, hydrogen bonded frame work of Pentagonal dodecahedron cages (Pauling, 1959, 1960; Frank, 1961).

The 'flickering cluster model' makes use of the partially covalent character of the hydrogen bond and assumes that H-bond formation in water is a cooperative phenomenon, in that the formation of a hydrogen bond between two water molecules reinforces that tetrahedral hybridization in oxygen atoms.

The 'mixture model' picture water as a mixture of 0-, 1-, 2-, 3- and 4- bonded water molecules engaging in the formation of various sized clusters (Frank, 1957; Walrafen, 1972). Finally, the 'bent bond model' assumes that few, if any, bonds between water molecules are broken upon melting of ice, but instead become bent to various degrees (Pople, 1951).

Experiments show that the structure of water is altered when water-soluble salts, in part dissociated into ions, are dissolved in water. The aqueous solution resulting from dissolving a salt in water would be an ideal solution if the dissolved salt molecules or ions in no way affected the water molecules (Haggis, 1952).

In any real aqueous solution this is not the case. For example, some of the salt molecules or ions do not fit into the water 'structure' and therefore distort it, causing a size effect. This effect is called hydration. Since large ions have weaker local electric field than small ions, the hydration effect is greater for small ions. In addition, hydration is more pronounced for positive ions than for negative ones, since a positive ion tends to interact with both ions electron pairs, which blocks the formation of two H-O group of a water molecule, which blocks the formation of only hydrogen bond.

1.8 WATER VAPOUR DISTRIBUTION IN INDIA:

Sarkar et al. (1982) brought about an atlas on water vapour distribution over India as a part of their programme under the project "Anomalous, Microwave Propagation and Prediction of Radar Performance over India." The list of sixteen regular radiosonde stations providing data is given in table (1.1).

Water vapour density was calculated from radiosonde data of four year (1968-71) using fixed pressure level data from 1000mb to 50mb level. Radiosonde flights were taken twice daily, one at 0000 GMT and the other at 1200 GMT corresponding to early morning and late evening in local time. Accuracy of relative humidity temperature and pressure obtained from radiosonde measurements are 5%, 0.25% and 2mb, respectively. Over the northern plains, the water vapour density is generally high during monsoon and post monsoon periods while the value are of moderate order during winter and summer months.

The water vapour density values are obtained from two observations per day; hence these values do not strictly indicate the percentage of time in a year when a particular water vapour density can be expected. It seems unlikely that the extremes of diurnal density variation could always occur at 0000GMT and 1200 GMT, and therefore cumulative distribution statistics have a tendency to be the case if the observations were made frequently, our data are especially useful for station to station in two regions, such as estimating the water vapour values for one region fig. (1.7) to fig. (1.14).

Table-1.1

List of Radiosonde Stations

		Elevation (m)
1.	Minicoy	2
2.	Visakhapatnam	3
3.	Cochin	3
4.	Calcutta	6
5.	Bombay	14
6.	Madras	16
7.	Gauhati	54
8.	Ahmedabad	55
9.	Trivandrum	64
10.	Port Blair	79
11.	Lucknow	128
12.	New Delhi	216
13.	Jodhpur	224
14.	Nagpur	310
15.	Bangalore	921
16.	Srinagar	1666

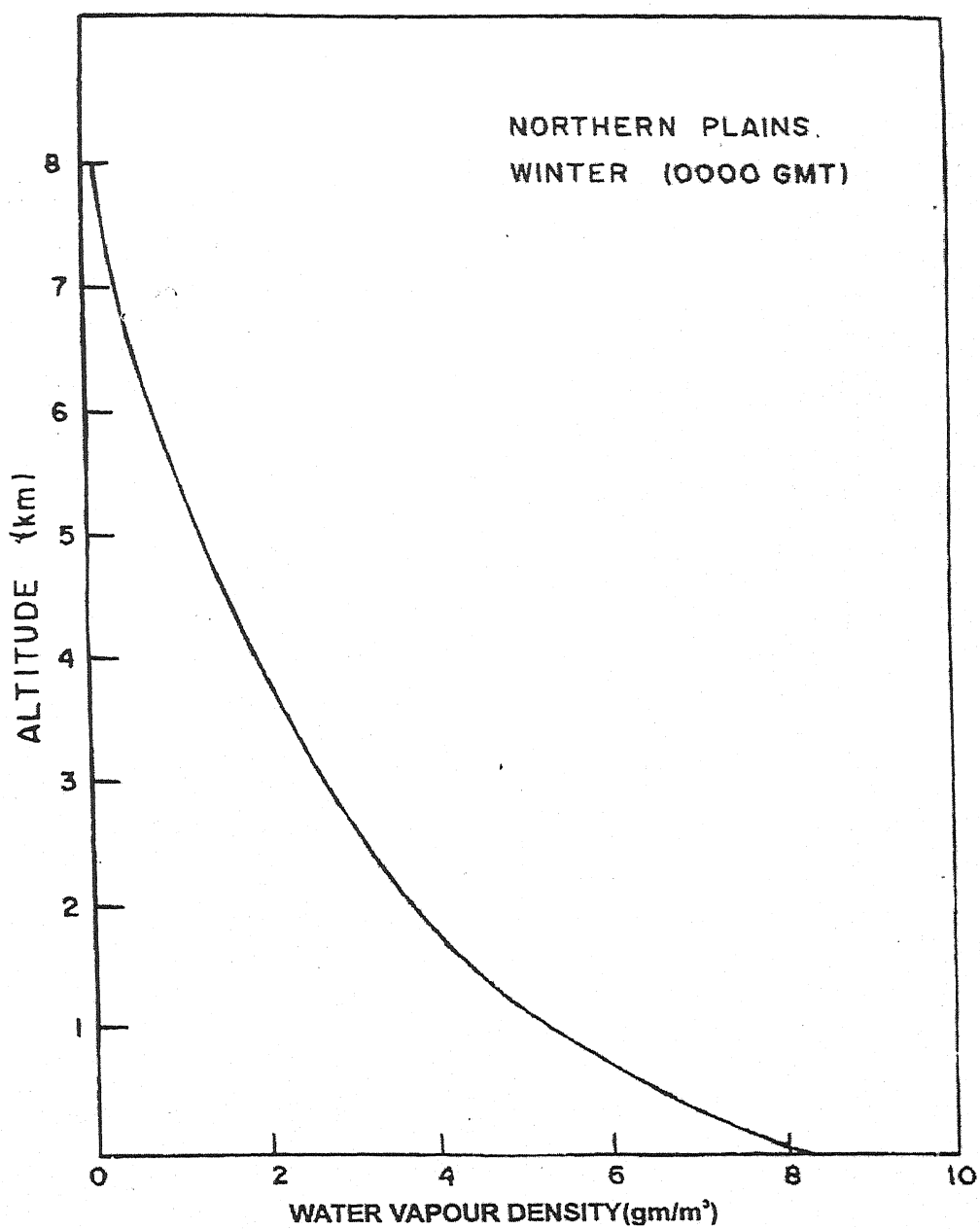


fig. 1.7 : Water Vapour density profile over Northern Plains in Winter (0000GMT).

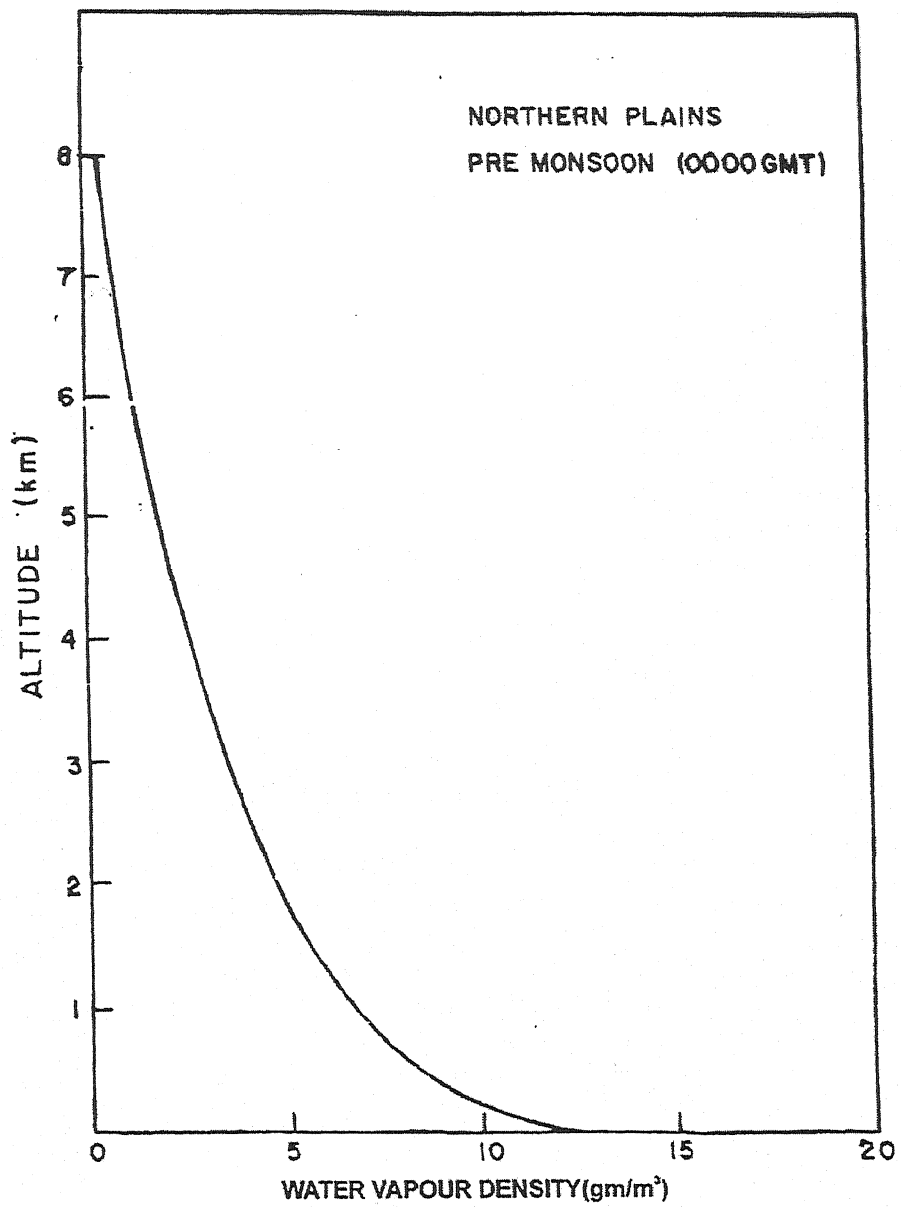


fig. 1.8 : Water Vapour density profile over Northern Plains in Pre monsoon (0000GMT).

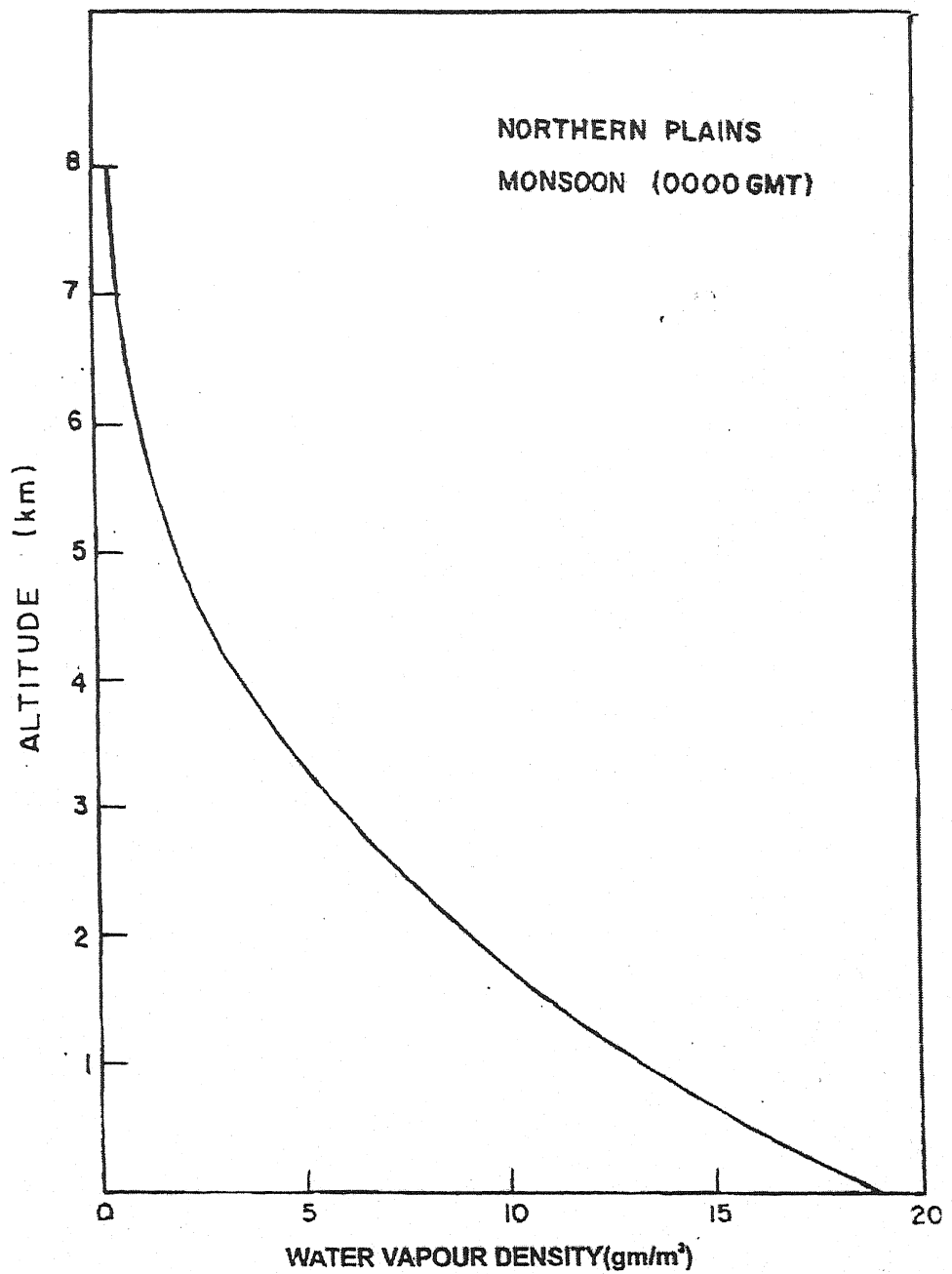


fig. 1.9 : Water Vapour density profile over Northern Plains in Monsoon (0000GMT)

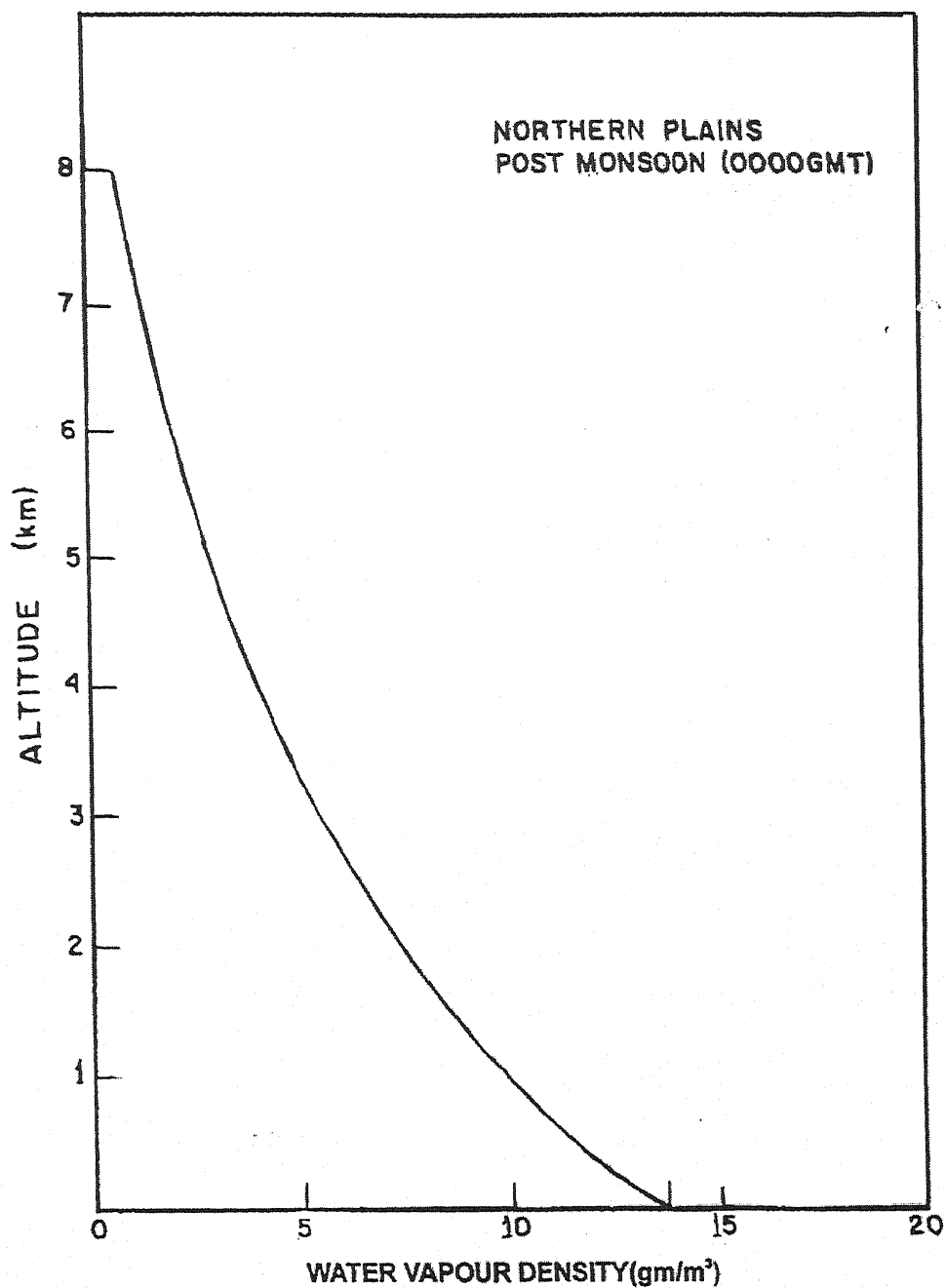


fig. 1.10 : Water Vapour density profile over Northern Plains in Post monsoon (0000GMT).

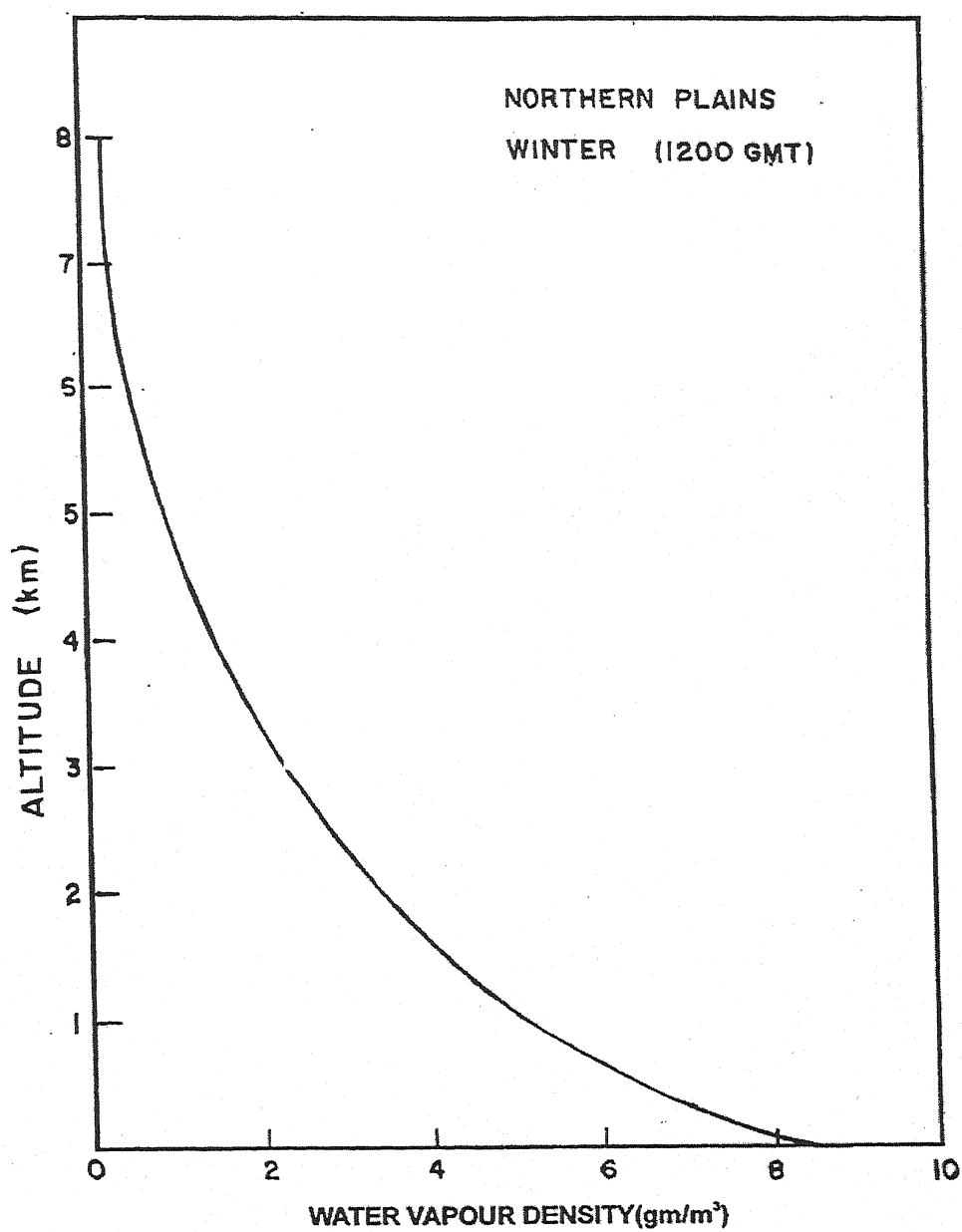


fig. 1.11 : Water Vapour density profile over Northern Plains in Winter (1200 GMT).

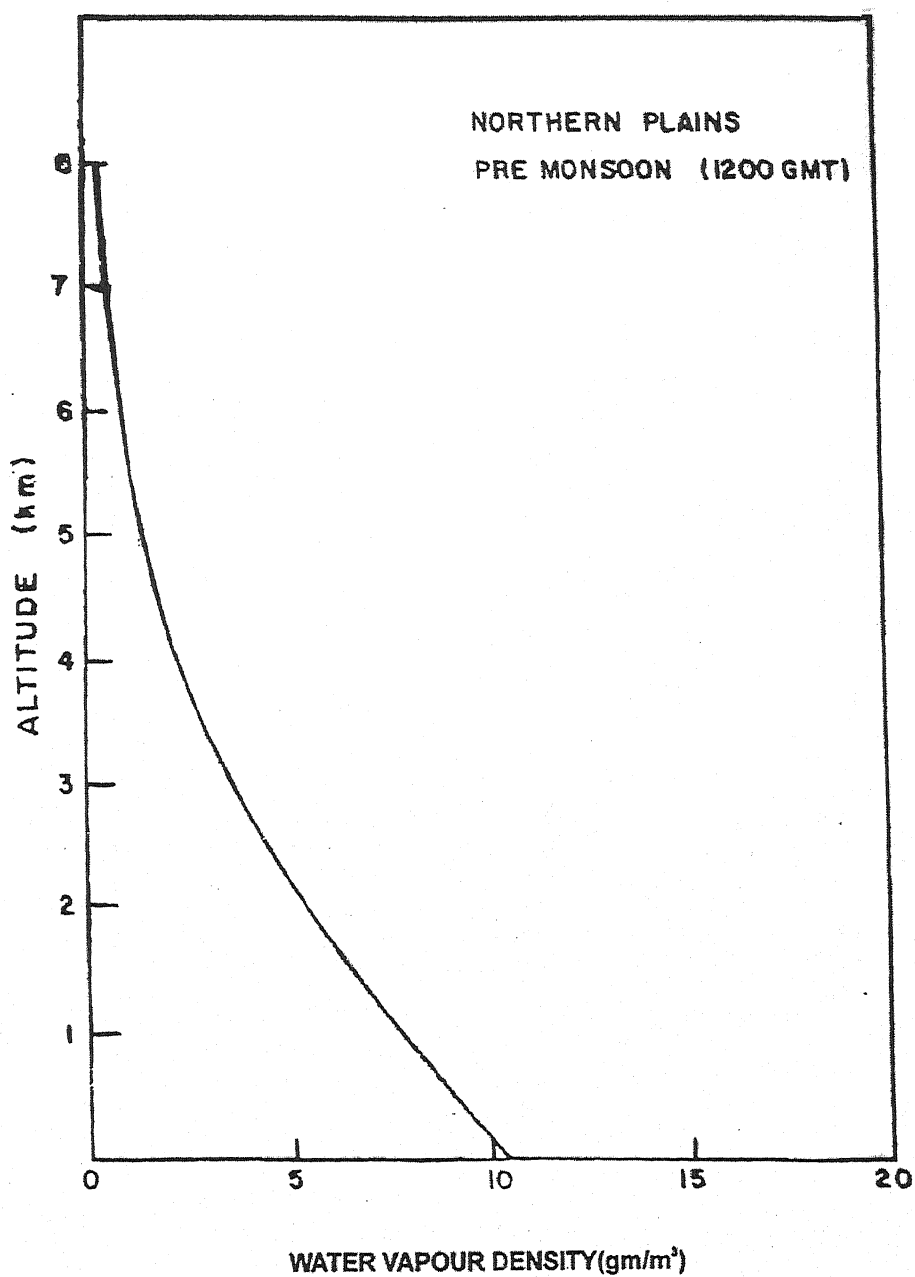


fig. 1.12 : Water Vapour density profile over Northern Plains in Pre monsoon (1200GMT).

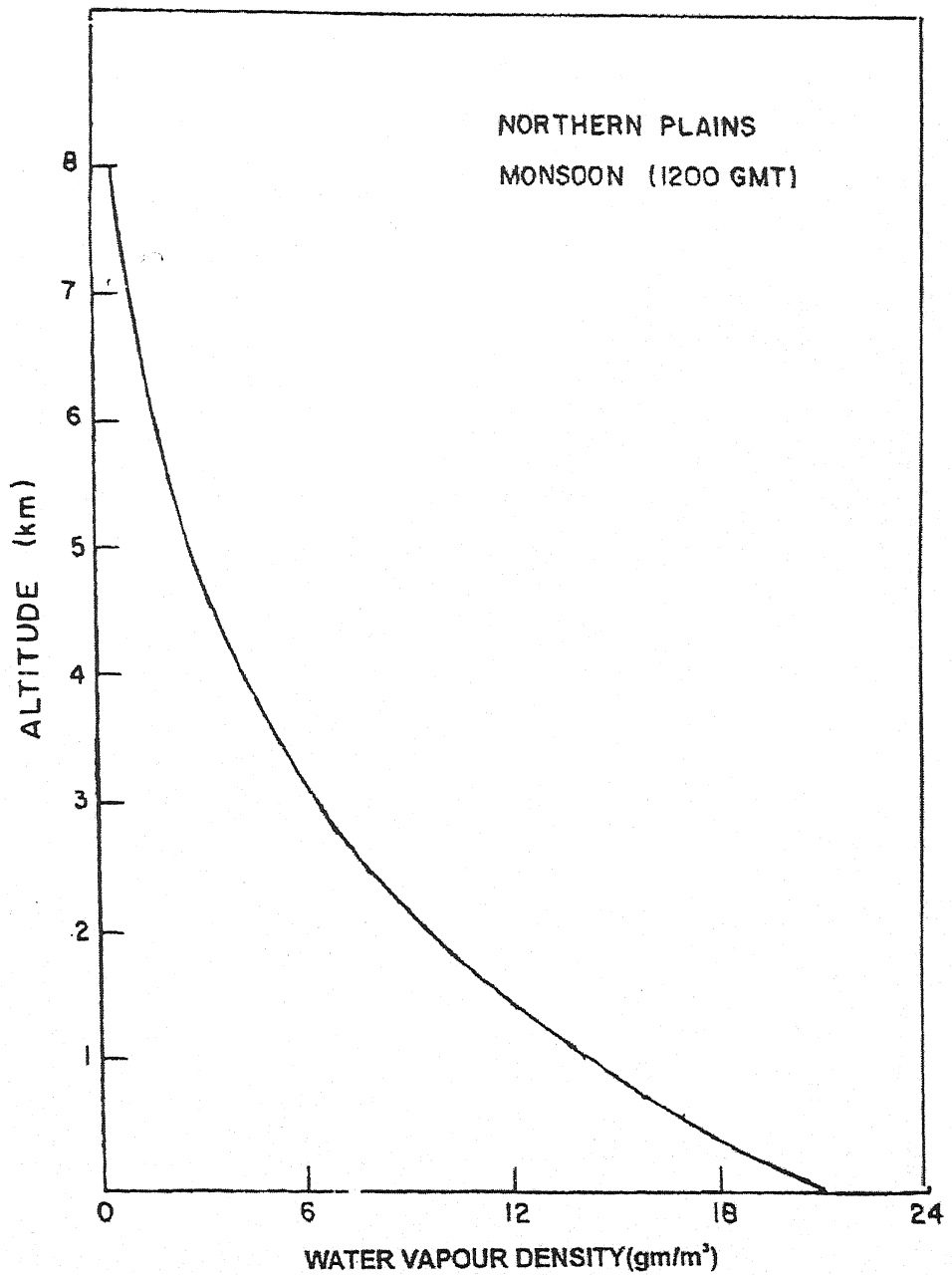


fig. 1.13 : Water Vapour density profile over Northern Plains in monsoon (1200GMT).

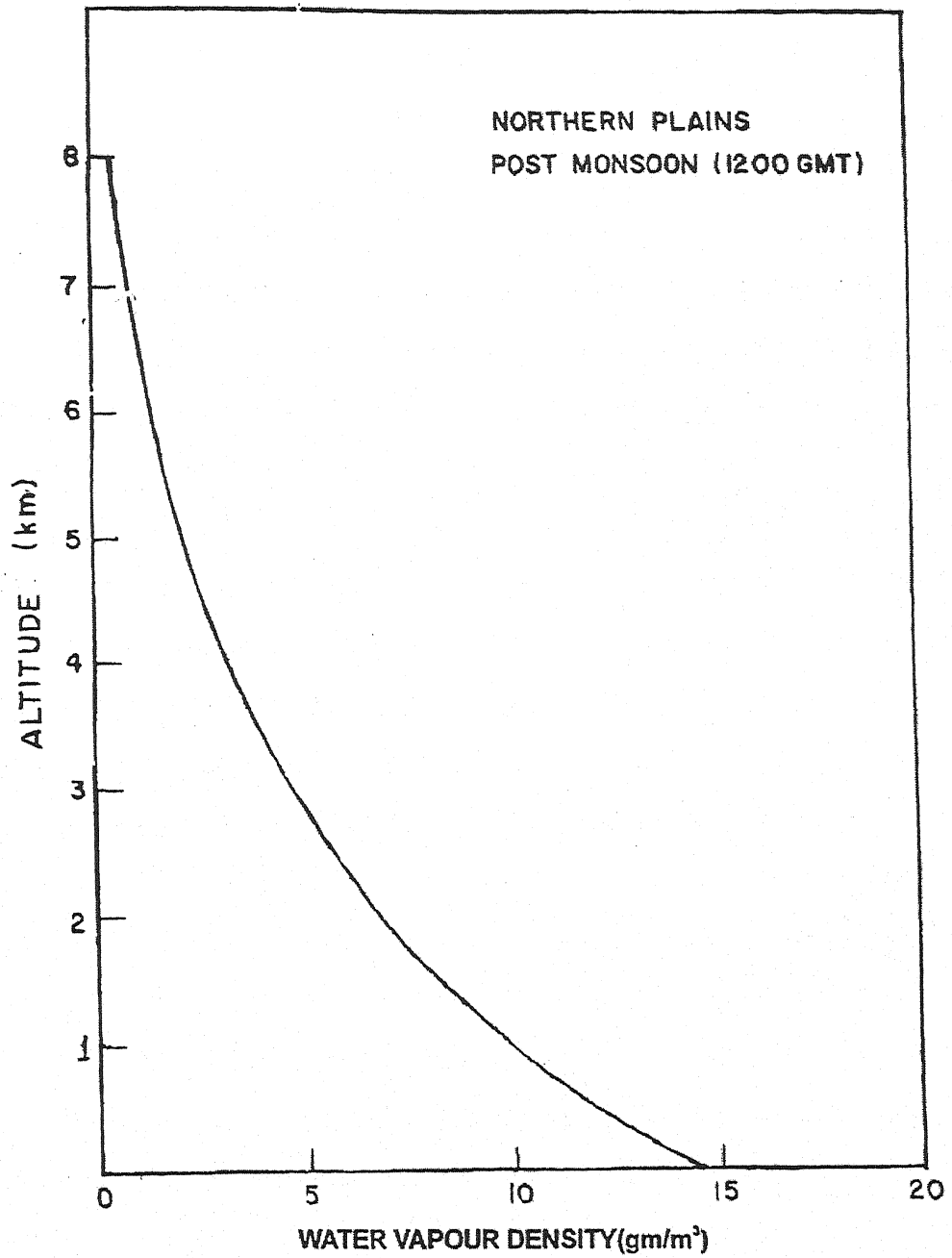


fig. 1.14 : Water Vapour density profile over Northern Plains in Post monsoon (1200GMT).

1.9 SURFACE PROPERTIES OF WATER SUBSTANCE:

Surface Tension:- Phases in contact are separated by a thin transitional region, generally only a few molecule thick; consequently, a useful abstracting regard. Such an interface as geometrical surface. To include surface effect, in complete analogy to the contribution-pdV of pressure volume work the internal energy contribution is given by σds , where S denotes the area of the surface of separation and σ the surface tension. The quantity σ is an intensive thermodynamic variable and has dimension of energy per unit area or force per unit length.

1.9 (i) Effect of Temperature On Surface Tension: The surface Tension of water decreases with increasing temperature, which is excepted on considering the effects of thermal agitation. This behaviour has been investigated experimentally by Dorsch and Hacker (1951) their results are shown in fig. (1.15). For the interval 0 to 40°C the data can be reproduced to within ± 0.02 dyne cm⁻¹ by the following expression;

$$\sigma_{w/a} = 76.10 - 0.155 T \quad (1.20)$$

Where $\sigma_{w/a}$ is in dyne cm⁻¹, i.e. Erg cm⁻², and T is in 0°C. From fig (1.5), it appears that eq. (1.18), also represents a reasonable extrapolation for the temperature interval 0 to -40°C.

1.9 (ii) Radius Dependence of Surface Tension: Surface Tension arises from attractive forces between molecules near the surface, hence we may expect that only and attraction of average geometrical configuration of these molecules on a size scale comparable to the effective range of the attractive forces would significantly affect the Surface tension. Thus we expect a dependence of $\sigma_{w/v}$ on size only for

extremely small drops, consistency of nearly a few tens or hundreds of water molecules. The surface tension of water decreases with decreasing radius of curvature of water surface. Tolman (1949a, 1949b), estimated that $\sigma_{w/v}$ for a drop, which consist of 13 water molecules (equivalent to a drop radius of 4.6×10^{-8} cm, based on $V_w = 30 \times 10^{-24} \text{ cm}^3$ and $\rho_w = 1.0 \text{ gm cm}^{-3}$) is 40% smaller than that for a plane water surface. Benson and Shuttleworth (1951) computed this surface tension of a small drop water molecules by counting the number of bonds, which had to be broken in order to cut off the group of molecules from the bulk water structure. In order to estimate the interaction energy between water molecules in water it was assumed that only the first and second nearest neighbour has to be considered. In this manner they predict that the surface tension of a drop of 13 water molecules is only 15% smaller than that for a plane water surface.

Following Defay et al. (1966) a simple, approximately quasi thermodynamic derivation of radius dependence of $\sigma_{w/v}$ is given by fig. (1.15)

$$\sigma_{w/v} = \frac{(\sigma_{w/v})_{\infty}}{1 + \left(\frac{2}{a}\right) \left[\Gamma_w^{(w/v)} / (\rho_w - \rho_v) \right]} \quad (1.21)$$

Where $(\sigma_{w/v})_{\infty}$ is surface tension of a plane water surface, $\Gamma_w^{(w/v)}$ the absorption and the term $\Gamma_w^{(w/v)} / (\rho_w - \rho_v)$ is independent of radius 'a' table (1.2) lists result of $\sigma_{w/v}$ (a) computed from eq.(1.21). Using $\Gamma_w^{(w/v)} \approx 0.87 \times 10^{-9} \text{ mol cm}^{-2}$ and approximation $\rho_v \ll \rho_w = 1 \text{ g.cm}^{-3}$. It is seen that the radius dependence becomes important for $a \ll 10^{-6} \text{ cm}$.

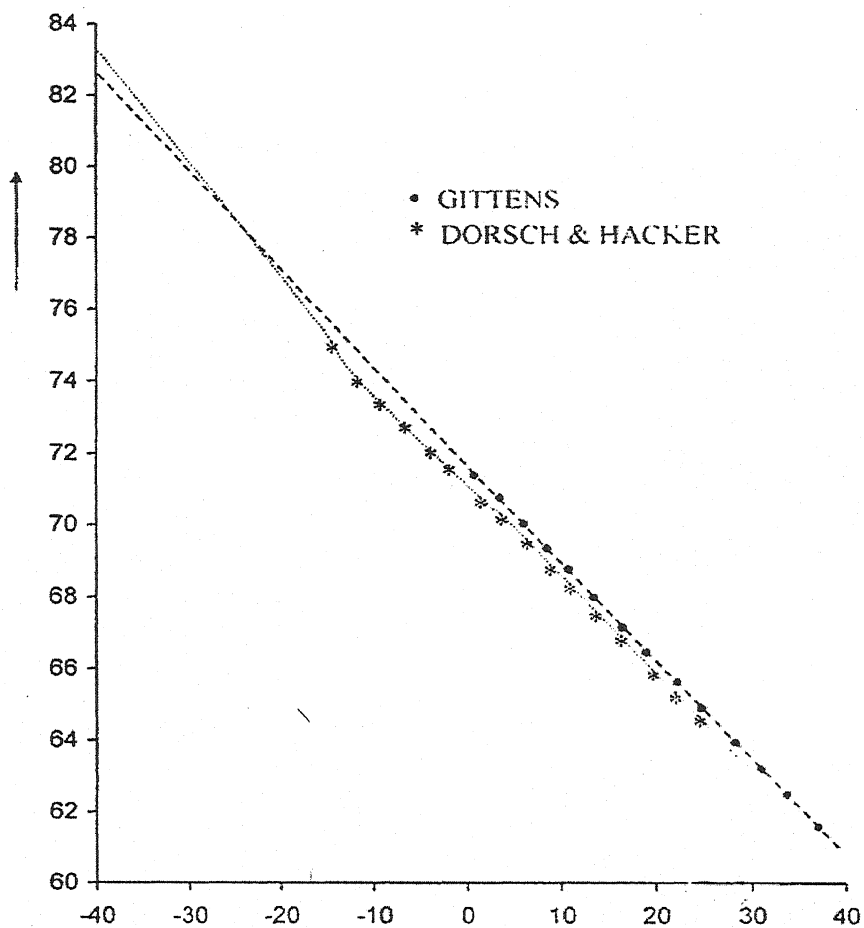


fig 1.15 : Variation of Surface tension of water (against air) with temperature according to Gittens & Dorsch & Hacker (1951).

Table-1.2

Variation Of Surface Tension Of Water For Drops Of Various Radii

a(cm)	$\sigma_{w/v}/(\sigma_{w/v})_{\infty}$	$[(\sigma_{w/v})_{\infty} - \sigma_{w/v}] / (\sigma_{w/v})_{\infty}$ (%)
∞	1.0	0
10^{-4}	0.9997	0
10^{-5}	0.9969	0.3
10^{-6}	0.9697	3.0
10^{-7} (140 molecules)	0.7622	23.8
4.6×10^{-8} (13 molecules)	0.5959	40.4

1.9 (iii) Surface Tension at Vapour Interface: The difference between the pressures p_w inside water drop of radius 'a' and the pressure $e_{sat.w}$ of vapour with which it is in equilibrium is given by

$$p_w - e_{sat.w} = \frac{2\sigma_{w/v}}{a} \quad (1.22)$$

Where now we have introduced the subscript w/v for the surface tension to emphasize that is the water vapour interface which is involved. Given that $\sigma_{w/v} \approx 76 \text{ dyne cm}^{-1}$ at 0°C , we see that the pressure difference is about 1.5 atm. For $a = 1\mu\text{m}$, smaller drops have correspondingly larger internal pressure.

For practical purposes one may replace $\sigma_{w/v}$ by $\sigma_{w/a}$, the surface tension for a water-humid air interface. Experimentally have shown that $\sigma_{w/a}$ increases by less than 0.05% if air at 1 atm is replaced by pure water vapour at saturation pressure (at the same temperature).

1.9 (iv) Surface Tension at Ice-Vapour Interface and Surface Energy of Ice: Surface energy of ice is the energy required to form a unit area of low surface. For ideal crystalline ice energy may be identified with one half of the energy per unit area, which is needed to split an infinite crystal parallel to a particular crystallographic plane and separate the two parts by one infinite distance. It is natural to take $\frac{W_c}{2}$, as the surface tension or interfacial energy $\sigma_{i/v}$ between the particular ice crystal face and water vapour or air, assuming the presence of such gases does not affect the surface energy. Disregarding the forces of interaction due to third or higher order nearest neighbour, energy per molecule required for cleavage of an ice crystal can be expressed as

$$E_m = U_1 + 6U_2 \quad (1.23)$$

Where U_1 & U_2 are the average interaction potentials between the molecules in the first and second interaction zones. The interaction potentials U_1 & U_2 for intermolecular spacing's of 2.76×10^{-8} cm. and 4.51×10^{-8} cm, respectively, were computed (Reuck, 1957) on the basis (Rowlinson, 1951) of force constants, which take account of the multiple electrostatic interaction forces, induction forces and repulsion forces. As a result, Reuck found $N_A E_m = 6.08 \text{ Kcal mole}^{-1}$ or $E_m = 4.22 \times 10^{-13} \text{ erg per molecules}$, for an ice crystal in vacuum at 0°K .

The estimated values of w_c for different shapes of ice crystals are $w_c^{(B)} = 238 \text{ erg cm}^{-2}$ for the basal faces of ice and $w_c^{(P)} = 253 \text{ erg cm}^{-2}$ for the prism faces; the corresponding values for the surface energies are $\sigma_{i/v}^{(B)} = 119 \text{ erg cm}^{-2}$ and $\sigma_{i/v}^{(P)} = 126 \text{ erg cm}^{-2}$. Similar estimates were made by Mc. Donald (1953b).

Mc. Donald (1953b) has pointed out that the surface energies thus computed pertain to "fresh" surface since molecules in a freshly cleaved surface will not remain in their original position but will relax into new equilibrium position, surface energy of an "aged" surface is somewhat less than that of fresh surface. Significance of such relaxation can be appreciated if we calculated $\sigma_{w/a}$ for water at 0°C in the same way as was just done for ice and compare results with the known values of surface Tension.

1.9 (v) Ice water Interface (State between ice and water):

Consider a system of consisting of an ice crystal surrounding by super cooled water. For sufficient small particles of ice such a system can be in stable equilibrium so that it is again possible to speak of surface tension

as interface energy of boundary separating the phases unfortunately it is very difficult to determine $\sigma_{i/w}$ by experimental technique, and the results of numerous attempts show considerable spread, fig. (1.16) (Wood, 1970; Dufour, 1963; Jacobi, 1955a; Ketcham, 1969; Kubelka, 1944; Turnbull, 1950, 1965).

A reasonable relation for the variation of $\sigma_{i/w}$ with the temperature as given by

$$\sigma_{i/w} = 28.5 + 0.25 T \quad (1.24)$$

Where σ is in erg cm^{-2} , and T is in $^{\circ}\text{C}$. Direct photographic evidence of the presence of steps at a growing ice-water interface has been provided (Ketcham, 1968; Hobb's, 1969).

Some of the observed steps had spiral forms appearing at a number concentration of about 10^2 cm^{-2} , with step heights between 0.1 and $4\mu\text{m}$, and spacing between the steps of 5 to $20\mu\text{m}$. No explanation for this observation is currently available except to say that, as in the case of step formation at the ice-air interface, some sort of bunching mechanism may be operating.

1.10 NUCLEATION:

The formation of a new phase at the expense of a metastable original phase ("Mother phase") does not begin in a continuous manner, but rather takes place spontaneously as result of temperature and density fluctuations (heterophase fluctuation) in the original phase, provided that a critical supersaturation is exceeded. This spontaneous process is called

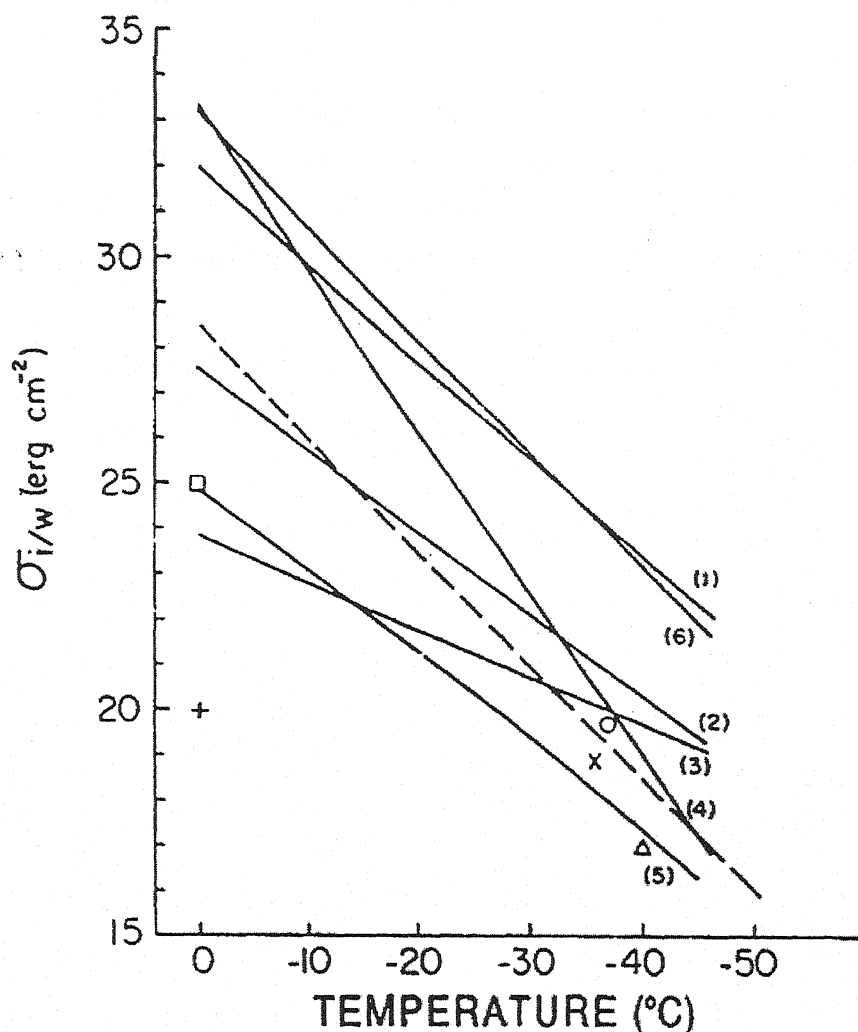


fig. 1.16 : variation with temperature of the surface tension of ice against supercooled water (1) Wood and Walton (1970) for spherical ice crystal, (2) Wood and Walton (1970) for Wulff crystal, (3) Dufour and Defay (1963) based on data of jacobi (1955 a), (4) Ketchman and Hobbs (1969), (5) Pruppacher (Unpub.) based on data of Kubelka and Prokscha (1944), (6) Pruppacher (Unpub.) based on (Turnbull, 1950, 1965).

nucleation. Thus the formation of critical nuclei of water or ice is called the nucleation phenomenon. Before the critical size the embryos are formed of different sizes. Beyond the critical size the nuclei are changed into drops by further condensation of water vapour. But below the critical size the embryos may be vapourized or dissociated.

The nucleation phenomenon has been divided in two categories-

1. Homogeneous Nucleation
2. Heterogeneous Nucleation.

1.10 (i) Homogeneous Nucleation of Water: Homogeneous Nucleation occurs when supersaturation ratio is several hundred percentages and it may be assumed that foreign substance are absent but in actual atmosphere only 0.01 and to 0.10 supersaturation (i.e. 1% to 10%) is present in the clouds, hence homogeneous nucleation is not possible generally. Nucleation generally occurs with much more difficulty in the interior of a uniform substance, by a process called homogeneous nucleation. The liquids which are cooled above the homogeneous nucleation temperature are said to be supercooled. Quantitative comparison of experiment and theory for the growth of homogeneously nucleated water droplets had been explained by Alexander Fladerer et al. (2003).

1.10 (ii) Heterogeneous Nucleation of Water: In the case of heterogeneous nucleation some energy is released by the partial destruction of the previous interface. For example, if a carbon dioxide

bubble forms between water and the inside surface of a bottle, the energy inherent in the water bottle interface is released wherever a layer of gas intervenes and this energy goes towards the formation of bubble water and bubble-bottle interface (Nickolay, 2005). Heterogeneous nucleation is generally responsible for cloud formation. Such nucleation is assisted if suitable solid surface or some foreign materials like dust particles, cloud seeding particles and ions are present. The heterogeneous nucleation also takes place when external electric field is applied to the cloud.

Thus heterogeneous nucleation may be of the following types,

- a. Ion induced nucleation
- b. The electric field induced nucleation
- c. Nucleation on certain solid surfaces of different shapes and materials.

Daniel Beysensa, b, (2006) explained that Dew is the condensation of water vapour into liquid droplets on a substrate. It is characterized by an initial heterogeneous nucleation on a substrate and a further growth of droplets.

1.11 CLOUD CONDENSATION NUCLEI (CCN): The drop formation in the atmosphere occurs via heterogeneous nucleation involving aerosol particles (A.P.). A.P. which are capable of initiating drop formation at the observed low supersaturation are called cloud condensation nuclei (CCN).

Cloud condensation nuclei or CCNs (also known as cloud seeds) are small particles (typically 0.0002mm or $1/100^{\text{th}}$ the size of a cloud

droplet. Water requires a non-gaseous surface to make the transition from a vapour to a liquid. In the atmosphere, this surface presents itself as tiny solid or liquid particles called CCNs. When no CCNs are present water vapour can be super cooled below 0°C (32°F). The number of CCNs in the air can be measured and ranges between around 100 to 1000 per cubic cm. The total mass of CCNs injected into the atmosphere has been estimated at 2×10^{12} kg over a year's time.

Aerosols play an important role in a variety of processes in the marine boundary layer. They transfer water vapour, heat and matter through the air sea interface, interact with the fields of temp and humidity by evaporation and condensation, and may act as condensation nuclei in the formation of clouds and fog (Van Eijk, 1996).

J.P.D. Abbat and Broekhuizen et al. (2005), the ability of mixed ammonium sulfate/organic acid particle to act as 'cloud condensation' nuclei (CCN) has been studied in the laboratory using a continuous flow, thermal gradient diffusion chamber operated at supersaturation at between 0.3% and 0.6%. The organic acid studied were malonic acid, azelaic-hexanoic acid, cis pionic acid, oleic acid and stearic, and the particles were largely prepared by 'Condensation' of the organic vapour onto a dry ammonium sulfate core. For malonic acid and hexanoic acid, the mixed particles activated as predicted by a simple Köhler theory model where both species are assumed to be fully soluble and the droplet has the surface tension of water. Three low solubility species, cis-pinonic acid, azelaic acid, oleic acid are well modeled where the acid was assumed to be either partially or fully insoluble. We observed no CCN behaviour that could be clearly attributed to lowering of the surface tension of the growing droplet by the presence of the organic constituents, some of which are highly surface active.

1.1.2 ICE FORMING NUCLEI (IN):

The cloud glaciations generally begins at temperature which too warm for homogeneous freezing of water. For example at one occasion (Mossop, 1968), observed ice crystals in a long lived cumulative cloud whose top was probably never colder than -4°C and which was not seeded with ice particles from clouds at higher altitude. Such behaviour indicates that some fraction of the local Aerosol particles (AP) also, can serve as ice forming Nuclei (IN).

1.1.3 NUMBER CONCENTRATION OF CCN:

Twomey and Wojciechowski(1969), comprehensively studied CCN concentration over various part of the world. The results of these studies are summarized in fig. (1.17 a,b,c). The result shows no systematic latitudinal variation in concentration. The observation also, confirm that continental air masses are generally richer in CCN than are maritime air masses with in a particular air mass at flight level the variation of median CCN concentration was surprisingly small. At supersaturation between 0.1 and 10% the median concentration of CCN was found to range from a few ten to a few hundred cm^{-3} in air over oceans and from a few hundred to a few thousand cm^{-3} in air over the continents fig. (1.17). It is indicated that the concentration of CCN (i.e. N_{CCN}) increases with increasing supersaturation $S_{v,w}$. This behaviour can be expressed in the form

$$N_{\text{CCN}} = CS_{v,w}^k \quad (1.25)$$

Where k and C are approximately constant.

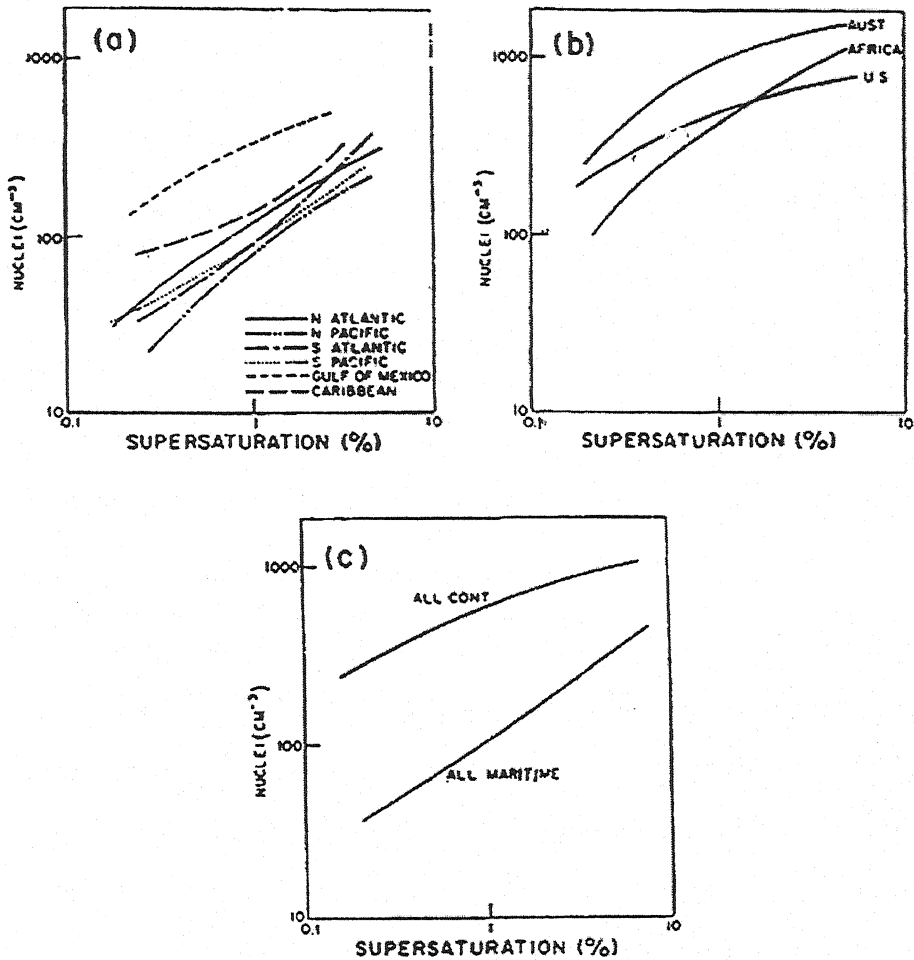
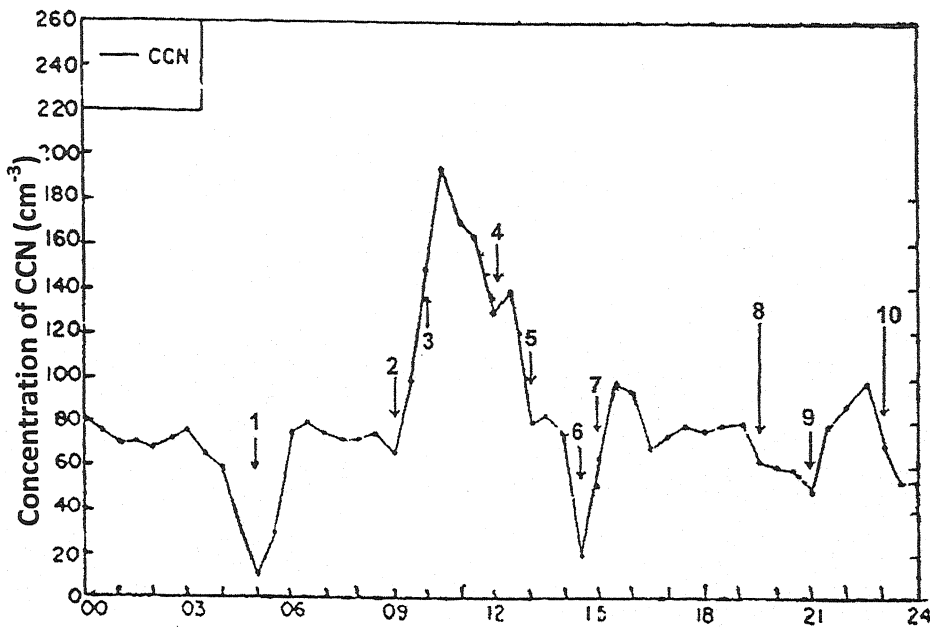


fig. 1.17 : Median world-wide concentration of CCN as a function of supersaturation required for activation; (a) in air over oceans, (b) in air over continents, (c) all observation (Twomey, 1969).

At a given location the CCN concentration is magnitude, depending upon approximately of sources and an metrological factors such as wind direction, air mass type, precipitation and decreasing or increasing cloudiness (Twomey, 1959a; Rodke, 1969).

Fig. (1.18) illustrates a typical time variation of CCN concentration (Twomey et al. 1970, 1971) showed that at given location, repeated patterns can be detected in the diurnal variation of the CCN concentration. This is a noon maximum and late evening maximum were observed during one year observation period at Robertson (N.S.W. Australia). Generally CCN concentration in maritime and modified maritime air masses which have been overland less than two days rarely exceed 100cm^{-3} are found in air which have been overland for several days.

Variation of CCN at different values of supersaturation are discussed by Jiusto (1968) shown in fig. (1.19). Fig. (1.20) describes the comparison between total concentration of aerosol particles and concentration of cloud condensation nuclei activated at 0.7% supersaturation of various locations (Hoppel, 1973). In table (1.3), the values of Ailken particles per cm^3 are given which were evaluated by Allee et al. (1970) and Twomey et al. (1964) at different places.



1.	This dip corresponds to the last storm cell recorded on the barograph
2.	Wind NW 10mph. light snow and fog-clearing
3.	Cu Breaking west
4.	Wind NW 5-10mph. light snow and fog.
5.	Wind SW 5mph. Snow and fog.
6.	Wind SW 2-5 mph light snow and fog.
7.	Wind WSW 5-10 mph Breaks in Cu.
8.	Wind WSW 5-10mph Fog
9.	Wind WNW 5-10 mph Clearing to west
10.	Wind W 2-5 mph light fog

fig. 1.18 : Variation with time of the CCN Concentration activated at 1% supersaturation during March 29, 1968, in air at observation station (2025m) in Olympic Mts., Washington State (Rodke, 1969).

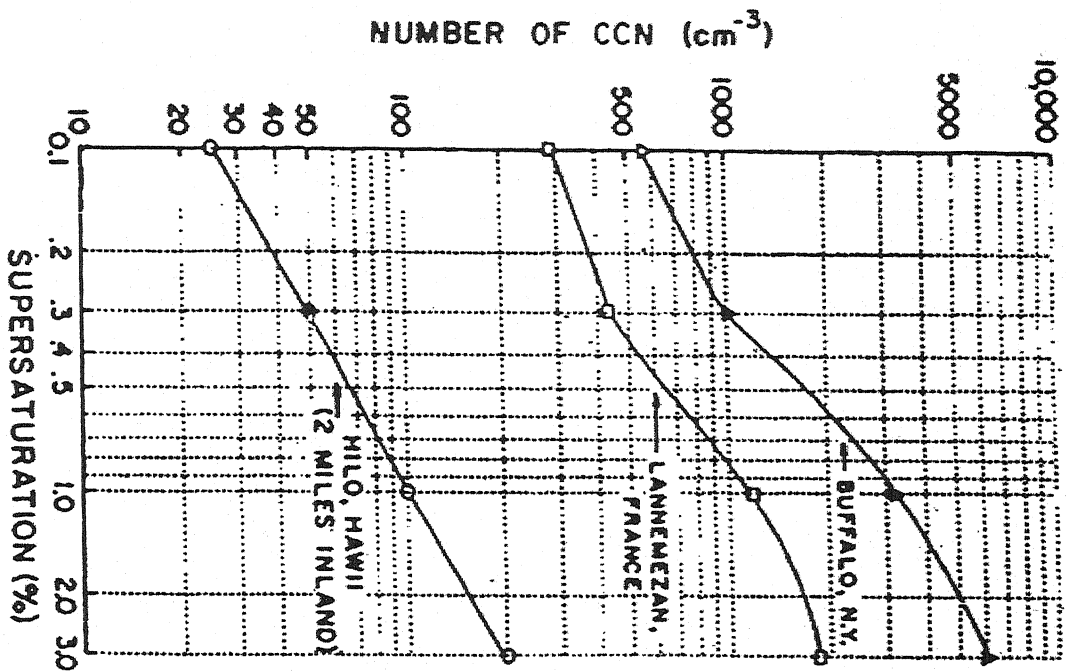


fig. 1.19 : Variation of the CCN concentration required for activation at various locations, as a function of supersaturation (Justo, 1968).

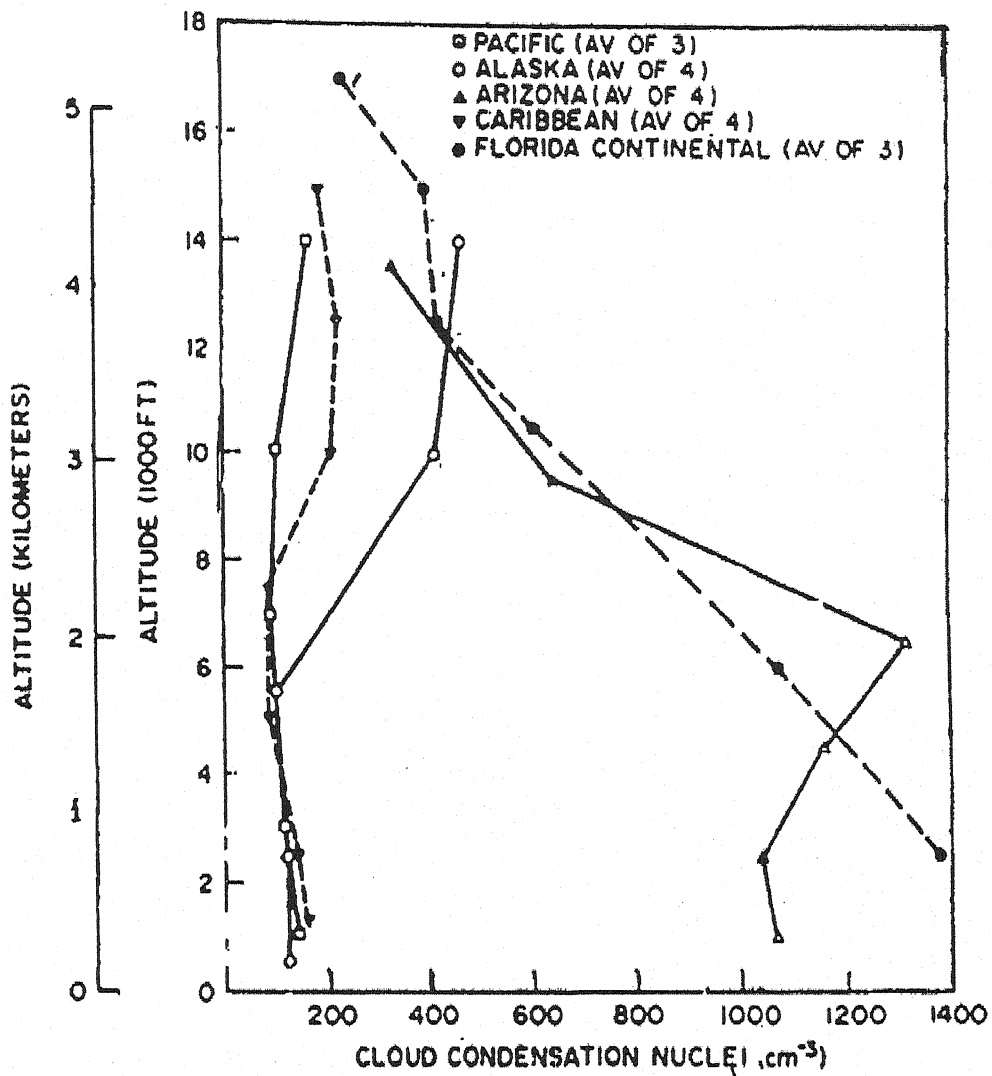


fig. 1.20 : Vertical variation of the CCN concentration activated at 0.7% supersaturation over various location (Hoppel, 1973).

Table-1.3

Type of nuclei Location	Number of Ailken Paticles (cm⁻³)	Number of CCN (cm⁻³)
Washington D.C. (Allee, 1970)	7800	2000
	6800	2000
	5700	5000
	50000	7000
Yellow Stone National Park (Wyoming)	1000	15
Long Island (N.Y.) (Twomey, 1964)	5700	30
	6500	150
	18000	110
	51000	220

1.14 A LABORATORY STUDY OF ICE NUCLEATION DUE TO ELECTRICAL DISCHARGE:

Experiments were performed (G.Mandal, 2002) in a walk- in cold room where the lowest attainable temperature is -30°C to investigate the effect of electrical discharge and high electric fields on ice nucleation. Experiments were carried out at cloud temperatures varying from -9 to -12°C . It was observed that ice nucleation does occur inside the cloud if there is an electrical discharge inside the cloud. However, not all electrical discharges resulted in ice nucleation. In no case was ice nucleation observed in the presence of high electric fields with no discharge. No ice nucleation was noted in the cloud when the Liquid water content (LWC) was greater than 2.1 gm^{-3} .

1.15 EXPERIMENTAL VERIFICATION OF HETEROGENEOUS WATER DROP NUCLEATION:

Once water soluble and mixed A.P., grow with increasing relative humidity, it is appropriate to test the theory of nucleation of such particles in two ways:

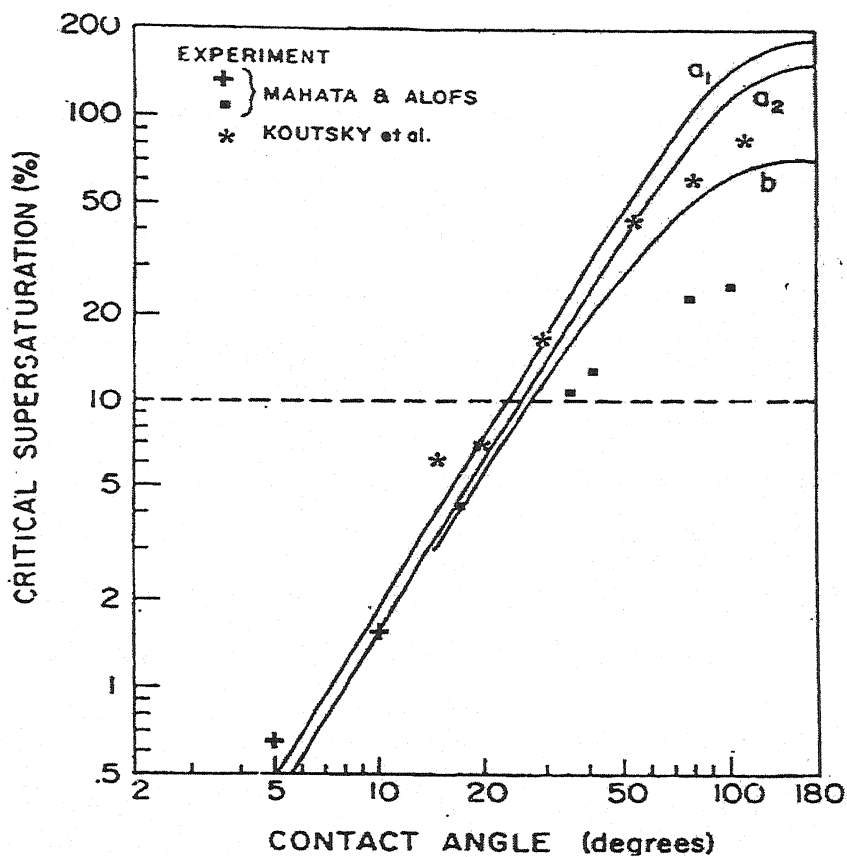
1. By experimentally determining the equilibrium growth of these particles and,
 2. By determining the number of particles of given size and composition which become activated at a given supersaturation.
- The agreement with theory is satisfactory as regards the shape of CCN Spectral actual concentration of activated drops.

Attempt to verify the prediction of water drop nucleation on water insoluble partially wettable substrates have been made (Isaka, 1972; Mahata, 1975).

These experiments were carried out in diffusion chamber where nucleation was forced to take place on plane substrate for which angle of contact of water had been measured separately. Considerable disagreement, while, the critical supersaturation necessary for onset of drop nucleation are sufficiently lower for all wetting angles than those predicted by theory.

The results of experiments carried out (Mahata, 1975) are reproduced in fig. (1.21). It is seen that the measured critical supersaturations as a function of contact angle agree fairly well with those of Koutsky et al. (1965), up to a supersaturation of 10% corresponding to a contact angle of about 25°C.

An overview of the two FEBUKO aerosol cloud interaction field experiments in the Thuringer Wald (Germany in October 2001 and 2002 and the corresponding modeling project MODMEP is given by Hermann et al. (2005). Experimentally, a variety of measurement methods were deployed to probe the gas phase, particles and cloud droplets at three sites upwind, downwind and within an orographic cloud with special emphasis on the budgets and inter conversions of organic gas and particle phase within 30 cloud events three events (E I, E II, E III) are selected for detailed analysis. At various occasions an impact of the cloud process on particle chemical composition such as on the organic compounds content, sulphate and nitrate and also on particle size distributions and particle mass is observed. Moreover, direct phase transfer of polar organic compound from the gas phase is found to be very important for the understanding of cloud water composition.



Theory

$$a_1 : j = 10^8 \text{ cm}^{-2} \text{ sec}^{-1}$$

$$a_2 : j = 1 \text{ cm}^{-2} \text{ sec}^{-1}$$

$$b : j = 1 \text{ cm}^{-2} \text{ sec}^{-1}$$

(With size correction to surface tension)

fig. 1.21 : Critical supersaturation for onset of water nucleation on a plane, waterinsoluble, partially wettable substrate, as a function of contact angle of water on substrate. Comparison of experiment with theory (Mahata, 1975; Koutsky, 1965).

1.16 ELECTRICAL INHOMOGENETIES OTHER THAN IONS:

The surface of the nucleation substrate consist of sharply defined boundaries between surface regions of different field sign, or of locations where the electric field vector in the substrate is oriented parallel to the surfaces. Growth of water cluster around electric inhomogeneties other than ions attract water molecules to the substrates and the dipole of a water molecule. Growth of water cluster at such sites can be aided if the diffusivity of water molecules of surface region with either an inward directed or an outward directed electric field is high as compared to the diffusivity over in a area where the electric field vector in the substrate is oriented parallel to the substrate, since than both the positive and negative ions of water molecules are partially tied down.

ref. ?
 Thomas evaluated both individual and combined effects of the horizontal and vertical variability of cumulus clouds on solar radioactive transfer are investigated using a two-dimensional (x-and z- directions) cloud radar data set. This high resolution dataset of typical fair weather marine cumulus is derived from ground based 94 GHz cloud radar observations. The domain averaged (along x-direction) radiative properties are computed by a Monte Carlo method. It is shown that (i) different cloud-scale resolutions can be used for accurate calculation of the mean absorption, upward and downward fluxes. (ii) the resolution effects can depend strongly on the solar zenith angle, and (iii) a few cloud statistics can be successfully applied for calculating the averaged radiative properties.

1.16 (i) Ice Forming Nuclei: Ice forming nuclei exhibit three basic modes of action:

1. In the first mode, water is absorbed directly from vapour phase on to the surface of IN where, at sufficiently low temperature, observed vapour is transformed into ice.
2. In the second mode, the IN initiates the ice phase from inside in supercooled water drop.
3. In third mode in the action the IN initiates the ice phase at the moment of contact with the supercooled droplets.

The first mode action is called deposition mode and AP which exhibit this behavior are called "deposition IN"; the second is called freezing mode and the corresponding 'AP' are "freezing nuclei", the third is called contact mode, participated in by contact angle.

1.16 (ii) IN Concentration: The IN concentration measurements are reproduced as a function of temperature and location in fig. (1.22, 1.23, 1.24), illustrates a day to day variation in IN concentration observed with one counting technique one particular site. Even at remote locations such as Antarctic, pronounced variation in the daily IN concentration do occur. Similar observation were made (Kikuchi, 1971), which were measured at an Antarctic station. IN concentration maxima as high as $30 \ell^{-1}$ at 20°C . Such high concentration counts were found to last up to two days fig. (1.21), also shows that the IN counts increase nearly exponentially with decreasing temperatures.

Fletcher (1970a) gave a convenient statement of this behaviour as,

$$N_{IN} = A \exp (\beta \cdot \Delta T) \quad (1.26)$$

Where $\beta = 0.6 (^{\circ}\text{C})^{-1}$, $A = 10^{-5} \ell^{-1}$, where N_{IN} is the number concentration of IN active at a temperature warmer than T and where

$$\Delta T = T_0 - T.$$

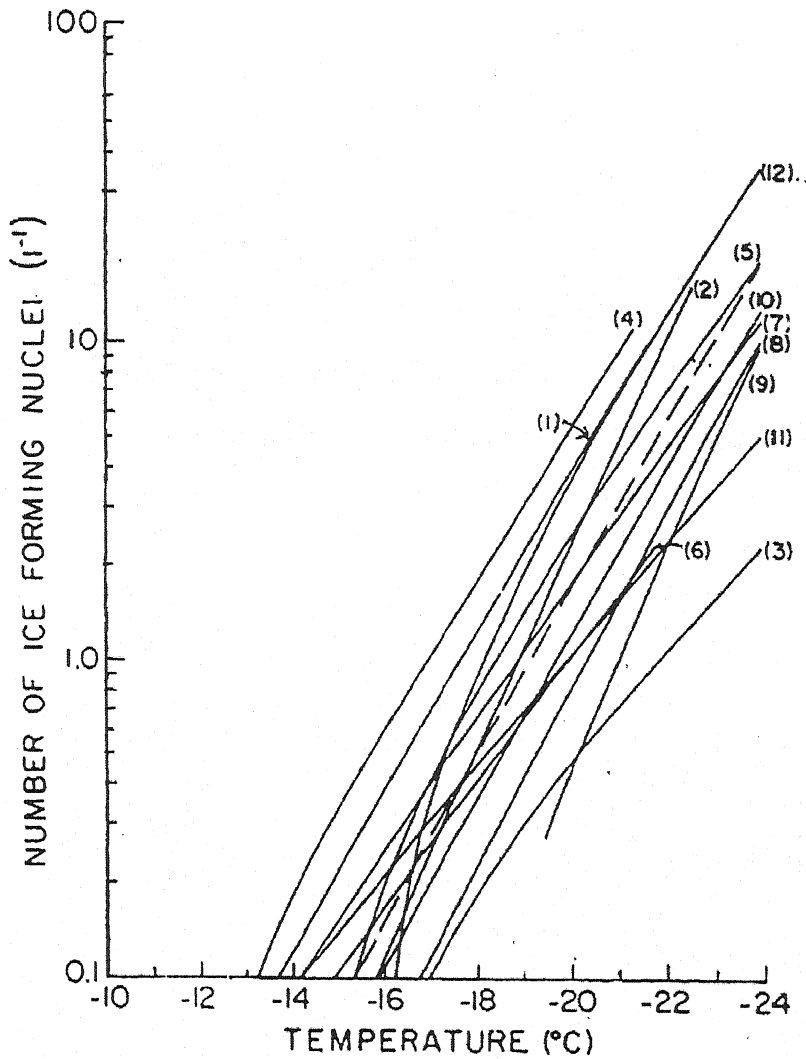


fig.1.22 : Variation of the mean or median number concentration of IN with temperature and geographic location. (1) Bracknell (England), 51° N, 0°W, (2) Clermont-Ferrand (France), 46° N, 3° E, (3) Corvallis (Oregon, U.S.), 44° N, 123°W, (4) Tokyo (Japan), 36°N, 140° E, (5) Tucson (Arizona, U.S.), 32° N, 111°W, (6) Jerusalem (Israel), 32° E, (7) Palmbeach (Florida, U.S.), 27°N, 80° W, (8) Hawaii (U.S.), 20° N, 158° W, (9) Swakopmund (S. Africa), 34° S, 14° E, (10) Sidney (Australia), 34° S, 151° E, (11) Tasmania (Australia), 43° S, 147° E, (12) Antarctica, 78° S, 166° E. The dashed line represent $N_{IN} = 10^5 \exp(0.6 \Delta T)$.

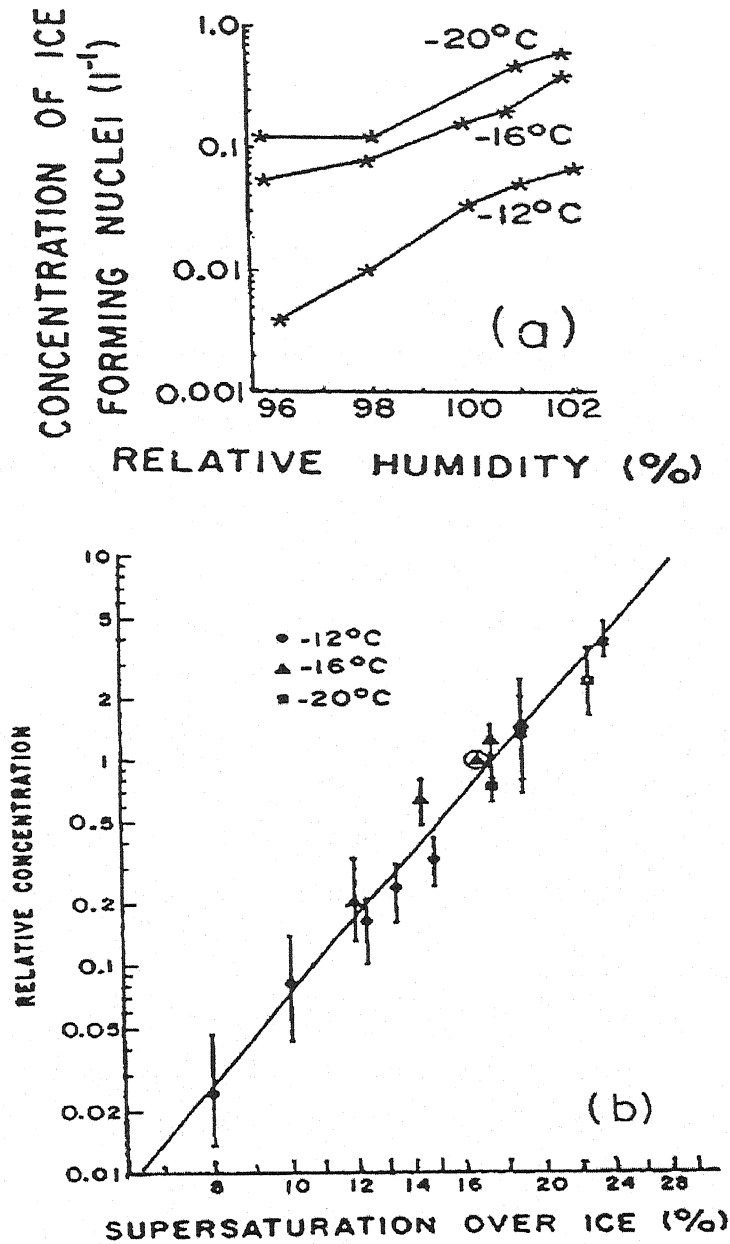


fig. 1.23 : Variation of the IN concentration with (a) relative humidity and with (b) supersaturation over ice. (Huffman, 1973 a).

Gagin (1972) and Huffman (1973a, 1973b) found that, at any given temperature the number concentration of IN increases with increasing relative humidity fig. (1.23a) and correlates logarithmically with the Supersaturation over ice, independently of temperature fig.(1.23b) according to the relation.

$$N_{IN} = CS_{V,i}^K \quad (1.27)$$

Where K and C are constant.

Huffman (1973b) observed that the vertical IN concentration profiles often exhibit a pronounced layer structure even in the lowest few Kilometers above ground. For example a strong concentration maximum was observed during a few days of summer time sampling at about 500 meter above ground over St. Louis and over N.E. Colarado, no temperature inversion was present at the time over N.E. Colarado and the inversion over St. Louis was considerably above the IN concentration maximum, thus the concentration maxima appear not to be co-related with the temperature inversion. Bigg et al. (1970, 1963) studied range of median number concentration of IN as function of temperature at various geographic locations and the variation of the daily number concentration of ice forming nuclei at -20°C measured during December, 1961 to Jan., 1962 at Antarctica station fig. (1.24) and fig (1.25).

1.17 ENHANCEMENT RATIO OR ENHANCEMENT FACTOR:

The enhancement ratio is defined as a ratio of ice crystal concentration determined at the cloud top temperature. This ratio can be as large as 10^4 to 10^5 at temperatures between -5°C to -15°C . Also, R_m tends to decrease with decreasing cloud top temperature and reaches unity between -25°C and -30°C . Fig. (1.26) (Hobb's, P.V., 1974) represents some observations of R_m over the cascade meters during winter of 1971 to 1973, which were summarized by the best fit relation.

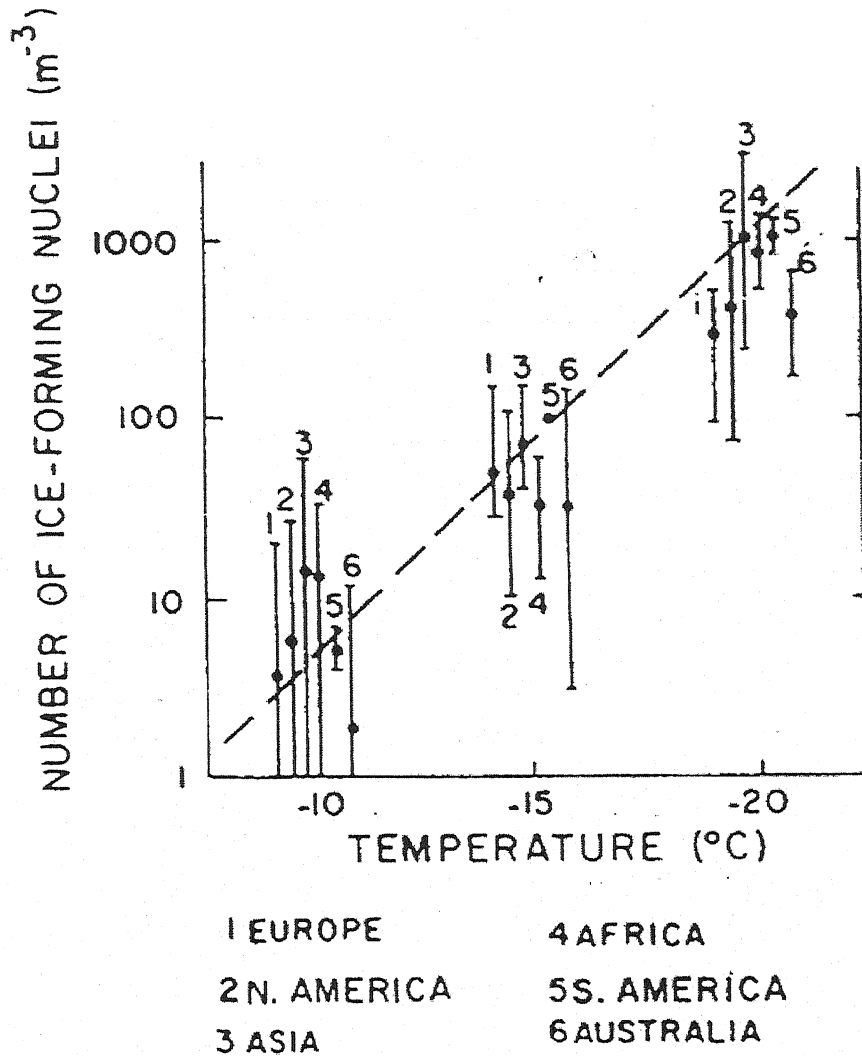


Fig. 1.24 : Range of median number concentration of IN as function of Temperature for various geographic location; 44 stations. The dashed line represent $N_{IN} = 10^{-5} \exp(0.6\Delta T)$ (Bigg, 1970).

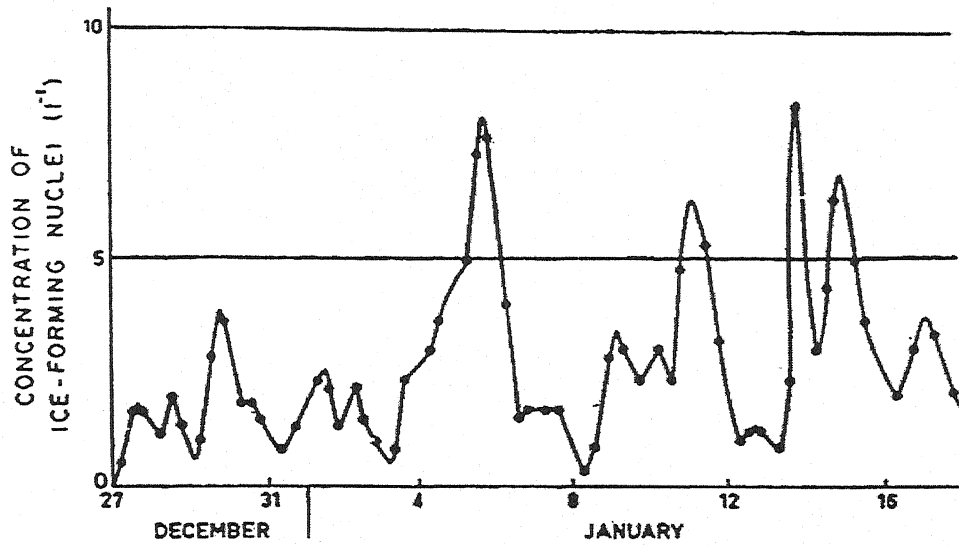


fig. 1.25 : Variation of the daily number concentration of ice forming nuclei at -20°C measured during December, 1961, to January, 1962, at Antarctica station. (Bigg, 1963).

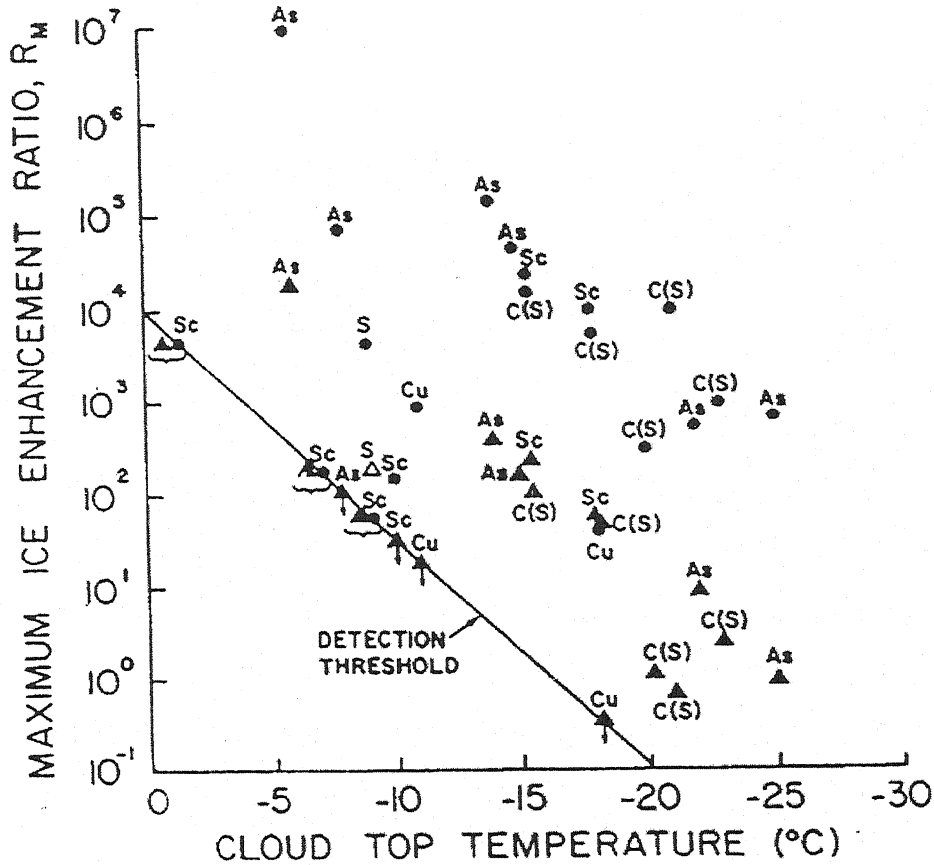


fig. 1.26 : Maximum ice enhancement ratio (R_M) in clouds over the Cascade Mts. (Washington State) during winter, 1971-72. (If value is below the detection threshold, it is show on the threshold line with an arrow attached.) Asaltostratus, S-stratus, Sc-stratocumulus, Cu-cumulus, C (S)-Cumulus with stratified tops. (Hobb's, P. V., 1974).

$$\text{Log } R_m = 5.02 + 0.204 T_c \quad (1.28)$$

Where T_c is called cloud top temperature in $^{\circ}\text{C}$.

1.17 (i) Ion Induced Nucleation: The observed anomaly of maximum enhancement ratio R_m ($\sim 10^4 - 10^5$) can be explained when we consider the effects of ions on ice formation. The ratio can be written as.

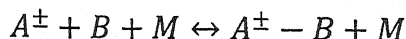
$$R_m = \left[\frac{N_{ice}}{IN} \right] = \left[\frac{\alpha N_{ion} + IN}{IN} \right] \quad (1.29)$$

Where N_{ion} is the concentration of ions ($\sim 10^8$ to $10^9 m^{-3}$), near the ground surface; IN , the concentration of ice forming nuclei at cloud top temperatures ($\sim 10^3 m^{-3}$); α , the efficiency of ions acting as IN . As a rough estimate the value of α can be taken as 0.1. For the above parameters the values of R_m comes out to be ($\sim 10^5$). This value is in excellent agreement with the experimental observations.

The ions provide a central force field, which is a simple form of attractive potential resulting in the formation of heterogeneous embryos. A basic understanding of ion induced nucleation, therefore, provides an important basis for further development in the theory of heteromolecular nucleation which is important in atmospheric process (Allen, 1969; Doyle, 1961).

Condensation of water vapour on ions was also mentioned (Mason, 1971). The possibility of ice germ formation in supercooled liquid, when ionizing radiations are passed through (Varshneya, 1969) is a milestone in the understanding of ions as centre of condensation. The pioneer works (Varshneya, 1971; Castelman, 1978; Mohnen, 1970, 1974; Chan, 1980a,

1980b) has placed the belief on a firm footing. Ion induced nucleation process via a sequence of clustering reactions. These may be considered to commence with the third order reaction.



M, being a third body. Here A^{\pm} represents the ion (of either sign) about which molecules B is clustering.

In the classical model of drop formation the Gibb's function has been taken into consideration. The energy of formation of a nucleus is given by

$$\Delta G_w = -4\pi\Delta G_v r_w^3/3 + 4\pi\sigma_{w/v} r_w^2 \quad (1.30)$$

Where r_w is the radius of water nucleus (assumed spherical). $\sigma_{w/v}$ the surface free energy per unit area of water nucleus in water vapour; ΔG_v , the volume free energy of condensate per unit volume per mole. In presence of ions the water vapour molecules form clusters with ion at the centre. In this case the Gibb's free energy is modified as eq. (1.31).

$$\Delta G_w = -(4\pi\Delta G_v r_w^3/3) + 4\pi\sigma_{w/v} r_w'^2 + (Ze)^2/5r_w' \quad (1.31).$$

The last term in eq. (1.31) is due to the electrostatic energy of the cluster in the presence of an ion of charge (Ze), Z being the charge number, e the electronic number.

Yuhang Wang and Russel (2005) positive matrix factorization (PMF) was used to infer the sources of PM_{2.5} observed at four sites in Georgia and Alabama.

1.17 (ii) Electric Field Induced Nucleation: Thunder clouds are known to have strong electric field. During a lightening discharge the maximum electric field (~ 10 e. s. u.) is produced near the channel. The electric field so generated affects the rated condensation of water vapour and ice deposition. It has been reported (Jalaluddin, 1962; Parmar, 1973, 1975) that the electric field induces nucleation in a liquid.

The supercooled drops of a few millimeter diameter resting on a chromium surface froze immediately when electric fields of 20 to 60 Kv/cm were applied. It has been observed that the supercooled water drops on a plastic surface froze when expressed to sparks from a Teslacoil. Sparks from the coil had no effect on the drop when they were not on a surface but suspended in the air (Evans, 1973; Singh, N., 1986).

Now we can also write the phase change of water vapour in following manners

1. Water vapour $\xrightleftharpoons[\text{Evaporation}]{\text{Condensation}}$ Liquid water (condensation)
2. Water vapour $\xrightarrow{\text{Condensation}}$ Liquid water $\xrightarrow{\text{Crystalization}}$ Solid water (ice).
3. Water vapour $\xrightarrow{\text{Glaciation}}$ solid water or (ice)

Nucleation is the key element in the understanding of many natural and industrial processes as well. It plays a prominent role in a wide variety of engineering process.

1.18 MODELS OF NUCLEATION:

1.18 (i) Classical Liquid drop Model: Within meta-steady state bulk phase of water vapour of small molecular clusters of liquid water, which results from the ions agglomeration of water molecules; these are generally referred to as embryos if the vapour pressure is below the critical value required for nucleation. Such embryos have small binding charges and usually disrupted by thermal agitation. However, at the critical vapour pressure some embryos will reach critical size, at which point will be unstable equilibrium with the mother phase. A germ will proceed to grow spontaneously and thereby produce a microscopic phase, if a result of fluctuation in the mother phase; its size increase by even an infinitesimal amount.

The workers description completely assumed that

1. Pre-nucleation embryos may be regarded water spheres characterized by the usual macroscopic densities and surface tension.
2. They are distributed according to the Boltzmann law.
3. The i-mers are in thermal equilibrium, and the probability that they have the certain energy $(\Delta\phi)_i$, is just the probability for their existence, if we interpret $(\Delta\phi)_i$, as the energy of formation of i-mer.

In this model embryos are considered as spherical of certain radius. The phase change occurs at constant temperature. The total volume of the system considered (the mother phase + the condensed phase) remains constant.

Volmer (1939) and co-workers evaluated the free energy of formation of water clusters by ascribing macroscopic thermodynamics properties to them. Thus the free energy of droplets is described as the sum of the surface term. An attractive feature of this approach is that it permits ready visualization of the origin of the free energy barrier to nucleation in terms of the maximum in the above sum as a function of size. However, a very unattractive aspect is that the calculated size of critical nucleus i.e. The cluster size at a top of the free energy barrier is only about 100 molecules which leads to doubt the applicability of macroscopic concept in the present examples following standard methods (Frenkel, 1946). This spherical drop models leads to directly to a rather simple expression for the rate of homogeneous nucleation of droplets from vapour.

The remarkable arrangement (Hirth, 1963; Volmer, 1939) of the macroscopic theory with observations of the critical supersaturation for appreciable nucleation rate of various liquids in cloud chambers stood for many years as the basis of our knowledge of nucleation. For example, referring to the data of Wilson (1899) and Powell (1928) who reported "fog limit" for homogeneous nucleation of water droplets at a Supersaturation ratio is about 5.0 at 273⁰ K, agreement with microscopic theory is excellent (Feder, 1966). However, it has been pointed out (Feder, 1966; Dunning, 1969; Lothe, 1969; Frenkel, 1946; Hirth, 1963) that the external partition fractions for free translation and rotation had been neglected in the macroscopic theory. According to Lothe and Pound (1969, 1962, 1966, 1968) the Helmholtz free energy of formation should be corrected to include the following contributions;

$$\Delta F' = \Delta F_i + \Delta F_{iT} + \Delta F_{iR} - \Delta F_{i-rep} \quad (1.32)$$

Where F_{iT} and F_{iR} results from the translational and rotational degrees of freedom of the embryo. The term ΔF_{i-rep} called replacement term by Lothe and Pound (1962) has been regarded as resulting from the deactivation of the vibrational degree of freedom, which the cluster would have possesses as bulk water (Lothe and Pound, 1962). Later, Lothe and Pound (1966) approximated ΔF_{i-rep} as due to translation and vibrations about the centre of the embryo water mass considered again as a spherical partition of bulk water not yet 'injected' into the vapour with the introduction of these contributions and by expressing the result in terms of portion functions, the size distribution according to Lothe and Pound become

$$N'_i = \left[\frac{Z_{iT}Z_{iR}}{Z_{i-rep}} \right] N_i = \phi_{LP} N_i \quad (1.33)$$

Where Z_{iT} and Z_{iR} are the translational and rotational partition functions of i-mer, Z_{i-rep} is the i-mer replacement partition function $[\approx \exp(\dot{S}/k)]$, where \dot{S} is the entropy per water molecules in the bulk state (Lothe and Pound, 1962). N_i is the uncorrected classical size distribution. Unfortunately, the correction factor ϕ_{LP} turns out to be of the order of 10^{17} , annihilating the classical theory and experiment.

With the inclusion of this contribution the theory predicts a critical supersaturation ratio of about 3.0 per water vapour at 250^0K in poor quantitative agreement with Powell's (1928) observations. This situation stimulated a great deal of experimental and theoretical work in the field on the experimental side (Franck, 1956), two new techniques were developed to measure critical supersaturation ratio for homogeneous nucleation;

1. The Diffusion cloud chamber (Katz, 1970; Frenkel, 1946)
2. The Supersonic Nozzle method (Wegner, 1977)

Work is still in progress, but it appears that virtually all substances with the possible exception of Argon (Hoare, 1980) and Ammonia (Dawson, 1969) follow the original macroscopic theory, which ignores the contribution from free translation and rotation. Since the innovative work of Wilson (1897) the expansion cloud chamber has been developed and used by numerous investigators to study homogeneous nucleation. Miller et al. (1983) presented experimental homogeneous nucleation rate data extending over an exceptionally large J_w - $S_{v,w}$ - T (Nucleation rate-supersaturation ratio- temp.) surface. Using the empirical nucleation rate formula (Miller et al., 1983).

$$J = S_{v,w}^2 \exp [328.124 - 5.58243T + 0.030365T^2 - 5.0319 \times 10^{-5}T^3 - (999.814 - 4.10087T + 3.01084 \times 10^{-3}T^2)\ell_n^{-2}S_{v,w}] \quad (1.34)$$

And adjusting only the sticking coefficient a good fit was obtained between classical nucleation theory and the experimental data (Hagen, 1984). Not surprisingly, the refinement (Lothe and Pound, 1969, 1962, 1966, 1968) to classical approach has been questioned (Kikuchi, 1971, 1969; Reiss, 1967, 1970) on theoretical side, much effort has been directed towards ascertaining the magnitude of another correction to the macroscopic theory, which tends to counter balance the effects of free translation and rotation. This is termed as replacement partition function, and it describes the free energy due to the six internal degrees of freedom. Efforts to calculate this quantity by classical phase internal methods (Reiss, 1977; Kikuchi, 1977; Nishioka, 1977) have not been entirely successful because of great difficulties in defining a cluster embedded in liquid. In fact, some treatments yields larger (Reiss, 1977; Kikuchi, 1977)

replacement partition functions while others give smaller ones (Nishioka, 1977). In summary one might conclude at the present time that the good agreement between the original macroscopic theory and experiments in liquids is fortuitous, but many appear genuine because of

1. A large replacement partition function, or
2. The observation of potential energy due to macroscopic surface tension (Abraham, 1974; Binder, 1980).

Kikuchi (1971) extended and refined the work of Reiss (1968) to obtain the following correction factor in place of $\phi_{L,P}$,

$$\phi_{RK} = \rho_w \dot{v}_v / kT \quad (1.35)$$

Where \dot{v}_v is the volume per molecule in the vapour phase.

At 303k, $\phi_{RK} = 3 \times 10^4$. Although, this is more than 12 order of magnitude smaller than $\phi_{L,P}$, it still constitutes a significant correction to classical results.

Unfortunately, the studies of Lothe and Pound (1969, 1962, 1966, 1968) and of Reiss (1977), Kikuchi (1977) and Reiss et al. (1968) suffer from fairly obvious short coming ; either the energy of formation of germ, or the correction factor itself, or both have to be evaluated, in terms of macroscopic values of parameters like surface tension $\sigma_{w/v}$ and density ρ_w . This tends to seriously compromise the microscopic point of view, which is taken when formulating modification to the classical model. Also, there are still partially unresolved conceptual problems, which arise in the attempt to merge the classical stationary drop model and statistical mechanics points of view.

1.18 (ii) Computer Simulation and Monte Carlo Method: One might think that the issue could be settled by computer calculation using fairly realistic potential functions to calculate the free energy of cluster. Much work has been done in this area (Hale, 1982; Sjolander, 1978; Ward, 1982; Abraham, 1974). In one of the more elaborate efforts (Miyazaki, 1977), Monte Carlo methods were used to calculate the surface tension and chemical potential of bulk argon using Lennard-Jones potential, and these results were applied to estimate the free energy of isolated argon droplets. The proposed approach is logical development of the statistical ions originally suggested for a single layer cluster (Thomas Ackermn, 2005).

The resulting free energies of formation were then compared with the actual Monte Carlo free energies of isolated argon clusters. It was found that the contributions from free translation and rotation were required to describe the Monte Carlo Cluster data. This means that, unlike the case of physical experiment on real liquids, the original macroscopic theory must be modified by the contribution from free translation and rotation in order to describe argon by L-J Potential. However, a major short coming of this and other computer calculations is that the pair wise potentials were used. This is a serious difficulty in view of the importance of three body potentials in describing surface properties. Further, a Monte Carlo procedure has been used to study the stability and structure of small water clusters absorbed on model basal and Prism faces of Hexagonal AgI (Ward, 1982) and to estimate the critical cluster size to calculate cluster free energies (Hale, 1982).

1.18 (iii) Molecular Model: For many years the pre nucleated embryos have been treated classically (Becker, 1935) i.e. as liquid drop or as a solid spherical caps rather than as a collection of water molecules inspite of the fact that these embryos consists of typically from two to less than a hundred molecules clearly. Surface tension and density of Liquid are not applicable in the description of such small embryos or clusters. Strongly, however at least in the case of homogeneous nucleation of liquid water from vapour, this extrapolated macroscopic model has provided qualitative agreement with the experiment (Allen, 1969; Russell, 1969; Lothe and Pound, 1969). The liquid drop model also has other difficulties, which should be mentioned. There are terms missing from the free energy of formation which questionable are supposed to be present (Frenkel, 1955; Lothe and Pound, 1962), but have been cancelled by so called 'replacement term'. There have been great deals of illuminating work directed towards evaluating the replacement terms (Dunning, 1965; Lothe, 1971; Lothe and Pound, 1962, 1966, 1968; Kikuchi, 1969; Reiss, 1967, 1970, 1968) and these contributions have done a great deal to aid our understanding of nucleation process. Molecular model proposed by Plummer and Hale (1972) had several advantage such as to predict.

1. Molecular properties such as binding energy and external energy of the water cluster stored in the form of inter and intermolecular vibrations.
2. The concentration of different sized water cluster or ice clusters.
3. The detailed information directly related to physically meaning full cluster properties such as cluster size, structure and stability.
4. It can serve as a frame work for the incorporation of molecules of other substance.

The basic assumptions of the Molecular model are as follows:

1. The cluster have a well defined structure,
2. The internal properties of the molecules are only slightly altered by cluster formation.
3. The life time of clusters is sufficiently large that its vibrational spectrum can be characterized, and.
4. The most stable clusters are approximately spherical in shape.

The assumed structure for water clusters in supersaturated vapour is that of a closed or partially closed clathrates composed of five membered rings. An example of such a structure for a 20-mer is show in fig.(1.27). These cluster forms fulfill the imposed criteria that the molecules associated by hydrogen bonding with bond angles, which are roughly tetrahedral, that the number of bonds be maximized, and the forms posses near spherical symmetry. This choice of geometry is supported by the studies of Searchy and Fenn (1974).

However, these perfectly ordered clatharate structures could not be used to represent arbitrarily large i-mers, since it becomes difficult to maintain the closed 'cages' without grossly distorting the bond angles and lengths. This results in the occurrence of considerable bond strain for $i \geq 80$, the effect of which has been studied by Hagen (1973). However, nucleation of ice is not a homogeneous nucleation process. Hale and Plummer (1974b) have extended the molecular model to include configurational entropy contributions to the partitions function for the study of prenucleation embryos of ice in vapour. They assumed an ice-I_h structure composed of rings containing six water molecules each. A typical structure with 20 molecules is shown in fig. (1.28).

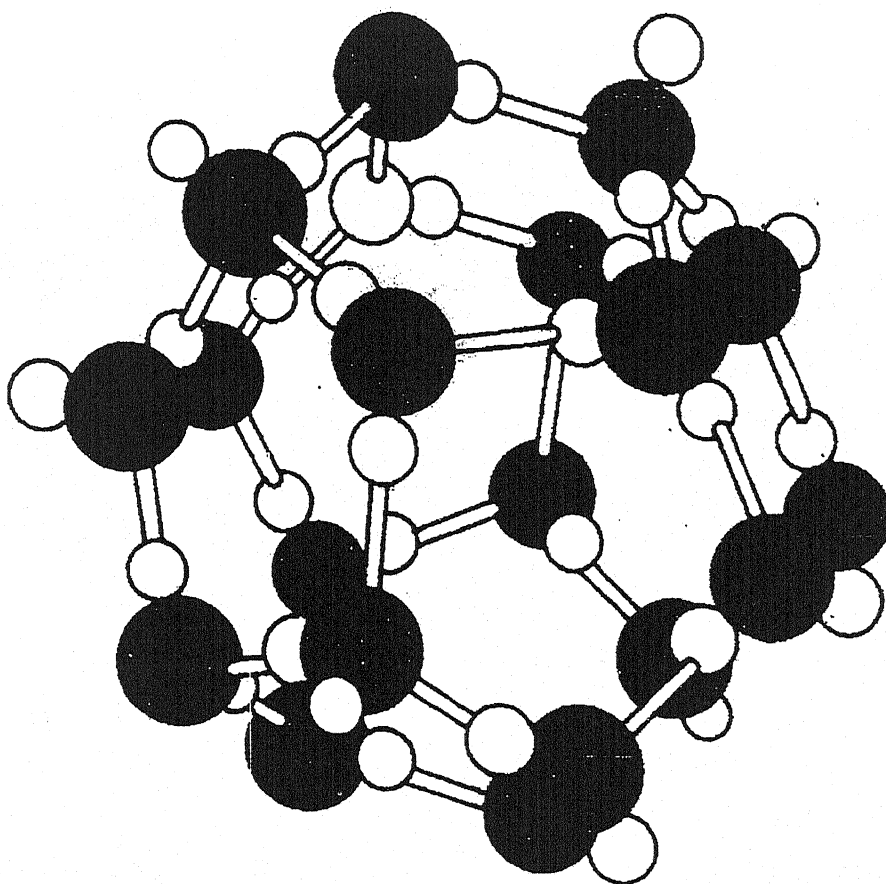


fig. 1.27 : The 20- molecule clathrate cluster composed of five-membered rings. From Hale and Plummer (1974 a).

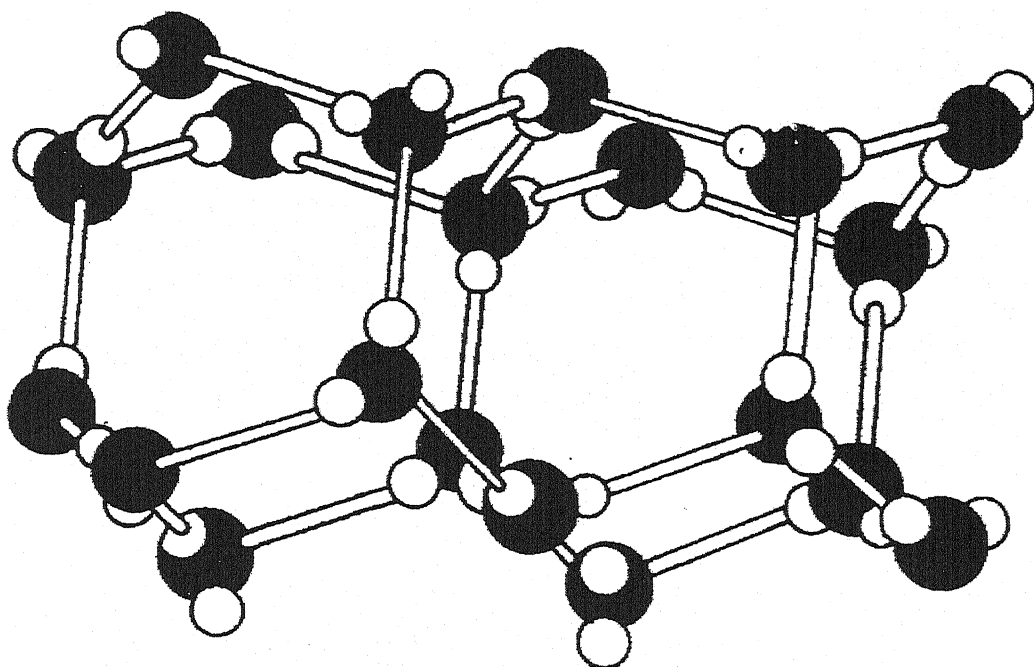


fig. 1.28 : The 20 molecule ice I_h structure. From Hale and Plummer (1974 b).

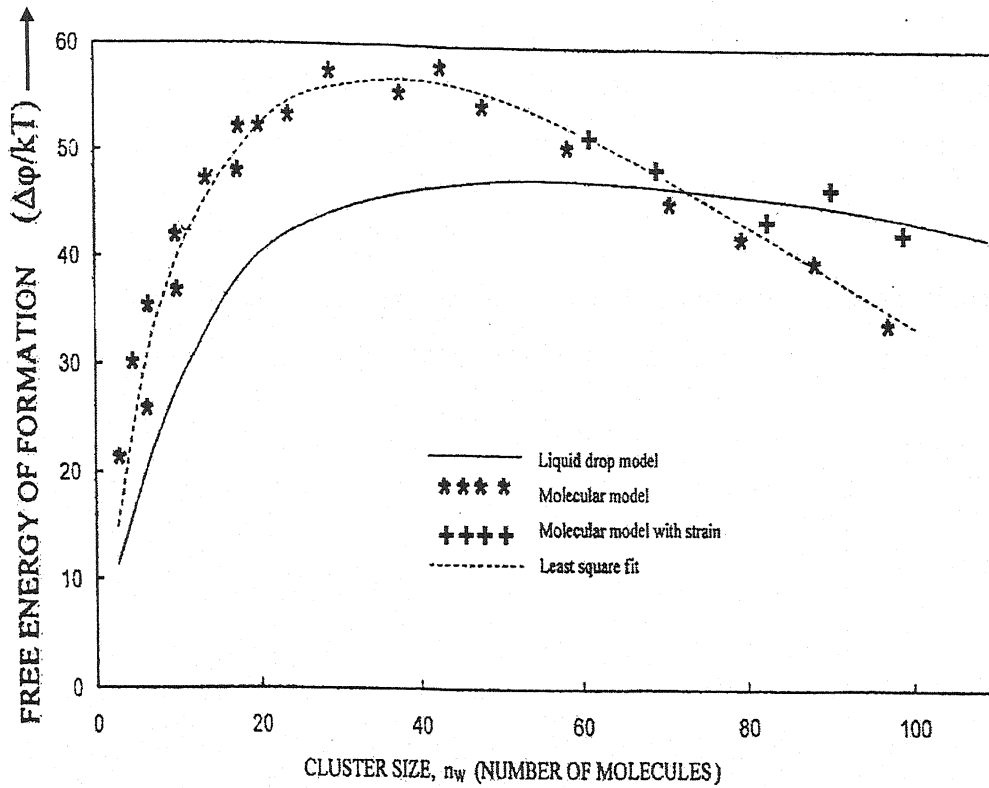


fig. 1.29 : The free energy of formation versus cluster size at $S_{v,w} = 5.0$ and $T=273$ k for (i) The liquid drop model, $\Delta G/kT=9.3 N_w^{2/3} - 1.6 n_w$; (ii) The molecular model, $\Delta\phi/kT$; (iii) Molecular model with strain and (iv) The least square fit to $\Delta\phi/kT=12.8n_w^{2/3} - 2.4n_w$, From Hale and Plummer (1974 a).

A comparison was made with the clathrate model and with a simple spherical cluster model using ice surface tension to evaluate energy of formation and to use it to calculate the nucleation rate and the exact critical supersaturation ratio. In this model, the Hamiltonian of the n - molecules cluster can be written as

$$H_{(n)} = H_T + H_R + H_v + H_B \quad (1.36)$$

Where H_T and H_R , are the rigid body translational and rotational energy operators for the cluster. H_v , the vibrational energy internal to the cluster and H_B , inter-molecular binding energy.

The partition function is given by

$$Z_{(n)} = \sum_i [-< i/H_n/kT >] \quad (1.37)$$

Where the summation 'i' is overall possible states of the system k being Boltzmann constant using eq.(1.36), we can write-

$$Z_{(n)} = Z_T Z_R Z_v Z_B Z_c \quad (1.38)$$

Where Z_c , represents the contribution from configuration entropy.

A comparison of $(\Delta\phi/kT)$ (molecular model) and $(\Delta\phi/kT)$ (liquid drop model) was made (Hale, 1974a). It was found that at supersaturation ratio $S_{v,w} = 1$, the energies of formation differed by about 5 to 10 kT (or 0.1 to 0.2 ev at 273^0 K) over a wide range of temperatures. The molecular model predicts consistently higher energies of formation than the liquid drop model. This is in contrast to the corrected liquid drop model with replacement terms, which give consistently liquid drop model, fig. (1.29) shows the least square fit to $(\Delta\phi/kT)$ for $S_{v,w} = 5.0$ and temp. 273^0 K.

1.18 (iv) Semi-Molecular Model: The Cluster model (Chan, 1980a), with ion at the centre features two separate regions and is, therefore, discontinuous. It consists of a hydration shell containing discrete water molecules. The molecules are strongly bonded to the ion and their orientation is determined by the ion. Statistical mechanics is applied to calculate the excess free energy of the micro clusters. In the outer region, the water is taken to be a dielectric continuum and the modified Fisher droplet model for ion-water nucleation is used.

This model has the advantage that it can be applied to both ends of the ions cluster spectrum. It predicts saturation ratio for condensation on ions close to values from cloud chamber experiments. A sufficient part of molecular approach has been included so that the model makes a distinction between positive and negative ions.

1.18 (v) Extension of Molecular Model to Heterogeneous Nucleation:

It is difficult to extend the molecular model to a study of heterogeneous nucleation. This is because very less is known about the mode and energy of interactions between clusters, of water molecules and substrate molecules. The major problem in determining the interaction energy is that it is specific to each solid and to each crystallographic arrangement. Further more it is a function of position on each crystallographic face, due to the heterogeneous nature of the surface. In spite of these difficulties, preliminary studies (Plummer, 1973) have produced at least qualitative agreement with observation by predicting that the weaker the interaction between the surface cluster and solid substrate, the more likely it is that the water molecules will arrange in isolated multi-layered structures instead of a single layer.

The conceptual difficulties associated with assigning surface tension and contact angles to microscopic embryos are avoided with a molecular model. The affinity of the surface for water and the strength of the water substrate interaction can be specifically included in this model. The model thus has the potential to predict which artificial nuclei should be the most effective in producing ice crystals or cloud droplets. The effect of temperature and supersaturation on nuclei activation can also be studied. The role of surface imperfection and contaminants can well be included.

1.19 MODELS FOR HETEROGENEOUS WATER NUCLEATION:

The classical model of nucleation theory is used for heterogeneous nucleation. The “replacement term” difficulties associated with the attempt to define the classical approach do not arise, since the nucleating substrate may be taken to be at rest. The modification has been made according to the geometry of surface.

1.19 (i) Nucleation on water in soluble, partially wettables CCN: It is assumed that water embryos or germ or nucleus, nucleated in supersaturated vapour on a water insoluble partially wettable surface assumes the shape of a cap.

1. Nucleation on a planar Substrate: Gibb's free energy for the formation of spherical embryos is given by

$$\Delta G_{i,s} = \left(\frac{\pi a_i^3}{3} \Delta G_{vol} + \pi a_i^2 \sigma_{w/v} \right) (2 + m_{w/v}) (1 - m_{w/v})^2 \quad (1.39)$$

Where a_i is the radius of embryo, $\sigma_{w/v}$, the surface tension of the water and $m_{w/v} = \cos\theta$, θ being the angle of contact of the surface with water.

2. **Nucleation on a curved substrate:** Fletcher (1958, 1959a) has extended the theory to include an amount of the effects of the finite size of the nucleating particle. In this extension the substrate is assumed to be a sphere of radius r_N .

Accordingly, the energy of germ formation becomes

$$\Delta G_{g.s} = \frac{16\pi M_w^2 \sigma_{w/v}^3}{3[RT \rho_w \ell_n S_{v,w}]^2} f(m_{v/w}, X) \quad (1.40)$$

where

$$2f(m, X) = 1 + \left(\frac{1 - mX}{\phi}\right)^3 + X^3 \left[2 - 3 \left(\frac{X - m}{\phi}\right) + \left(\frac{X - m}{\phi}\right)^3 \right] + 3mX^2 \left(\frac{X - m}{\phi} - 1\right) \quad (1.41)$$

$$\text{With } \phi = (1 - 2mX + X^2)^{\frac{1}{2}}, \quad X = r_N/a_g \quad (1.42)$$

Twomey (1964) modified the heterogeneous nucleation theory of Fletcher to consider nucleation on an insoluble, partially wettable spherically concave substrate of nucleus r_N . The only change in theory is one of geometry. The volume energy in this case is given by changed value of

$$2f(m, X) = 1 - \left(\frac{1 + mX}{\phi}\right)^3 - X^3 \left[2 - 3 \left(\frac{X + m}{\phi}\right) + \left(\frac{X + m}{\phi}\right)^3 \right] + 3mX^2 \left(\frac{X + m}{\phi} - 1\right) \quad (1.43)$$

$$\text{and } \phi = (1 + 2mX + X^2)^{\frac{1}{2}}, \quad X = r_N/a_g \quad (1.44)$$

Mahata's computations indicate that concave surface features can sufficiently enhance the capacity AP to serve as CCN.

1.20 ELECTRIC FIELD AND ELECTRIFICATION OF CLOUDS:

Here we shall describe various types of clouds and cloud particle acquire their characteristic state of electrification.

1.20 (i) Electric State of cloudless Atmosphere: Under clear sky conditions, flat portions of the conducting earth carry a negative surface energy density σ_o which is approximately $\sigma_o = -3.4 \times 10^{-4}$ e.s.u. cm^{-2} . By Gauss's law there is a corresponding downward directed surface electric field of magnitude $E_o = 4\pi\sigma_o(\text{e.s.u.}) = 3 \times 10^4 \text{Vm}^{-1}$. The field strength in the atmosphere varies with height in accordance to Coulomb's law (i.e. as d^{-2}) where 'd', denotes distance from centre of the earth. However, in the rate of attenuation is much greater than this due to the existence of positive space charge, which rapidly screens out the surface field with increasing height.

An approximate empirical description of the variation of the electric field strength with height is

$$E(\text{Vm}^{-1}) = 81.8e^{-4.52z} + 38.6e^{-0.375z} + 10.27e^{-0.121z} \quad (1.45)$$

Where z is in Km. from Gauss's law,

$$\nabla \cdot \vec{E} = \frac{\rho}{\epsilon_o} \quad (1.46)$$

The corresponding positive space charge density ρ (elementary charges cm^{-3}) is

$$\rho = 20.4e^{-4.52z} + 0.8e^{-0.37z} + 0.069e^{-0.121z} \quad (1.47)$$

Thus at ground level the charge density is about $21e \text{ cm}^{-3}$, while the average over the first Kilometer of the atmosphere is about $5e \text{ cm}^{-3}$.

The small ions produced by cosmic rays and radioactive substances are generally singly charged molecules. They may become large ions by attaching themselves too much larger aerosol particles. Since the mobilities of large ions is usually 10^{-2} to 10^{-4} times less than those of small ions, they contribute relatively little to the total ion current. Measurements show that the represented mobilities B_- of the small negative ions are greater than the corresponding mobilities B_+ of the positive ions according to Bricard (1969).

$$B_+ = 1.4\text{cm}^2\text{v}^{-1}\text{sec}^{-1} \text{ and } B_- = 1.9\text{cm}^2\text{v}^{-1}\text{sec}^{-1} \text{ at STP.}$$

An extrapolation of these values to elevations $Z \leq 10\text{km}$ in the standard atmosphere has been computed (Shreve, 1970)

$$B_+ = 1.4e^{0.14z}, \quad B_- = 1.9e^{0.14z} \quad (1.48)$$

Where z is in km. Shreve also obtained expressions for the variation with altitude of the corresponding diffusivities (in $\text{cm}^2\text{sec}^{-1}$) for example

$$D_+ = 3.6 \times 10^{-2}e^{0.092z}, \quad D_- = 4.8 \times 10^{-2}e^{0.092z} \quad (1.49)$$

The vales for $Z=0$ were obtained by substituting the corresponding mobilities and $T=273\text{K}$. In recent years the propagation effects on the electric field time derivative generated by return strokes in lightning flashes has been studied by Mahendra Fernando, Vernon Cooray (2007).

1.20 (ii) Electrical state of the Atmospheric Aerosol: Aerosol particles acquire charge through Brownian deposition of ions. In term, such

charged particles experience Brownian coagulation, which is enhanced or suppressed by electrostatic forces. Under fair weather conditions aerosol charging is approximately symmetrical, since small ions are created in air and have roughly equal mobilities. Therefore, in equilibrium particles of any size have a charge distribution approximately symmetrical about Zero charge, so that for every V_j particle bearing charge q_j . Besides acquiring charge through ionic diffusion, aerosol particles polarized in the fair weather electric field and thereby received an additional ionic drift current.

According to Brian A. Tinsleya (2005) et al. the electrical charges on aerosol particles and droplets modify the droplet-particle collision efficiencies involved in scavenging, and the droplet- droplet and particle-particle collision efficiencies involved in coalescence of droplets and particles, even in only weakly electrified clouds and aerosol layer.

1.20 (iii) Cloud Electrification (Models for cloud electrification):

There are a number of models for electrification of clouds. A few of them are given below:

1. Convection charging
2. Particle charging by selective ion capture
3. Particle charging by thermoelectric effect.
4. Particle charging by induction.
5. Non-inductive charge transfer process.
6. Electrification of thundercloud by an entrainment mechanism of charge separation.
7. Electrochemical charge separation in clouds.

1. Convection Charging: Vonnegut (1955) independently proposed that a convective cloud may operate as an electrostatic energy generator according to the following scenario: Initially, an up draft carries positive space charge from the lowest levels of the troposphere into the growing cloud, the electric field cloud soon acquires a negative charge screening layer at its edges due to cloud, the electric field cloud soon acquires a negative charge screening layer at its edges due to cloud particle capture of ions drifting from clear air to cloud under the influence of the main positive charge, finally, downdrafts carry the negative charge closer to the ground, thereby increasing the (reversed) electric field at the earth sufficiently to initiate positive point discharge which enhances the positive charge entering the cloud via the updraft.

The time dependent model for cloud electrification has been developed (Mathpal, 1982) in which both convection and gravitational separation of charged precipitation particles work simultaneously towards its electrification. Not only the generated electric field but also the current density have been calculated for various values of precipitation intensity P_0 , liquid water content L , rebound mean angle probability $\langle P \rangle$, relaxation time τ , fractional constants of space charge and electric field $f_1 f_2$ and the vertical air motion U . It has been found that an electric field of about $4.0 \times 10^5 \text{ Vm}^{-1}$ and a current density of about $0.1 \mu\text{Am}^{-2}$ may normally be achieved for a vertical air motion $U \approx 4\text{ms}^{-1}$, at a precipitation intensity of about 10mmh^{-1} . However, occurrence of the first lightning flashes may also be explained even at precipitation intensity 5mmh^{-1} ($U \approx 8\text{ms}^{-1}$). Thus it appears that the thundercloud electrification may be explained by the combined precipitative and

convective (CPC) charging mechanisms and the vertical air motion in the cloud plays an important role in its electrification. The role of parallel electric fields in the mass-dependent effects in ion conic production had been studied by E.J. Lund et al.(1999).

2. Particle charging by selecting ion Capture: Wilson (1929) described how an electrically polarized cloud particle may selectively capture ions of one sign as it falls. This happens, because while the lower surface of the particle may easily attract and capture ions which carry a sign opposite to the local surface charge, the upper surface is not as effective in this respect since ions attracted to it must first catch up with it in order to be captured. The net effect of this selective process is a large-scale separation of charge from due to the sedimentation of the charged cloud particles. This reinforces the existing field, so that its occurrence in the clouds would cause a field enhancement in qualitative agreement with what is expected for thunderstorm.

Mathematical model for the “Wilson Process”, based on spherical particles in stokes flow has been worked out by Whipple and Chalmers (1944). The equilibrium charge for this process is proportional to the ambient field strength and particle surface area. Also, the process becomes ineffective for large fields, since then the ionic drift velocity greatly exceed drop terminal velocities. A simple estimate (Mason, 1971) suggests the mechanism may produce fields only as large as 100 Vcm^{-1} , which is still three orders of magnitude below characteristics thunderstorm values.

3. Particle charging by thermoelectric effects: Reynolds et al. (1957) obtained laboratory evidence that a Hail Pellet may become

charged as a result of collisions with ice crystals having a temperature different from that of the pellet. The physical basis of the charge transfer was suggested as being due to the diffusion of hydrogen ions down the temperature gradient existing in the region of momentary contact (Brook, 1961). Thus, Since H^+ ions have a greater mobility in the ice lattice than OH^- ions, a temperature gradient maintained across a piece of ice will result in an excess of positive charge on the colder portion. Mason formulated a one-dimensional model for this process on the basis of an ideal ice structure and found that magnitude of equivalent surface charge density σ on the ends of an ice rod having prescribed steady state temperature gradient dT/dx ($^{\circ}C. cm^{-1}$) is given approximately by $\sigma \approx 5 \times 10^{-5} \frac{dT}{dx}$ e.s.u. cm^{-2} . Similar results follow from a more complete theory of the process in real ice having orientational defects worked out by Jaccard (1963). Apparently the results depend sensitivity on such factors as the time of contact, micro-topography of the areas of contact, presence of impurities in the ice, and the relative velocity of impact. All of these factors are difficult to control in an experimental situation and hence their effects are not easily evaluated.

4. Particle charging by induction: An uncharged drop polarized in the fair-weather electric field carries a surface charge density.

$$\sigma \text{ e.s.u} = (4\pi)^{-1}(Er)_{r=a} = 3E \cos\theta / 4\pi \quad (1.50)$$

θ , being the polar angle measured from the lowest point on the drop: thus the lower hemisphere is positively charged, and the upper hemisphere negatively charged. Therefore, if such a drop were to experience on its lower hemisphere a momentarily electrical contact with and subsequent separation from a similarly polarized smaller drop, there

would result a net negative charge on the larger drop and a positive charge of equal magnitude on the smaller drop. The first to point out that such a process of inductive charge transfer, occurring throughout a cloud and followed by the large scale separation of charge through relative sedimentation under gravity, would serve to increase the in-cloud electric field in the sense normally observed in thunderstorms.

5. Non-inductive charge transfer process: These processes occur during particle collisions in which charge is transferred independently of the local electric field strength. It is perhaps unusual for a process to be named in terms of what it is not however, a more succinct and yet all encompassing little has yet to emerge. Beared and Ochs (1986) use the term "interface charging" for charge transfers driven by differences in contract potential.

Detailed laboratory Studies of the above charging processes have been carried out over the last ten year. Jayaratne et al. (1983) confirmed that the sign of graupel charging reverses as a function of temperature and that this "reversal temperature", moves to higher (warmer) values with decreased cloud liquid water content. They also found that the amount of charge transferred depends on impact velocity and on the size of the small ice crystals used.

Keith and Saunders (1990) extended the previous work by using larger ice crystals, up to 800 μ m diameter, and found that the charge transfer increases rapidly with crystal size for small crystals but increases at a lower rate for larger crystals. They suggested that high values of charge transfer are limited by the reverse charge transfer of some of the charge residing on the surfaces when the particle in the dark. A study of

crystal-graupel interactions in the dark revealed light emission associated with this reverse charge transfer in the form of Corona (Keith, 1988). From their charge transfer experiments; they formulated relationships between charge transfer, crystal size, and impact velocity for positive and negative charging situations.

6. Electrification of thundercloud by an entrainment mechanism of charge Separation: Wagner and Telford (1981) proposed an entrainment mechanism for cloud electrification in which the micro-scale charge separation can take place at the interface. This conductivity in homogeneity has been postulated to result either from the one set of ice process or from the evaporative depletion of small ice or water particles in cloud particles, diluted by dry air entrained at the cloud top. They consider that the turbulence inside the thermals and the prevailing updrafts and downdrafts within the cloud are responsible for macro-physical charge separation. The ion pairs produced due to cosmic rays, as in the convective theory, provide the convective space charge in this mechanism. Sapkota and Varshneya (1988) examined the extent to which the leakage current produced by the electrical forces acting on the descending thermals influences the net charge separation caused by the entrainment mechanism. P.T. Tonev, a. and P.I.Y. Velinova (2007) examined Atmosphere-ionosphere vertical electric coupling about thunderstorms of different intensity.

7. Electrochemical charge Separation in clouds: Pathak et al.(1980) presented a self-sustaining mechanism for the continuous and rapid lightning flashes. It has been shown that the initial discharge provides sufficient number of ions for the electrochemical charging mechanism proposed (Wahlin, 1973) to be operative for the rapid separation of charges within a thundercloud.

The mechanism is based on experimental observations by Wahlin and uses electrophillic property of NO_2 and O_2 molecule present in the air, when any surface is ventilated to ionized air, these molecules with electrons attached to them react with surface material transferring negative charge to it. The positive ions are left in surrounding air. They form an electrical double layer with charged surface at a distance equal to the average distance between ions in air (about 1mm).

The Coulomb force does not bring them closer to oppositely charged surface. The surface is negatively charged because negative NO_2 and O_2 ions can react with surface material to transfer negative charged and thus a net positive charge is swept with air. For a spherical surface of radius R the maximum charge that can be separated at equilibrium is given by

$$q_{\max} = V_0 4\pi\epsilon_0 R [1 + (R/d)] \quad (1.51)$$

Where V_0 , is the oxidation reduction potential of the surface material; d , the thickness of electrical double layer.

1.21 EFFECT OF ELECTRIC FIELD OF MICROPHYSICAL PROCESS:

1.21 (i) Drop and Ice Crystal Nucleation: In the present work we have examine a number of physical parameters such as Gibb's free energy, critical radius, equilibrium concentrations and nucleation rate, related with nucleation of water drop and ice crystal affected by the external electric field.

1.22 CONDUCTION IN THE ATMOSPHERE:

The surface of the Earth and highly conduction layer of ionosphere may be treated as the plates of spherical condenser. Ions caused by various ionizing agencies e.g., Cosmic rays radio activity in air and ground etc. exist between the above mentioned plates. Possible influence of cosmic rays on climate through thunderstorm clouds were studied by Lev'I. Dormana, B, and Irena V. Dormanc (2005). With decreasing of cosmic rays intensity caused by increasing of solar activity or in some short periods of Forbush decreases, the intensity of secondary CR relativistic electrons decreases and the probability of formation of thunder storm is also expected to decrease. Cosmic ray-induced ionization in the atmosphere had been studied by I.G. Usoskin (2004).

Electric field changes of lightning observed in thunderstorms had been studied (William H. Beasley, 2000). Wilson's (1920) Thunderstorm theory could explain reasonably some of the necessary conditions, such as explanation to unitary diurnal variation in potential gradient, for the fundamental question in atmosphere electricity. "How the atmosphere has a permanent electric field in spite of its conductivity." The conductivity was measured by Gerdein's Chamber described by Khera (1994).

Gondot et al. (1988) have developed a new type of sensor to measure ionic electrical conductivity around and inside convection clouds. The resulting technical note is rather complicated and difficult to understand but it certain much material with regard the investigation it self, an attempt was made to utilize existing stations and network by combining their measurements in a sophisticated system which was called the "atmospheric electricity".

1.23 VERTICAL STRUCTURES OF TROPICAL PRECIPITATING CLOUD SYSTEMS:

Krishna Reddy (2003) studied temporal variation of vertical structure of precipitating cloud in tropical India based on the observations of 1.357 GHz lower atmospheric wind profilers (LAWP) at GADANKI. The occurrence of deep convection in the tropics plays an important role in global circulation, since it transports heat, water vapour and so on to the upper troposphere.

Kandalgaonkar et al. (2003) analysed the data of point discharge current (PDC) measurements during a total of 65 thunderstorm at Pune ($18^{\circ} 32'N$, 73° , $51'E$) to study the (PDC) local diurnal variation and some issues related with the current. Majority of the studies were carried out sporadically during time bound field experiments to accomplish specific objectives of the study but the significant issue of the diurnal variation of PDC received a little attention (Williams, 1985) except a few studies (Whipple, 1936; Ette, 1980).

In 80's positive charge deposition by lightening (Holden et al., 1983), phenomenon for the polarity of the thunderclouds and charge reversal microphysics (Jayratne, 1985) have been supported by the evidence now available from both field and laboratory.

The laboratory result on charge reversal microphysics for the infrared charge transfer per collision is strongly dependent on crystal size over a range from 10-100 microns, and then levels off for larger crystal sizes (Marshall, 1988).

Bourdeau and Chauze (1988) studied numerically two process that contributed to the limitations of hydrometer electricity charge in an

ambient field Frozen hydrometers the net charge is only limited by corona emission. Vonnegut (1988) proposed the mechanism to explain thunderstorm electrification differ greatly in how they might affect or be affected by the cloud and the clouds environment depending upon which mechanisms predominant, atmospheric electrification phenomenon may for some cases be in little influenced by environmental factors or exert only a minor influence on meteorological process.

Thorpe (1981) in a discussion of thunderstorm dynamics, "It has long been established that although thunder and lightning are the most spectacular, they are the least important in the storm structure and evolution. This is not to say that understanding of the electrification does not represent an enormous challenge, lightning causes a lot of damage, but the storm dynamics would almost identical if thunder and lightning were not present."

During water vapour condensation the equivalence between supersaturation ratio and the external electric field has been established recently (Dwivedi, D.et al., 2008).

CHAPTER-2

**MODIFICATION IN THE
NUCLEATION OF WATER VAPOUR
CONDENSATION AND ICE
GLACIATION, DUE TO EXTERNAL
ELECTRIC FIELD.**

CHAPTER-2

MODIFICATION IN THE NUCLEATION OF WATER VAPOUR CONDENSATION AND ICE GLACITION, DUE TO EXTERNAL ELECTRIC FIELD

2.1 INTRODUCTION:

There exists normally an electric field in the clouds. When the electric field becomes enough an electrical discharge (the bolt of lightning) occurs with clouds or between clouds and the grounds. During the strike, successive portion of air becomes a conductive discharge channel as the electrons and the ions of air molecules are pulled away from each other and forced to flow in opposite direction. During a lightning discharge the maximum electric field (~ 10 e.s.u.) is produced near the channel.

Upward-propagating discharges from thunderstorms called “blue jets” and “blue starters” and high altitude near-cloud top discharges have been reported over strong convective storm systems (Glenn E. Shaw, 1998). The electric field so generated may affect the rate of condensation of water vapour.

It has been reported (Jalaluddin et al., 1972; Parmar et al., 1973; Parmar et al., 1975) that the electric field induces nucleation in liquid. Schaefer (1953), Salt (1961) and Pruppacher (1963) observed the freezing of water due to passage of electric discharge through it. It has been observed that electrical charges on aerosol particle and droplets modify the droplet particle collision efficiencies involved in scavenging and the droplet-droplet and particle-particle collision efficiencies involved in coalescence of droplets and particles, even in only weakly electrified clouds and aerosol layers (Brian A. Tinsley et al., 2005).

Poc (1967) , Schaefer (1968) , Garraud (1969), Roulleau et al. (1971), demonstrated that the electric field is mainly responsible for enhanced ice crystal production with in the supercooled fogs. G. Mandal and P. Pradeep Kumar (2002) observed experimentally that ice-nucleation does occur inside the cloud if there is an electrical discharge inside the cloud. However not all electrical discharges resulted in ice nucleation. In no case was ice nucleation observed in the presence of high electric fields with no discharge. Varshneya (1969, 1971) and Pruppacher (1973) found that when charged ions and aerosols come in contact with the neutral drops, the nucleation process is enhanced. Barlett et al. (1963), as well as Maybank et al. (1967) reported the tendency of generation of few ice splinters during ice crystal growth in strong electric field.

Loeb (1963) discussed the disruptive effect of an electric field and suggested that the nucleation of the fragments of a drop is responsible for the observed enhancement in nucleation. Later Abbas and Latham (1969) gave a possible mechanism. Doolittle and Vali (1975) studied the effect of an electric field on sample of water at different time temperature cycles. No intrinsic effect was observed up to 6000 V cm⁻¹. Evans (1973) experimentally demonstrated the effect of an electric field on the production of ice crystals in cloud chambers and argued that the accelerated charged water molecules moves to crystal tips, thereby increasing the nucleation rates.

The effect of electric field on condensation and further polarizability of water-vapour molecules have been discussed by Singh, N., et al. (2000, 2001). A calculation of electric and magnetic fields at the Earth's Surface due to an ionospheric electrojet system is done by Risto J. Pirijola (1998).

Murino (1979) studied theoretically the effect of an electric field on the condensation of water vapour and concluded that under similar temperature conditions a bigger size of drop can be produced in a given time than the one obtained in the absence of an electric field. He observed the polarization of water vapour molecules in the electric field of the central dipole (embryo of water) alone.

Singh, N., et al. (1986) discussed the effect of external electric field on the relaxation time in the nucleation process of water vapour condensation and ice glaciations. The similar study has been extended (Sharma, A.R., et al., 1992) and concluded that a small value of electric field is equivalent to very high supersaturation ratio to get a nucleus of given size under similar conditions of temperature.

The effect of electric field is dominant over the Indian subcontinent (Manohar, G.K., et al., 1999). Shaw (1998) has been shown the effect of electrical discharge in the nucleation of water droplets. Kumar, A., et al. (1998) discussed the effect of orographic features on atmospheric electrical parameters of different cities of India. Recently Dwivedi D., et al. (2008) has established equivalence between the external electric field and supersaturation ratio during water vapour condensation.

According to Pinksy et al. (1999), the inertia of cloud droplets plays a crucial role in the evaluation of the spectral during drop growth by diffusion. But, the electrical analogy does not apply to modeling dry deposition of particle (Venkatran, 1999). The fair weather electric field occurring soon after sunrise has been observed (Marshall et al., 1999). The changes in electric field due to lightening in thunderstorms have been

observed by Beasley et al. (2000). The most important features of quasi-electrostatic fields and currents, generated in the region between a thunderstorm and the ionosphere between lightning discharges, are theoretically investigated by P.T. Tonev et al. (2007). The electric field alignment of ice crystals in thunderstorms has been studied by Saunders et al. (1999). Although lightning flashes in thunderstorms are among the most ancient natural phenomenon known by human kind, several important physical processes related to them are not understood in detail yet (Lyons et al., 1999; Mac Gorman et al., 1998). In order to contribute to this understanding, recent effort has been done, for instance; the studies of the effects of thunderstorm and lightning on upper atmosphere (Sentman et al., 1998), and the development of a 3 dimensional detection of lightning path, as the recent methodology using GPS-based mapping system (Krehbiel et al., 2000). Electrical conductivity effects on lightning path simulation has been studied by Odum Mendes Jr. et al. (2005). The formulation of relaxation time required for the attainment of the steady state concentration of embryos of the critical size has been discussed previously (Kantrowitz, 1951; Probstein, 1951; Wakeshima, 1954; Collins, 1955). Following Kinetic theory (Collins, 1955) inferred that the relaxation time is independent of the free energy of formation of the nucleus, but it varies as the square of the radius of the critical nucleus.

2.2 THEORETICAL CONSIDERATION:

In the nucleation process of water vapour condensation and ice glaciations the fundamental quantity of importance is the Helmholtz or Gibb's free energy of germ formation. But the relaxation time is found to be independent of the Gibb's free energy. However, at normal electric fields the electrostatic energy of germ formation is very small compared

to the volume and surface energy terms. It becomes appreciable only at high electric fields at which break down in air might occur. Also the critical size of nucleus is produced quickly. Therefore, in this chapter we consider only the relaxation time of germ formation and thereby study the effect of an electric field on the process of self-nucleation (homogenous case) only. While calculating the relaxation time of water phase we have taken the variation of surface energy and density of water according to the different temperatures given by Edward, W.W et al, (2003) as following.

Tabel-2.1(A)

T (Kelvin)	$\rho_w(gm/cm^3)$	$\sigma_{w/v}(dynes/cm)$
273	0.999841	75.7
278	0.999965	74.9
283	0.999700	74.2
288	0.999099	73.6
293	0.998203	72.8
298	0.997044	72.0
303	0.995646	71.2

Similarly for ice phase Smitha R. P. et al. (1986) observed from the Antonow's formula that for ice phase the surface energy of ice vapour interphase also changes according to the temperatures.

$$\sigma_{i/v} = \sigma_{i/w} + \sigma_{w/v}$$

In which the value of ($\sigma_{i/w} = 33$ dynes/cm) which is independent of temperature. Thus in calculating $\sigma_{i/v}$ for ice phase we will add $\sigma_{i/w}$ into the surface energy of water vapour. Now the values of surface energy of ice phase will be as following:

Table-2.1 (B)

T (Kelvin)	ρ_i (gm/cm ³)	$\sigma_{w/v}$ (dynes/cm)	$\sigma_{i/v}$ (dynes/cm)	$\sigma_{i/v} = \sigma_{i/w} + \sigma_{w/v}$ (dynes/cm)
273	0.917	75.7	33	108.7
278	0.917	74.9	33	107.9
283	0.917	74.2	33	107.2
288	0.917	73.6	33	106.6
293	0.917	72.8	33	105.8
298	0.917	72.0	33	105.0
303	0.917	71.2	33	104.2

2.2.1 Homogeneous Nucleation Process:

2.2.1 (i) In The Absence of An Electric Field:

For the formation of a new phase a substantial supersaturation of the mother phase is required to provide the nuclei necessary for initiating the growth of this phase. In some very rapid process involving the formation of aerosols. There are indications that at supersaturation sufficient to provide nucleation according to steady state theories, there may be a measurement delay in nucleation. Probstein (1951), Wakeshima (1954) and Kantrowitz (1951) have shown that such delays in nucleation may be anticipated on the basis of the relaxation time required for the attainment of the steady state concentration of embryos of various sizes.

The frequency of growth of embryos beyond a critical size in the nucleation process corresponds to a free energy maximum. This energy is

$$\Delta G_w = -(\mu_v - \mu_l)n_w + \sigma_{w/v}S_n \quad (2.1)$$

Where μ_v , is the chemical potential of vapour and μ_l , chemical potential of liquid. $\sigma_{w/v}$, the surface free energy of water vapour interface; and S_n , surface area of embryo; n_w , is the number of water molecules in the embryo.

Corresponding to the free energy maximum for a critical size nucleus, we have,

$$\frac{\partial \Delta G_w}{\partial n_w} = 0$$

and thus the eq. (2.1) becomes

$$\Delta G_w^* = \frac{2\sigma_{w/v}\mu'_w}{3n_w^{*1/3}}n_w + \sigma_{w/v}\mu'_wn_w^{2/3} \quad (2.2)$$

$$\text{Where } \mu'_w = 4\pi \left(\frac{3m_w}{4\pi\rho_w} \right)^{2/3} \quad (2.3)$$

m_w , being the molecular mass and ρ_w the density of water.

The growth of the embryo involves the step wise gain or loss of single molecules so that the embryo undergoes an analog of a random walk among its various sizes. Similar to the classical diffusion equation, the transformation equation of the set of differential equations representing this process is.

$$\frac{\partial c}{\partial t} = \frac{\partial}{\partial n_w} \left(D \frac{\partial c}{\partial n_w} \right) + \frac{\partial}{\partial n_w} \left(DC \frac{\partial \Delta G_w}{\partial n_w} \right) \quad (2.4)$$

Where $C = C(n_w, t)$ is the concentration of embryos of the size n_w at the time t , and the (Diffusion Constant) $D = D(n)$ is

$$D = S_n \beta_w \quad (2.5)$$

Where β_w is the frequency of collision of single molecules per unit area. In the case of self nucleation.

$$\beta_w = n_1 (kT/2\pi m_w)^{1/2} \quad (2.6)$$

Where n_1 is the concentration of water vapour molecules; k , the Boltzmann constant; T , the temperature of the system.

Case I - Steady State Case: For the steady state case eq. (2.4) becomes:

$$\frac{d}{dn_w} \left[D \frac{dc}{dn_w} + DC \frac{d\Delta G_w}{dn_w} \right] = 0 \quad (2.7)$$

With the assumption that the concentration of single molecules is constant and that for some embryo containing molecules, where $n'_w > n_w^*$, the probability of decomposition is zero. Hence the boundary condition are:

$$C(1) = n_1 : C(n'_w) = 0 \quad (2.8)$$

The flow of embryos past the critical size is

$$I = D^* n_1 e^{-\Delta G_w^*} \left(\frac{\gamma}{2\pi kT} \right)^{1/2} \quad (2.9)$$

Where

$$\gamma = \frac{2}{9} 4\pi \left(\frac{3m_w}{4\pi\rho_w} \right) \sigma_w/v n_w^{*-4/3}$$

Case II – Non Steady State Case: To calculate the minimum limit of relaxation time in the non-steady-state case, a constant value D^* has been assumed disregarding its dependent on n_w .

The equation (2.4) then becomes

$$\frac{\partial C}{\partial t} = D^* \frac{\partial^2 C}{\partial n_w^2} + D^* \frac{\partial}{\partial n_w} \left(C \frac{d\Delta G_w}{dn_w} \right) \quad (2.10)$$

The solution of this equation gives the time-dependent flux for small values of t .

$$I(t) = 2n_1 e^{-\Delta G_w^*} \left(\frac{D^*}{\pi t} \right)^{1/2} \exp \left(\frac{-2\pi kT}{\gamma D^* t} \right) \quad (2.11)$$

The relaxation time may be written as

$$\tau = 2\pi kT / \gamma D^* \quad (2.12)$$

The relaxation time is the characteristic time to achieve the quasi-steady-state (germ concentration equilibrium). In the absence of an electric field Collins (1955) evaluated the relaxation time.

$$\tau_0 = 9\pi kT (n_w^*)^{2/3} / \mu_w'^2 \beta_w \sigma_{w/v} \quad (2.13)$$

The number of water molecules in a critical nucleus is given by:

$$n_w^* = \left(\frac{r_w^*}{1.958 \times 10^{-8}} \right)^3 \quad (2.14) \quad \checkmark$$

Where r_w^* is the radius of the critical nucleus (Pruppacher and Klett, 1978) with

$$r_w^* = \frac{2\sigma_{w/v} M_w}{\rho_w RT \ln S_{v,w}} \quad (2.15) \quad \checkmark$$

In this expression $S_{v,w}$ is the supersaturation ratio of vapour over the plane water surface.

2.2.1 (ii) In The Presence of An External Electric Field:

Water is a strongly polarizable medium with an electric dipole moment of 1.83×10^{-18} e.s.u. cm. (Eisenberg, 1969; Hobb's, 1974). A perturbation by an external electric field induces an electric dipole moment on the embryo of water as well as on the surrounding water vapour molecules.

The moment induced on the embryo is

$$\vec{M} = \vec{E} r_w^3 \quad (2.16)$$

Where r_w , is the radius of the water embryo and \vec{E} is the inducing electric field. The moment induced on a water vapour molecules (Kittel, 1966) is given by

$$\vec{M}_1 = \alpha \vec{E} \quad (2.17)$$

Where ($\alpha = 5 \times 10^{-23} \text{cm}^3$) is the polarizability the electric field generated at any point (A) due to the embryo dipole, fig. (2.1), is

$$\vec{E}_1 = [3(\vec{M} \cdot \vec{X})\vec{X} - X^2 \vec{M} / X^5] \quad (2.18)$$

Where \vec{X} is the radius vector joining the centre of an embryo and the water vapour molecules, shown in fig. (2.1).

However, the vapour molecules experience the external electric field as well as the field produced due to the embryo dipole.

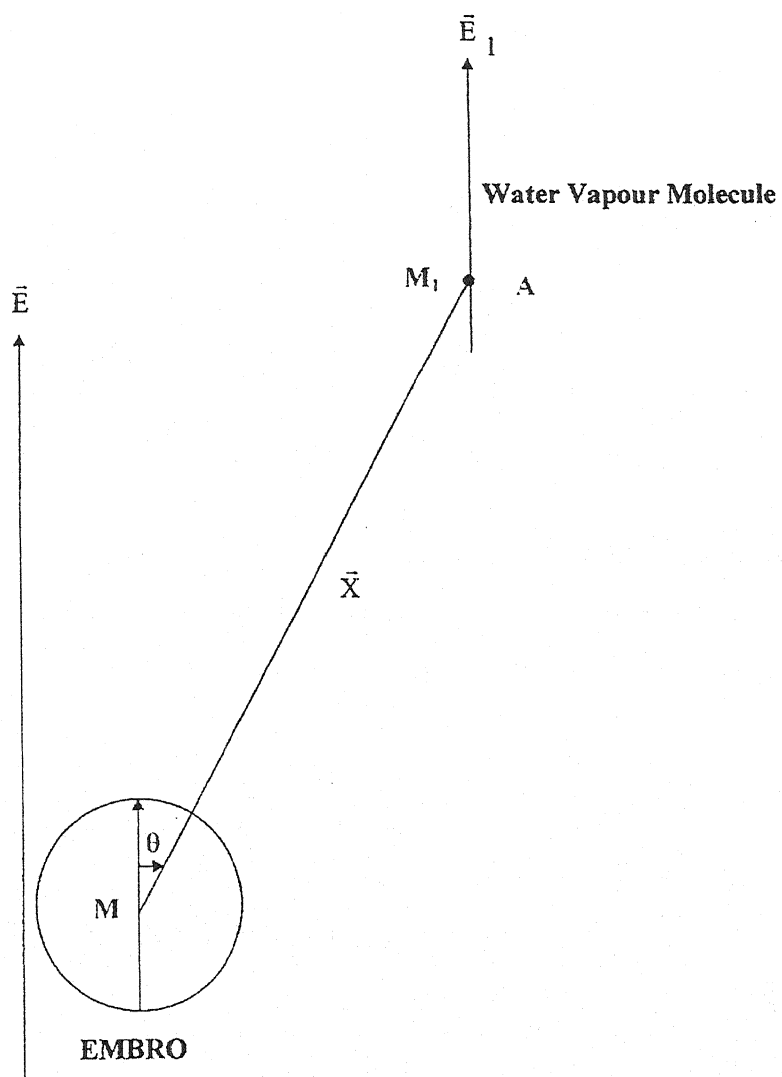


fig. 2.1 : Geometry for electric field \vec{E}_1 , generated at point (A) by the water embryo placed in an external electric field \vec{E} .

Taking into account the total electric field ($\vec{E} + \vec{E}_1$), the induced moment on a vapour molecule can be written as

$$\vec{M}'_1 = \alpha (\vec{E} + \vec{E}_1) \quad (2.19)$$

Using eq. (2.18) and eq. (2.19), the potential energy of a vapour molecule becomes.

$$\begin{aligned} U &= -\vec{E}_1 \cdot \vec{M}'_1 \\ &= -\alpha [3\cos^2\theta - 1][(E^2 r_w^3 X^3) + (E^2 r_w^6 X^6)] \end{aligned} \quad (2.20)$$

Where θ is the direction of point (A) with respect to the direction of the electric field. The molecules can have any orientation ranging from 0 to 2π . For simplicity we are replacing $(3\cos^2\theta - 1)$ by its average value

$$\langle 3\cos^2\theta - 1 \rangle = \frac{1}{2\pi} \int_0^{2\pi} (3\cos^2\theta - 1) d\theta = \frac{1}{2}$$

The average potential energy is given by

$$\bar{U} = -\frac{\alpha}{2} [(E^2 r_w^3 / X^3) + E^2 r_w^6 / X^6] \quad (2.21)$$

The negative sign in the expression for the potential energy shows that the potential is attractive and hence there is a flux of water molecules towards the embryo dipole. From the kinetic theory of gases (Engel, 1955) it is assumed that in a non-uniform field, the drift velocity is given by the transformation of potential energy lost in one mean free path into kinetic energy. The loss in potential energy in one mean free path is

$$\bar{U}' = -\frac{\alpha}{2} \left[\left(\frac{E^2 r_w^3}{(X+\lambda)^3} + \frac{E^2 r_w^6}{(X+\lambda)^6} \right) \right] \quad (2.22)$$

Where λ is the mean free path ($\sim 10^{-5}$ cm), from eq. (2.21) and eq. (2.22) substituting $X = r_w$, the change in potential energy is given by

$$d\bar{U} = -(9 \propto \lambda E^2 / 2r_w) \quad (2.23)$$

(i.e. the change in potential energy of a molecule in a transition through a distance λ onto the surface of the embryo of radius r_w)

The corresponding gain in kinetic energy is given by

$$K.E. = \frac{1}{2} m_w v^2 \quad (2.24)$$

Where m_w is the mass of one molecule and v its velocity. From eq. (2.23) and eq. (2.24) one can write from the law of conservation of energy that

$$(9 \propto \lambda E^2 / 2r_w) = \frac{1}{2} m_w v^2$$

Therefore

$$v = (9 \propto \lambda E^2 / m_w r_w)^{1/2} \quad (2.25)$$

The increase in mass (dm_w) of the embryo in time (dt) is

$$\frac{dm_w}{dt} = \rho_v S_n v \quad (2.26)$$

Where S_n is the surface area of the water embryo of radius r_w and ρ_v is the density of the water vapour molecules, from eq. (2.25) and eq. (2.26) we have

$$\frac{dm_w}{dt} = \left(\frac{\rho_v}{\rho_w}\right) \left(\frac{9\alpha\lambda E^2}{m_w r_w}\right)^{1/2} \quad (2.27)$$

Rewriting this in terms of the increase in radius with respect to time, we have

$$\frac{dr_w}{dt} = \left(\frac{\rho_v}{\rho_w}\right) \left(\frac{9\alpha\lambda E^2}{m_w r_w}\right)^{1/2} \quad (2.28)$$

Integrating within the limits $r_w = 0$ to r_w^* (critical radius of nucleus) and $t = 0$ to $t = \tau_N$ (relaxation time), we get

$$r_w^* = [3\rho_v(9\alpha\lambda E^2/m_w)^{1/2}\tau_N/2\rho_w]^{2/3} \quad (2.29)$$

Putting, $\lambda \approx 10^{-5} \text{ cm}$, $\alpha = 5 \times 10^{-23} \text{ cm}^3$, $m_w = 3.0 \times 10^{-23} \text{ gm}$

$\rho_w = 1$ and $\rho_v = 10^{-5} \text{ (at } \sim 10^0 \text{ c)}$ we get

$$r_w^* = (3.18 \times 10^{-7} E \tau_N)^{2/3} \quad (2.30)$$

From eq.(2.30) the relaxation time in the presence of an electric field is,

$$\tau_N = r_w^{*3/2} / 3.18 \times 10^{-7} E \quad (2.31)$$

Thus the relaxation time for the growth of a nucleus in the presence of an electric field varies inversely with the applied electric field. Under the combined effect of an electric field and diffusion the reduced relaxation time τ_{0N} is given by

$$\frac{1}{\tau_{0N}} = \frac{1}{\tau_0} + \frac{1}{\tau_N}$$

$$\tau_{0N} = \frac{\tau_0 \tau_N}{\tau_0 + \tau_N} \quad (2.32)$$

Where τ_0 is the relaxation time in absence of electric field with only diffusion of water vapour molecules.

2.2.2 Ice Nucleation in the presence of an Electric field:

In the atmosphere the water vapour changes its phase via either of following thermodynamic processes

1. Water vapour $\xrightarrow{\text{Condensation}}$ Liquid water.
2. Water vapour $\xrightarrow{\text{deposition}}$ Solid Water (ice)
3. Water vapour $\xrightarrow{\text{Condensation}}$ Liquid water $\xrightarrow{\text{freezing}}$ ice

The process concerned in the present discussion is of type (i) or (ii) only. For the purpose of type (iii) a more rigorous mathematical treatment is required.

The above derivations are applicable equally well to the ice formation from the vapour phase (type iii) by introducing the following replacements

$$\rho_w \rightarrow \rho_v, \sigma_{w/v} \rightarrow \sigma_{i/v}, r_w^* \rightarrow r_i^* \text{ and } S_{v,w} \rightarrow S_{v,i}$$

2.3 DISCUSSION OF THE RESULTS:

In homogeneous nucleation in absence of external electric field Collins (1955) evaluated the relaxation time for the growth of a nucleus is given by eq. (2.13)

$$\tau_0 = 9\pi kT (n_w^*)^{2/3} / \mu_w'^2 \beta_w \sigma_{w/v}$$

In homogeneous nucleation in presence of external electric field taken into account the induced dipole by eq.(2.31)

$$\tau_N = r_w^{*2/3} / 3.18 \times 10^{-7} \cdot E$$

Murino (1979) also, obtained an expression for the drop growth in presence of an electric field without considering dipole contribution. With some manipulations the relaxation time on the bases of Murino's theory can be written as

$$\tau_M = r_w^{*3/2} / 1.8 \times 10^{-7} E \quad (2.33)$$

The relaxation time, in the absence of an electric field, varies directly with the radius of the nucleus, but in the presence of an electric field, it varies as $r_w^{*3/2}$. In the absence of an electric field one can write from eq. (2.14)

$$n_w^* = (r_w^* / 1.958 \times 10^{-8})^3$$

And from eq.(2.15) we get

$$r_w^* = 2\sigma_{w/v} M_w / \rho_w RT \ell n S_{v,w}$$

From eq. (2.6) we have

$$\beta_w = n_1 (kT / 2\pi m_w)^{1/2}$$

Where, n_1 is the concentration of water vapour molecule; k , the Boltzmann constant; T , the temperature of the system. Here

$$n_1 = \frac{\text{n.of molecule}}{\text{unit volume}} = \frac{N}{22.4 \times 10^3} \quad (2.34)$$

Putting the values of $n_w^*, r_w^*, \beta_w, n_1, \mu'_w$ in eq. (2.31) and putting
 $m_w = 3 \times 10^{-23} \text{ gm.}; M_w = 18; N = 6.023 \times 10^{23}; k = 1.38 \times 10^{-16} \text{ erg K}^{-1};$
 $R = 8.317 \times 10^7 \text{ erg K}^{-1} \text{ mole}^{-1}; \mu'_w = 2.1792 \times 10^{-29}.$ We have

$$\tau_0 = 3782.026 \times 10^{-9} \times \frac{\sigma_{w/v}}{\rho_w^2 T^{3/2} (\ell n S_{v,w})^2} \quad (2.35)$$

From eq. (2.35) we can calculate the different values of τ_0 at different σ, ρ, T .

Similarly the values of τ_N and τ_M have been calculated from eq. (2.31) and eq. (2.33) respectively.

The variation of r_w^* and τ_0 with supersaturation ratios are given in table 2.2 to table 2.7. The relaxation time for the formation of critical nucleus in absence of electric field is determined by temperature and supersaturation. Typical values of relaxation time ($\tau_N, \tau_M, \tau_{0N}$) at $E = 2, 4, 6$ e.s.u. are given in table (2.2) to table (2.7) for both water and ice phase in Homogeneous nucleation. Graphs between variation of critical radius and relaxation times with supersaturation ratios and $E = 2, 4, 6$ (e.s.u.) have been plotted from fig. 2.2(a) to fig. 2.2(e iii) at $T=278\text{K}$ for water phase. Similarly for $T=298\text{K}$ graphs are plotted from fig. 2.3(a) to fig. 2.3(e iii). Similarly graphs have been plotted for ice phase also from fig. 2.4(a) to fig. 2.4(e iii) for $T=278\text{K}$ and $E = 2, 4, 6$ e.s.u. and from fig. 2.5 (a) to fig. 2.5 (e iii) for $T=298\text{K}$ and $E=2, 4, 6$ e.s.u.

2.4 CONCLUSION:

In the present study, we have calculated the relaxation time (τ_0) in absence of electric field during homogenous nucleation process. Also, the composition has been made with the relaxation times calculated in

presence of external electric field during these nucleation process using Murino's expression (τ_M) and the expression obtained by eq. (2.31) for τ_N . The reduced relaxation time (τ_{ON}) has also been calculated both for water vapour condensation and ice glaciations as the function of supersaturation. Thus from these results it may be concluded that under the combined effect of external electric field, the droplets and ice crystals are nucleated in very less time. From the tables we conclude that the radius of critical nucleus of embryo is inversely proportional to the applied supersaturation ratios. Thus if supersaturation ratio is increased, small drops of water and ice crystals are formed. Similarly the relaxation times decreases with increase in applied electric field and is inversely proportional to the applied supersaturation ratios.

Table-2.2

Value of Critical radius (r_w^* Å) and relaxation time in water vapour condensation at T=278 K and E= 2, 4, 6 e.s.u. as a function of supersaturation ratio($S_{v,w}$), for homogenous nucleation. Suffix w stands for water phase

S. No.	$S_{v,w}$	r_w^* (Å)	τ_0 (μ Sec.)	E (e.s.u.)	τ_N (μ Sec.)	τ_M (μ Sec.)	τ_{0N} (μ Sec.)
1.	1.005	2340.2765	2456.9510	2	178009.6918	314483.7889	105396.6620
				4	89004.8459	157241.8945	66200.4469
				6	59336.5640	104827.9296	48254.8399
2.	1.01	1173.0491	617.2975	2	63170.9126	111601.9456	42460.2256
				4	31585.4563	55800.9728	25392.6186
				6	21056.9709	37200.6485	18112.1379
3.	1.05	239.2332	25.6747	2	5818.0174	10278.4974	4767.7928
				4	2909.0087	5139.2487	2620.4042
				6	1939.3391	3426.1658	1806.6835
4.	1.5	28.7873	0.3718	2	242.8528	429.0400	225.6136
				4	121.4264	214.5200	116.9580
				6	80.9509	143.0133	78.9403
5.	2	16.8395	0.1272	2	108.6514	191.9508	102.6523
				4	54.3257	95.9754	52.7833
				6	36.2171	63.9836	35.5251
6.	3	10.6245	0.0506	2	54.4511	96.1970	52.0356
				4	27.2256	48.0985	26.6080
				6	18.1504	32.0657	17.8738
7.	3.05	10.4670	0.0491	2	53.2449	94.0661	50.8997
				4	26.6225	47.0330	26.0230
				6	17.7483	31.3554	17.4799

Table-2.3

Value of Critical radius (r_w^* Å) and relaxation time in water vapour condensation at T=288 K and E= 2, 4, 6 e.s.u. as a function of supersaturation ratio($S_{v,w}$), for homogenous nucleation. Suffix w stands for water phase

S. No.	$S_{v,w}$	r_w^* (Å)	τ_0 (μ Sec.)	E (e.s.u.)	τ_N (μ Sec.)	τ_M (μ Sec.)	τ_{0N} (μ Sec.)
1.	1.005	2221.7324	2293.6307	2	164657.1213	290894.2476	100567.9930
				4	82328.5606	145447.1238	62434.6465
				6	54885.7071	96964.7492	45269.4048
2.	1.01	1113.6296	576.2640	2	58432.4399	103230.6438	40265.4886
				4	29216.2200	51615.3219	23838.5018
				6	19477.4800	34410.2146	16931.1520
3.	1.05	227.1151	23.9680	2	5381.60582	9507.5036	4470.6935
				4	2690.8029	4753.7518	2442.0198
				6	1793.8686	3169.1679	1679.7823
4.	1.5	27.3291	0.3470	2	224.6364	396.8576	209.8074
				4	112.3182	198.4288	108.4849
				6	74.8788	132.2859	73.1553
5.	2	15.9865	0.1188	2	100.5014	177.5525	95.3472
				4	50.2507	88.7762	48.9282
				6	33.5005	59.1842	32.9075
6.	3	10.0863	0.0473	2	50.3667	88.9812	48.2931
				4	25.1834	44.4906	24.6541
				6	16.7889	29.6604	16.5520
7.	3.05	9.9368	0.0459	2	49.2510	87.0101	47.2378
				4	24.6255	43.5051	24.1117
				6	16.4170	29.0034	16.1871

Table-2.4

Value of Critical radius (r_w^* Å) and relaxation time in water vapour condensation at T=298 K and E= 2, 4, 6 e.s.u. as a function of supersaturation ratio($S_{v,w}$), for homogenous nucleation. Suffix w stands for water phase

S. No.	$S_{v,w}$	r_w^* (Å)	τ_0 (μ Sec.)	E (e.s.u.)	τ_N (μ Sec.)	τ_M (μ Sec.)	τ_{0N} (μ Sec.)
1.	1.005	2104.8292	2140.5773	2	151833.7055	268239.5376	95634.7698
				4	75916.8503	134119.7688	58676.4891
				6	50611.2335	89413.1792	42321.3170
2.	1.01	1055.0326	537.8101	2	53881.7484	95191.0888	38050.9649
				4	26940.8742	47595.5444	22301.6644
				6	17960.5828	31730.3630	15773.1536
3.	1.05	215.1647	22.3686	2	4962.4888	8767.0636	4177.5877
				4	2481.2444	4383.5318	2268.1684
				6	1654.1629	2922.3545	1556.6718
4.	1.5	25.8911	0.3239	2	207.1418	365.9505	194.4674
				4	103.5709	182.9753	100.3023
				6	69.0473	121.9835	67.5791
5.	2	15.1453	0.1108	2	92.6744	163.7248	88.2742
				4	46.3372	81.8624	45.2104
				6	30.8915	54.5749	30.3866
6.	3	9.5556	0.0441	2	46.4442	82.0514	44.6753
				4	23.2221	41.0257	22.7713
				6	15.4814	27.3505	15.2797
7.	3.05	9.4140	0.0428	2	45.4154	80.2338	43.6981
				4	22.7077	40.1169	22.2701
				6	15.1385	26.7446	14.9427

Table-2.5

Value of Critical radius (r_i^*) and relaxation time in ice deposition at $T=278$ K and $E= 2, 4, 6$ e.s.u. as a function of supersaturation ratio($S_{v,i}$), for homogenous nucleation. Suffix i stands for ice phase

S. No.	$S_{v,i}$	$r_i^*(\text{\AA})$	τ_0 ($\mu\text{Sec.}$)	E (e.s.u.)	τ_N ($\mu\text{Sec.}$)	τ_M ($\mu\text{Sec.}$)	τ_{0N} ($\mu\text{Sec.}$)
1.	1.005	3676.3958	4208.8848	2	350490.5271	619199.9000	153685.9000
				4	175245.2635	309600.0000	106838.5000
				6	116830.1757	206400.0000	81879.5100
2.	1.01	1842.7706	1057.4627	2	124379.7808	219737.6000	65235.7000
				4	62189.8904	109868.8000	42791.8700
				6	41459.9260	73245.8700	31838.2000
3.	1.05	375.8171	43.9821	2	11455.3312	20237.7500	8127.6400
				4	5727.6656	10118.8800	4754.3760
				6	3818.4437	6745.9170	3359.8970
4.	1.5	45.2226	0.6368	2	478.1629	844.7544	418.6970
				4	239.0814	422.3772	223.2292
				6	159.3876	281.5848	152.1830
5.	2	26.4535	0.2179	2	213.9281	377.9397	192.9670
				4	106.9641	188.9698	101.4538
				6	71.3094	125.9799	68.8176
6.	3	16.6903	0.0867	2	107.2110	189.4061	98.6953
				4	53.6055	94.7031	51.3885
				6	35.7370	63.1354	34.7379
7.	3.05	16.4429	0.0842	2	104.8361	185.2105	96.5662
				4	52.4181	92.6053	50.2657
				6	34.9454	61.7368	33.9755

Table-2.6

Value of Critical radius (r_i^* Å) and relaxation time in ice deposition at $T=288$ K and $E= 2, 4, 6$ e.s.u. as a function of supersaturation ratio ($S_{v,i}$), for homogenous nucleation. Suffix i stands for ice phase

S. No.	$S_{v,i}$	r_i^* (Å)	τ_0 (μ Sec.)	E (e.s.u.)	τ_N (μ Sec.)	τ_M (μ Sec.)	τ_{0N} (μ Sec.)
1.	1.005	3505.9873	3943.4947	2	326406.1904	576650.9000	148869.3000
				4	163203.0952	288325.5000	102239.3000
				6	108802.0635	192217.0000	77853.5000
2.	1.01	1751.3543	990.7846	2	115832.8893	204638.1000	62805.1300
				4	57916.4447	102319.1000	40724.2500
				6	38610.9631	68212.7000	30130.9000
3.	1.05	358.3972	41.2088	2	10668.1657	18847.0900	7723.3090
				4	5334.0828	9423.5460	4479.9860
				6	3556.0552	6282.3640	3155.0540
4.	1.5	43.1264	0.5967	2	445.3054	786.7062	393.2867
				4	222.6527	393.3531	208.8418
				6	148.4351	262.2354	142.1671
5.	2	25.2273	0.2042	2	199.2278	351.9691	180.9252
				4	99.6139	175.9846	94.8180
				6	66.4093	117.3230	64.2430
6.	3	15.9167	0.0813	2	99.8439	176.3909	92.4178
				4	49.9219	88.1954	47.9937
				6	33.2813	58.7970	32.4131
7.	3.05	15.6808	0.0789	2	97.6322	172.4836	90.4207
				4	48.8161	86.2418	46.9441
				6	32.5441	57.4945	31.7013

Table-2.7

Value of Critical radius (r_i^*) and relaxation time in ice deposition at $T=298$ K and $E= 2, 4, 6$ e.s.u. as a function of supersaturation ratio($S_{v,i}$), for homogenous nucleation. Suffix i stands for ice phase

S. No.	$S_{v,i}$	r_i^* (Å)	τ_0 (μ Sec.)	E (e.s.u.)	τ_N (μ Sec.)	τ_M (μ Sec.)	τ_{0N} (μ Sec.)
1.	1.005	3337.4799	3690.4361	2	303159.2778	535581.4000	143838.7000
				4	151579.6389	267790.7000	97553.1000
				6	101053.0926	178527.1000	73803.8800
2.	1.01	1672.8910	927.2049	2	107583.1774	190063.6000	60298.0900
				4	53791.5887	95031.8100	38640.7600
				6	35861.0591	63354.5400	28429.6500
3.	1.05	341.1716	38.5644	2	9908.3703	17504.7900	7317.1020
				4	4954.1852	8752.3940	4208.9160
				6	3302.7901	5834.9290	2954.0730
4.	1.5	41.0536	0.5584	2	413.5904	730.6763	368.3410
				4	206.7952	365.3382	194.8282
				6	137.8635	243.5588	132.4402
5.	2	24.0148	0.1911	2	185.0387	326.9016	169.1463
				4	92.5193	163.4508	88.3680
				6	61.6796	108.9672	59.8065
6.	3	15.1517	0.0761	2	92.7329	163.8282	86.2928
				4	46.3665	81.9141	44.6985
				6	30.9110	54.6094	30.1607
7.	3.05	14.9271	0.0738	2	90.6788	160.1992	84.4250
				4	45.3394	80.0996	43.7201
				6	30.2263	53.3997	29.4979

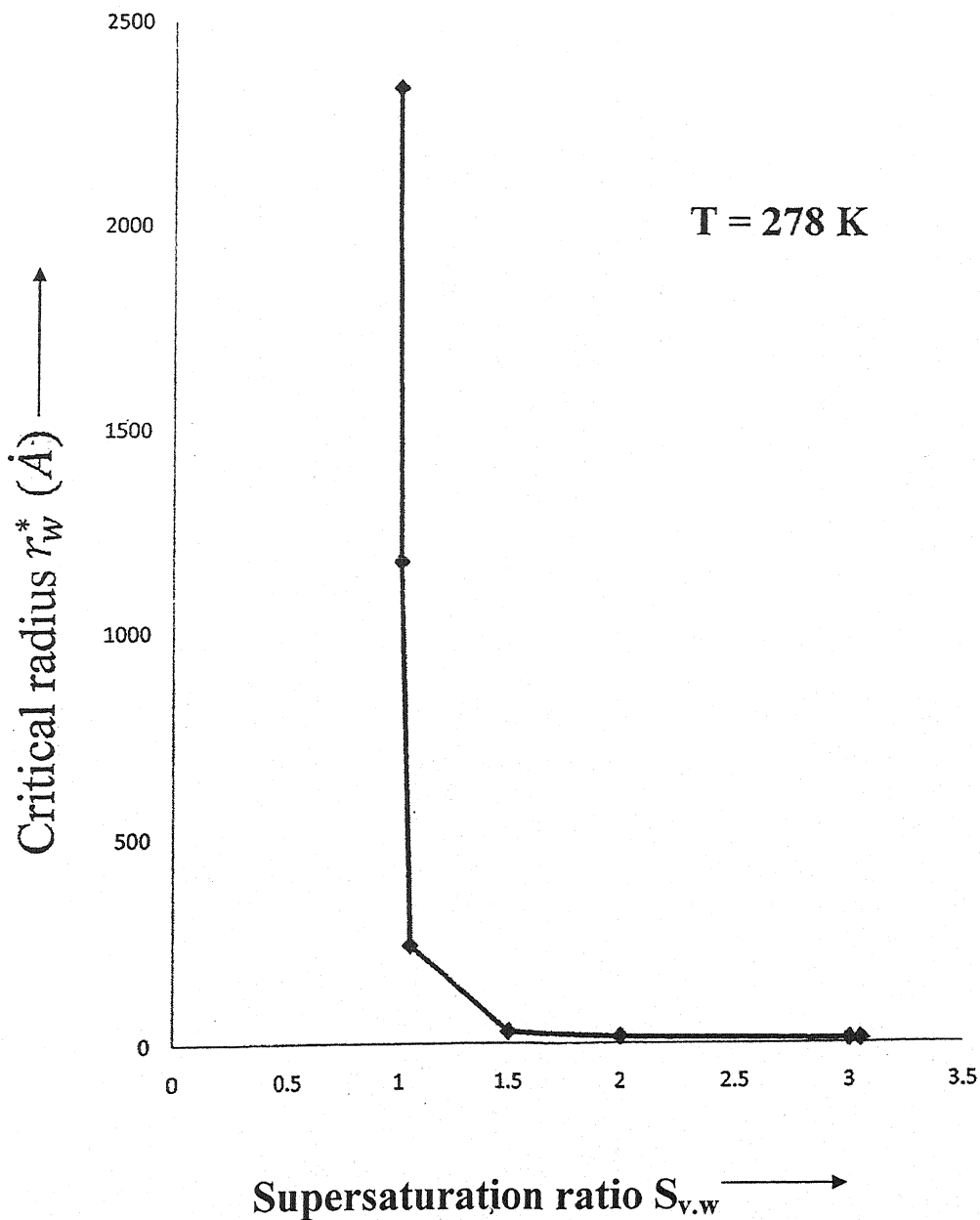


fig. 2.2 (a) variation of critical radius of water molecule r_w^* (Å) with supersaturation ratio $S_{v,w}$ at $T=278\text{K}$.

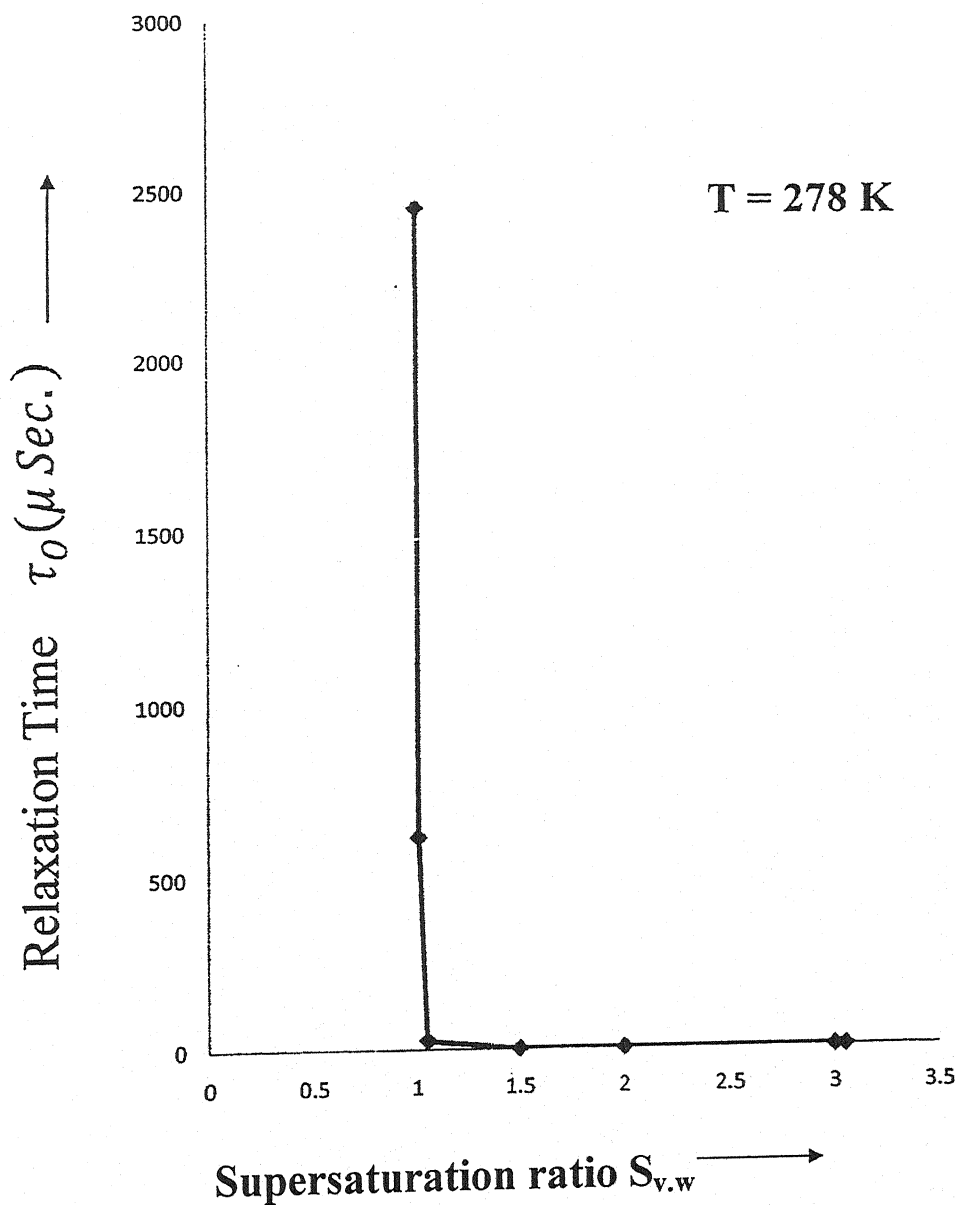


fig. 2.2 (b) Variation of Calculated relaxation time $\tau_0 (\mu \text{ Sec.})$ with supersaturation ratio $S_{v,w}$ at $T=278\text{K}$.

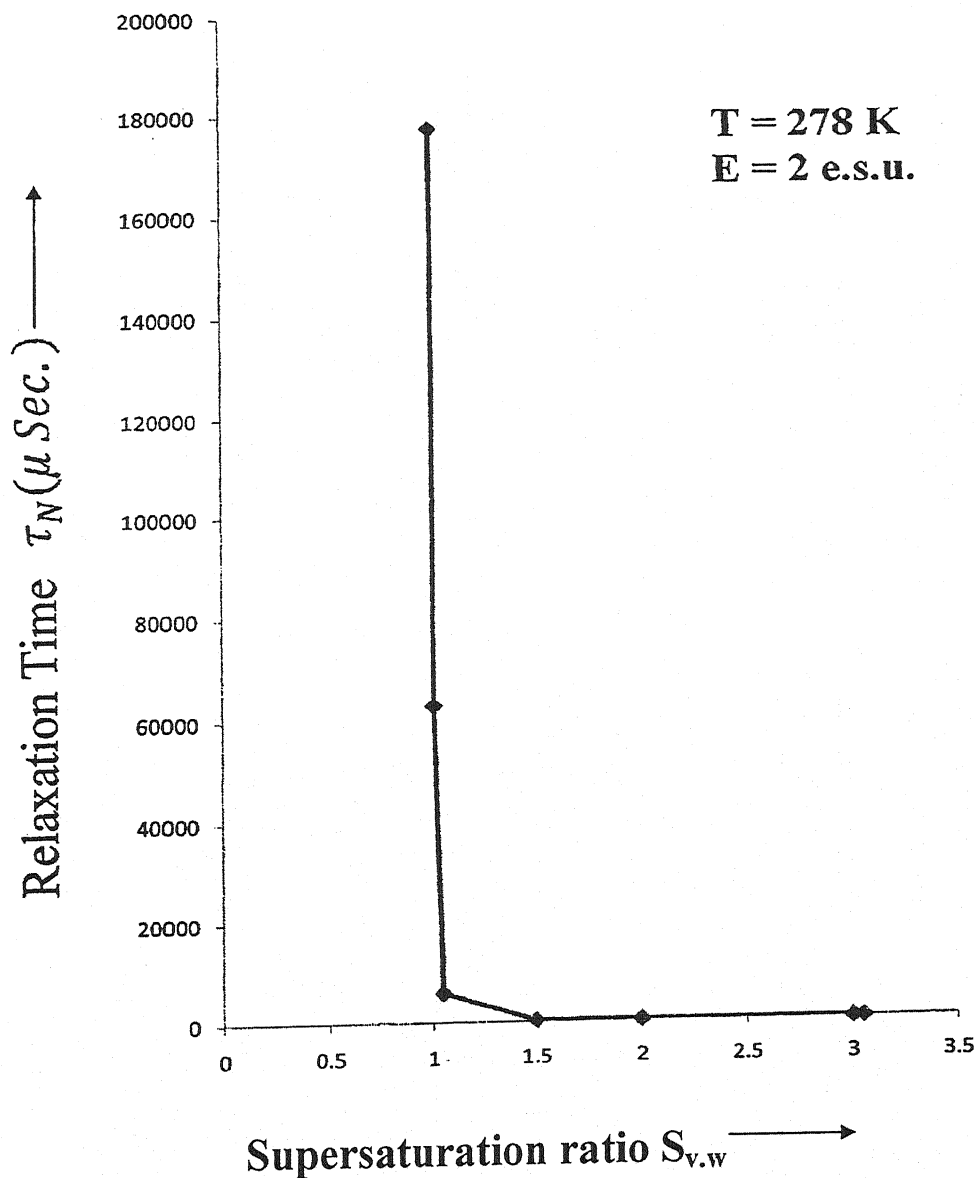


fig. 2.2 (c-I) Variation of relaxation time τ_N (μ Sec.) with supersaturation ratio $S_{v,w}$ at $T=278$ K and $E=2$ e.s.u.

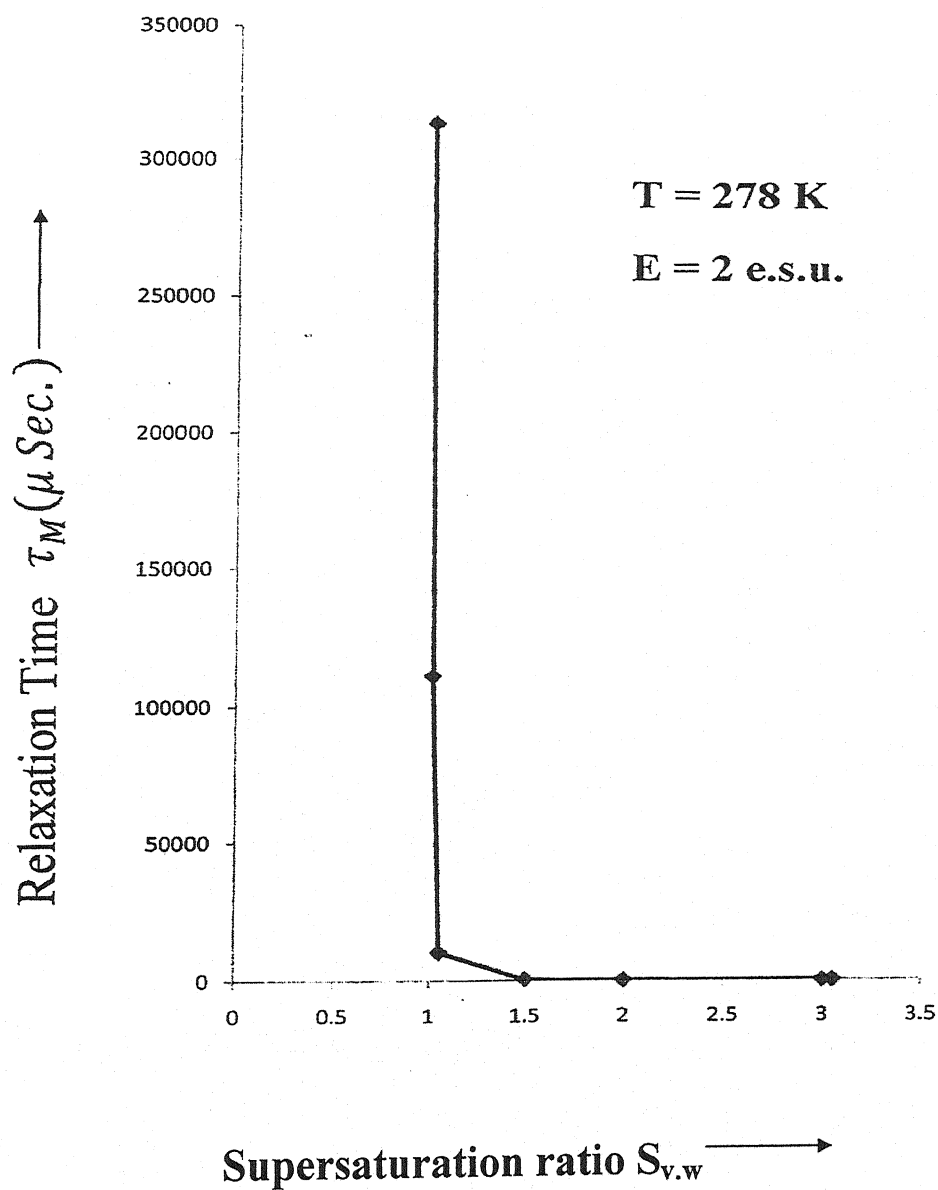


fig. 2.2 (d-I) Variation of relaxation time τ_M (μ Sec.) with supersaturation ratio $S_{v,w}$ at $T=278\text{K}$ and $E=2 \text{ e.s.u.}$

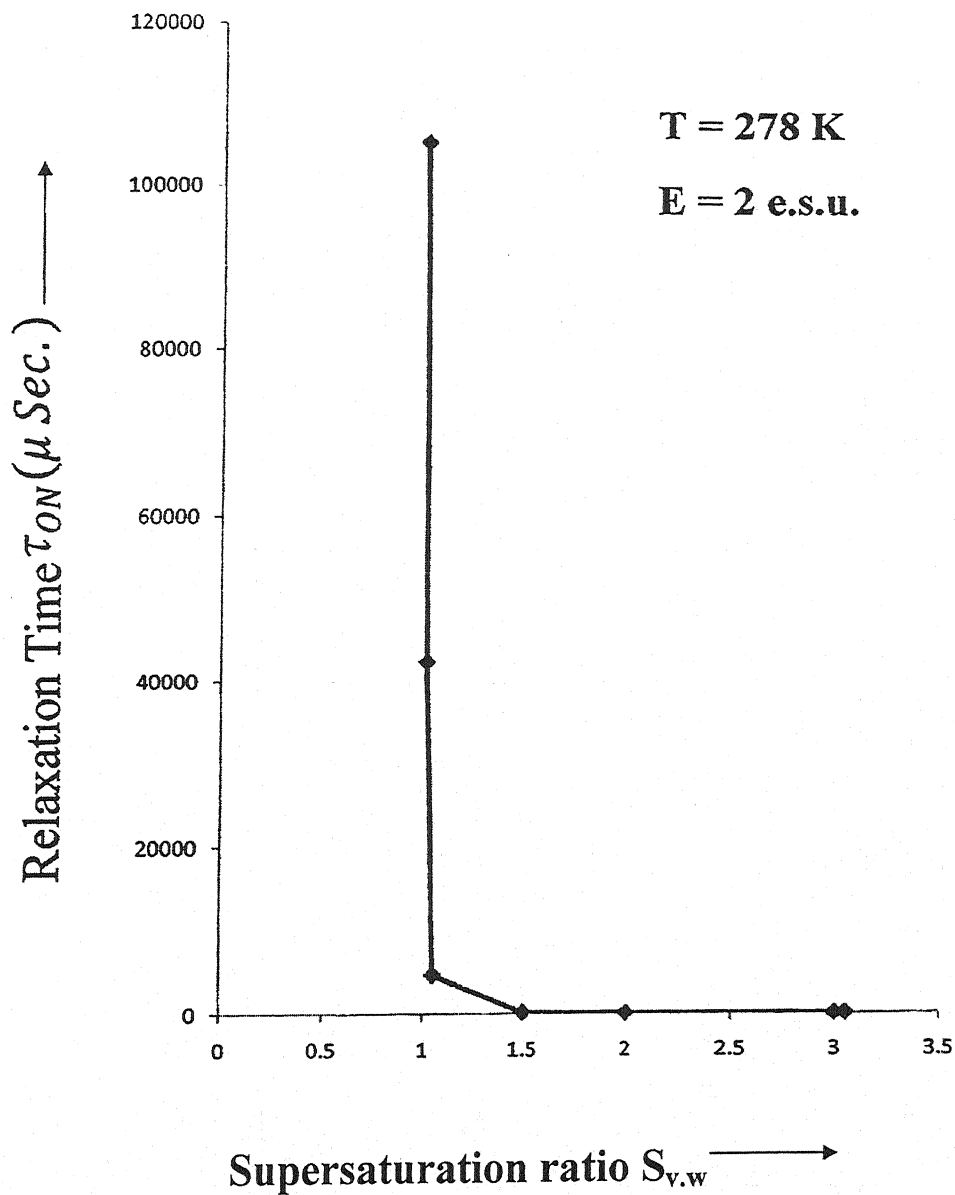


fig. 2.2 (e-I) Variation of relaxation time $\tau_{ON} (\mu \text{ Sec.})$ with supersaturation ratio $S_{v,w}$ at $T=278\text{K}$ and $E=2 \text{ e.s.u.}$

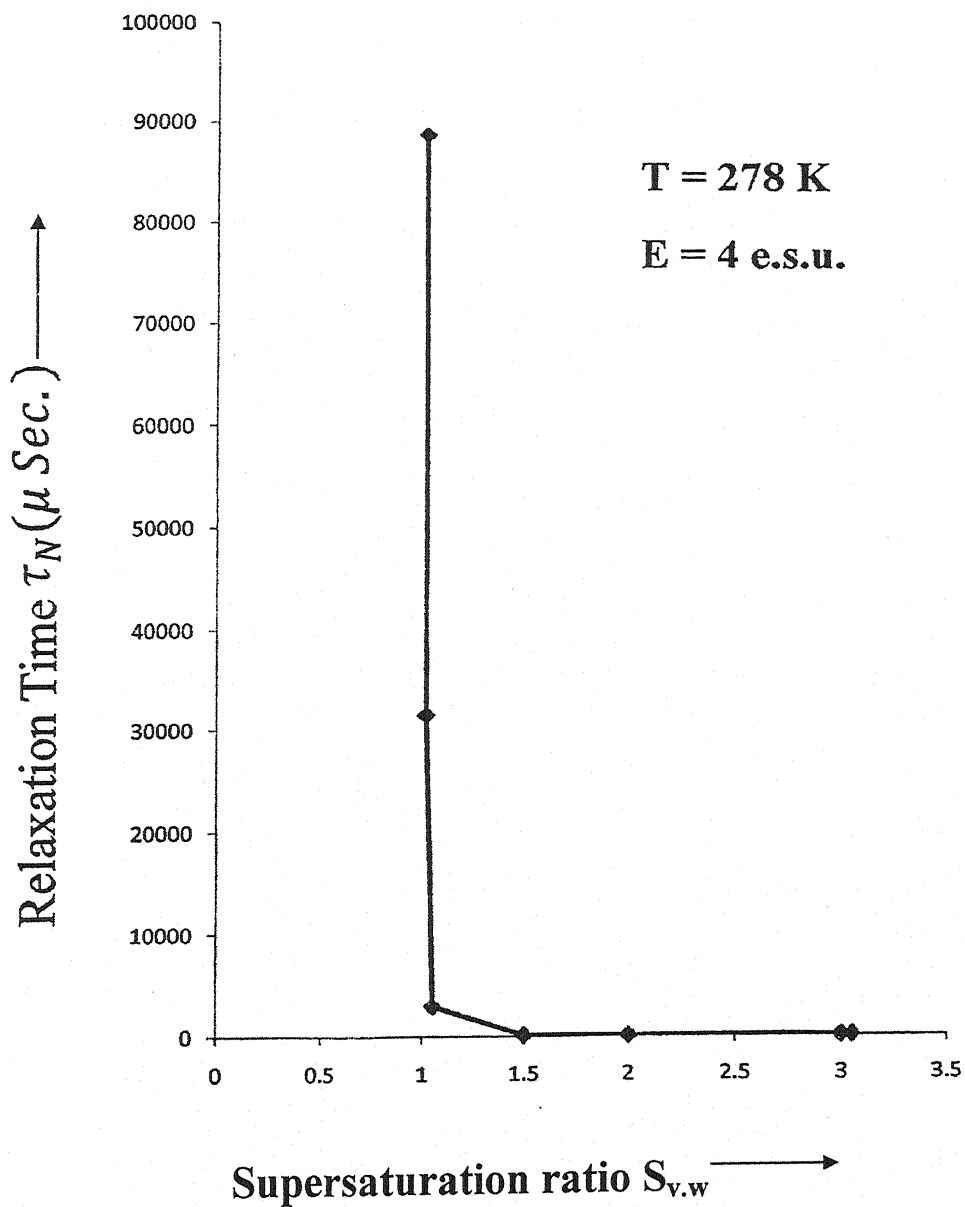


fig. 2.2 (c-II) Variation of relaxation time τ_N (μ Sec.) with supersaturation ratio $S_{v,w}$ at $T=278$ K and $E=4$ e.s.u.

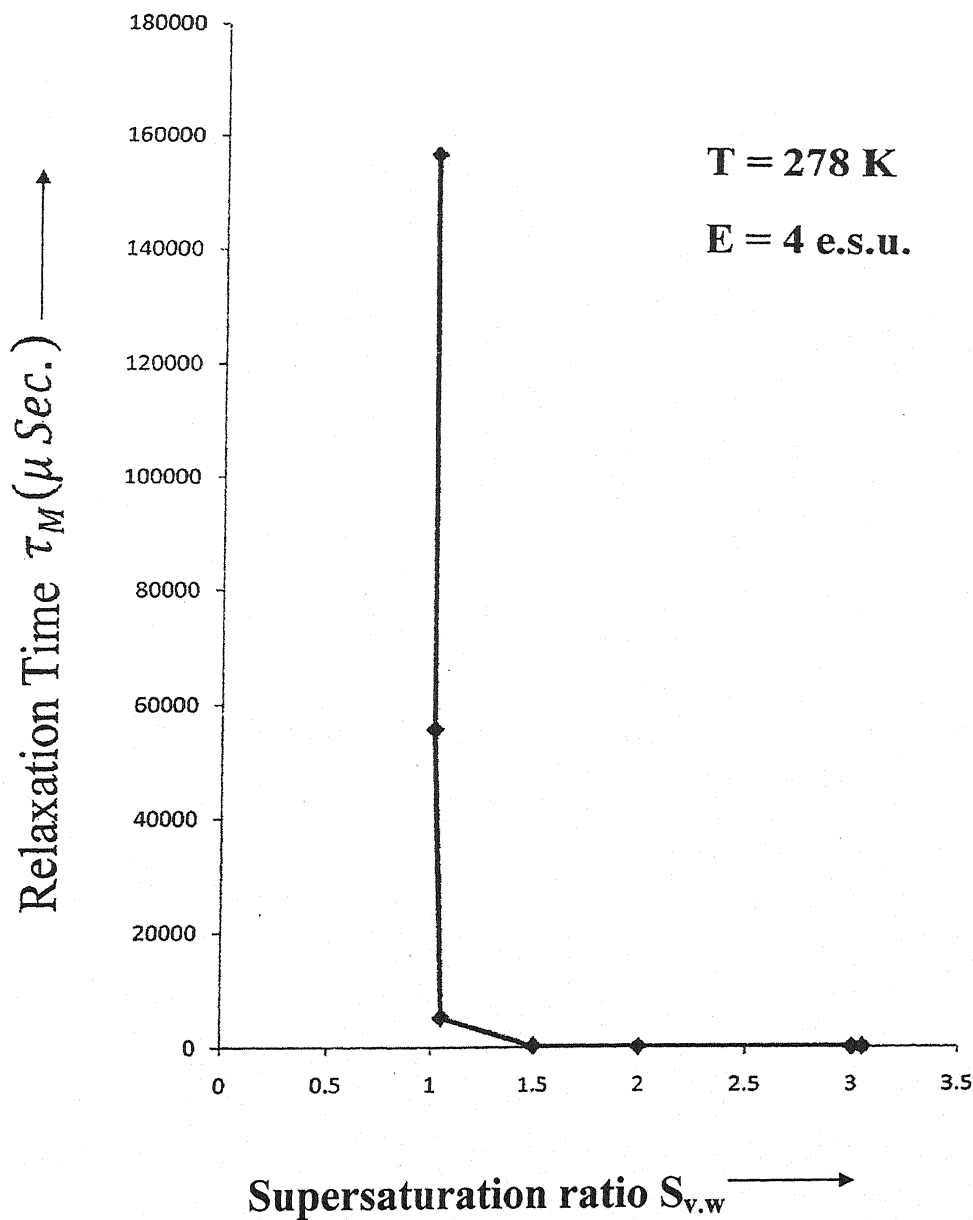


fig. 2.2 (d-II) Variation of relaxation time τ_M (μ Sec.) with supersaturation ratio $S_{v,w}$ at $T=278$ K and $E=4$ e.s.u.

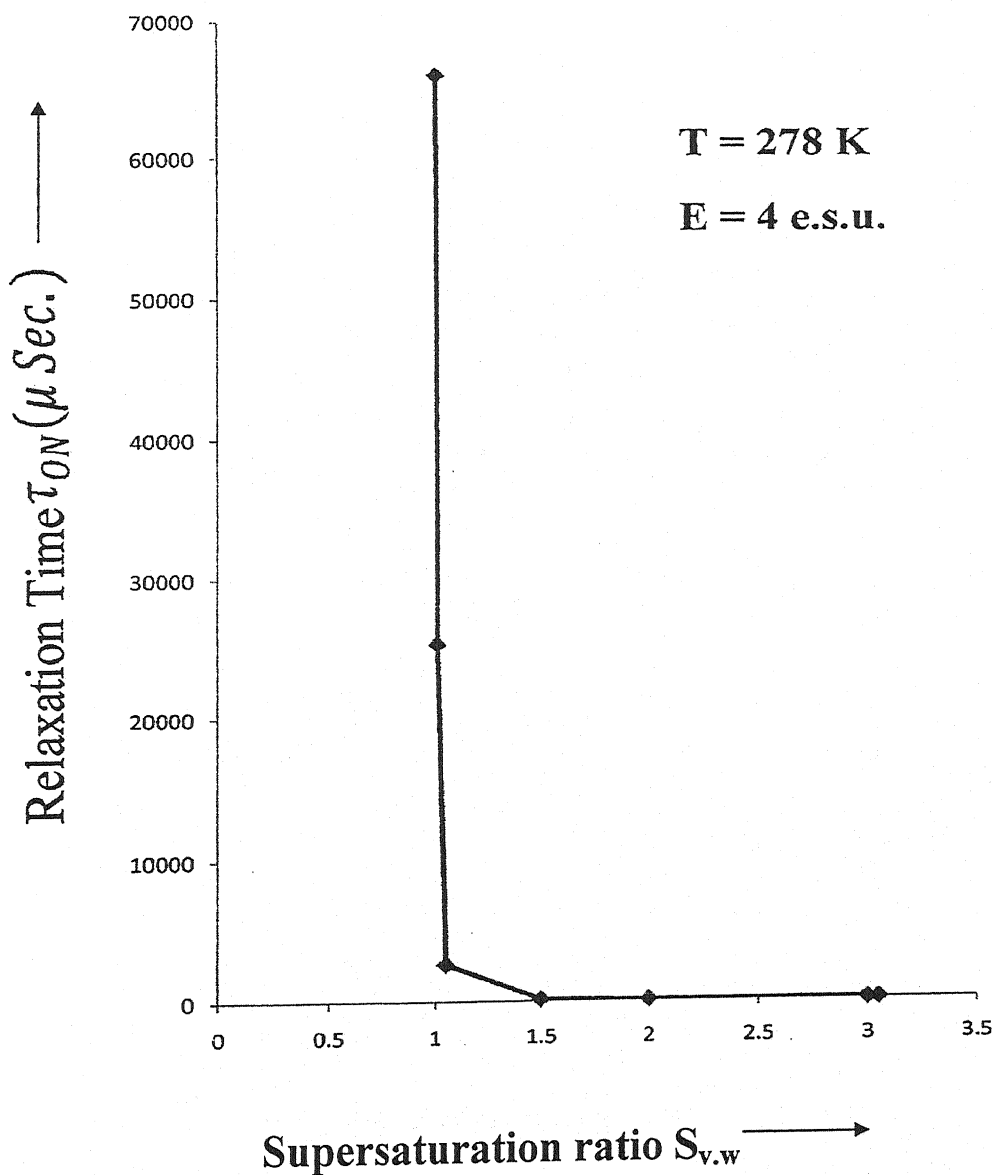


fig. 2.2 (e-II) Variation of relaxation time τ_{ON} (μ Sec.) with supersaturation ratio $S_{v,w}$ at $T=278$ K and $E=4$ e.s.u.

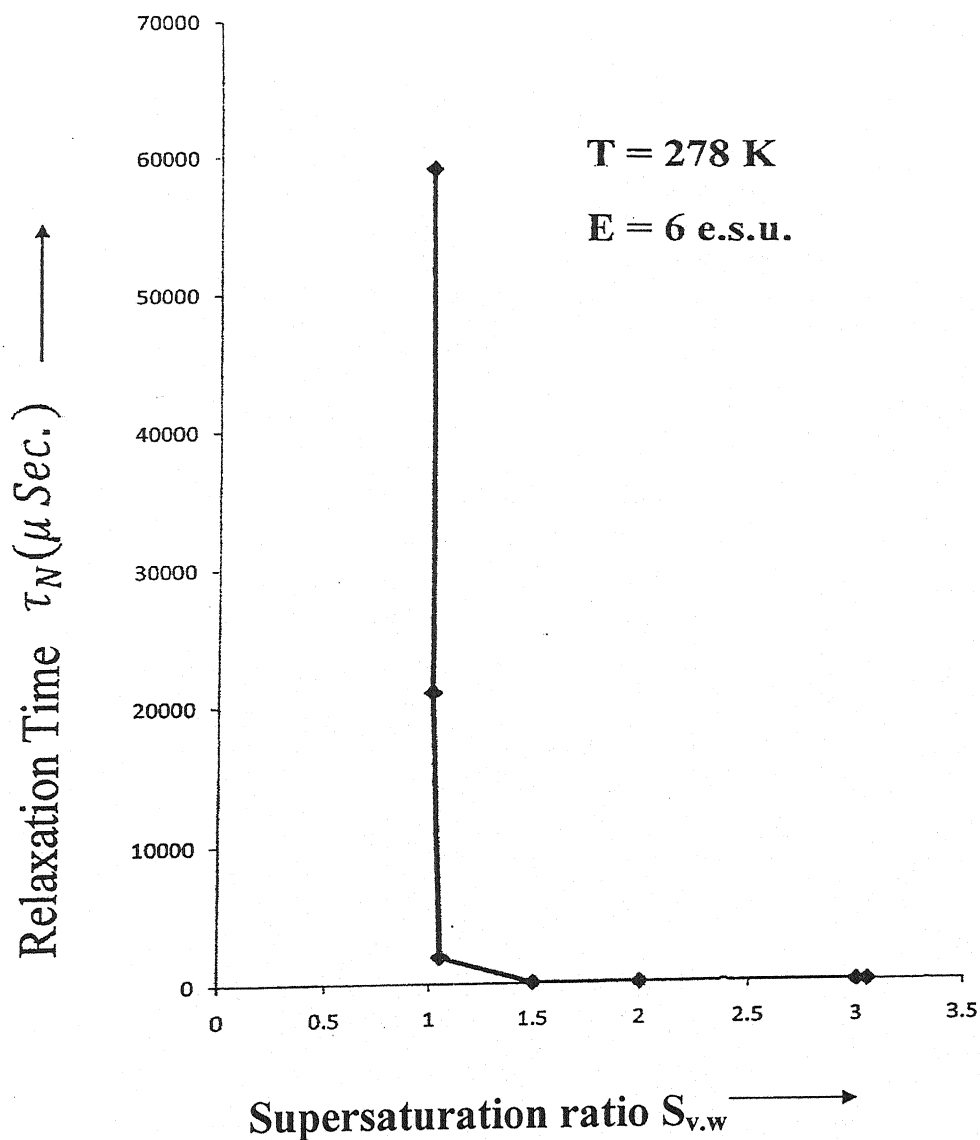


fig. 2.2 (c-III) Variation of relaxation time τ_N (μ Sec.) with supersaturation ratio $S_{v,w}$ at $T=278$ K and $E=6$ e.s.u.

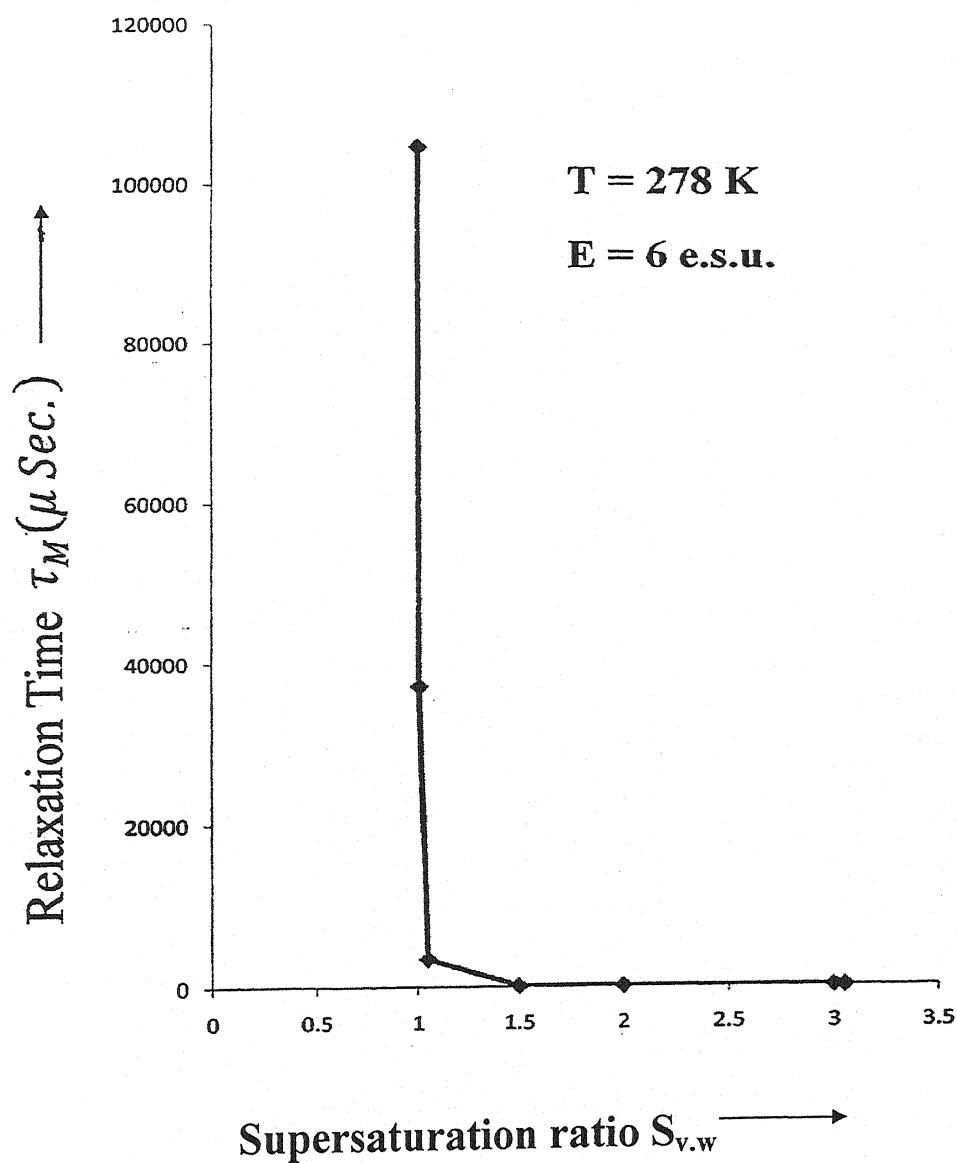


fig. 2.2 (d-III) Variation of relaxation time τ_M (μ Sec.) with supersaturation ratio $S_{v,w}$ at $T=278\text{K}$ and $E=6 \text{ e.s.u.}$

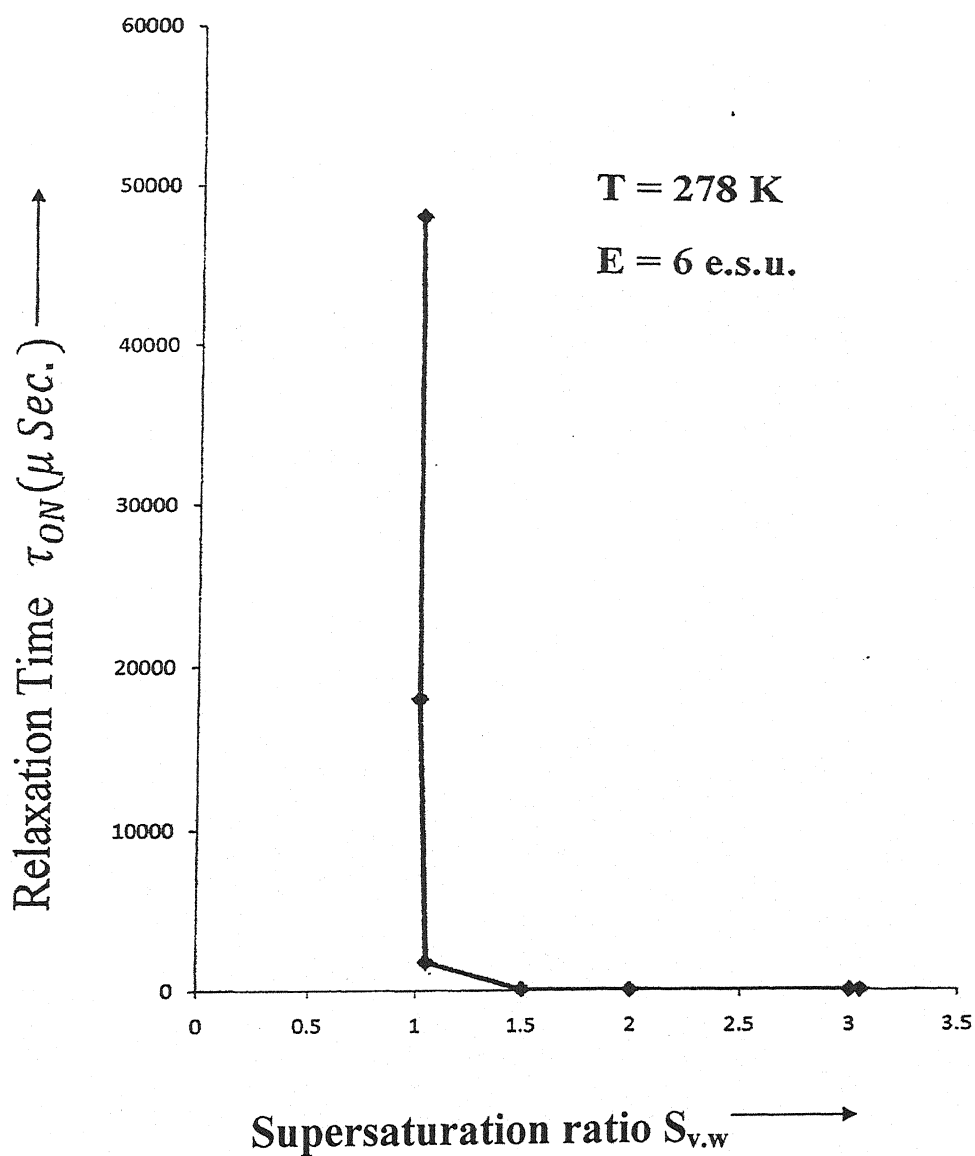


fig. 2.2 (e-III) Variation of relaxation time τ_{ON} (μ Sec.) with supersaturation ratio $S_{v,w}$ at $T=278K$ and $E=6$ e.s.u.

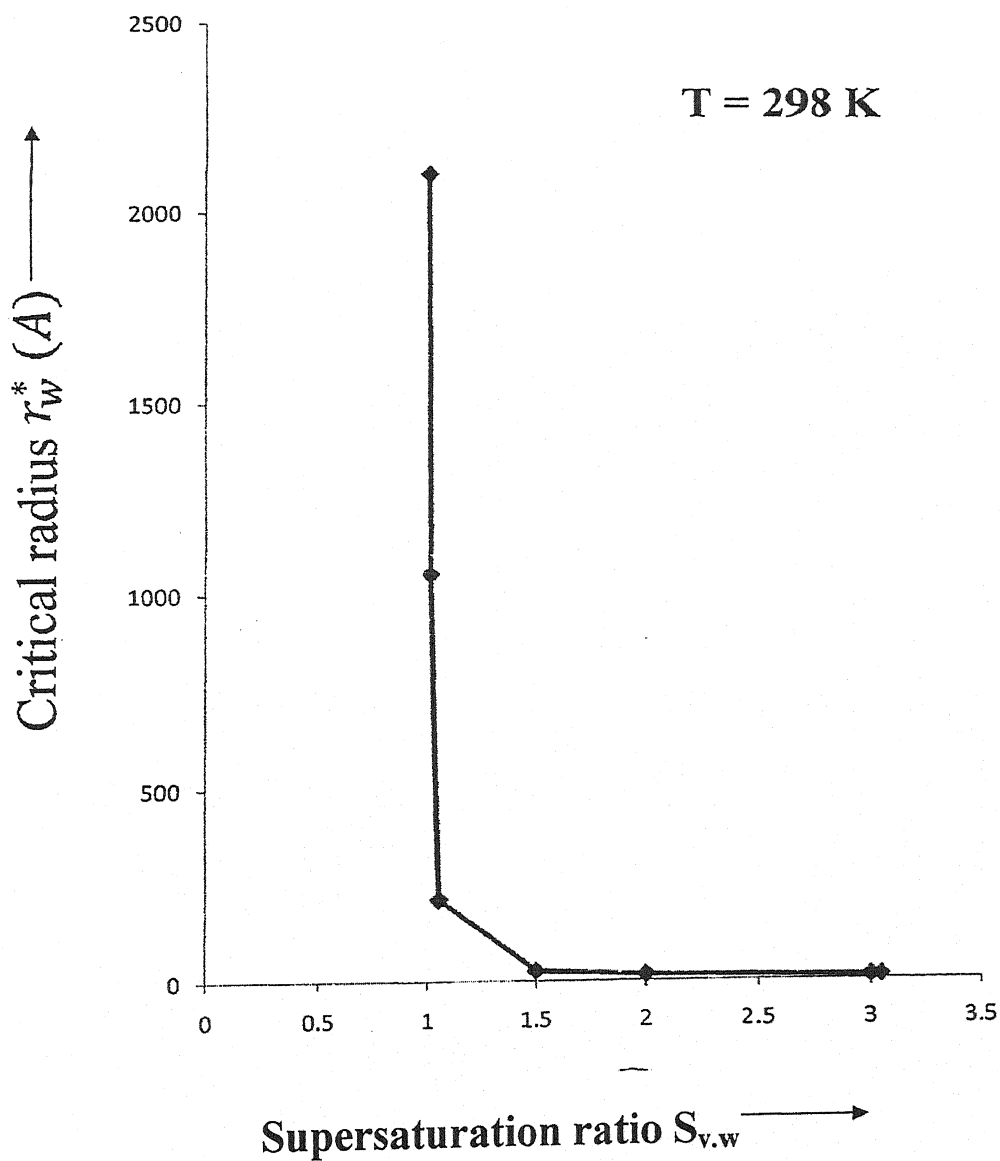


fig. 2.3 (a) Variation of critical radius of water molecule $r_w^* (\text{\AA})$ with supersaturation ratio $S_{v,w}$ at $T=298\text{K}$.

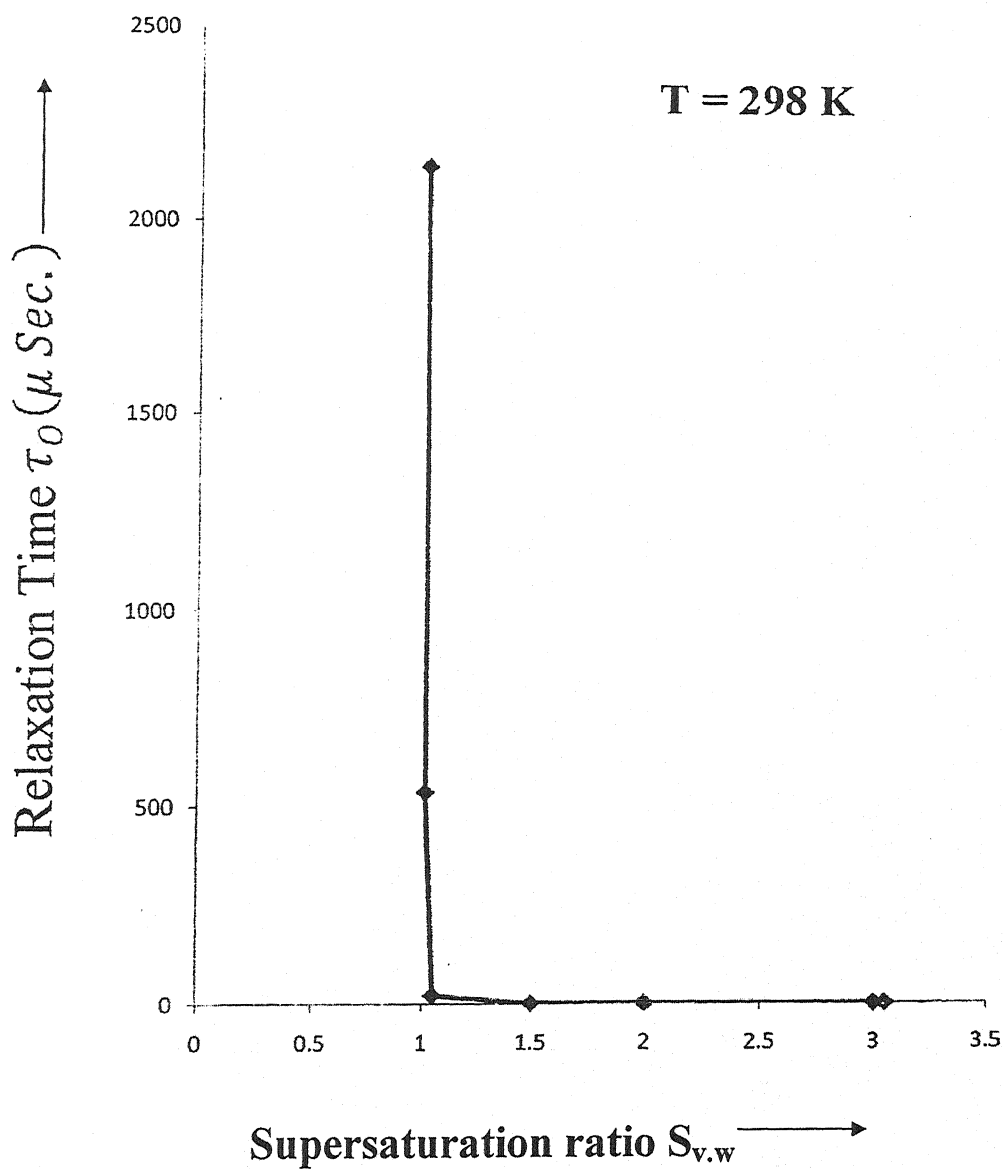


fig. 2.3 (b) Variation of Calculated relaxation time τ_0 ($\mu \text{ Sec.}$) with supersaturation ratio $S_{v,w}$ at $T=298\text{K}$.

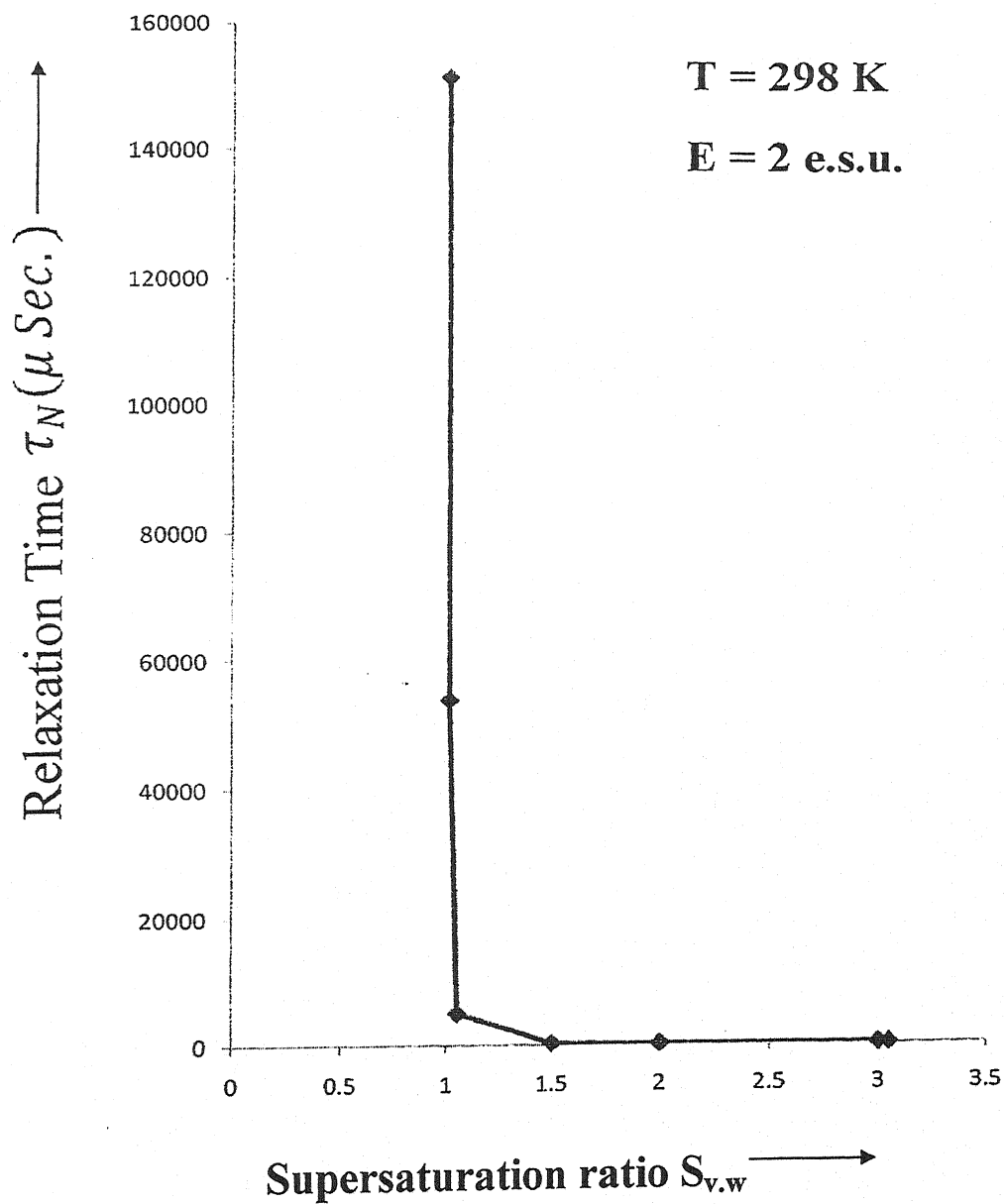


fig. 2.3 (c-I) Variation of relaxation time τ_N (μ Sec.) with supersaturation ratio $S_{v,w}$ at $T=298$ K and $E=2$ e.s.u.

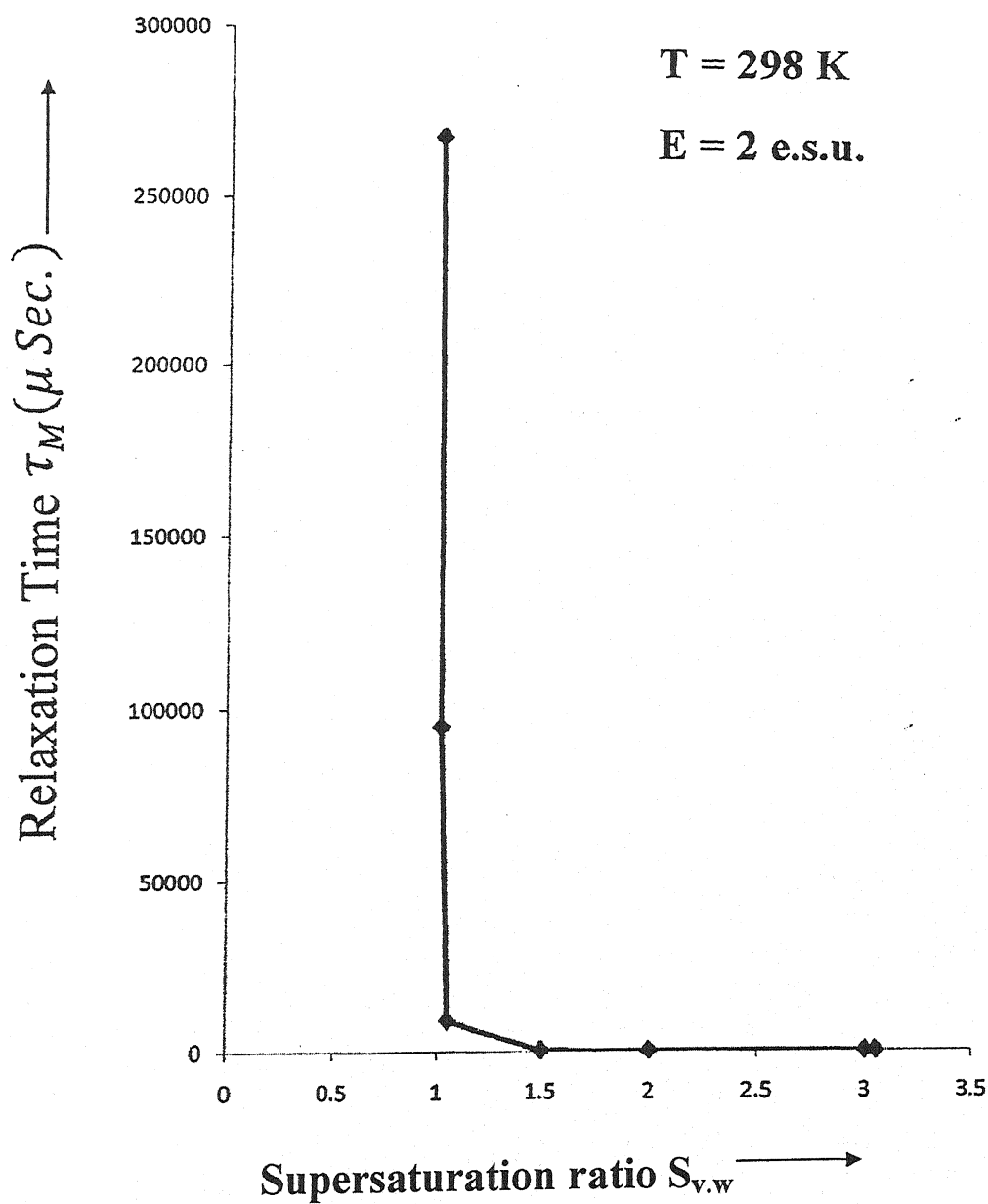


fig. 2.3 (d-I) Variation of relaxation time $\tau_M (\mu \text{ Sec.})$ with supersaturation ratio $S_{v,w}$ at $T=298\text{K}$ and $E=2 \text{ e.s.u.}$

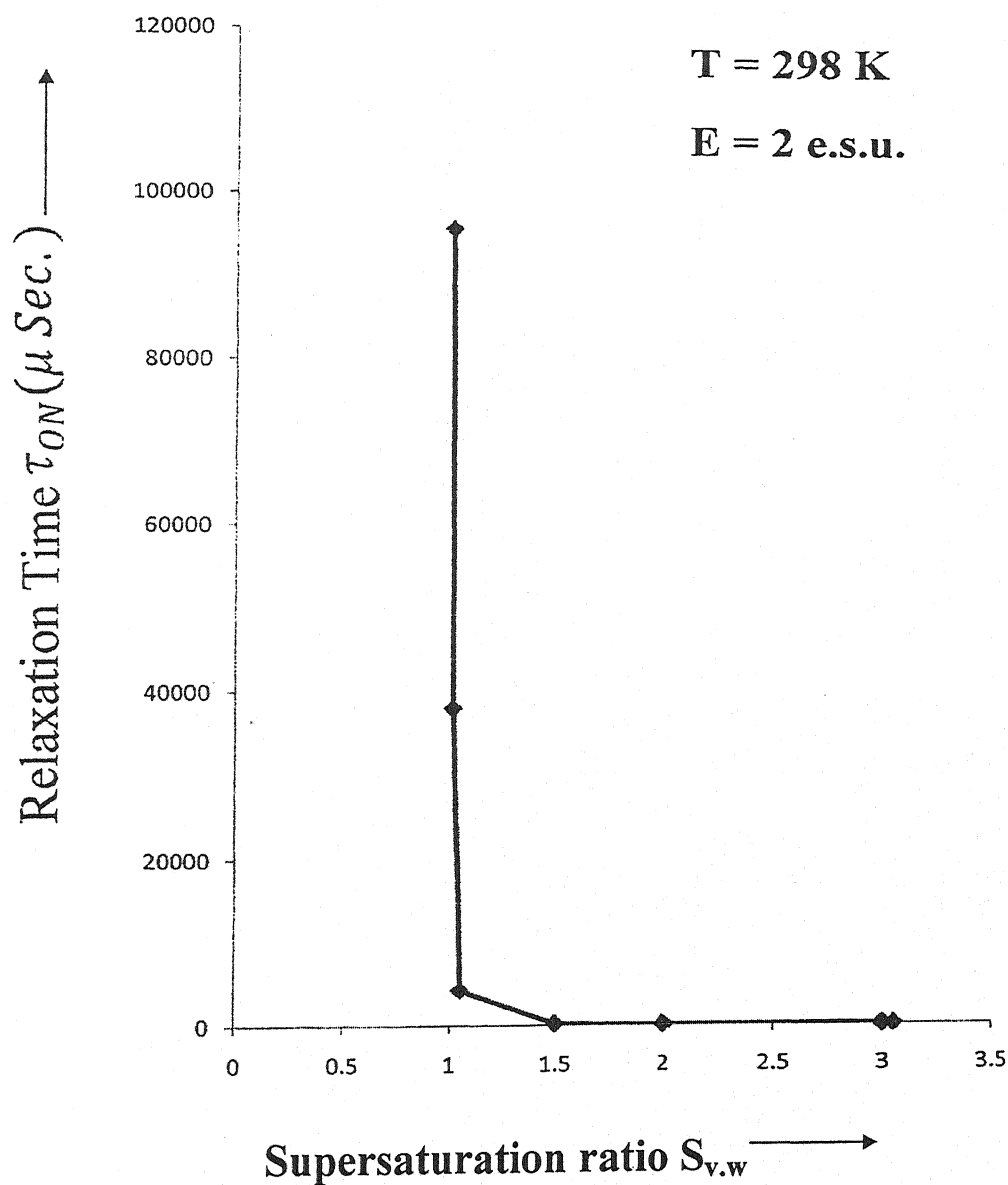


fig. 2.3 (e-I) Variation of relaxation time $\tau_{ON} (\mu \text{ Sec.})$ with supersaturation ratio $S_{v,w}$ at $T=298\text{K}$ and $E=2 \text{ e.s.u.}$

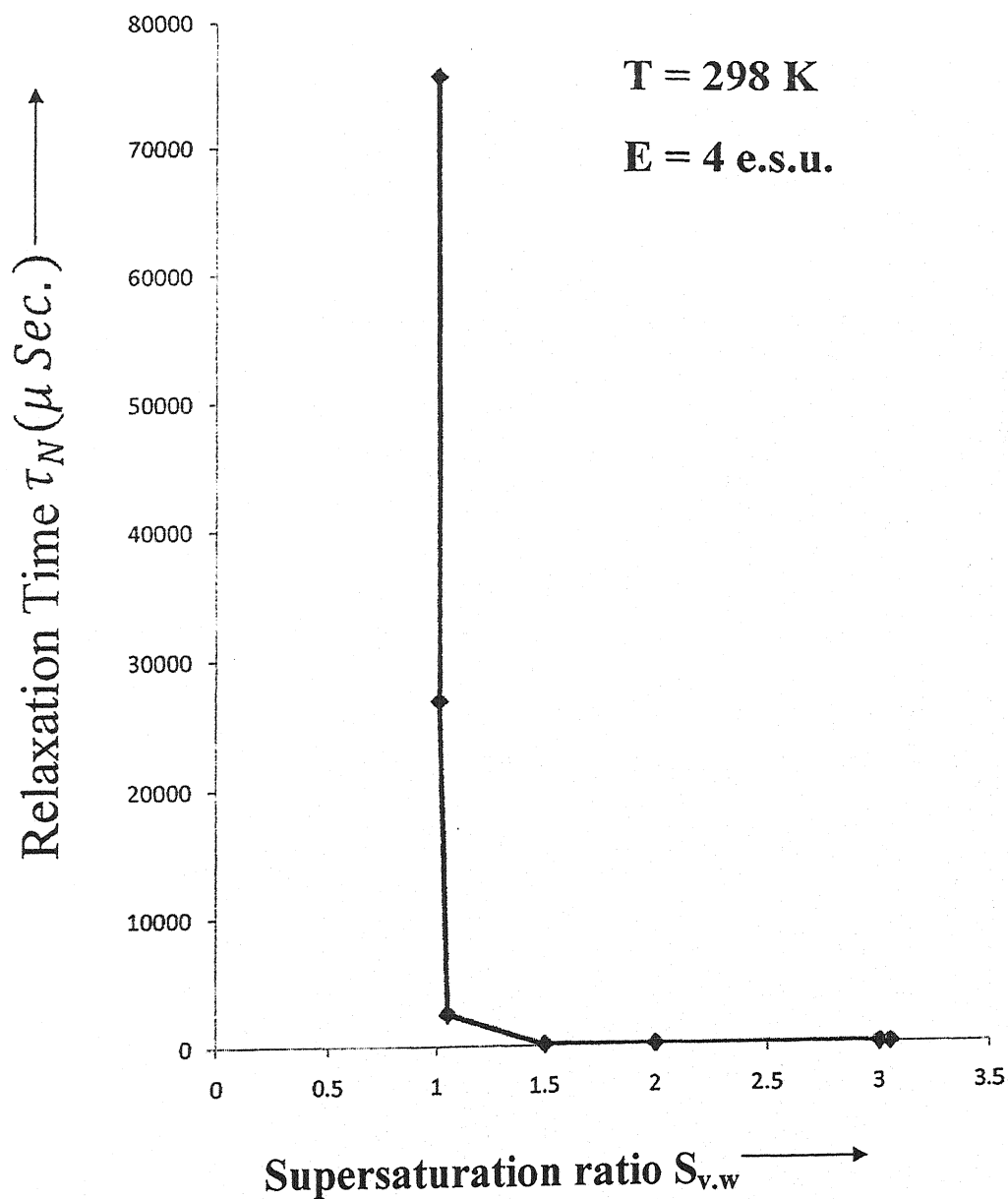


fig. 2.3 (c-II) Variation of relaxation time $\tau_N (\mu \text{ Sec.})$ with supersaturation ratio $S_{v,w}$ at $T=298\text{K}$ and $E=4 \text{ e.s.u.}$

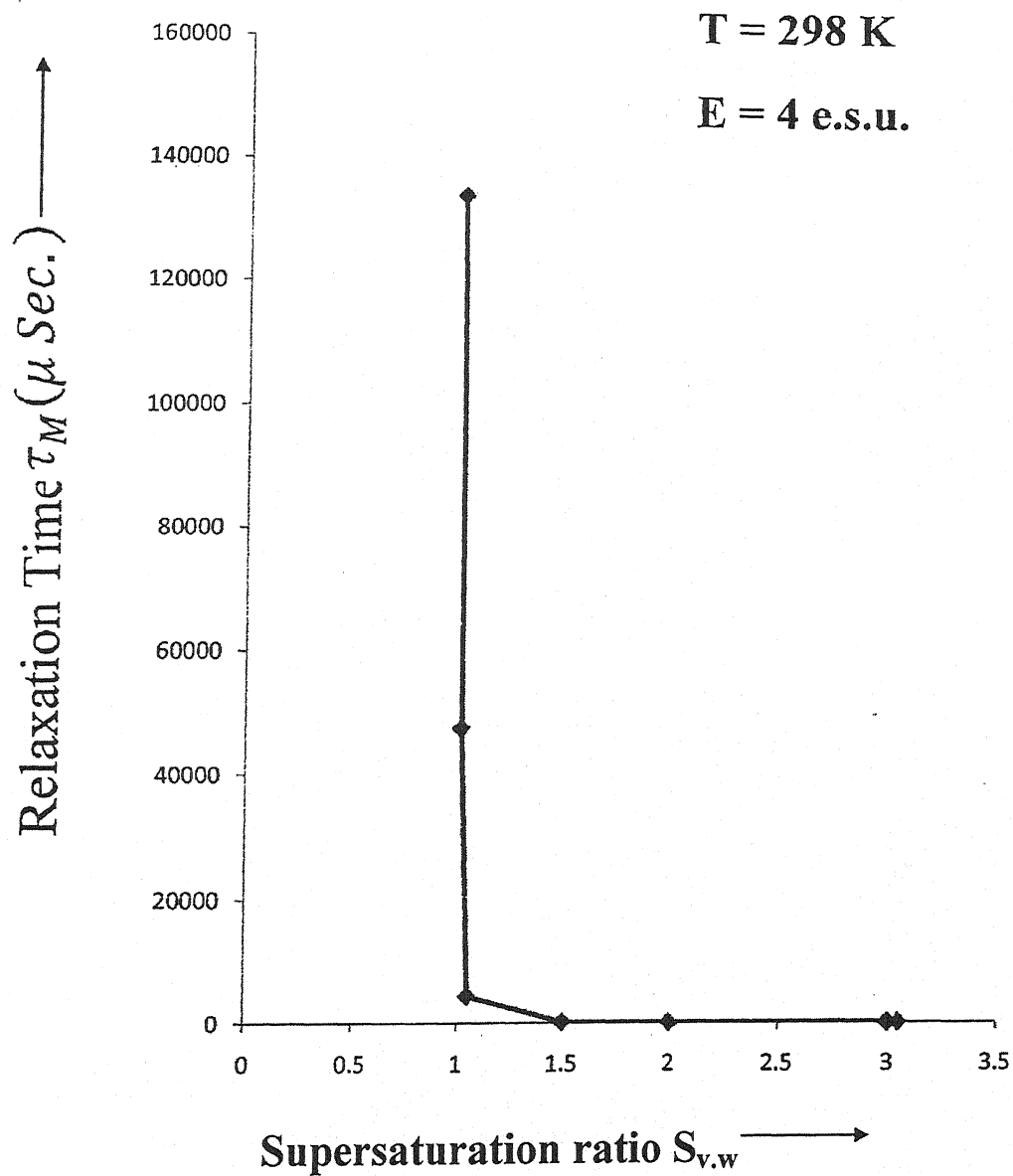


fig. 2.3 (d-II) Variation of relaxation time $\tau_M (\mu \text{ Sec.})$ with supersaturation ratio $S_{v,w}$ at $T=298\text{K}$ and $E=4 \text{ e.s.u.}$

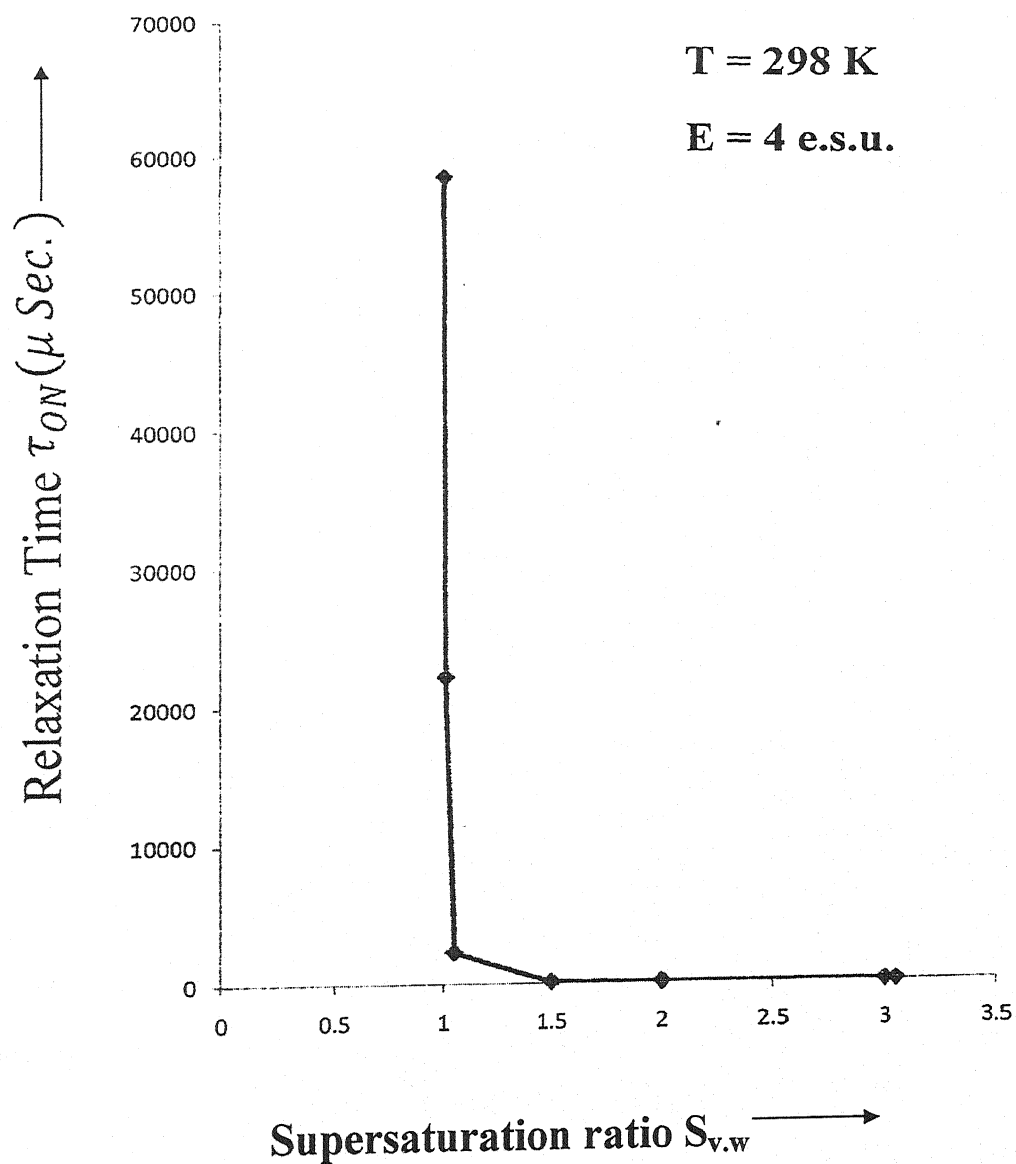


fig. 2.3 (e-II) Variation of relaxation time $\tau_{ON} (\mu \text{ Sec.})$ with supersaturation ratio $S_{v,w}$ at $T=298\text{K}$ and $E=4 \text{ e.s.u.}$

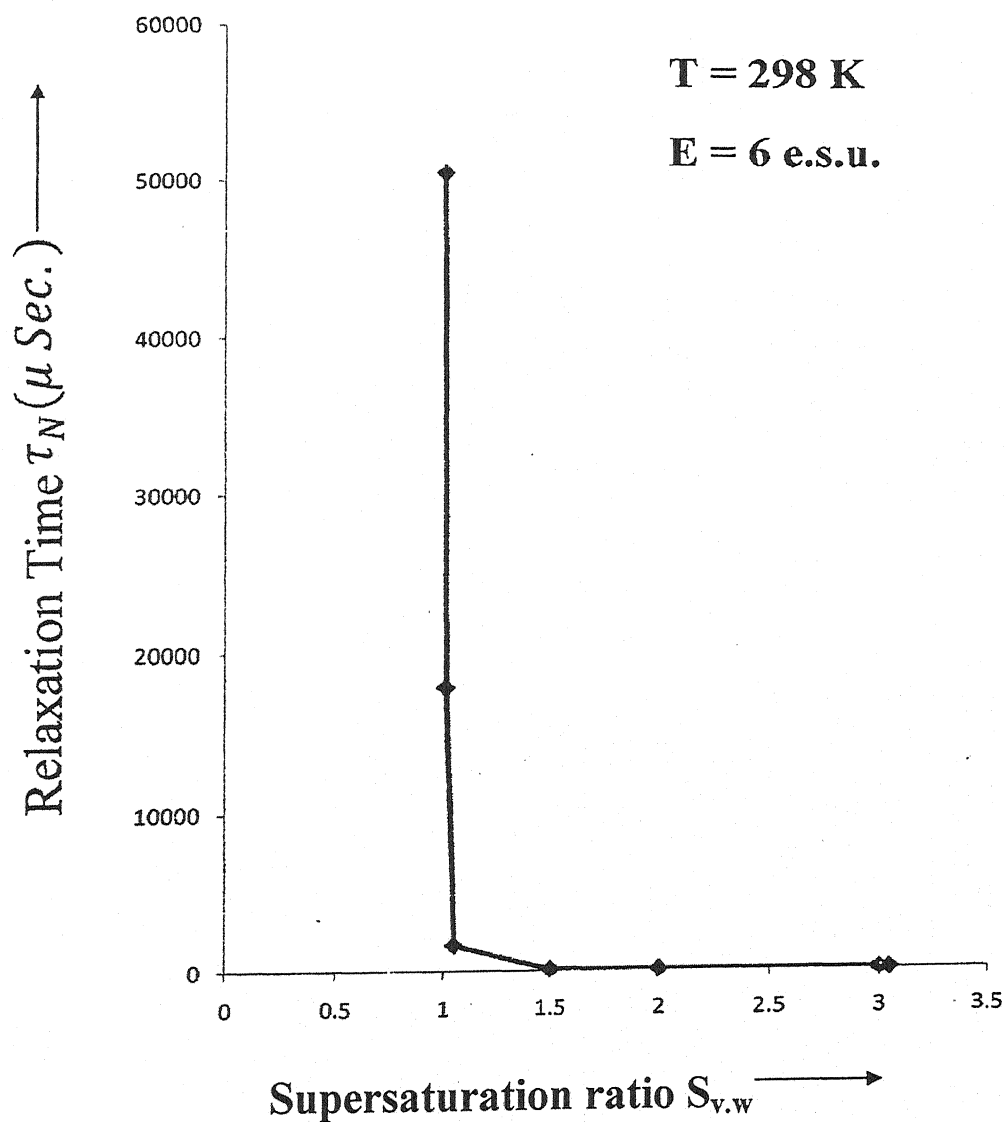


fig. 2.3 (c-III) Variation of relaxation time τ_N (μ Sec.) with supersaturation ratio $S_{v,w}$ at $T=298K$ and $E=6$ e.s.u.

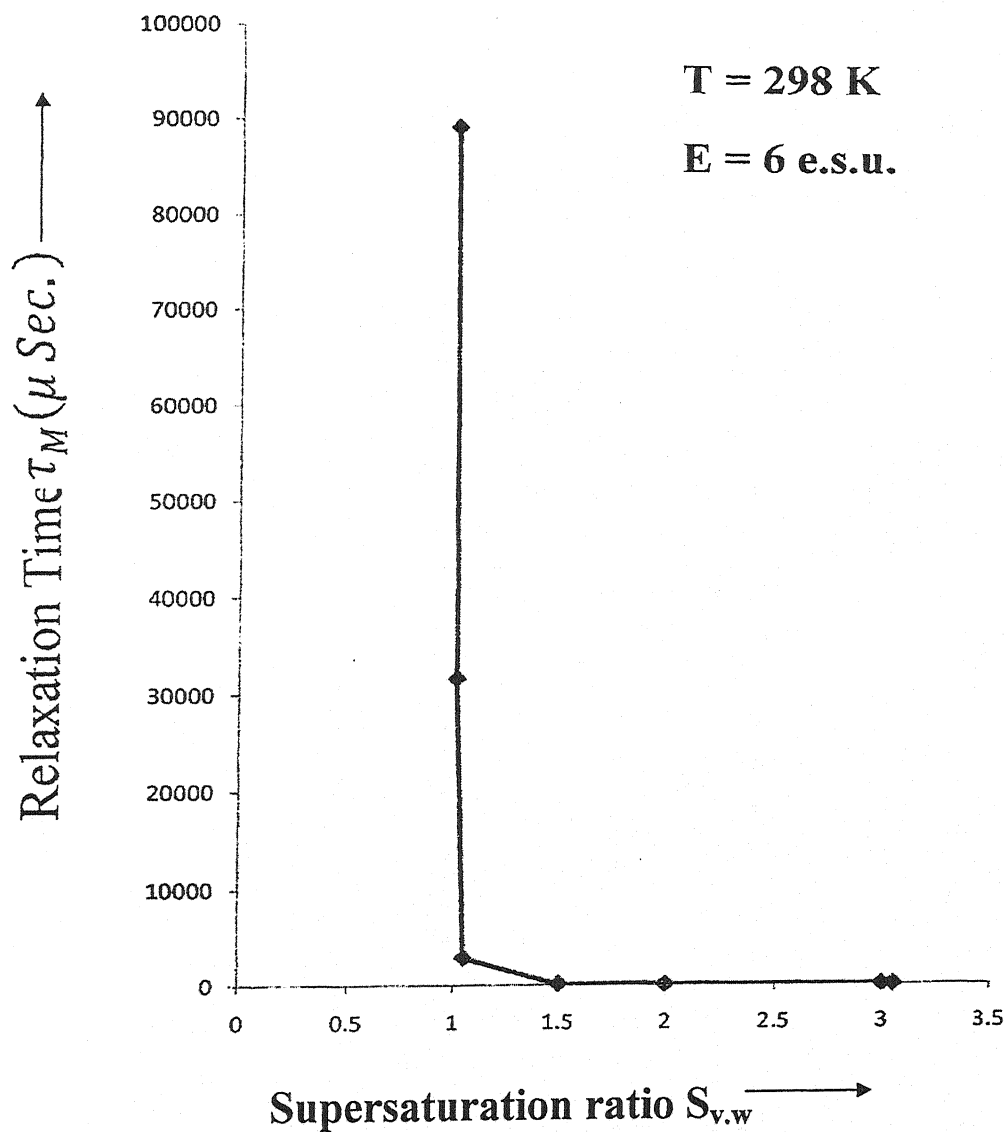


fig. 2.3 (d-III) Variation of relaxation time τ_M (μ Sec.) with supersaturation ratio $S_{v,w}$ at $T=298K$ and $E=6$ e.s.u.

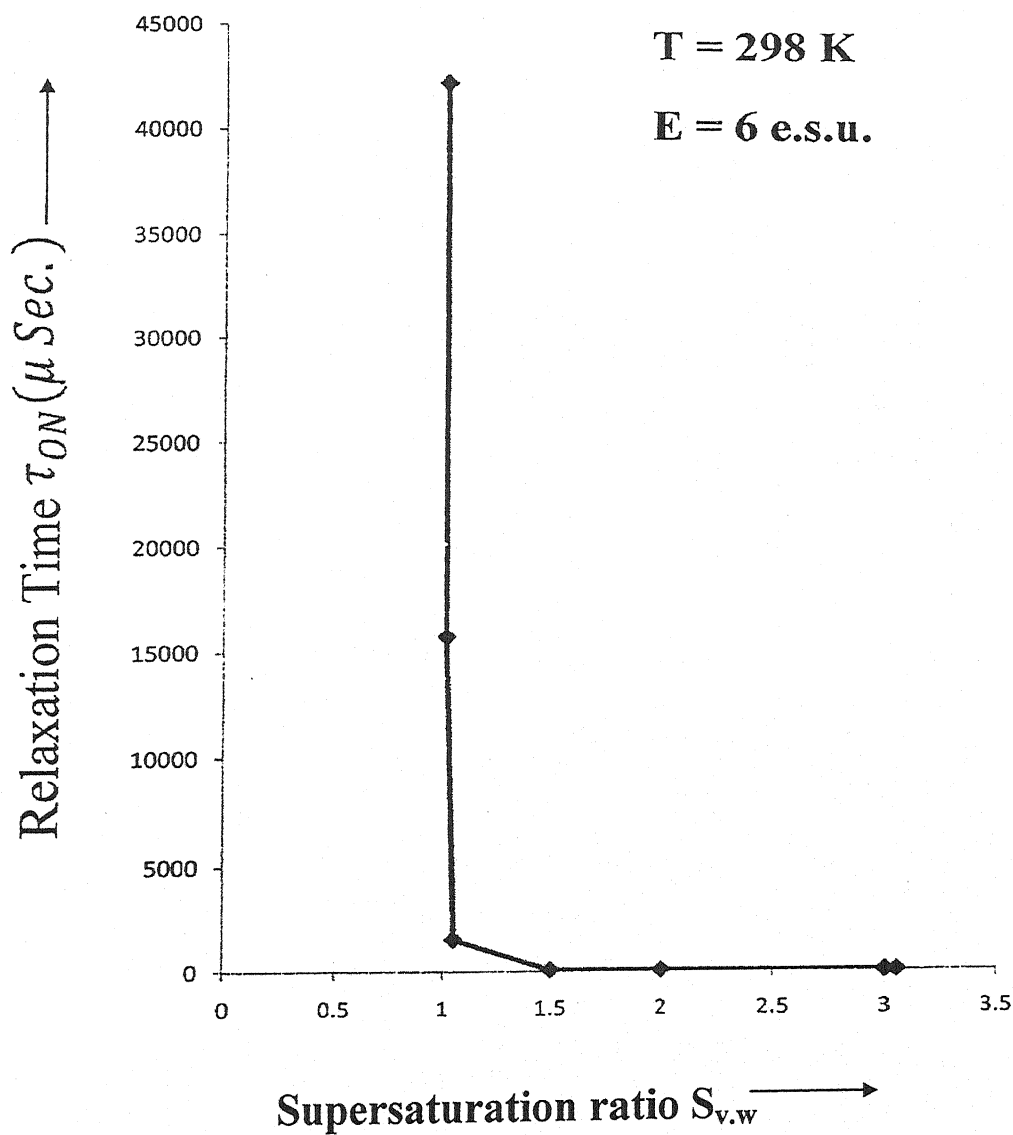


fig. 2.3 (e-III) Variation of relaxation time $\tau_{ON} (\mu \text{ Sec.})$ with supersaturation ratio $S_{v,w}$ at $T=298\text{K}$ and $E=6 \text{ e.s.u.}$

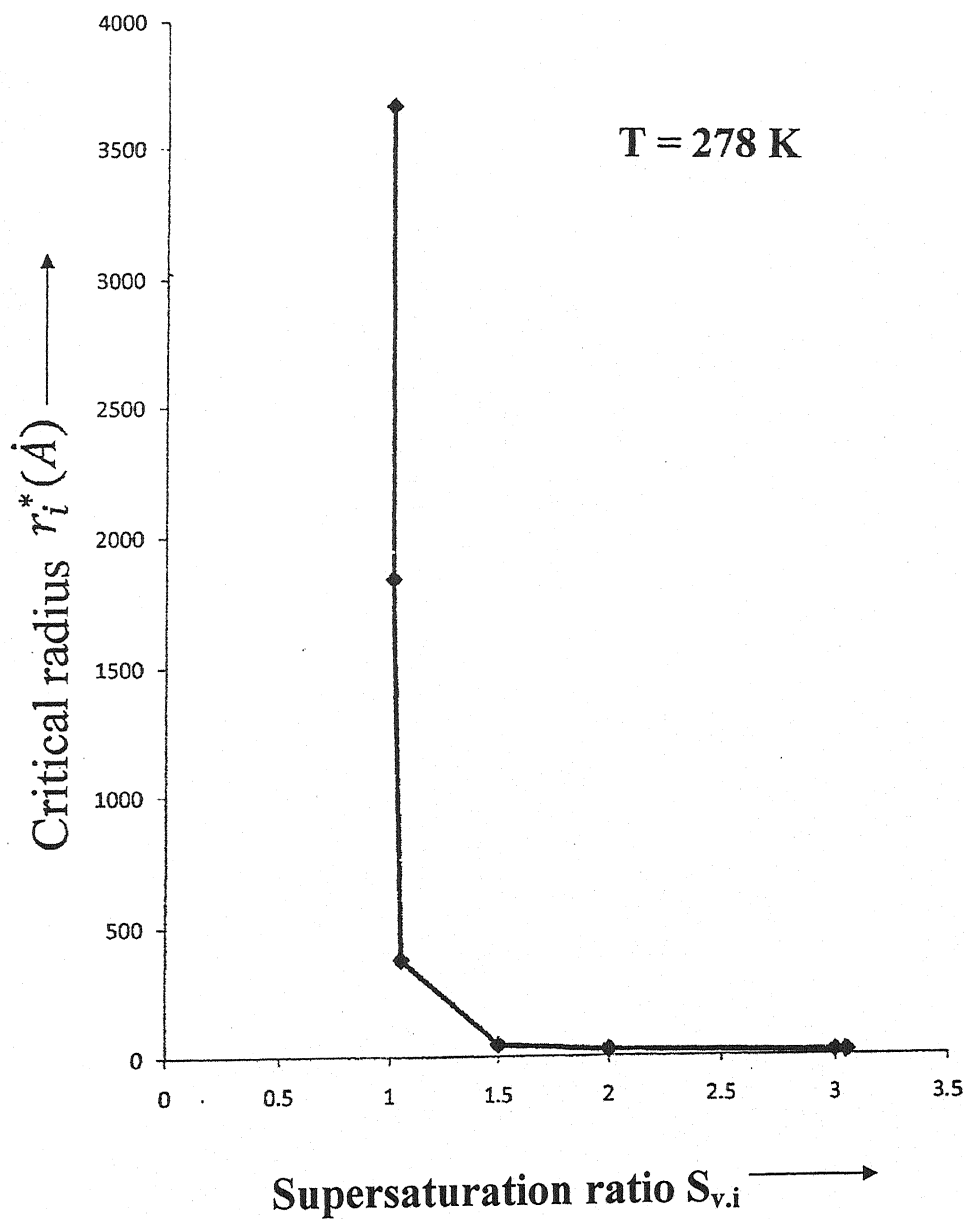


fig. 2.4 (a) Variation of critical radius of ice molecule $r_i^* (\text{\AA})$ with supersaturation ratio $S_{v,i}$ at $T=278\text{K}$.

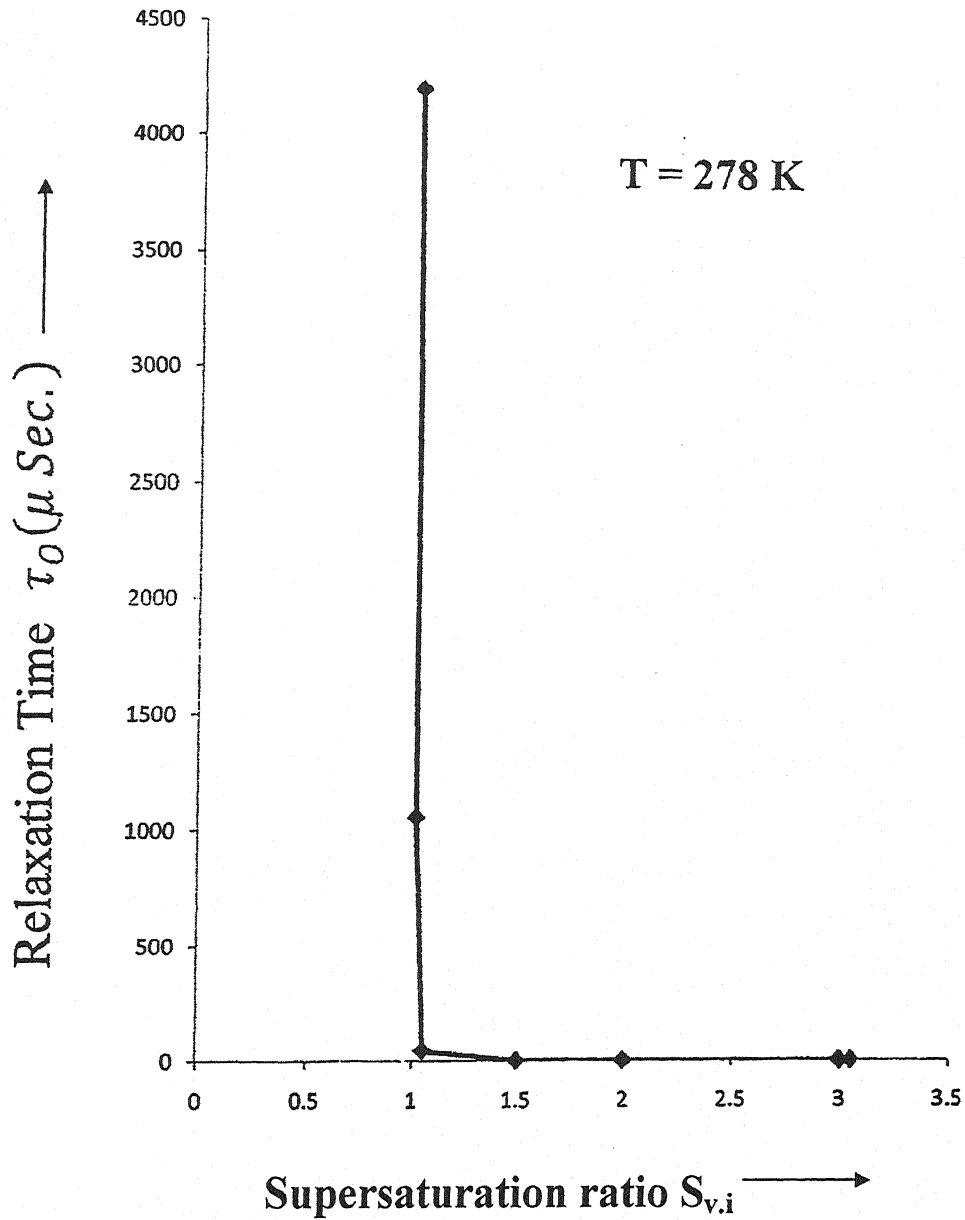


fig. 2.4 (b) Variation of Calculated relaxation time $\tau_0 (\mu \text{ Sec.})$ with supersaturation ratio $S_{v,i}$ at $T=278\text{K}$.

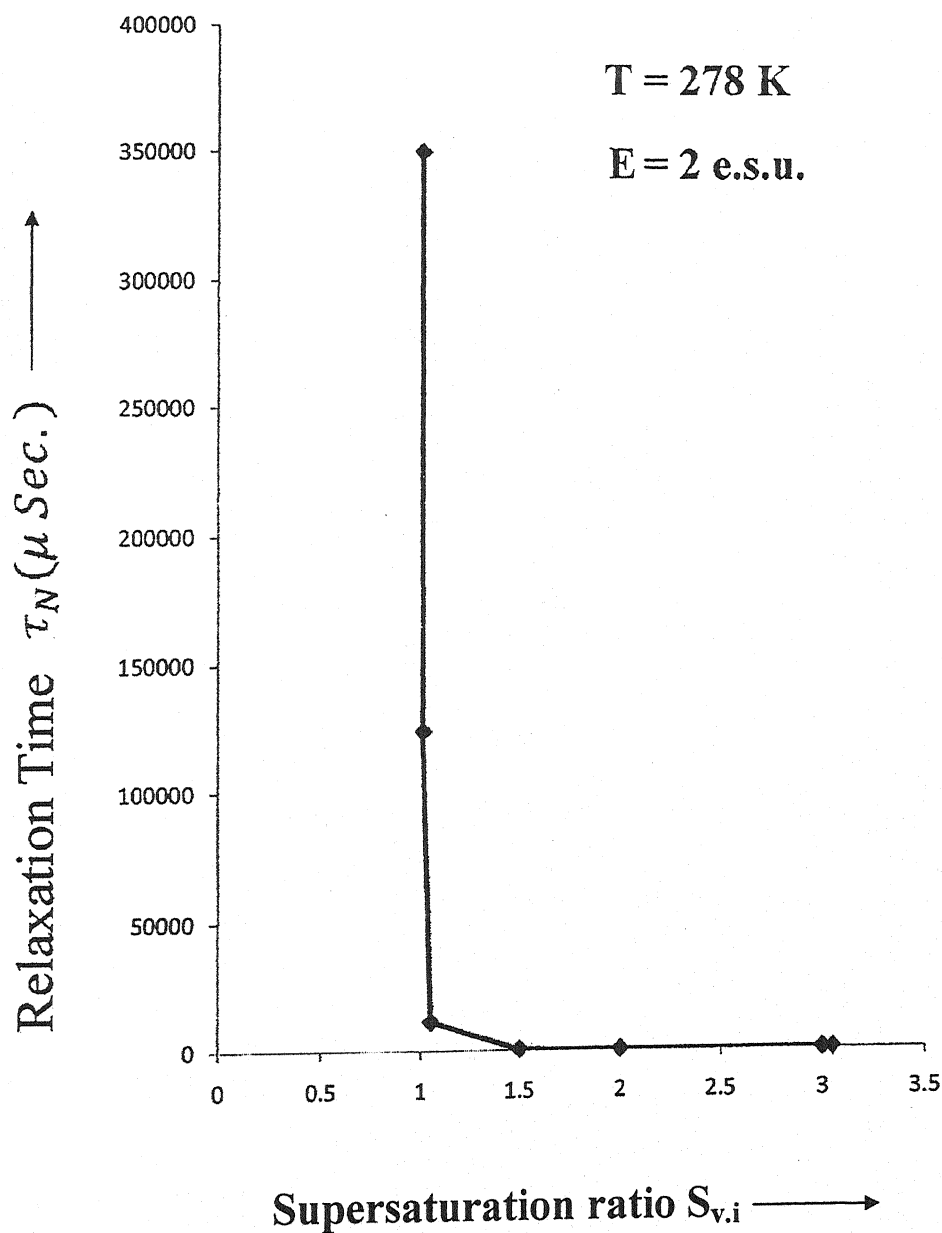


fig. 2.4 (c-I) Variation of relaxation time $\tau_N (\mu \text{ Sec.})$ with supersaturation ratio $S_{v,i}$ at $T=278\text{K}$ and $E=2 \text{ e.s.u.}$

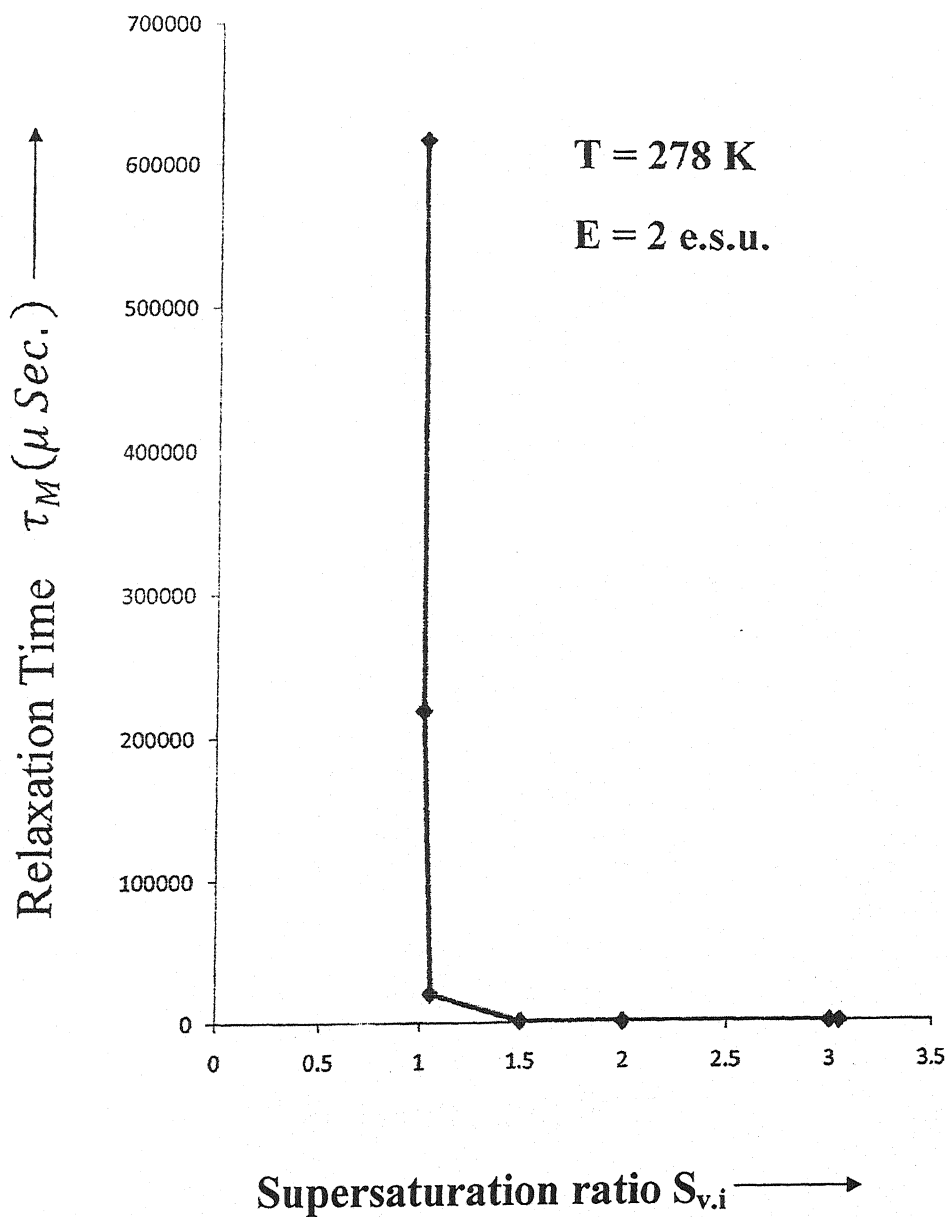


fig. 2.4 (d-I) Variation of relaxation time τ_M (μ Sec.) with supersaturation ratio $S_{v,i}$ at $T=278\text{K}$ and $E=2 \text{ e.s.u.}$

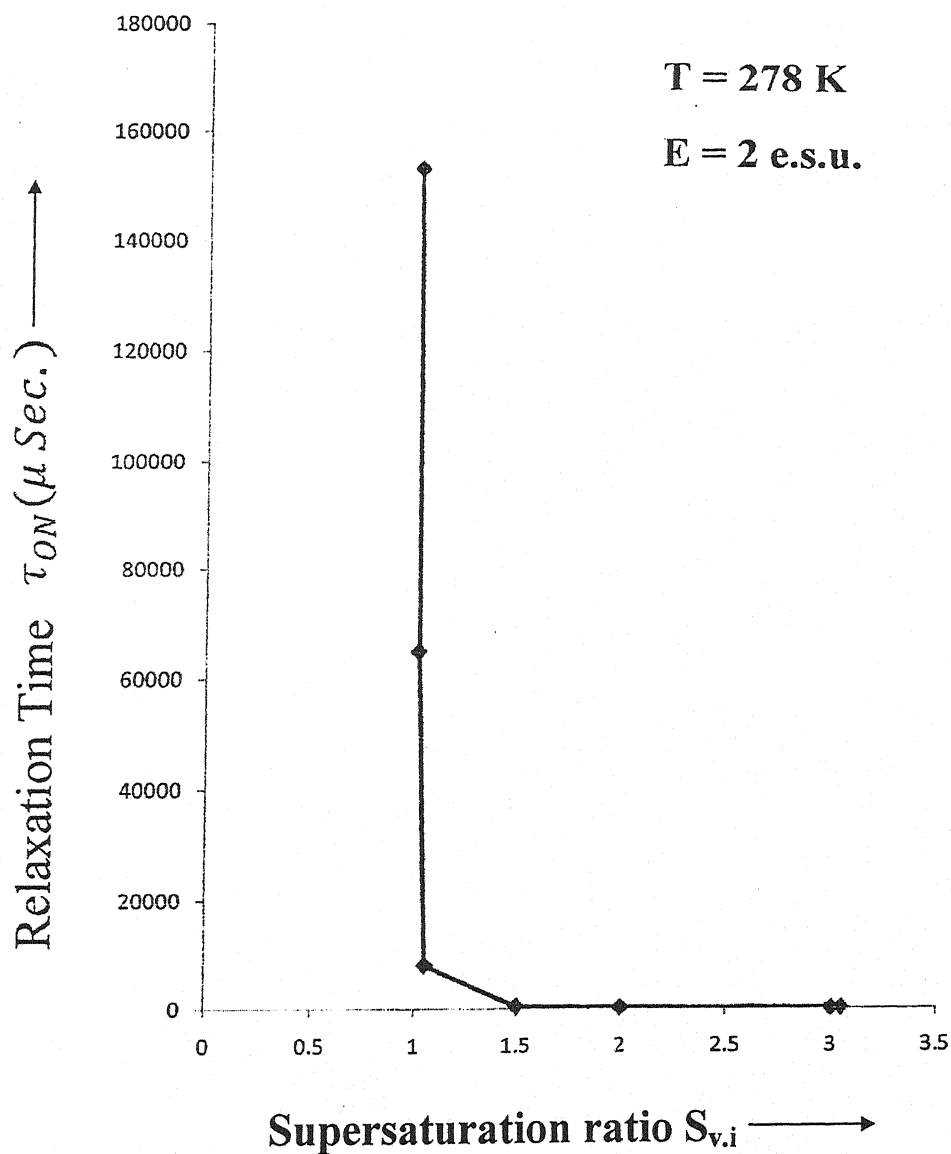


fig. 2.4 (e-I) Variation of relaxation time $\tau_{ON} (\mu \text{ Sec.})$ with supersaturation ratio $S_{v,i}$ at $T=278\text{K}$ and $E=2 \text{ e.s.u.}$

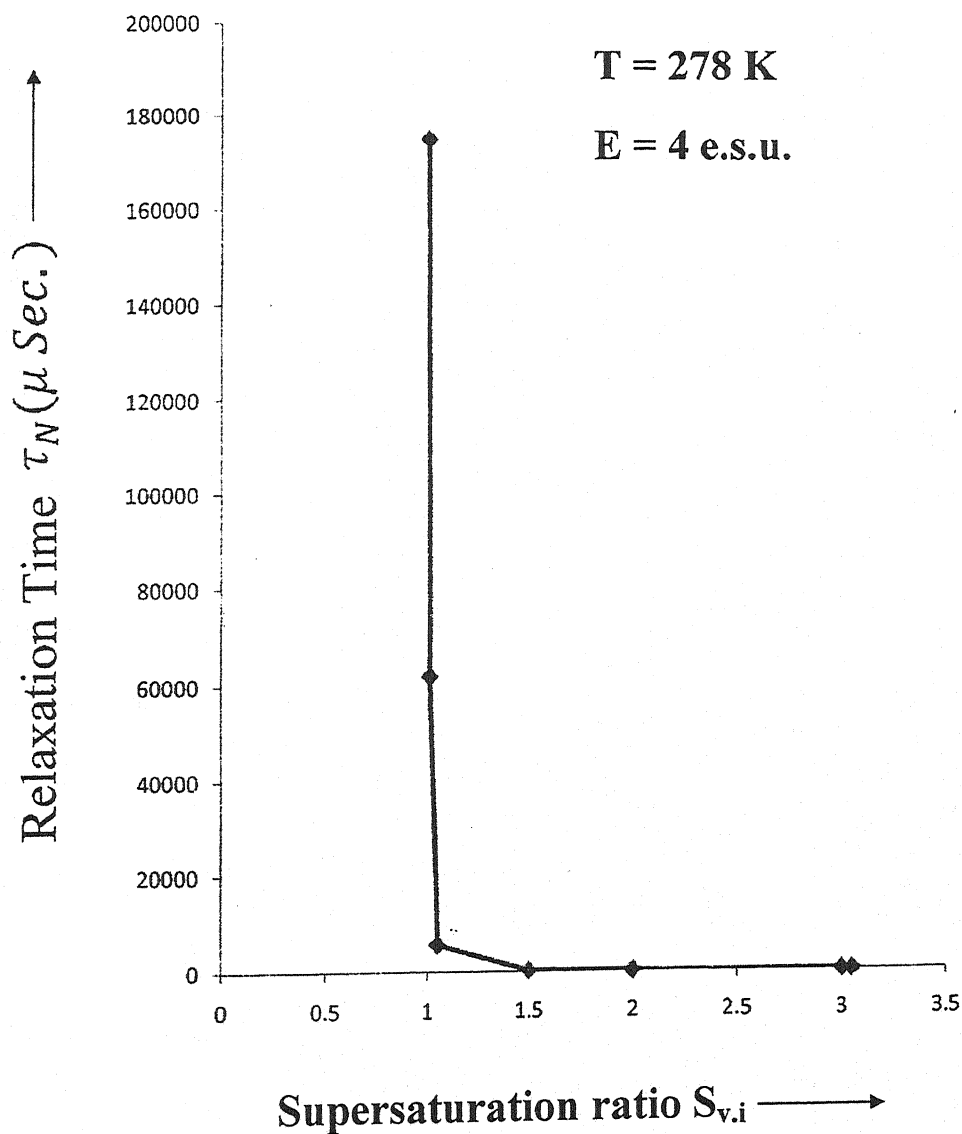


fig. 2.4 (c-II) Variation of relaxation time τ_N (μ Sec.) with supersaturation ratio $S_{v,i}$ at $T=278K$ and $E=4$ e.s.u.

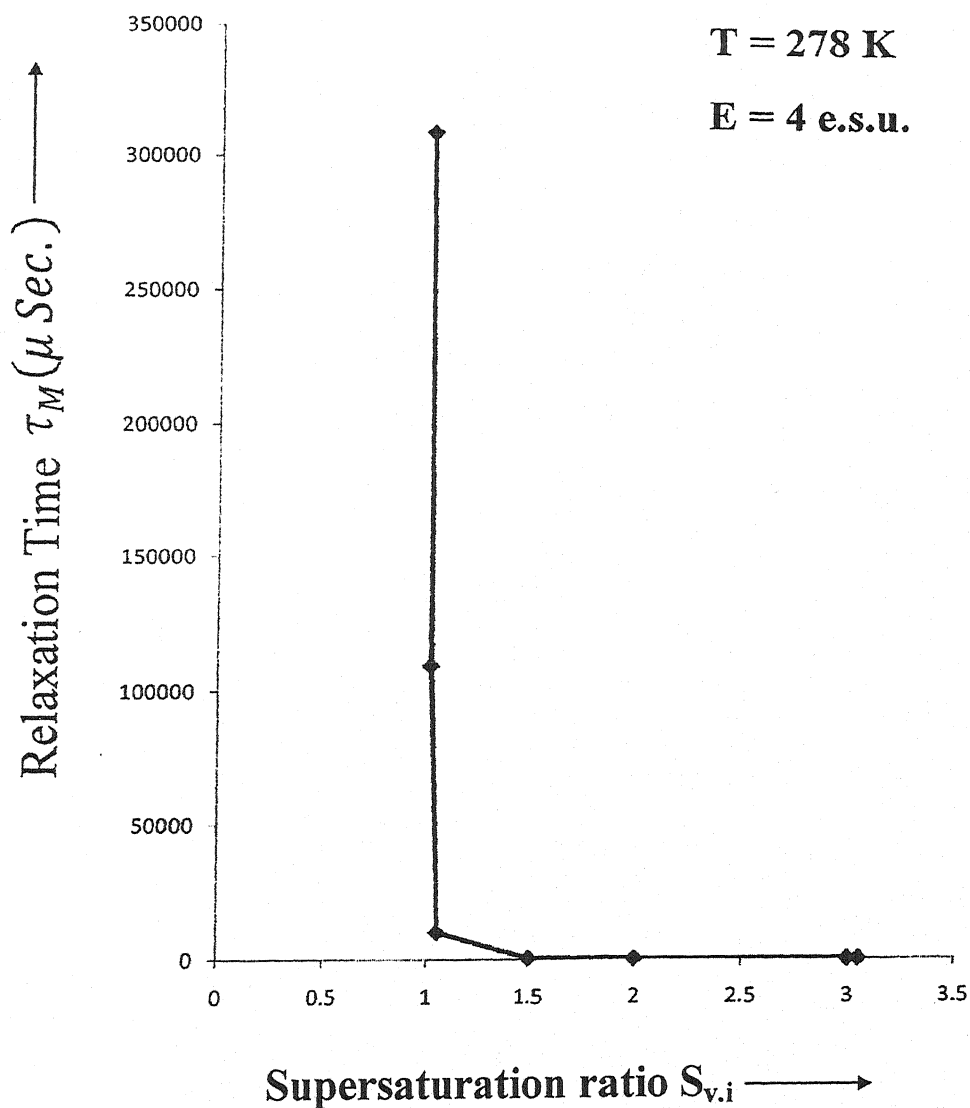


fig. 2.4 (d-II) Variation of relaxation time $\tau_M (\mu \text{ Sec.})$ with supersaturation ratio $S_{v,i}$ at $T=278\text{K}$ and $E=4 \text{ e.s.u.}$

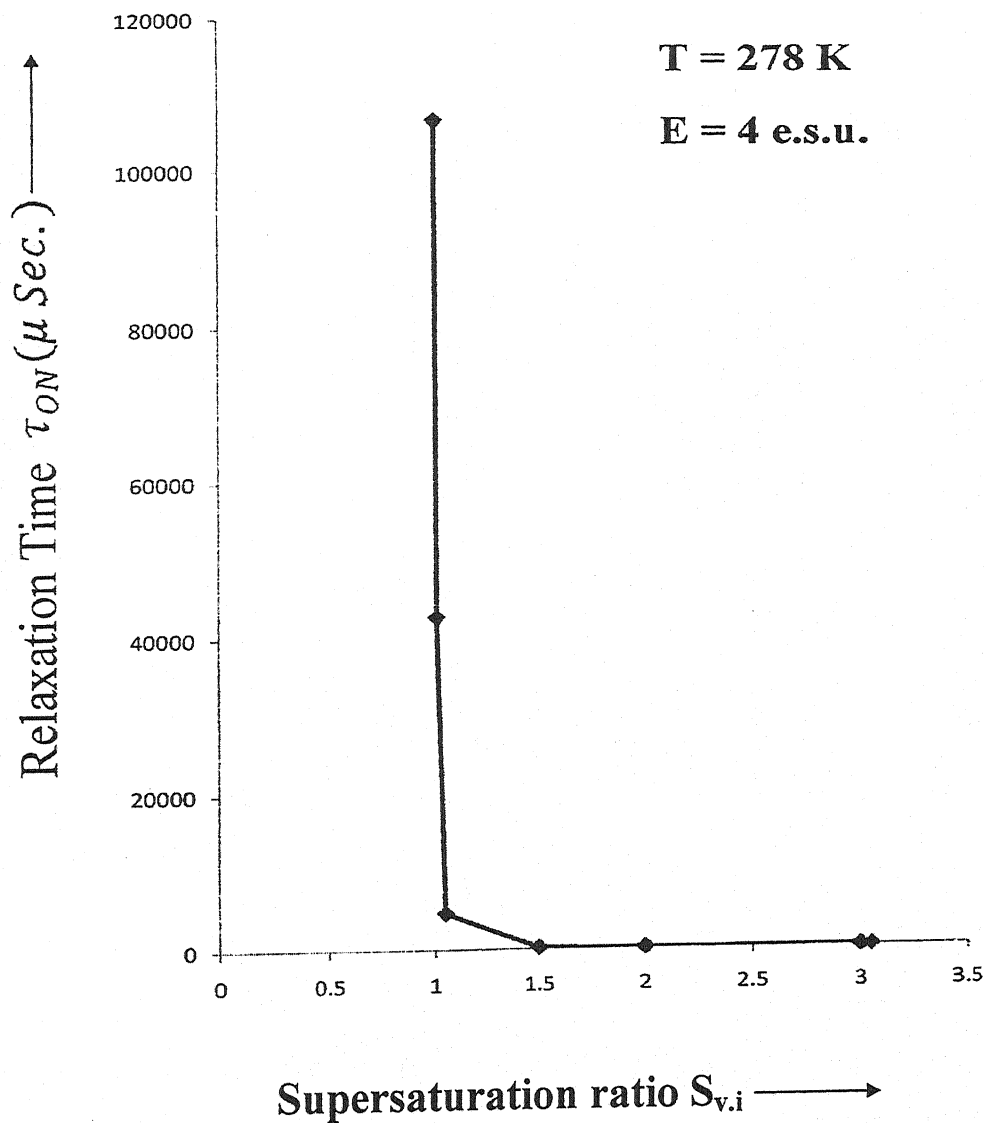


fig. 2.4 (e-II) Variation of relaxation time τ_{ON} (μ Sec.) with supersaturation ratio $S_{v,i}$ at $T=278K$ and $E=4$ e.s.u.

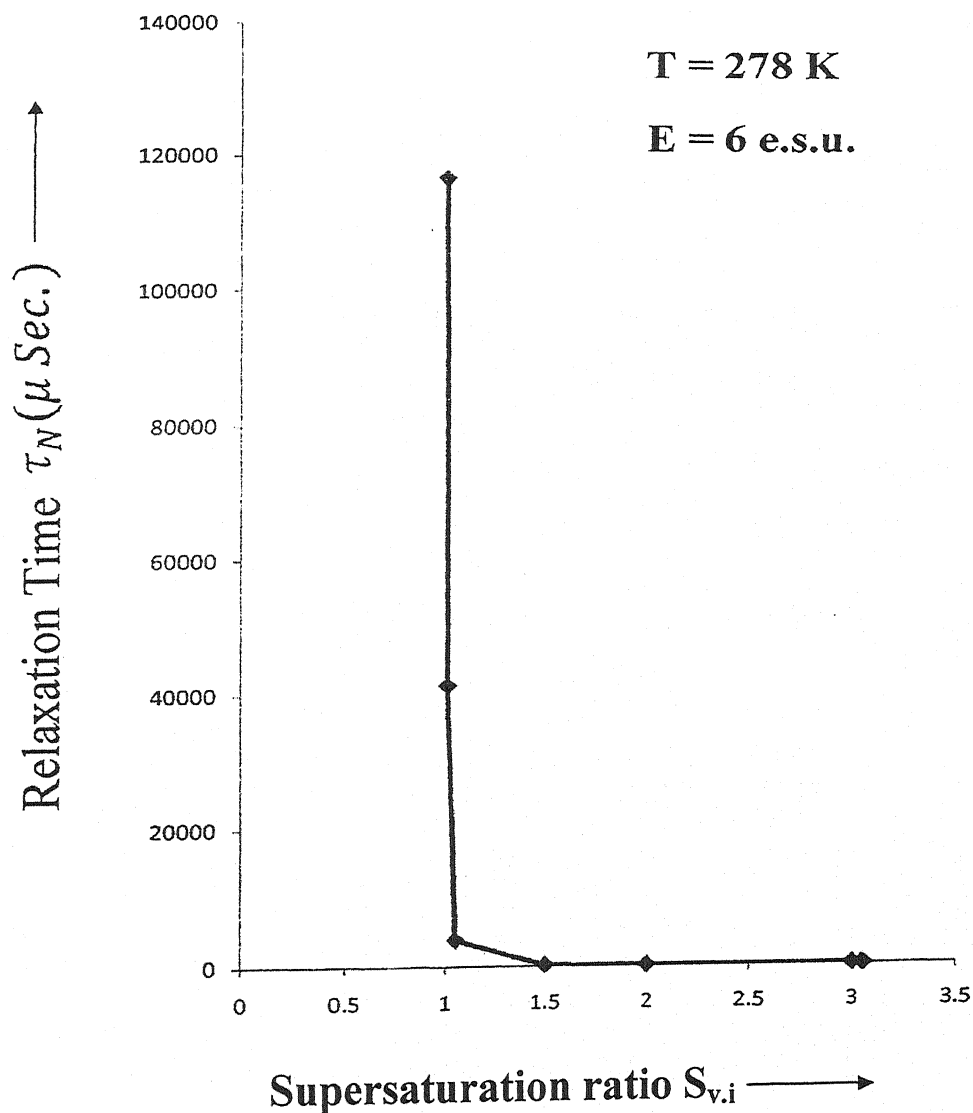


fig. 2.4 (c-III) Variation of relaxation time $\tau_N (\mu \text{ Sec.})$ with supersaturation ratio $S_{v,i}$ at $T=278\text{K}$ and $E=6 \text{ e.s.u.}$

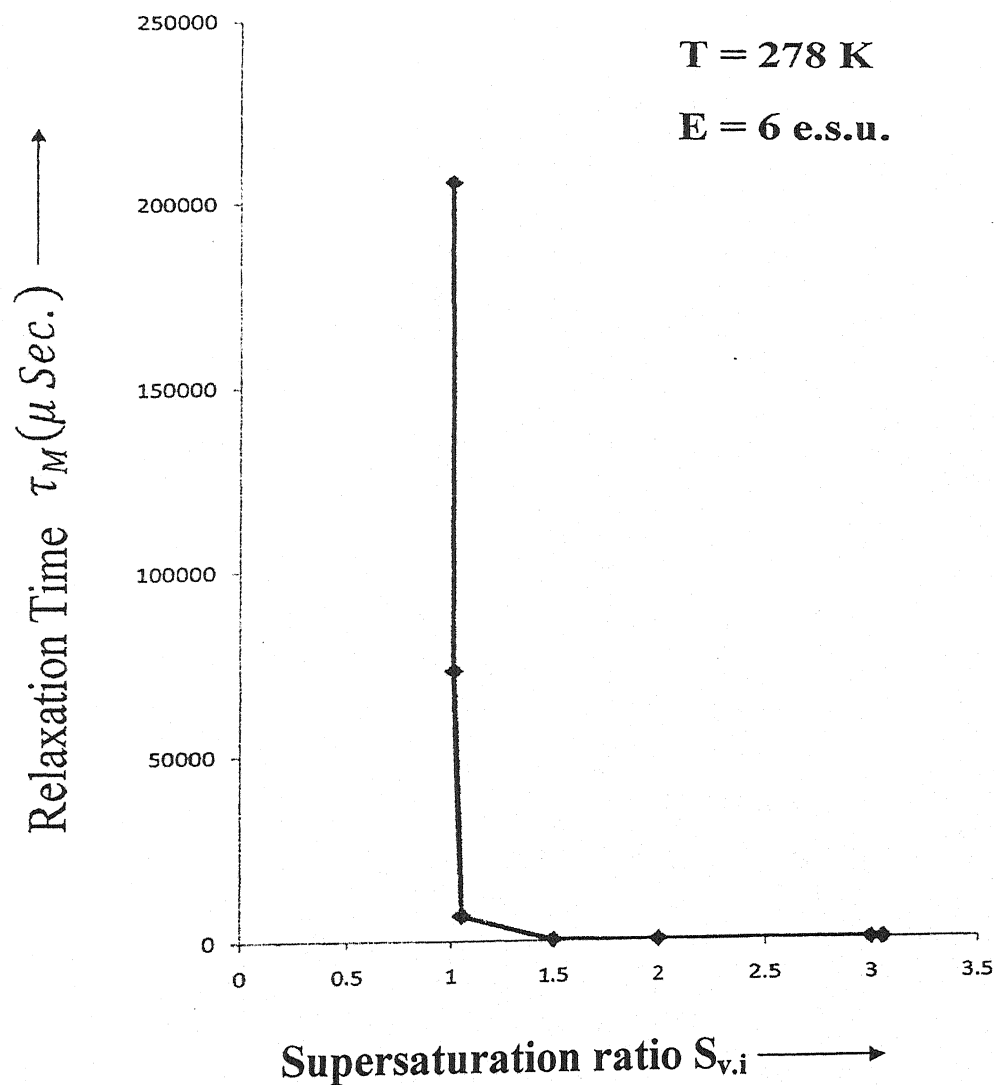


fig. 2.4 (d-III) Variation of relaxation time τ_M (μ Sec.) with supersaturation ratio $S_{v,i}$ at $T=278$ K and $E=6$ e.s.u.

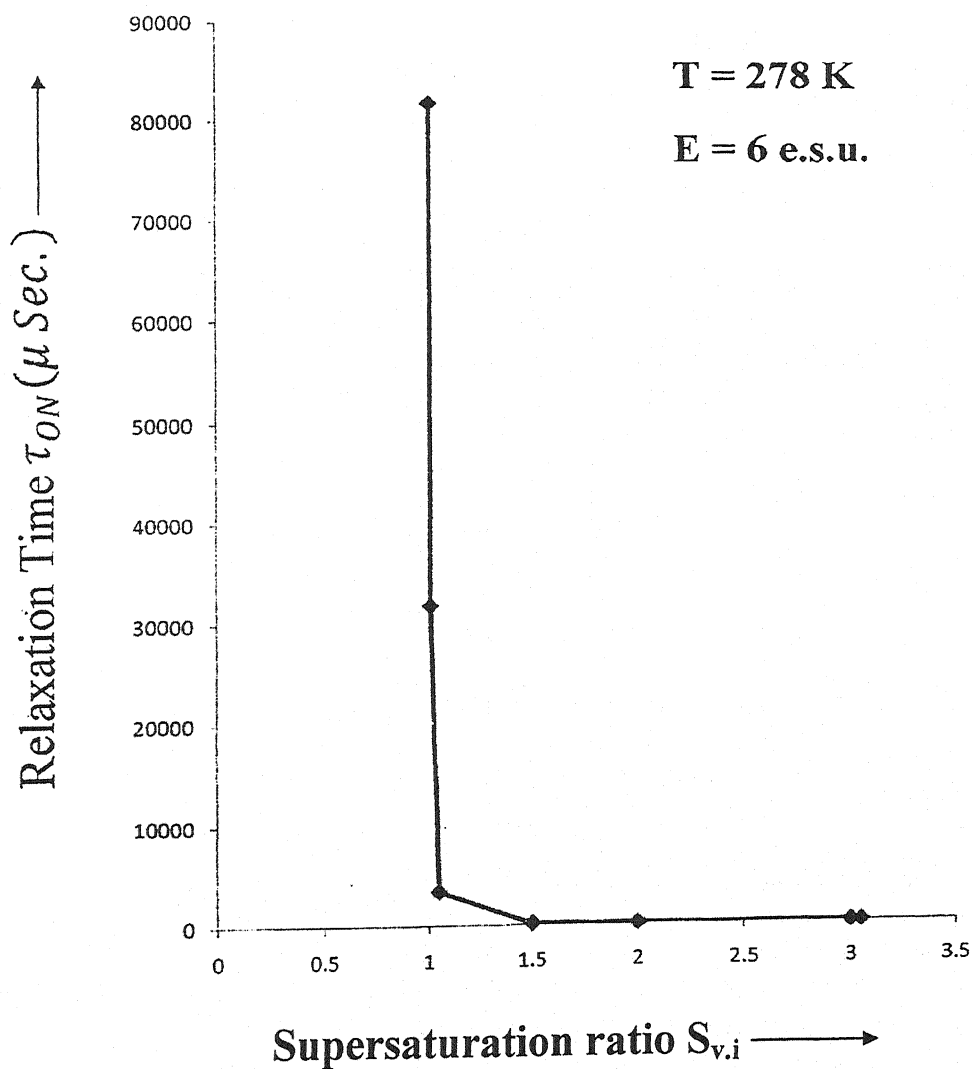


fig. 2.4 (e-III) Variation of relaxation time τ_{ON} (μ Sec.) with supersaturation ratio $S_{v,i}$ at $T=278$ K and $E=6$ e.s.u.

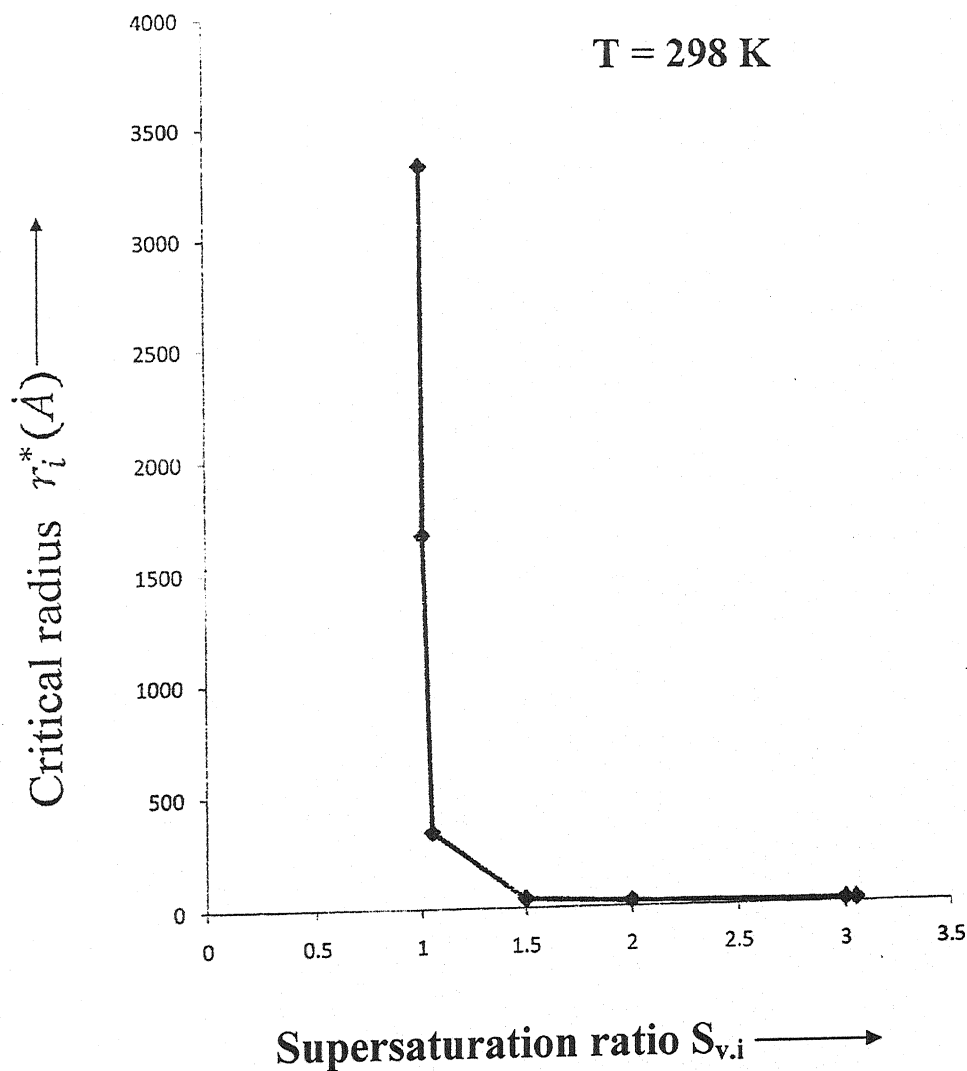


fig. 2.5 (a) Variation of critical radius of ice molecule $r_i^* (\text{\AA})$ with supersaturation ratio $S_{v,i}$ at $T=298\text{K}$.

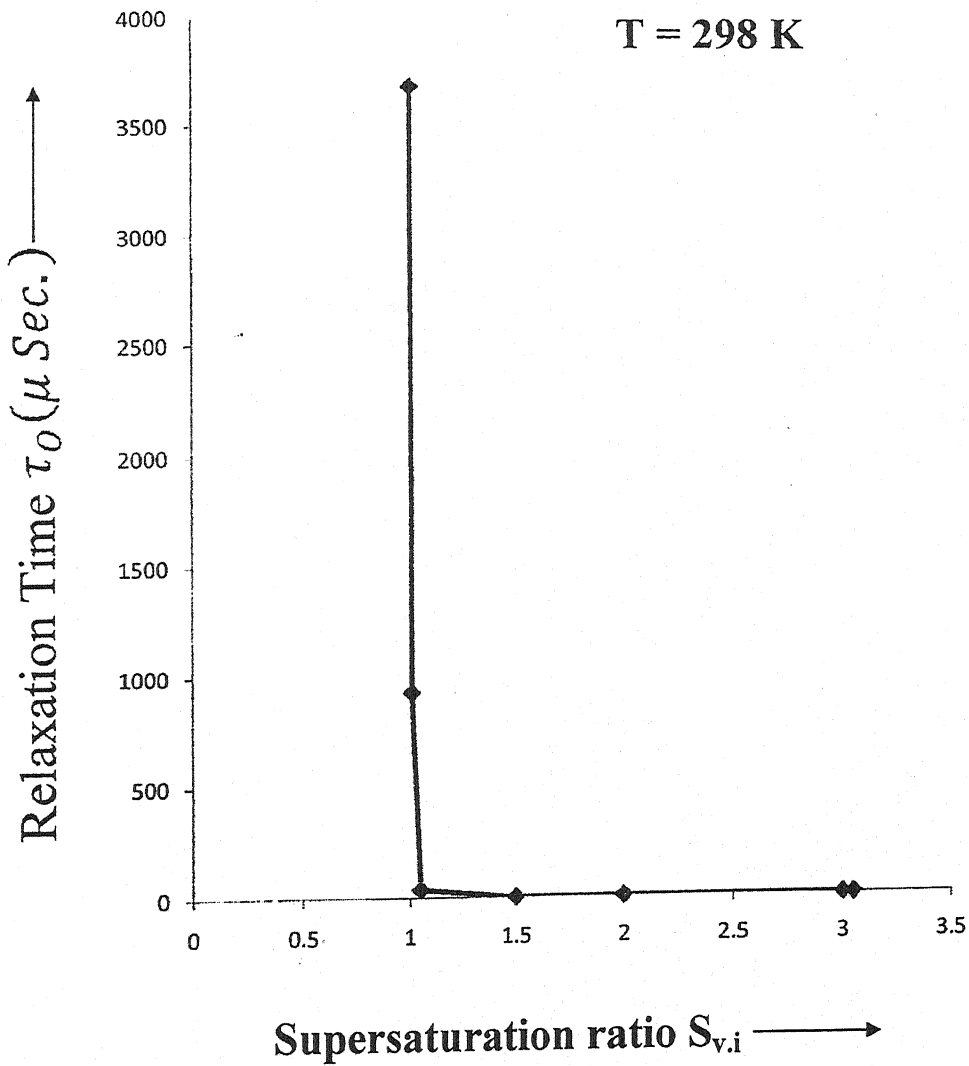


fig. 2.5 (b) Variation of Calculated relaxation time τ_0 ($\mu \text{ Sec.}$) with supersaturation ratio $S_{v,i}$ at $T=298\text{K}$.

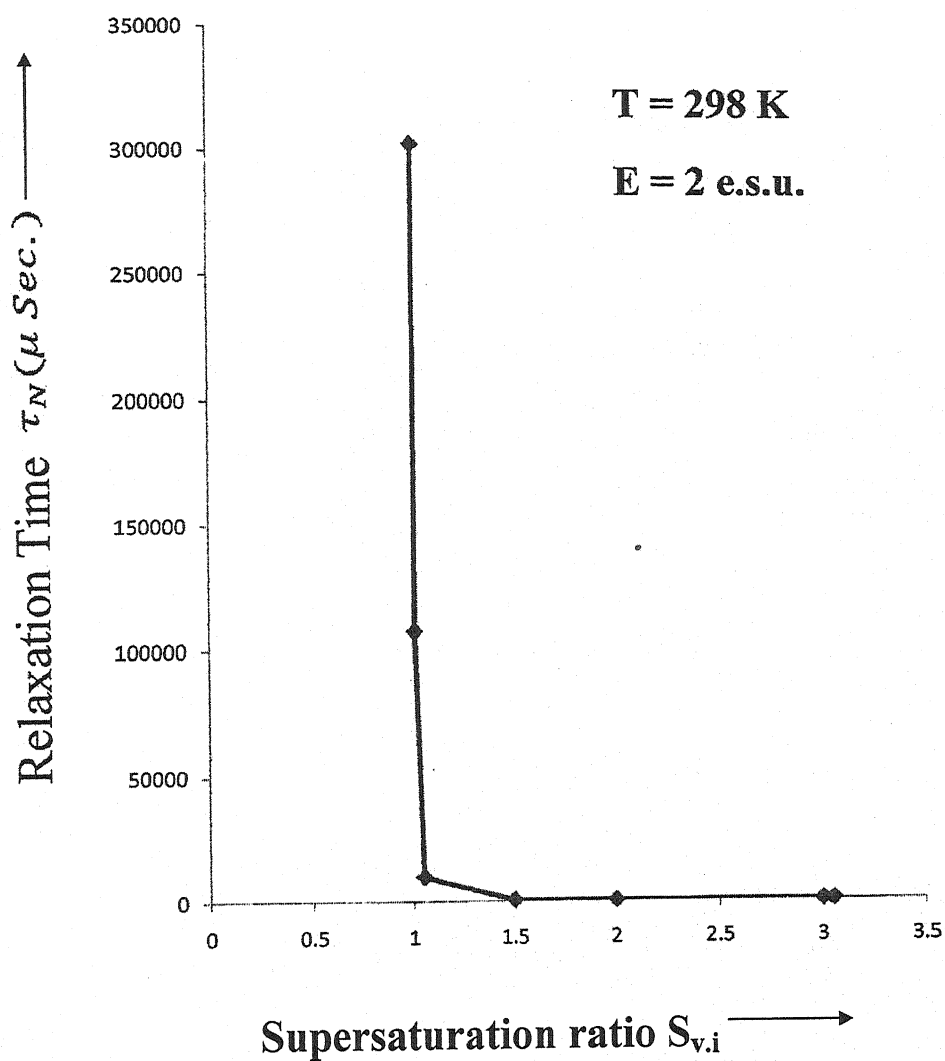


fig. 2.5 (c-I) Variation of relaxation time τ_N (μ Sec.) with supersaturation ratio $S_{v,i}$ at $T=298K$ and $E=2$ e.s.u.

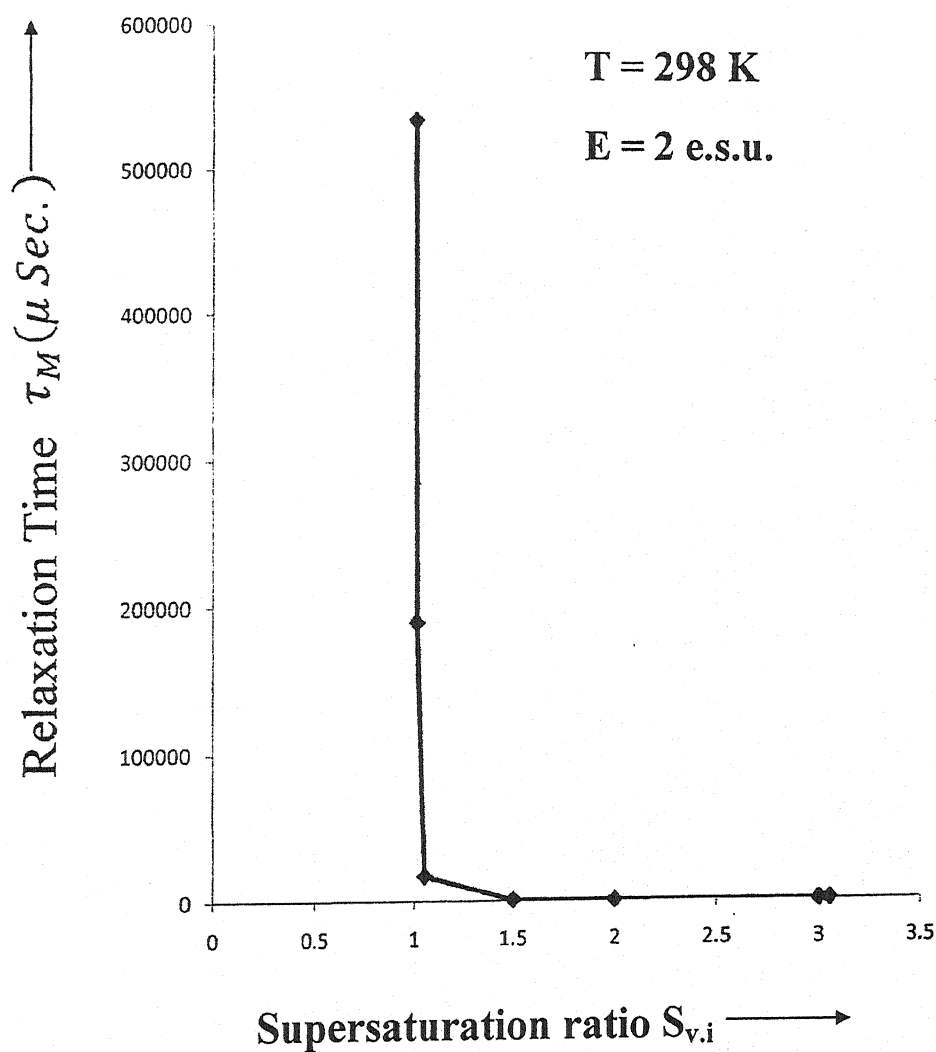


fig. 2.5 (d-I) Variation of relaxation time τ_M (μ Sec.) with supersaturation ratio $S_{v,i}$ at $T=298K$ and $E=2$ e.s.u.

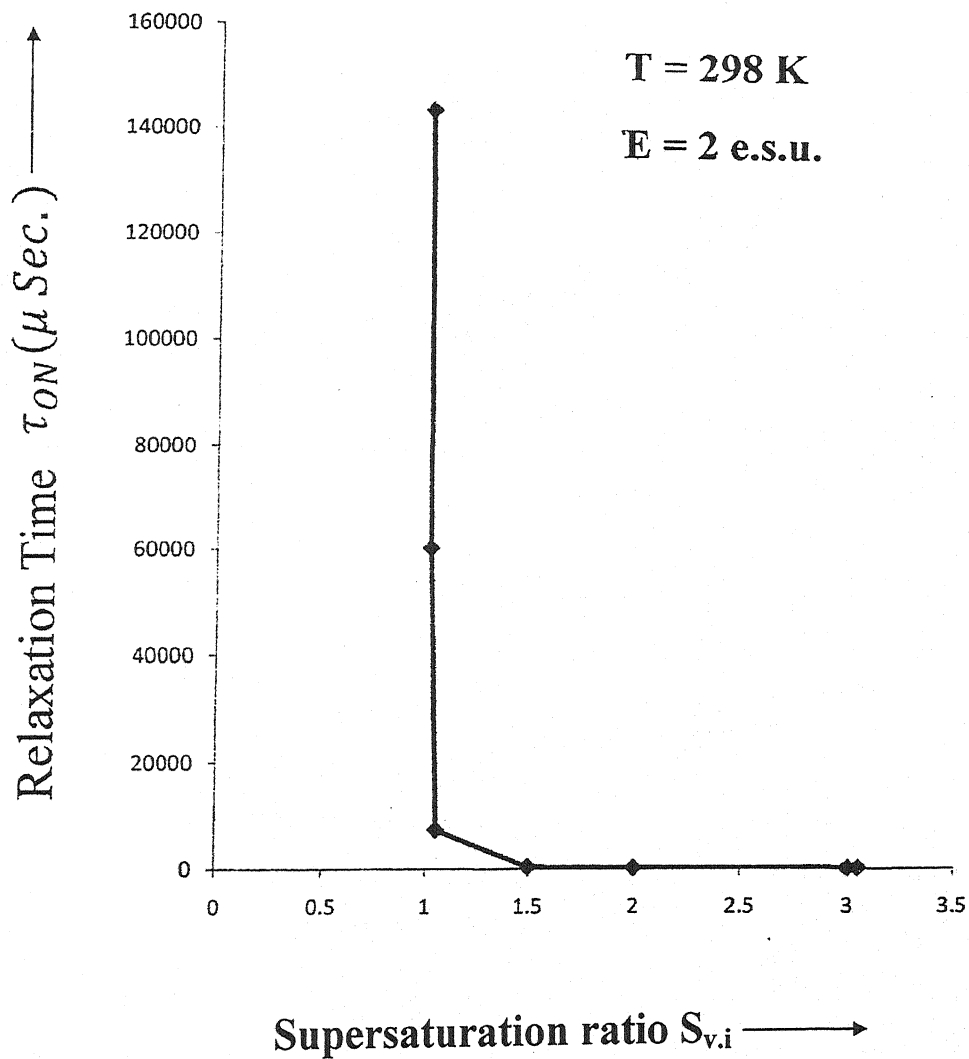


fig. 2.5 (e-I) Variation of relaxation time $\tau_{ON} (\mu \text{ Sec.})$ with supersaturation ratio $S_{v,i}$ at $T=298\text{K}$ and $E=2 \text{ e.s.u.}$

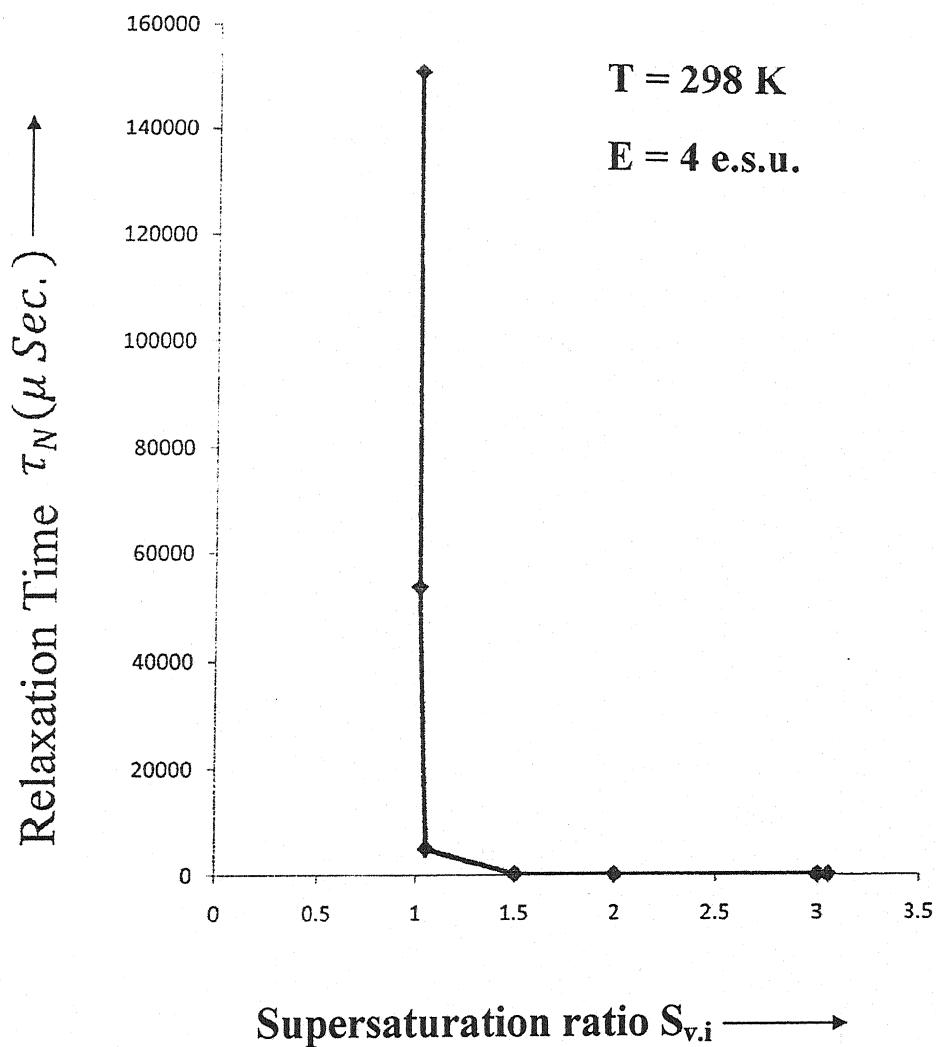


fig. 2.5 (c-II) Variation of relaxation time $\tau_N (\mu \text{ Sec.})$ with supersaturation ratio $S_{v,i}$ at $T=298\text{K}$ and $E=4 \text{ e.s.u.}$

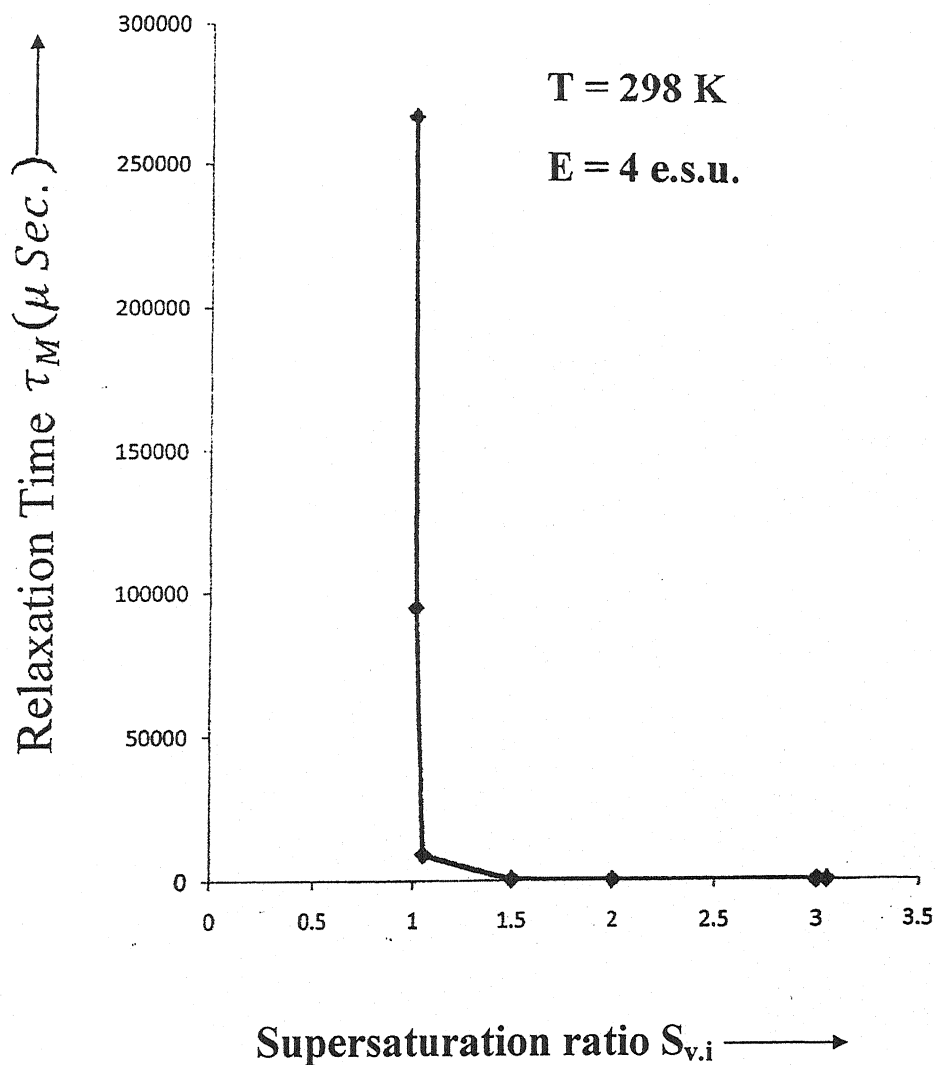


fig. 2.5 (d-II) Variation of relaxation time $\tau_M (\mu \text{ Sec.})$ with supersaturation ratio $S_{v,i}$ at $T=298\text{K}$ and $E=4 \text{ e.s.u.}$

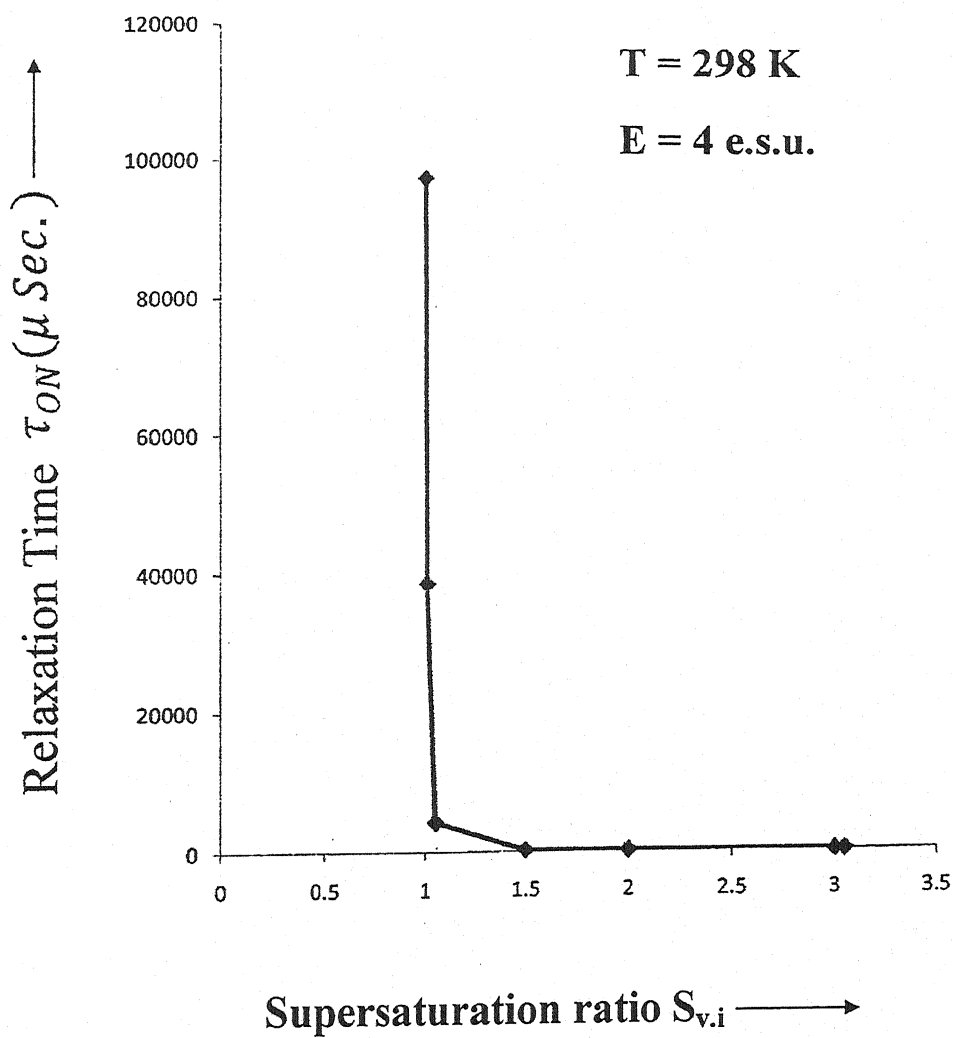


fig. 2.5 (e-II) Variation of relaxation time $\tau_{ON} (\mu \text{ Sec.})$ with supersaturation ratio $S_{v,i}$ at $T=298\text{K}$ and $E=4 \text{ e.s.u.}$

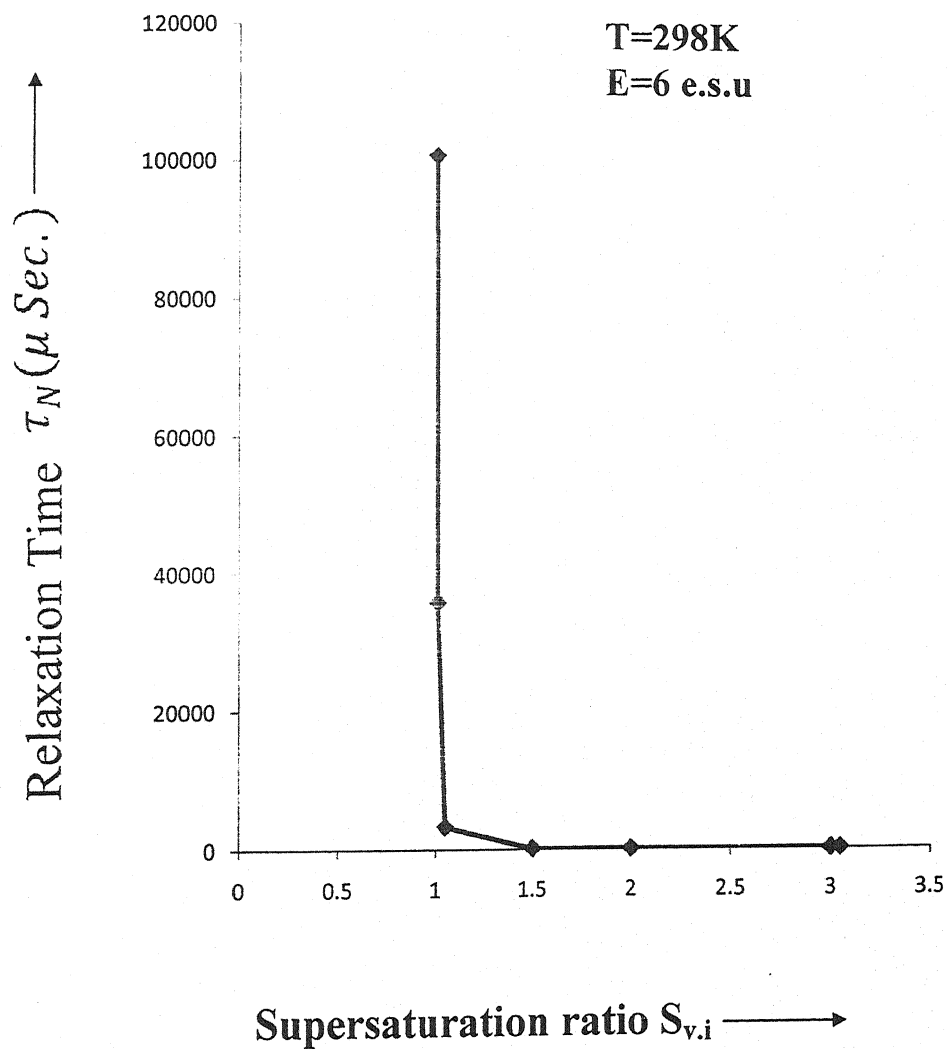


fig. 2.5 (c-III) Variation of relaxation time $\tau_N (\mu \text{ Sec.})$ with supersaturation ratio $S_{v,i}$ at $T=298\text{K}$ and $E=6 \text{ e.s.u.}$

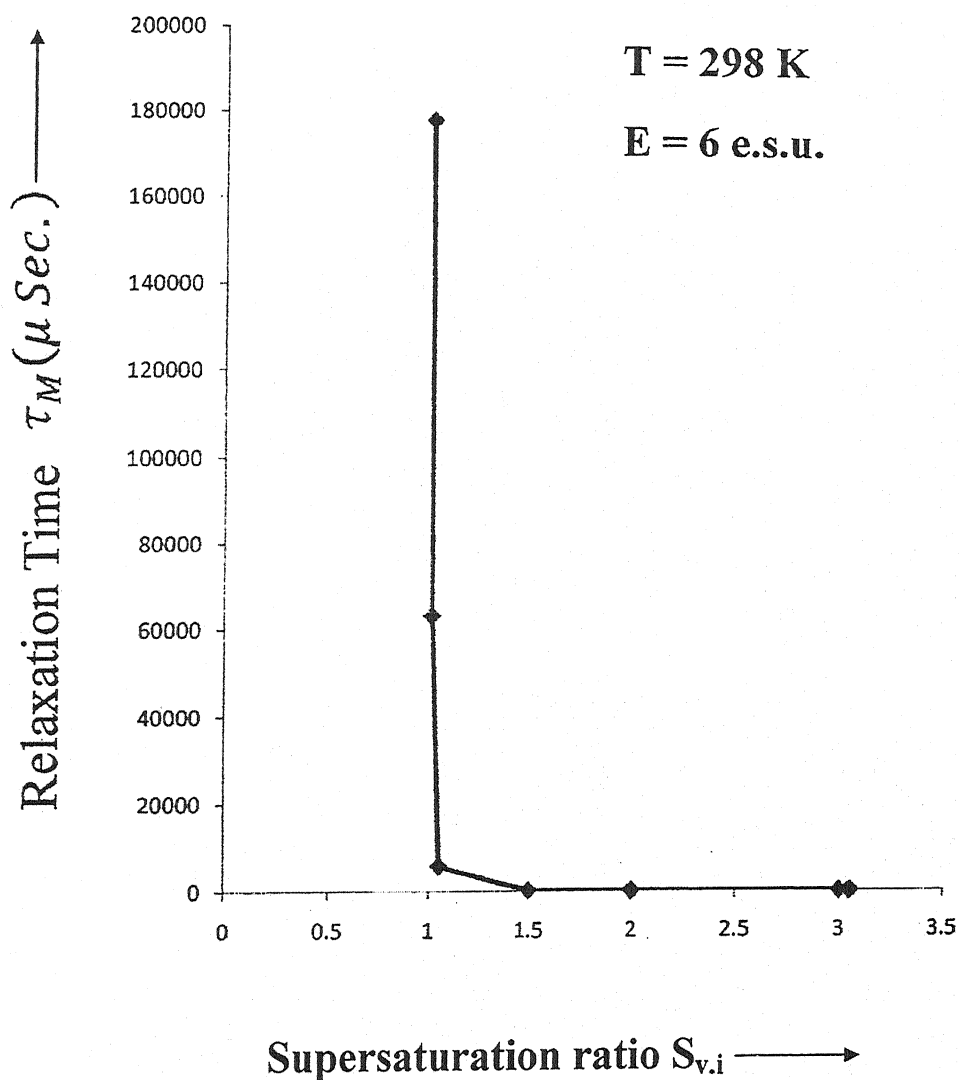


fig. 2.5 (d-III) Variation of relaxation time $\tau_M (\mu \text{ Sec.})$ with supersaturation ratio $S_{v,i}$ at $T=298\text{K}$ and $E=6 \text{ e.s.u.}$

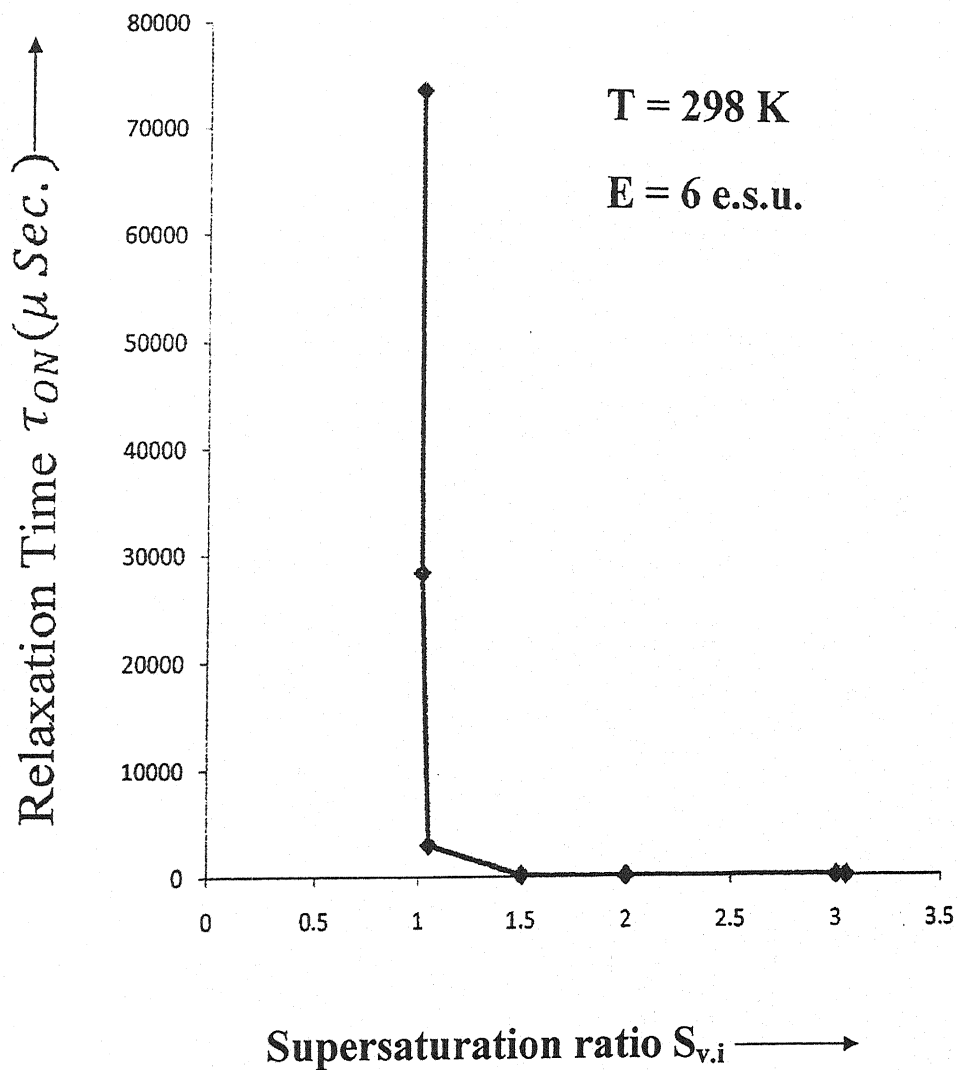


fig. 2.5 (e-III) Variation of relaxation time $\tau_{ON}(\mu \text{ Sec.})$ with supersaturation ratio $S_{v,i}$ at $T=298\text{K}$ and $E=6 \text{ e.s.u.}$

CHAPTER-3

**EQUIVALENCE OF THE
EXTERNAL ELECTRIC FIELD
WITH SUPERSATURATION RATIO
DURING WATER VAPOUR
CONDENSATION AND
GLACIATIONS.**

CHAPTER-3

EQUIVALENCE OF THE EXTERNAL ELECTRIC FIELD WITH SUPERSATURATION RATIO DURING WATER VAPOUR CONDENSATION AND GLACIATION

3.1 INTRODUCTION:

Water in atmosphere exists in all three forms-vapour, liquid and solid (ice). The phase changes take place due to change in temperature in its cycle through the atmosphere. First we will briefly discuss the basic stages of the cycle and examine the details later.

1. Water is transferred from the earth surface, primarily the oceans, into the atmosphere in the first stage of evaporation liquid water undergoes what is known as a change of phase; it vaporizes and becomes water vapour, a gas.
2. This water vapour condenses and forms cloud. In this second stage the water vapour undergoes the reverse change of phase and again becomes water or ice.
3. In the third stage drops of water fall back to earth from the clouds.

Supersaturation ratio is defined as

$$S_v = e/e_{sat.w}$$

Where 'e' is vapour pressure of water vapour over water and $e_{sat.w}$, the maximum possible saturated values.

Air for which relative humidity $\Phi_v = 1(100\%)$ is saturated, if $\Phi_v > 1 (= > 100\%)$, it is said to be supersaturated, corresponding to Supersaturation $S_v > 0$.

According to Goff (1965), $e_{sat.w}(T_{ir} = 0.01^{\circ}C) = 6.1112\text{mb}$, and $e_{sat.w}(T_0 = 0^{\circ}C, p=1\text{atm}) = 6.1067\text{ mb}$. The former result is in excellent agreement with the most recent experimental values obtained as U.S. National Bureau of standards (Guider, 1977). The temperature variation of saturation pressure is shown in fig. (3.1). For $T < 0^{\circ}C$, $e_{sat.w} > e_{sat.i}$. The maximum difference of $e_{sat.w} - e_{sat.i}$, can be calculated by the figure. The variation of $e_{sat.w} - e_{sat.i}$ is illustrated in fig. (3.2). The interesting point to emphasis here is that air saturated with respect to water, with the consequence that supercooled water drops and ice crystals cannot coexist in equilibrium.

It is also worth emphasizing that at sufficiently low temperatures, air may be ice supersaturated but water sub saturated. This is illustrated in fig. (3.3) similarly fig. (3.4) shows the ice supersaturation, which are required for water saturation to occur also.

We shall study the equilibrium of (i) a pure water or aqueous solution drop surrounded by water vapour or humid air and (ii) an ice crystal in humid air. We shall see later that the relationships provided by these case studies are needed in order to formulate the conditions for which cloud drops and ice crystals are nucleated in the atmosphere.

3.2 EQUILIBRIUM BETWEEN A PURE WATER DROP AND PURE WATER VAPOUR OR HUMID AIR:

The Kelvin equation has been derived by W. Thomson according

$$\text{to which } \frac{e_{a.w}}{e_{sat.w}} = \exp\left(\frac{2v_{w.o}\sigma_{w/a}}{RTa}\right) = \exp\left(\frac{2M_w\sigma_{w/a}}{RT\rho_w a}\right) \quad (3.1)$$

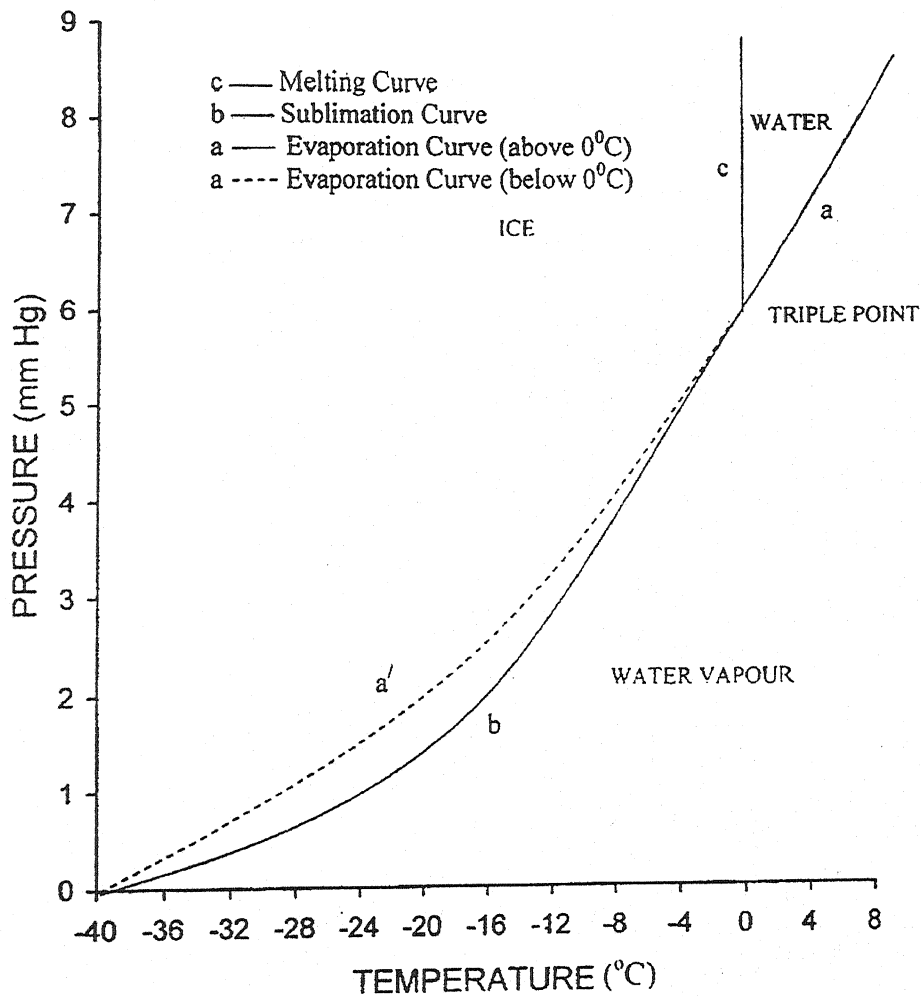


fig. 3.1: P-T phase diagram for bulk water substance.

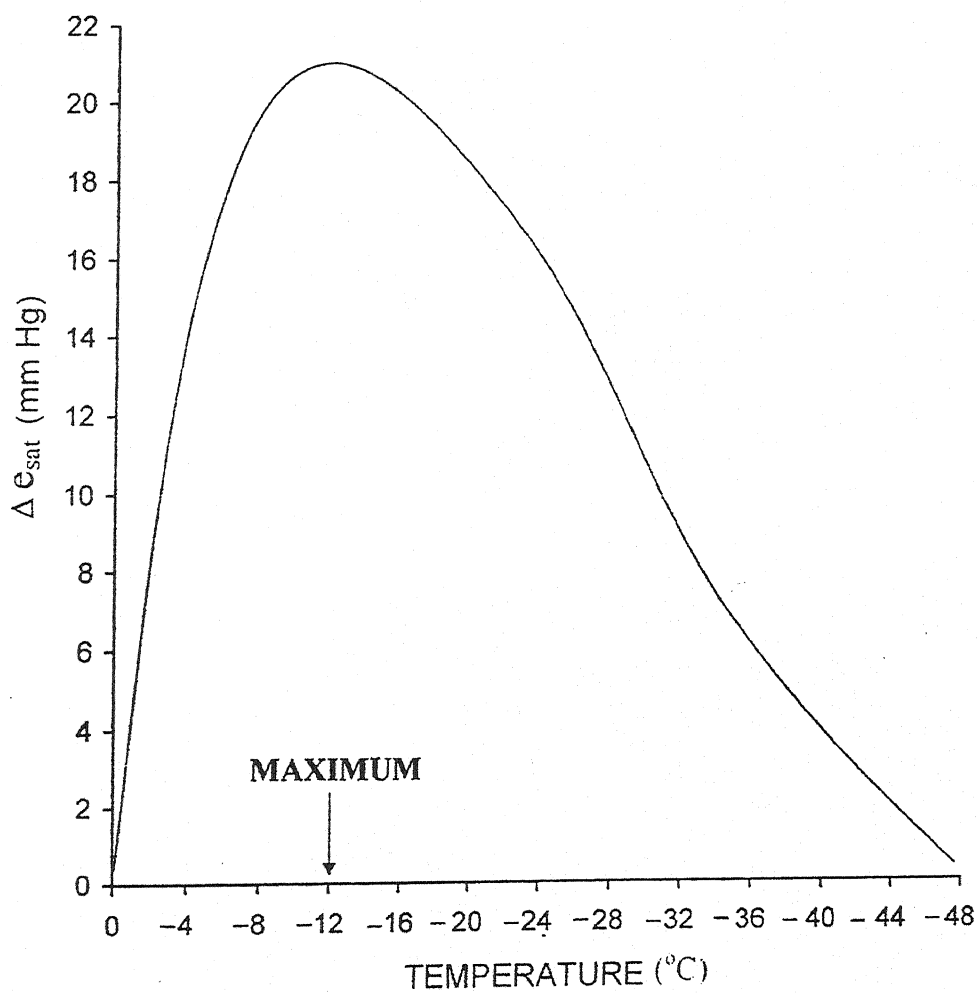


fig. 3.2 : Variation of $\Delta e_{\text{sat}} = e_{\text{sat.w}} - e_{\text{sat.i}}$ with temperature.

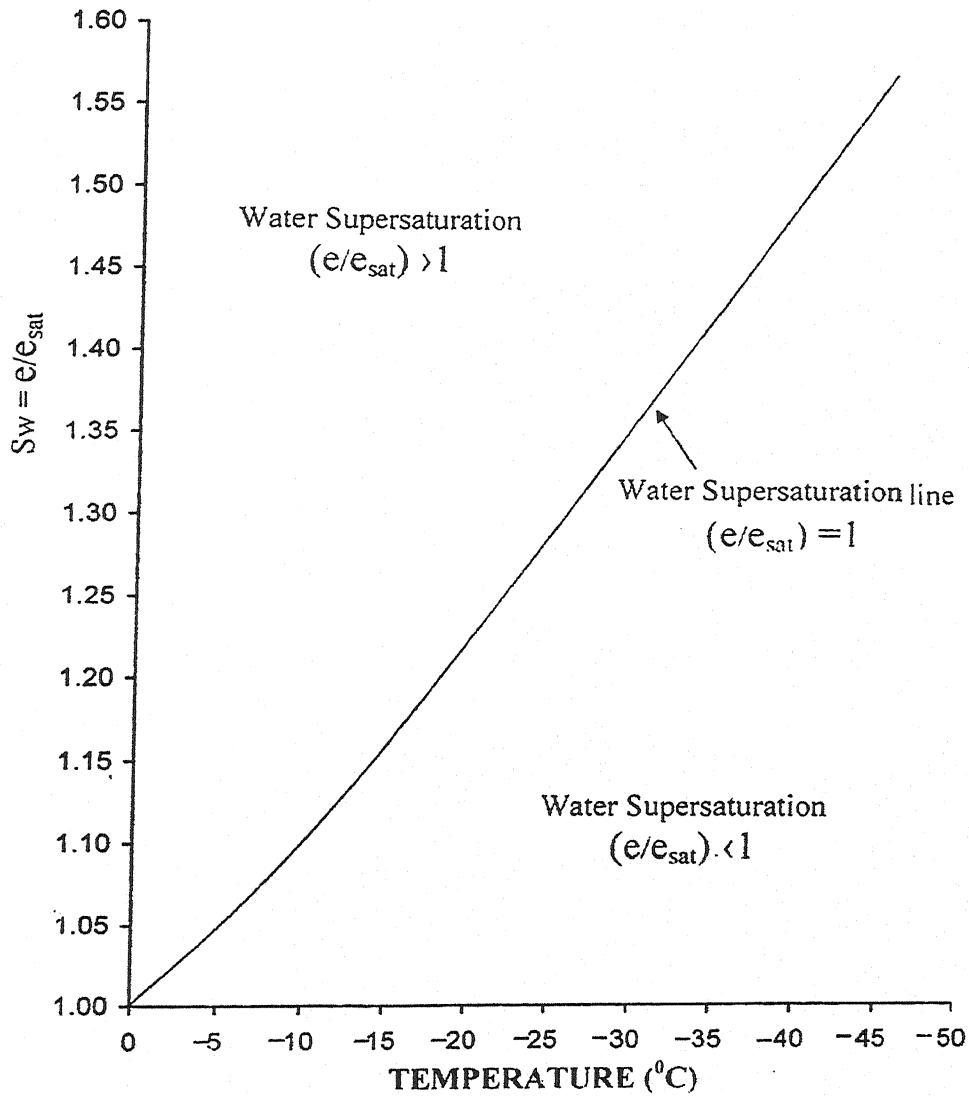


fig. 3.3 : Water Supersaturation as a function of saturation ratio with respect to ice at temperature below 0°C .

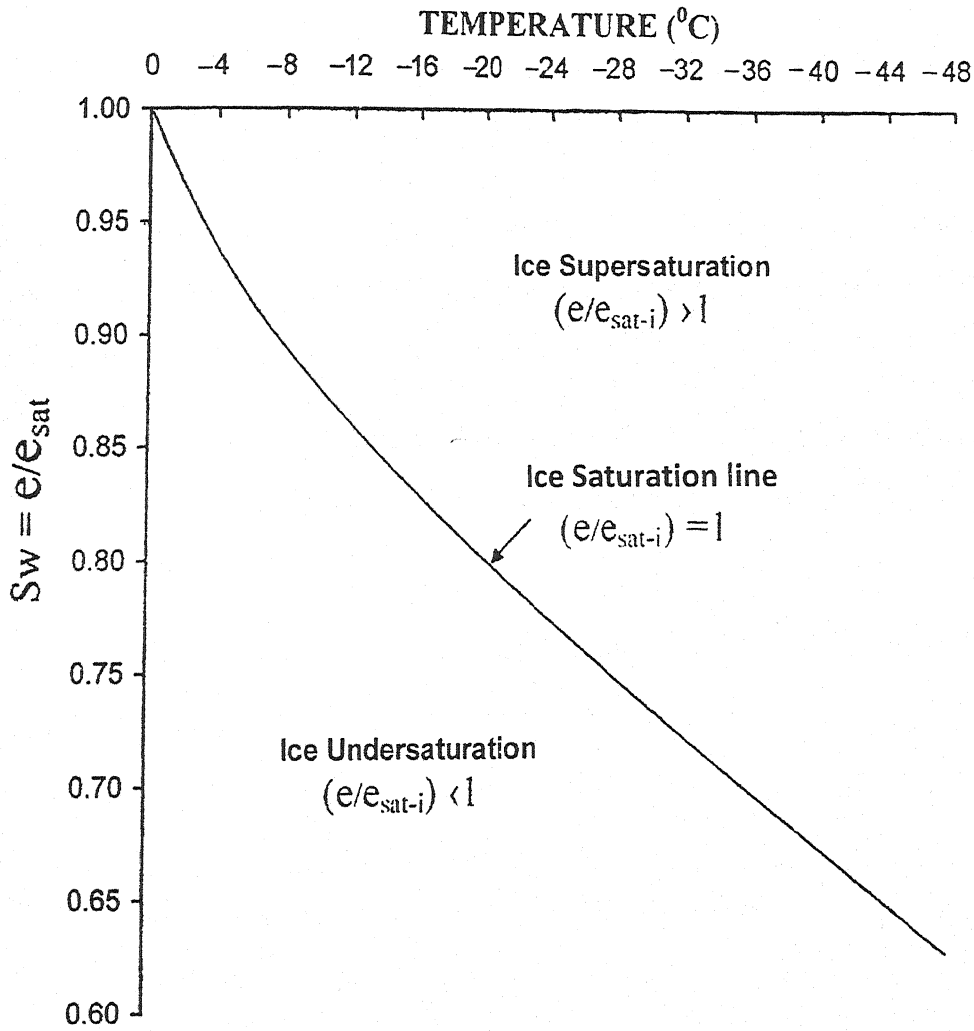


fig. 3.4 : Ice Supersaturation as a function of saturation ratio with respect to ice at temperature below 0°C .

where M_w is the molecular weight of water; $\sigma_{w/a}$, the surface free energy of water air interface; a the radius of water droplet; ρ_w , the density of water; T , the temperature; R , the universal gas constant and $v_{w.0} = \frac{M_w}{\rho_w}$ is the molar volume of pure water in bulk.

According to this equation at any given temperature saturated vapour pressure over the surface of water drop is larger than that over flat surface, and increases as the decreasing radius.

Since Kelvin equation assumes equilibrium between the drop and its environment. We have $e_{a.w} = e$, the partial pressure of vapour in the environment.

Hence we can say that equilibrium requires an environment supersaturation of

$$S_{v.w} = \left(\frac{e_{a.w}}{e_{sat.w}} \right) - 1 > 0$$

Also the Kelvin equation may be expressed in terms of the saturation ratio $S_{v.w} = e_{a.w}/e_{sat.w}$ in form.

$$\ln S_{v.w} = \frac{2v_{w.0}\sigma_{w/a}}{RTa} = \frac{2M_w\sigma_{w/a}}{RT\rho_{w.a}} \quad (3.2)$$

A numerical evaluation of eq. (3.2) is plotted in fig. (3.5) for 20°C and -20°C . Dufour (1963) in deriving the Kelvin equation assumed that compressibility of water is negligible.

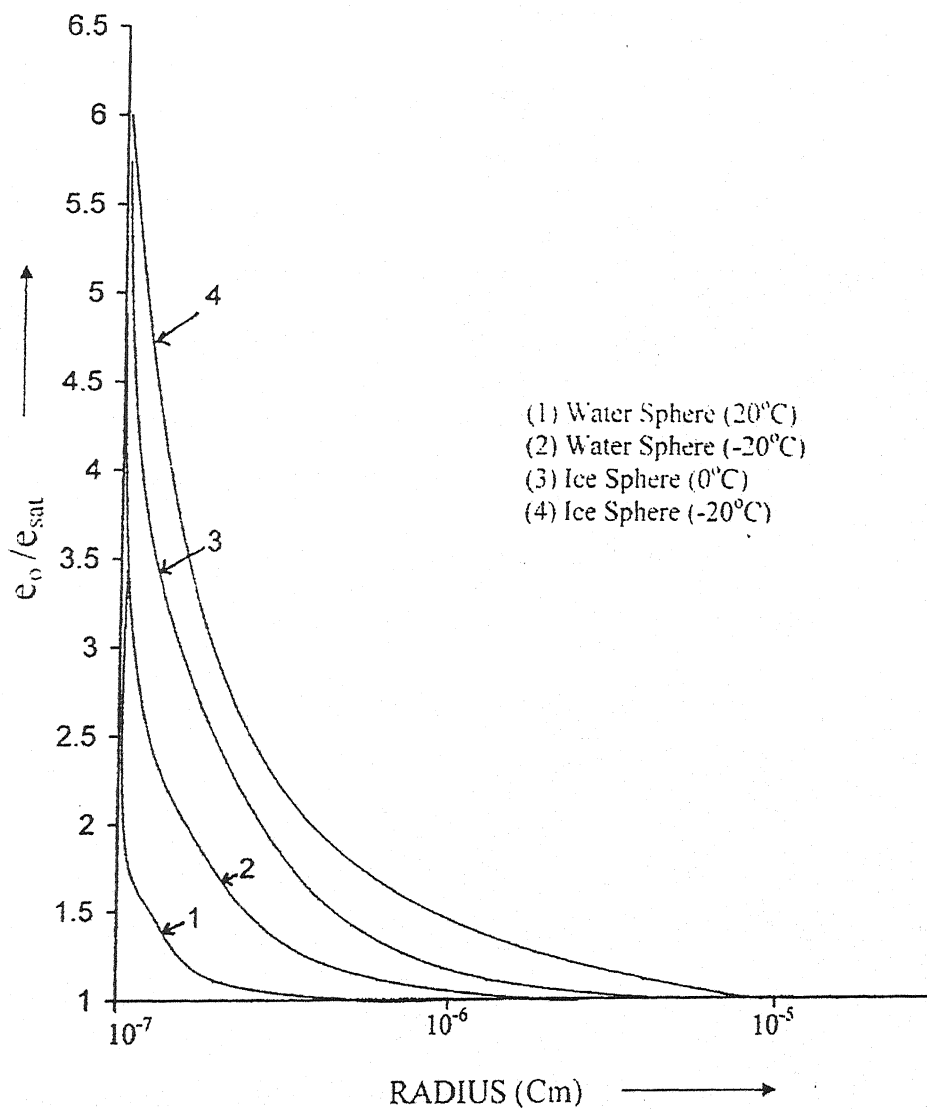


fig. 3.5 : Variation of the equilibrium vapour pressure over a water sphere and over an ice sphere with sphere size, for different temperatures. For (1) and (2), ordinates represents $e_0/e_{sat.w}$ for (3) and (4), ordinates represent $e_0/e_{sat.\lambda}$.

3.3 EQUILIBRIUM OF ICE CRYSTAL IN HUMID AIR:

There are three equilibrium situations involving the ice phase.

1. An ice particle in Humid air
2. An ice particle and separated supercooled solution drop in Humid air.
3. An ice particle in supercooled solution drop in humid air.

These three cases are illustrated in fig. (3.6)

In present case we analyze only case (1) and assuming that ice particle is spherical in strict analogy to the derivation of eq. (3.1) and define the saturation vapour pressure over ice, $e_{a,i}$ varies with radius according to

$$S_{v,w} = \frac{e_{a,i}}{e_{sat,i}} = \exp\left(\frac{2v_i\sigma_{i/a}}{RT_a}\right) = \exp\left(\frac{2M_w\sigma_{i/a}}{RT\rho_{ia}}\right) \quad (3.3)$$

This result is calculated for $T = 263^0\text{K}$. Shown in fig. (3.7) (a,b). The behaviour is seen to be very similar to that for a pure water drop, except that at small radii, $S_{v,i} \gg S_{v,w}$.

3.4 ELECTRICAL STATE OF ATMOSPHERE:

We shall describe some observed and predicated modification in the behaviour of isolated and interacting cloud particle in consequence of the ambient electrical field.

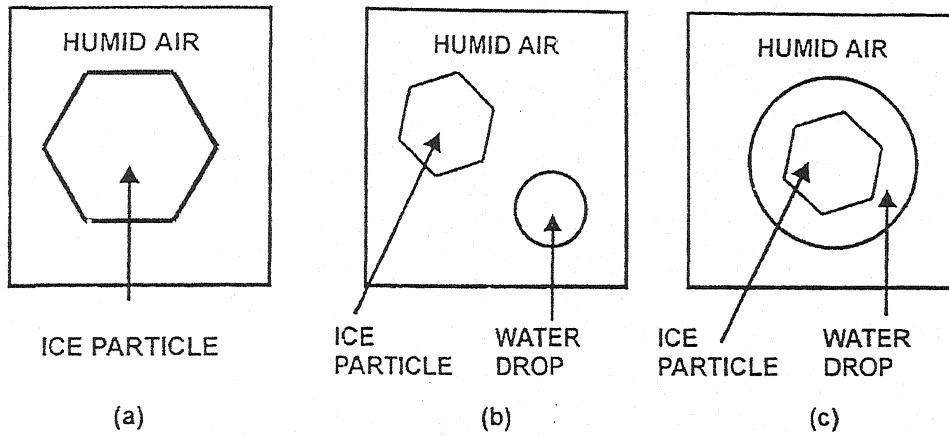


fig. 3.6 : The three basic equilibrium types involving ice crystals.

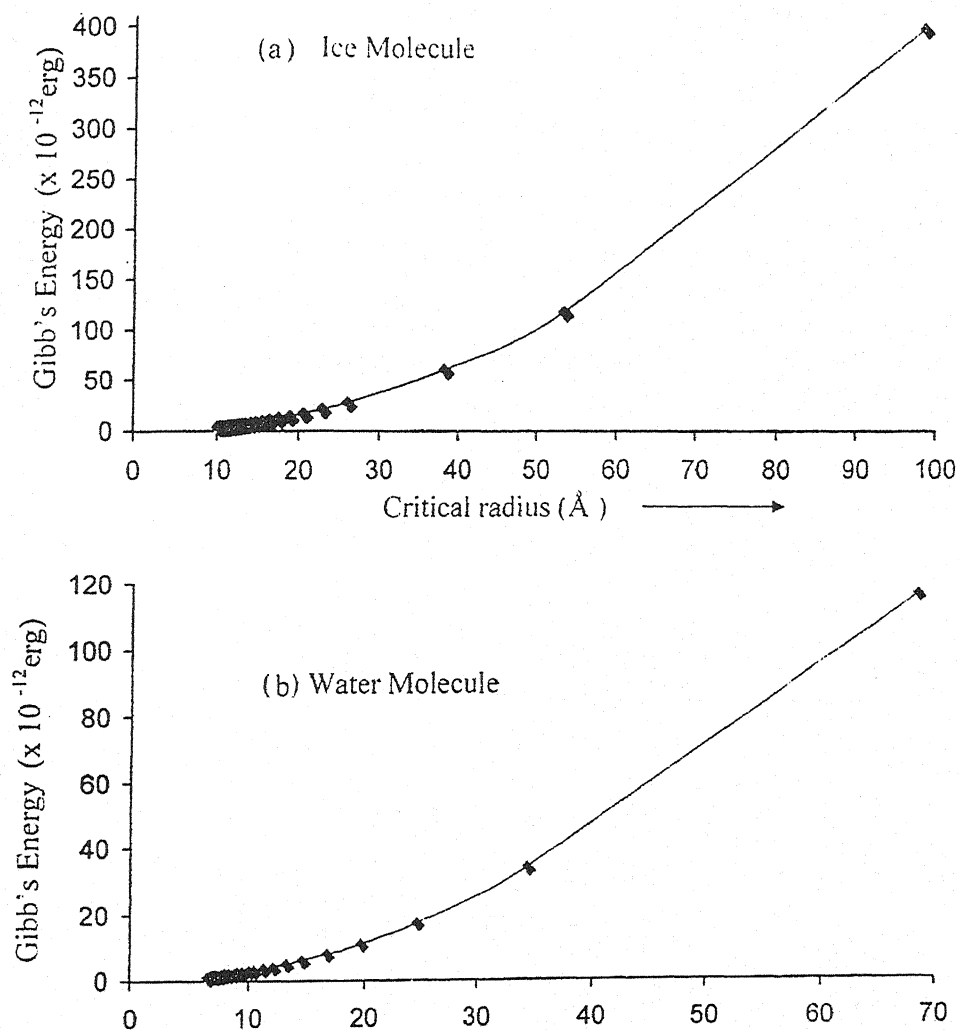


fig. 3.7 : Variation of Critical radius of water and ice molecule and Gibb's energy function for water and ice molecule at $T = 263$ K.

Work carried out prior to 1963 suggested qualitatively that electric fields and the charges enhance ice nucleation (Pruppacher, 1963). Gabarashvili and Glik (1967) and Gabarshvili and Kartsivadze (1968,1969) found that supercooled drops containing particles of quartz or naphthalene were nucleated to ice at significantly warmer temperatures when the particles carried a net negative charge than when they were neutral or carried a net positive charge. Abbas and Latham (1969), Morgan and Langer (1973) observed that charge nuclei produced during corona discharges or by sparks promoted ice nucleation of supercooled drops. The negatively charged ions are more effective than the positively charged ions (Singh, N., et al., 1985). Pruppacher (1973) found that the freezing temperature of supercooled water drops of 100 to 350 μm radius, freely suspended in the air stream of a wind tunnel, was raised considerably when contacted by predominantly negatively charged amorphous sulfur particles which, when unchanged, are known to be poor ice forming nuclei.

The effect of external electrical fields on ice nucleation has been studied under essentially two different experimental conditions. Pruppacher (1963) observed in laboratory experiments that millimeter sized drops, forced in an external electric field to deform and thus to rapidly spread over a solid surface, froze at temperatures up to 10⁰C warmer than when the drops were unaffected by the field. These results are consistent with the observations (Doolittle, 1975), who found that an electric field had no effect on the freezing of supercooled drops if they remained motionless with respect to the supporting surface. Other studies

have dealt with drops in free fall. For example (Dawson et al., 1973), observed millimeter sized drops suspended in the air stream of wind tunnel at temperatures -8 to -15°C , and detected no electro freezing effect for external field upto 4 KVcm^{-1} . Coalescence between drops did not alter this outcome. In contrast to these studies, however (Smith et al., 1971; Abbas and Latham, 1969) found that millimeter sized drops falling in air of -5 to -12°C through intense fields froze if disruptions caused small filaments to be drawn out from or between drops.

The theory of droplet growth in presence of external electric field has been applied to water vapour condensation (Singh, N., et al., 1986). The radius of critical nucleus is found to depend on electric field and relaxation time. Further in presence of electric field, Gibb's free energy of formation of water molecules about a critical nucleus is found to be much less than that in absence of the field, but equilibrium concentration of nuclei is very much large. From the observations we come to know that a small value of electric field is equivalent to very high supersaturation ratio to get nucleus of given size under similar conditions of temperature.

It is well know fact that there exists a vertical electric field in free and undisturbed atmosphere. Also, intense electric fields are generated in thunder clouds (Sapkata et al., 1989). The intense electric fields in thunder clouds are not widespread and the charge and intense electric fields seem to be concentrated in relatively very small volume. Under cloud condition the rate of growth of electric field varies considerably and has been calculated by Winn et al. (1974).

Moore et al. (1962) and Levin and Ziv (1974) reported a raingush following lightning stroke. Murino (1974) has shown that action of a constant and uniform electric field accelerated the condensation of water vapour by a factor depending upon the intensity of electric field. Changes in scavenging of particles due to weak electrification has been studied (Brian A. Tinsley et al., 2006). Mahendra Fernando (2007) studied propagation effects on the electric field time derivatives generated by return strokes in lightning flashes.

In this chapter, we have considered the resultant effect due to an external electric field and the field due to the central dipole. Following Kinetic theory (Collins, 1955), inferred that the relaxation time is independent of the free energy of formation of the nucleus but it varies as the square of the radius of the critical nucleus.

3.5 THEORETICAL CONSIDERATION:

3.5.1 Water Vapour Condensation:

In atmosphere under suitable conditions the phase change of water vapour may take place from,

1. Water vapour to liquid water (Condensation)
2. Water vapour to ice (deposition)
3. Water vapour to ice via liquid phase.

It has been reported that the last mode of phase change is less effective than in (2) and rigorous mathematical consideration is required. Therefore, we consider the first two cases only. In the classical model of

drop formation the Gibb's function has been taken into consideration. However (Abraham, F.F., 1968; Dufour et al., 1963), have shown that the Helmholtz free energy is the proper thermodynamic potential and Gibb's function is only its approximation. For practical purposes, the resulting difference turns out to be negligible. This energy of the formation of nucleus is given by

$$\Delta G_w = \frac{-4}{3} \pi r_w^3 \Delta G_v + 4 \pi r_w^2 \sigma_{w/v} \quad (3.4)$$

With $\Delta G_v = \frac{\rho_w R T \ln S_{v,w}}{M_w}$, the volume free energy of condensate per unit volume per mole where r_w is the radius of water nucleus; $\sigma_{w/v}$, surface free energy per unit area (surface) of water vapour interface; ρ_w , the density of water; T , the temperature; M_w , the molecular weight of water; R , the universal gas constant and $S_{v,w}$, the supersaturation ratio of water vapour over water surface.

The Gibb's free energy at a given temperature and supersaturation increases first with increasing radius of the condensed drop attains a maximum and then decreases monotonically. The critical radius corresponding to the maximum, Gibb's free energy is significant in the sense that above this value the embryo will grow to form a drop because it comes to the lower state in doing so. This critical radius obtained by setting.

$$\frac{\partial(\Delta G_w)}{\partial r_w} = 0 \quad (3.5)$$

From equation (3.4) and (3.5) we have the radius of critical nucleus as

$$r_w^* = \frac{2\sigma_{w/v}}{\Delta G_v} = \frac{2M_w\sigma_{w/v}}{\rho_w RT \ln S_{v,w}} \quad (3.6)$$

Substituting equation (3.6) back into (3.5) the critical Gibb's energy of formation of a critical nucleus is

$$\Delta G_w^* = \frac{4\pi r_w^{*2} \sigma_{w/v}}{3}$$

$$\Delta G_w^* = \frac{16\pi M_w^2 \sigma_{w/v}^3}{3(\rho_w RT \ln S_{v,w})^2}$$

$$\Delta G_w^* = \frac{16\pi \sigma_{w/v}^3}{3(\Delta G_v)^2} \quad (3.7)$$

The number of water molecules in a critical nucleus is given by

$$n_w^* = \frac{4\pi r_w^{*2} \rho_w N}{3M_w} \quad (3.8)$$

Where N is Avogadro's number. The critical supersaturation ratio can be obtained from eq. (3.5) for a neutral drop, it is given by

$$\ln S_{v,w} = \frac{2M_w\sigma_{w/v}}{\rho_w RT} \left(\frac{1}{r_w^*} \right) \quad (3.9)$$

Which is Kelvin classical formula, also sometimes called the Thomson, or Gibb's Thomson formula. The expression for equilibrium concentration for the critical nuclei is

$$C(n_w^*) = C(1)_0 \exp[-\Delta G_w^*/kT] \quad (3.10)$$

Where $C(n_w^*)$ is the equilibrium concentration of critical nuclei having n_w^* water molecules in it; $C(1)_0$, concentration of monomers (water vapour molecules) and k Boltzmann constant.

3.5.2 Nucleation Rate (J):

When homogenous nucleation of water from the vapour occurs, what is observed is the formation of a cloud of small drops. Thus the experimental quantity of interest is the rate at which drops appear in the system as a function of the prevailing saturation ratio $S_{v,w}$ let us denote this rate by J , measured as the number of drops appearing per unit volume and per unit time. We shall make the traditional assumption that J corresponds completely to the rate of germ formation; i.e., it is the nucleation rate.

Further the rate of nucleation of critical nuclei is given by Pruppacher and Klett (1978),

$$J_w = \frac{\alpha_c}{\rho_w} \left[\frac{2N^3 M_w \sigma_{w/v}}{\pi} \right]^{1/2} \left(\frac{e_{sat,w}}{RT} \right)^2 S_{v,w} \exp \left[\frac{-\Delta G_w^*}{kT} \right] \quad (3.11)$$

Where α_c is condensation coefficient

An inspection of the above equation shows that $C(n_w^*)$ and J_w are extremely sensitive to supersaturation. This behaviour enables us to define a critical supersaturation ratio at which drops suddenly appear in vapour. By convention this is taken to correspond to $J_w = 1 \text{ germ cm}^{-3} \text{ sec}^{-1}$. Pruppacher et al. (1978) calculated the pre-exponential factor for $\alpha_c = 1$ is $9 \times 10^{21} \text{ cm}^{-3} \text{ sec}^{-1}$ and $3.7 \times 10^{25} \text{ cm}^{-3} \text{ sec}^{-1}$ at -30°C and 30°C

respectively. Although pre-factor changes with temperature and supersaturation ratio, but it has been assumed constant for present calculations; because the nucleation rate is mainly dependent on the exponential term.

Hence eq. (3.11) become

$$J_w = 9 \times 10^{21} \exp \left[\frac{-\Delta G_w^*}{KT} \right] \quad (3.12)$$

The computed results for, r_w^* , n_w^* , ΔG_w^* and J_w are given in table (3.1).

3.5.3 Water Vapour Ice Nucleation:

The equation analogous to eq.(3.1), eq.(3.10), eq.(3.11) for homogeneous water condensation hold good for spherical ice germ nucleation from water vapour with

$$\alpha_c \rightarrow \alpha_d, S_{v.w} \rightarrow S_{v.i}, \rho_w \rightarrow \rho_i, \sigma_{w/v} \rightarrow \sigma_{i/v} \text{ and } e_{sat.w} \rightarrow e_{sat.i}.$$

The suffix 'i' stands for ice and α_c being deposition coefficient.

The computed results for r_i^* , n_i^* , ΔG_i^* and J_i are given in table (3.2) with $\rho_i = 0.917 \text{ gm cm}^{-3}$, $\sigma_{i/v} = 100 \text{ dynes cm}^{-2}$ and $\alpha_d = 1$.

From equation (3.9) shows that $\ln S_{v.w}$ varies approximately as $(r_i^*)^{-1}$ for neutral drop.

3.6 EFFECT OF EXTERNAL ELECTRICAL FIELD ON NUCLEATION DURING WATER VAPOUR CONDENSATION AND ICE GLACIATIONS :

As water is strongly polarisable medium, an electric dipole moment on both the water droplet and surrounding water vapour. The moment induced on the drop is given by (Kittle et al., 1966).

$$\vec{M} = \vec{E}r_w^3 \quad (3.13)$$

Where r_w is the radius of droplet and \vec{E} the inducing electric field. The moment induced on water vapour molecules is given by

$$\vec{M} = \alpha\vec{E} \quad (3.14)$$

Where α is polarizability.

Water is strongly polarizable medium. An external electric field induces an electric dipole moment on both the water droplet and surrounding water vapour. The expression for rate of increase in the radius of water droplet has been derived as

$$\frac{dr'_w}{dt} = \left(\frac{\rho_v}{\rho_w}\right) [9\alpha\lambda E^2 / (m_w r_w^*)]^{1/2} \quad (3.15)$$

Where λ is the mean free path of water vapour molecule; E , the external electric field; m_w , the mass of water vapor; α , is polarizability; ρ_v , the density of water vapour; r_w^* , the radius of water nucleus in presence of electric field. Integrating the above equation within limits $r'_w = 0$ to $r'_w = \underline{r_w'^*}$ (critical radius of water nucleus) and $t=0$ to $\underline{\tau}$ (relaxation time), we get

$$r_w'^* = \left[\frac{3\rho_v \tau [9\alpha \lambda E^2 / m_w]^{1/2}}{2\rho_w} \right]^{2/3} \quad (3.16)$$

The expression for the Gibb's free energy for the formation of critical water nucleus.

$$\Delta G_w'^* = \frac{4\pi r_w'^2 \sigma_w / v}{3} \quad (3.17)$$

And the equilibrium concentration of the critical nuclei is given by

$$C(n_w'^*) = C(1)_0 \exp(-\Delta G_w'^* / kT) \quad (3.18)$$

Where k is Boltzmann constant and $C(1)_0$ the number of water molecules (monomers) at temperature T .

3.7 EQUIVALENCE BETWEEN ELECTRIC FIELD AND SUPERSATURATION RATIO:

From above we see that in absence of electric field the main parameters to the nucleation of water droplets and ice glaciation are temperature and supersaturation. By thermal fluctuation at given supersaturation the water droplets are nucleated. Hence, supersaturation is the main parameter in the nucleation phenomenon.

Similarly in presence of electric field the main parameter to the nucleation phenomenon is the magnitude of electric field.

Thus, it appears that supersaturation and external electric field are analogous to each other. In the absence of electric field the radius of critical nucleus has been calculated (Gupta, N. et al., 2007). Recently the

equivalence between electric field and supersaturation ratio has been studied briefly (Dwivedi, D. et. al., 2008). In present study, we discussed the equivalence between the two parameters. If the same size of the water nucleus is obtained in the two cases; in absence of electric field and in presence of external field, we may equate eq.(3.6) with eq.(3.16), Thus:

$$\frac{2M_w\sigma_{w/v}}{\rho_w RT \ln S_{v,w}} = \left[\frac{3\rho_v \tau E}{2\rho_w} \left(\frac{9\alpha\lambda}{m_w} \right)^{1/2} \right]^{2/3} \quad (3.19)$$

$$\left[\frac{2M_w\sigma_{w/v}}{\rho_w RT \ln S_{v,w}} \right]^{3/2} \times \frac{2}{3} \frac{\rho_w}{\rho_v \tau} \left(\frac{m_w}{\alpha\lambda} \right)^{1/2} \times \frac{1}{3} = E$$

$$4 \left[\frac{M_w\sigma_{w/v}}{RT \ln S_{v,w}} \right]^{3/2} \times \frac{1}{9} \frac{1}{\rho_v \tau} \left(\frac{2m_w}{\rho_w \alpha\lambda} \right)^{1/2} = E$$

or

$$E = \left[\frac{4}{9\rho_v \tau} \times \left(\frac{2m_w}{\rho_w \alpha\lambda} \right)^{1/2} \times \left(\frac{M_w\sigma_{w/v}}{RT \ln S_{v,w}} \right)^{3/2} \right] \quad (3.20)$$

eq. (3.20) may be written as

$$E_{eq} = \left[\frac{4}{9\rho_v \tau} \times \left(\frac{2m_w}{\rho_w \alpha\lambda} \right)^{1/2} \times \left(\frac{M_w\sigma_{w/v}}{RT \ln S_{v,w}} \right)^{3/2} \right] \quad (3.21)$$

Where $E = E_{eq}$, is equivalent electric field corresponding to supersaturation ratio $S_{v,w}$.

From eq. (3.20) we can write

$$E^{2/3} = \left(\frac{4}{9\rho_v \tau} \right)^{2/3} \times \left(\frac{2m_w}{\rho_w \alpha\lambda} \right)^{1/3} \times \left(\frac{M_w\sigma_{w/v}}{RT \ln S_{v,w}} \right) \quad (3.22)$$

From eq. (3.22) we can write

$$\ln(S_{v,w})_{eq} = \left(\frac{4}{9\rho_v \tau E} \right)^{2/3} \times \left(\frac{2m_w}{\rho_w \alpha\lambda} \right)^{1/3} \times \left(\frac{M_w\sigma_{w/v}}{RT} \right) \quad (3.23)$$

From eq.(3.23) we can calculate $(S_{v,w})_{eq}$ (equivalent supersaturation ratio at a given electric field) and the values of E_{eq} has been calculated from eq. (3.21).

3.8 RESULT AND DISCUSSION:

In table (3.1) and table (3.2) the critical properties of uncharged water and ice molecules at $T=273K$ as a function of supersaturation ratios have been calculated. The graphs of these tables have been plotted from fig. 3.8 (a-c) to fig. 3.9 (a-c). From the graphs it is clear that at high supersaturation ratio the critical radius of the molecule decreases and the no. of molecules also decreases. The Gibb's free energy decreases accordingly increase in supersaturation ratios. From eq. (3.21) the values of equivalent electric field E_{eq} in table (3.3 a) to table (3.3 i) and critical radius r_w^* have been calculated ^{$(\chi_{eq}?)$} for different values of supersaturation ratio at given temperature. Similarly the values of $(S_{v,w})_{eq}$ in table (3.4) are calculated by eq. (3.22) and $r_w'^*$ are calculated by eq. (3.16).

In Present conditions the constant values used are: $\lambda = 10^{-5}cm$; $\rho_v = 10^{-5}cm^{-3}$ at 10^0C ; $\alpha = 5 \times 10^{-23}cm^3$; $\rho_w = 1$; $m_w = 3 \times 10^{-23}g$; $R = 8.31 \times 10^7 erg K^{-1}mole^{-1}$; $\beta = 1.1267 \times 10^{-4}m^{-1}$; $k = 1.38 \times 10^{-16} erg K^{-1}$; $N = 6.023 \times 10^{-23}$.

From the tables, it is clear that at a given relaxation times and temperature, the equivalent electric field decreases with increase in supersaturation ratio. Also, the equivalent electric field decreases with

increasing temperature. Corresponding to a given supersaturation ratio at a constant relaxation time.

Table (3.3a) to table (3.3i) represents the equivalence of supersaturation ratio with the electric field at $T=278\text{K}$, 288K , 298K and relaxation times $\tau = 5, 6, 7 (\times 10^{-6}\text{sec.})$. The equivalence depends on temperature and relaxation time as well. The graphs are plotted from fig. (3.10a) to fig. (3.10i) in supersaturation ratio and equivalent electric field.

Similarly, Table (3.4) compares the equivalence of electric field with supersaturation ratio as function of temperature and relaxation time. The graphs have been plotted from fig. (3.11a) to fig. (3.11c).

From Table (3.4) it is clear that at a given relaxation time and temperature, the equivalent supersaturation ratio decreases with increase in electric field.

3.9 CONCLUSION:

The nucleation rate of water condensation increases very much due to applied external electric field. Hence the electric field is very much effective in nucleation process. A small external electric field is equivalent to be large value of supersaturation ratio, which otherwise never exist in the clouds. In electric field induced nucleation, critical nuclei of smaller size are formed having smaller number of water molecules and require less Gibb's free energy for there formation and equilibrium concentration of critical nuclei is enhanced as compared with the homogeneous nucleation.

Also, from the equivalence of supersaturation ratio with external electric field, it appears that electric field is more efficient than supersaturation. Although, there are a number of mechanisms giving possible explanation for raingush after lightning discharge, creating ionization of medium and a large number of ions are formed. Most of these ions get attached with water embryos of critical nuclei. Further condensation of water vapour on critical nuclei have less radii, requiring less energy of formation (Sapkata, et.al., 1989). The number of critical nuclei is enormously increased using eq. (3.8). Hence, for a given amount of liquid water a large number of droplets of smaller size are formed immediately following lightening. Hence, Lightening seems to be cause of raingush and not the effect.

Table-3.1

Critical Properties of Uncharged water molecules at T=273K, as a function of supersaturation ratio $S_{v,w}$

S. No	$S_{v,w}$	$r_w^*(\text{\AA})$	$n_w^*(\text{cm}^{-3})$	$\Delta G_w^*(\times 10^{-12})$ ergs.	$\Delta G_w^*/kT$	$\ell n J_w$
1.	1.2	64.40691969	37410.19383	128.5183564	3411.32761	-3360.8376
2.	1.4	34.89966953	5951.909441	37.73485919	1001.615416	-951.12542
3.	1.6	24.98442381	2183.737266	19.33921229	513.3304744	-462.84047
4.	1.8	19.97794534	1116.46428	12.3652171	328.2161994	-277.7262
5.	2	16.94123585	680.8126814	8.891812202	236.0198599	-185.52986
6	2.2	14.89334802	462.5613956	6.872025784	182.4076494	-131.91765
7.	2.4	13.41312301	337.8952551	5.57390958	147.9510957	-97.461096
8.	2.6	12.28951252	259.8940517	4.67917639	124.201741	-73.711741
9.	2.8	11.40496155	207.7178637	4.029839556	106.9660656	-56.476066
10.	3	10.68872976	170.9899803	3.539584614	93.95298121	-43.462981
11.	3.2	10.0956555	144.0774249	3.157687508	83.81609353	-33.326094
12.	3.4	9.59552673	123.7082973	2.852579413	75.71745535	-25.227455
13.	3.6	9.167350763	107.8757721	2.603681168	69.11082358	-18.620824
14.	3.8	8.796075268	95.29260112	2.397054886	63.62623788	-13.136238
15.	4	8.470617926	85.10158518	2.22295305	59.00496497	-8.514965
16.	4.2	8.18263291	76.71346079	2.074370086	55.06105234	-4.5710523
17.	4.4	7.925711309	69.71193195	1.94615131	51.65767665	-1.1676767

Table-3.2

Critical Properties of Uncharged ice molecules at T=273K, as a function of supersaturation ratio $S_{v,i}$

S. No	$S_{v,i}$	$r_i^*(\text{\AA})$	$n_i^*(\text{cm}^{-3})$	$\Delta G_i^*(\times 10^{-12})$ ergs.	$\Delta G_i^*/kT$	$\ell n J_i$
1.	1.2	94.91426167	109788.317	377.1649546	10011.27979	-9960.7898
2.	1.4	51.4304423	17467.16747	110.7411179	2939.457394	-2888.9674
3.	1.6	36.8186858	6408.650017	56.75510746	1506.479468	-1455.9895
4.	1.8	29.44081073	3276.506262	36.28840795	963.2215307	-912.73153
5.	2	24.96571642	1997.992282	26.09494892	692.6514021	-642.1614
6	2.2	21.94781458	1357.486609	20.16744818	535.3147577	-484.82476
7.	2.4	19.76645791	991.6268161	16.357845	434.1945375	-383.70454
8.	2.6	18.11063179	762.7153893	13.73205665	364.4969118	-314.00691
9.	2.8	16.80709946	609.5930639	11.82643706	313.915089	-263.42509
10.	3	15.75161331	501.8071345	10.38767774	275.7253741	-225.23537
11.	3.2	14.87762017	422.8264113	9.266917965	245.9764815	-195.48648
12.	3.4	14.14059762	363.0487945	8.371512172	222.2092736	-171.71927
13.	3.6	13.50960942	316.5848197	7.641066359	202.8206816	-152.33068
14.	3.8	12.9624735	279.6567789	7.034676779	186.7249769	-136.23498
15.	4	12.48285821	249.7490352	6.523737231	173.1628505	-122.67285
16.	4.2	12.0584646	225.1322673	6.087688338	161.5885846	-111.09858
17.	4.4	11.67984808	204.5847643	5.711402567	151.6006415	-101.11064

Table-3.3 (a)

Values of E_{eq} Corresponding to supersaturation ratio $S_{v,w}$ for given r_w^* as the function of $\tau = 5 \times 10^{-6}$ sec. and $T=278K$

S. No.	$S_{v,w}$	$r_w^*(\times 10^{-8}cm.)$	$E_{eq}(\times 10^5 v/cm.)$
1.	1.2	64.02416305	258.4834456
2.	1.4	34.69226821	103.1017204
3.	1.6	24.83594669	62.45079161
4.	1.8	19.85922066	44.65397978
5.	2	16.84055769	34.86996997
6.	2.2	14.80484002	28.7423615
7.	2.4	13.33341167	24.56568064
8.	2.6	12.21647856	21.54447546
9.	2.8	11.33718429	19.26081583
10.	3	10.62520891	17.47523747
11.	3.2	10.03565916	16.04115827
12.	3.4	9.538502553	14.86405042
13.	3.6	9.112871145	13.88032751
14.	3.8	8.743802061	13.04569876
15.	4	8.420278843	12.32839611
16.	4.2	8.134005261	11.70505727
17.	4.4	7.878610491	11.15812736
18.	4.6	7.649118222	10.67416543
19.	4.8	7.441582701	10.24270909
20.	5	7.25283342	9.855494585
21.	5.2	7.080292365	9.505909083
22.	5.4	6.921840798	9.188598576
23.	5.6	6.775720573	8.899182246
24.	5.8	6.640459938	8.634041082
25.	6	6.514817016	8.390159218

Table-3.3 (b)

Values of E_{eq} Corresponding to supersaturation ratio $S_{v,w}$ for given r_w^* as the function of $\tau = 6 \times 10^{-6}$ sec. and $T=278K$

S. No.	$S_{v,w}$	$r_w^*(\times 10^{-8}cm.)$	$E_{eq}(\times 10^5 v/cm.)$
1.	1.2	64.02416305	215.4028713
2.	1.4	34.69226821	85.91810037
3.	1.6	24.83594669	52.04232634
4.	1.8	19.85922066	37.21164982
5.	2	16.84055769	29.05830831
6.	2.2	14.80484002	23.95196792
7.	2.4	13.33341167	20.47140053
8.	2.6	12.21647856	17.95372955
9.	2.8	11.33718429	16.05067986
10.	3	10.62520891	14.56269789
11.	3.2	10.03565916	13.36763189
12.	3.4	9.538502553	12.38670868
13.	3.6	9.112871145	11.56693959
14.	3.8	8.743802061	10.87141563
15.	4	8.420278843	10.27366343
16.	4.2	8.134005261	9.754214389
17.	4.4	7.878610491	9.29843947
18.	4.6	7.649118222	8.895137858
19.	4.8	7.441582701	8.535590908
20.	5	7.25283342	8.212912155
21.	5.2	7.080292365	7.921590902
22.	5.4	6.921840798	7.65716548
23.	5.6	6.775720573	7.415985205
24.	5.8	6.640459938	7.195034235
25.	6	6.514817016	6.991799348

Table-3.3 (c)

Values of E_{eq} Corresponding to supersaturation ratio $S_{v,w}$ for given r_w^* as the function of $\tau = 7 \times 10^{-6}$ sec. and $T=278K$

S. No.	$S_{v,w}$	$r_w^*(\times 10^{-8} cm.)$	$E_{eq}(\times 10^5 v/cm.)$
1.	1.2	64.02416305	184.6310325
2.	1.4	34.69226821	73.64408603
3.	1.6	24.83594669	44.60770829
4.	1.8	19.85922066	31.89569984
5.	2	16.84055769	24.90712141
6.	2.2	14.80484002	20.53025821
7.	2.4	13.33341167	17.54691474
8.	2.6	12.21647856	15.38891104
9.	2.8	11.33718429	13.7577256
10.	3	10.62520891	12.48231248
11.	3.2	10.03565916	11.45797019
12.	3.4	9.538502553	10.61717887
13.	3.6	9.112871145	9.914519649
14.	3.8	8.743802061	9.318356255
15.	4	8.420278843	8.805997223
16.	4.2	8.134005261	8.36075519
17.	4.4	7.878610491	7.970090974
18.	4.6	7.649118222	7.624403878
19.	4.8	7.441582701	7.316220779
20.	5	7.25283342	7.03963899
21.	5.2	7.080292365	6.789935059
22.	5.4	6.921840798	6.563284697
23.	5.6	6.775720573	6.356558747
24.	5.8	6.640459938	6.167172202
25.	6	6.514817016	5.99297087

Table-3.3 (d)

Values of E_{eq} Corresponding to supersaturation ratio $S_{v,w}$ for given r_w^* as the function of $\tau = 5 \times 10^{-6}$ sec. and $T=288K$

S. No.	$S_{v,w}$	$r_w^*(\times 10^{-8}cm.)$	$E_{eq}(\times 10^5 v/cm.)$
1.	1.2	60.78316285	251.8965789
2.	1.4	32.936093	100.474406
3.	1.6	23.57871341	60.85937426
4.	1.8	18.8539168	43.51607398
5.	2	15.98806312	33.98138756
6.	2.2	14.05539657	28.00992735
7.	2.4	12.65845416	23.93967976
8.	2.6	11.59806189	20.99546317
9.	2.8	10.76327883	18.76999745
10.	3	10.08734473	17.02992052
11.	3.2	9.527638879	15.63238559
12.	3.4	9.055649093	14.48527367
13.	3.6	8.651563792	13.52661872
14.	3.8	8.301177545	12.71325859
15.	4	7.994031562	12.01423479
16.	4.2	7.722249583	11.40678032
17.	4.4	7.479783283	10.87378769
18.	4.6	7.261908261	10.40215844
19.	4.8	7.064878503	9.981696788
20.	5	6.885683997	9.60434957
21.	5.2	6.721877231	9.263672464
22.	5.4	6.571446723	8.954447899
23.	5.6	6.432723325	8.672406691
24.	5.8	6.304309789	8.41402205
25.	6	6.185027102	8.176354964

Table-3.3 (e)

Values of E_{eq} Corresponding to supersaturation ratio $S_{v,w}$ for given r_w^* as the function of $\tau = 6 \times 10^{-6}$ sec. and $T=288K$

S. No.	$S_{v,w}$	$r_w^*(\times 10^{-8}cm.)$	$E_{eq}(\times 10^5 v/cm.)$
1.	1.2	60.78316285	209.9138157
2.	1.4	32.936093	83.72867168
3.	1.6	23.57871341	50.71614522
4.	1.8	18.8539168	36.26339498
5.	2	15.98806312	28.31782296
6.	2.2	14.05539657	23.34160612
7.	2.4	12.65845416	19.94973314
8.	2.6	11.59806189	17.49621931
9.	2.8	10.76327883	15.64166454
10.	3	10.08734473	14.19160043
11.	3.2	9.527638879	13.02698799
12.	3.4	9.055649093	12.07106139
13.	3.6	8.651563792	11.27218227
14.	3.8	8.301177545	10.59438216
15.	4	7.994031562	10.01186232
16.	4.2	7.722249583	9.50565027
17.	4.4	7.479783283	9.061489745
18.	4.6	7.261908261	8.668465364
19.	4.8	7.064878503	8.318080656
20.	5	6.885683997	8.003624642
21.	5.2	6.721877231	7.719727053
22.	5.4	6.571446723	7.462039916
23.	5.6	6.432723325	7.227005576
24.	5.8	6.304309789	7.011685042
25.	6	6.185027102	6.813629137

Table-3.3 (f)

Values of E_{eq} Corresponding to supersaturation ratio $S_{v,w}$ for given r_w^* as the function of $\tau = 7 \times 10^{-6}$ sec. and $T=288K$

S. No.	$S_{v,w}$	$r_w^*(\times 10^{-8}cm.)$	$E_{eq}(\times 10^5 v/cm.)$
1.	1.2	60.78316285	179.9261278
2.	1.4	32.936093	71.76743286
3.	1.6	23.57871341	43.47098162
4.	1.8	18.8539168	31.08290999
5.	2	15.98806312	24.27241968
6.	2.2	14.05539657	20.00709096
7.	2.4	12.65845416	17.09977126
8.	2.6	11.59806189	14.99675941
9.	2.8	10.76327883	13.40714104
10.	3	10.08734473	12.16422894
11.	3.2	9.527638879	11.16598971
12.	3.4	9.055649093	10.34662405
13.	3.6	8.651563792	9.661870513
14.	3.8	8.301177545	9.080898996
15.	4	7.994031562	8.581596277
16.	4.2	7.722249583	8.147700232
17.	4.4	7.479783283	7.76699121
18.	4.6	7.261908261	7.430113169
19.	4.8	7.064878503	7.12978342
20.	5	6.885683997	6.860249693
21.	5.2	6.721877231	6.616908903
22.	5.4	6.571446723	6.396034214
23.	5.6	6.432723325	6.194576208
24.	5.8	6.304309789	6.01001575
25.	6	6.185027102	5.840253546

Table-3.3 (g)

Values of E_{eq} Corresponding to supersaturation ratio $S_{v,w}$ for given r_w^* as the function of $\tau = 5 \times 10^{-6}$ sec. and $T=298K$

S. No.	$S_{v,w}$	$r_w^*(\times 10^{-8}cm.)$	$E_{eq}(\times 10^5 v/cm.)$
1.	1.2	57.58170636	243.9717028
2.	1.4	31.20134503	97.31339753
3.	1.6	22.33681975	58.94468767
4.	1.8	17.86087874	42.14702206
5.	2	15.14596992	32.91230481
6.	2.2	13.31509714	27.12871171
7.	2.4	11.99173186	23.1865175
8.	2.6	10.98719058	20.33492842
9.	2.8	10.19637564	18.1794777
10.	3	9.556043069	16.49414504
11.	3.2	9.025816995	15.14057772
12.	3.4	8.578686968	14.0295549
13.	3.6	8.195884888	13.10106003
14.	3.8	7.863953527	12.31328889
15.	4	7.57298496	11.63625696
16.	4.2	7.315517771	11.04791352
17.	4.4	7.0858222	10.53168928
18.	4.6	6.879422681	10.07489787
19.	4.8	6.692770504	9.667664295
20.	5	6.523014194	9.302188735
21.	5.2	6.36783515	8.972229615
22.	5.4	6.225327835	8.672733512
23.	5.6	6.093911015	8.399565555
24.	5.8	5.972261036	8.14930991
25.	6	5.859260982	7.919120029

Table-3.3 (h)

Values of E_{eq} Corresponding to supersaturation ratio $S_{v,w}$ for given r_w^* as the function of $\tau = 6 \times 10^{-6}$ sec. and $T=298K$

S. No.	$S_{v,w}$	$r_w^*(\times 10^{-8}cm.)$	$E_{eq}(\times 10^5 v/cm.)$
1	1.2	57.58170636	203.3097523
2	1.4	31.20134503	81.09449795
3	1.6	22.33681975	49.12057306
4	1.8	17.86087874	35.12251838
5	2	15.14596992	27.42692067
6	2.2	13.31509714	22.60725976
7	2.4	11.99173186	19.32209792
8	2.6	10.98719058	16.94577368
9	2.8	10.19637564	15.14956475
10	3	9.556043069	13.74512087
11	3.2	9.025816995	12.6171481
12	3.4	8.578686968	11.69129575
13	3.6	8.195884888	10.91755003
14	3.8	7.863953527	10.26107408
15	4	7.57298496	9.696880798
16	4.2	7.315517771	9.206594598
17	4.4	7.0858222	8.776407733
18	4.6	6.879422681	8.395748225
19	4.8	6.692770504	8.056386913
20	5	6.523014194	7.751823946
21	5.2	6.36783515	7.476858012
22	5.4	6.225327835	7.227277927
23	5.6	6.093911015	6.999637962
24	5.8	5.972261036	6.791091592
25	6	5.859260982	6.599266691

Table-3.3 (i)

Values of E_{eq} Corresponding to supersaturation ratio $S_{v,w}$ for given r_w^* as the function of $\tau = 7 \times 10^{-6}$ sec. and $T=298K$

S. No.	$S_{v,w}$	$r_w^*(\times 10^{-8} cm.)$	$E_{eq}(\times 10^5 v/cm.)$
1.	1.2	57.58170636	174.265502
2.	1.4	31.20134503	69.50956967
3.	1.6	22.33681975	42.10334834
4.	1.8	17.86087874	30.10501576
5.	2	15.14596992	23.50878915
6.	2.2	13.31509714	19.37765122
7.	2.4	11.99173186	16.56179822
8.	2.6	10.98719058	14.52494887
9.	2.8	10.19637564	12.98534122
10.	3	9.556043069	11.78153217
11.	3.2	9.025816995	10.81469837
12.	3.4	8.578686968	10.02111064
13.	3.6	8.195884888	9.357900022
14.	3.8	7.863953527	8.795206352
15.	4	7.57298496	8.311612112
16.	4.2	7.315517771	7.891366798
17.	4.4	7.0858222	7.522635199
18.	4.6	6.879422681	7.196355622
19.	4.8	6.692770504	6.905474497
20.	5	6.523014194	6.644420525
21.	5.2	6.36783515	6.408735439
22.	5.4	6.225327835	6.194809651
23.	5.6	6.093911015	5.999689682
24.	5.8	5.972261036	5.82093565
25.	6	5.859260982	5.656514306

Table-3.4
Values of $(S_{v,w})_{eq}$ Corresponding to E as the function of τ and T

τ ($\times 10^{-6}sec.$)	E ($\times 10^5V/cm.$)	r_w^* ($\times 10^{-8}cm.$)	equivalent supersaturation ($S_{v,w})_{eq}$ at			
			273K	280K	290K	300K
5	1.2	4.953	10.023	9.462	8.756	8.145
	1.4	5.489	8.002	7.597	7.084	6.637
	1.6	6.000	6.704	6.392	5.996	5.649
	1.8	6.490	5.806	5.557	5.237	4.956
	2.0	6.962	5.153	4.946	4.681	4.446
	2.2	7.419	4.659	4.483	4.257	4.056
	2.4	7.862	4.272	4.119	3.923	3.748
	2.6	8.293	3.961	3.827	3.654	3.500
6	1.2	5.593	7.699	7.316	6.831	6.407
	1.4	6.198	6.308	6.024	5.662	5.344
	1.6	6.775	5.392	5.169	4.885	4.633
	1.8	7.329	4.748	4.566	4.333	4.127
	2.0	7.862	4.272	4.119	3.923	3.748
	2.2	8.378	3.906	3.775	3.606	3.455
	2.4	8.878	3.618	3.503	3.355	3.222
	2.6	9.365	3.384	3.282	3.150	3.032
7	1.2	6.198	6.308	6.024	5.662	5.344
	1.4	6.869	5.269	5.055	4.780	4.537
	1.6	7.509	4.574	4.403	4.184	3.989
	1.8	8.122	4.078	3.937	3.755	3.593
	2.0	8.713	3.707	3.587	3.432	3.295
	2.2	9.285	3.420	3.316	3.182	3.061
	2.4	9.839	3.191	3.099	2.981	2.874
	2.6	10.110	3.004	2.922	2.816	2.721

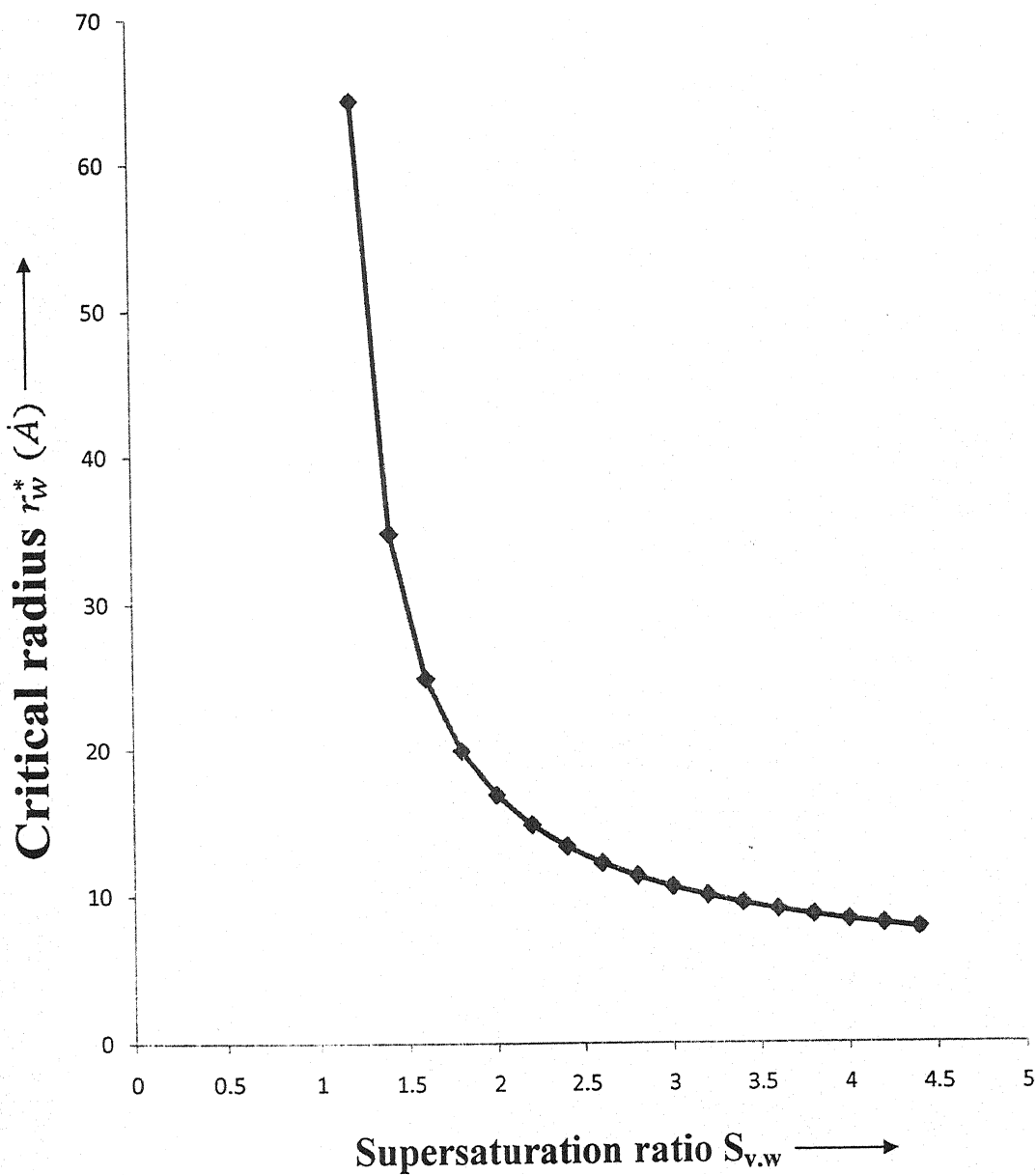


fig. 3.8 (a) Variation of Critical radius of water molecules r_w^* (Å) with supersaturation ratio $S_{v,w}$ at $T=273K$.

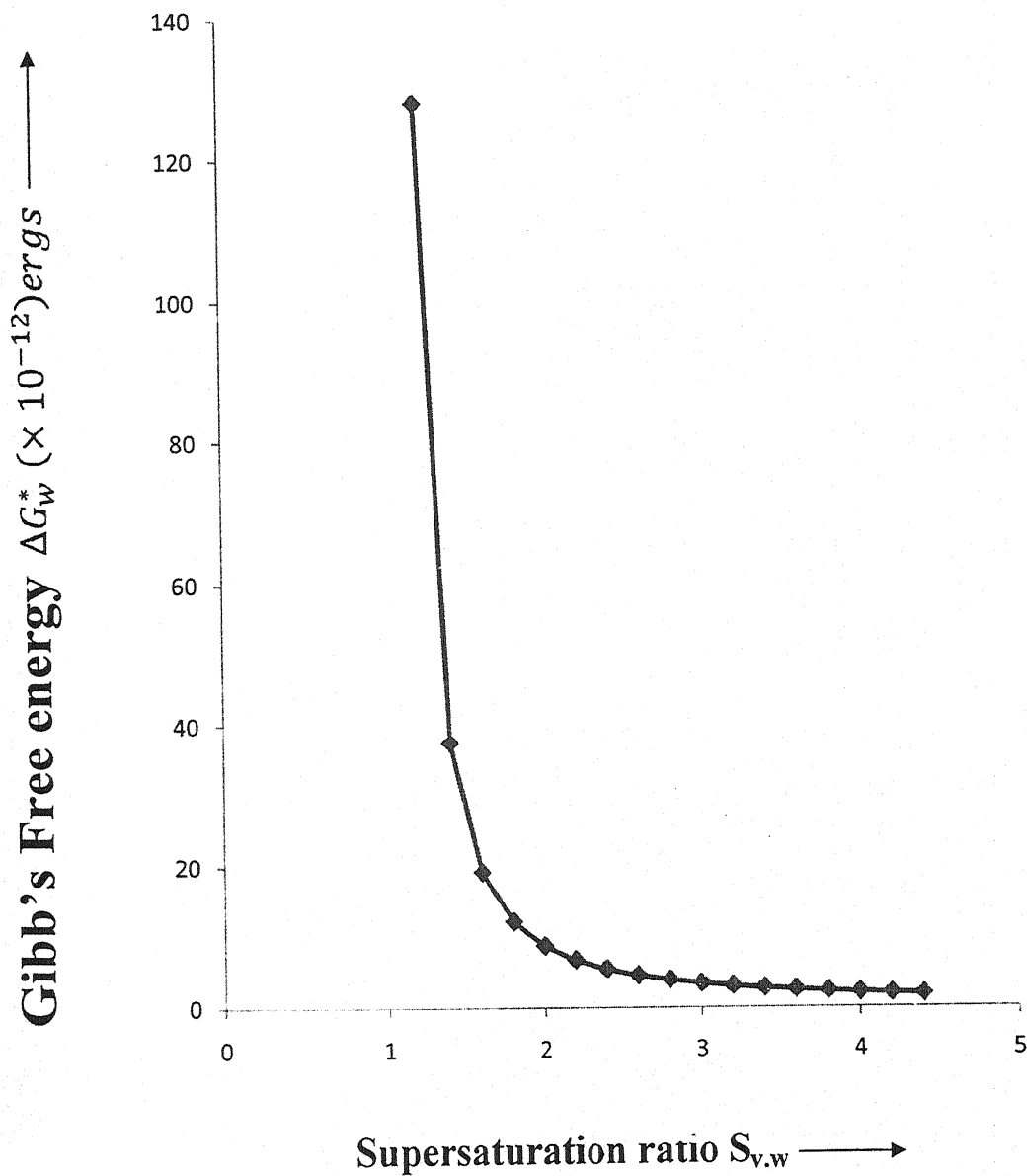


fig. 3.8 (b) Variation of Gibb's Free energy $\Delta G_w^* (\times 10^{-12}) \text{ ergs}$ with supersaturation ratio $S_{v,w}$ at $T=273\text{K}$.

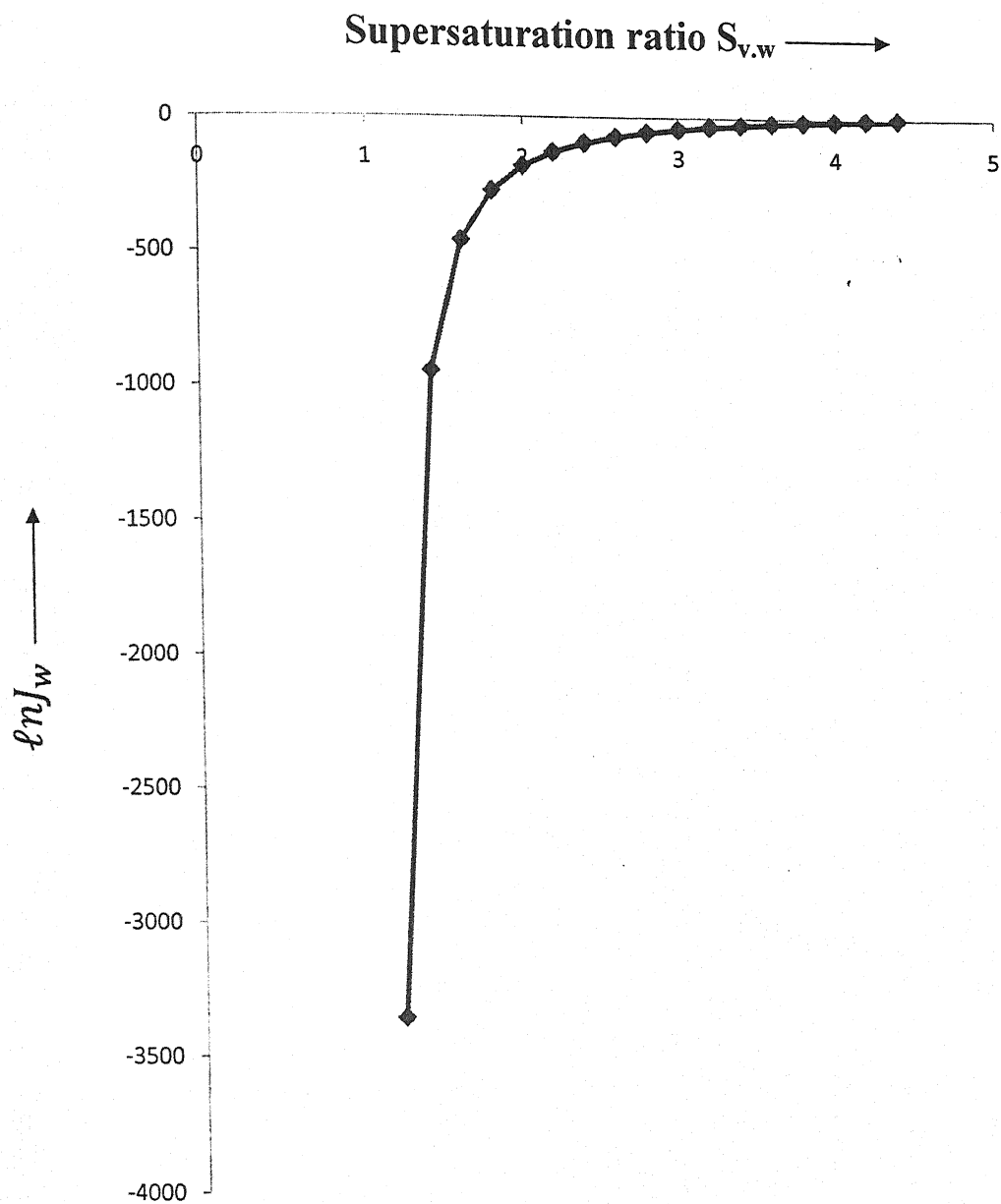


fig. 3.8 (c) Variation of natural log of rate of nucleation $\ln J_w$ with supersaturation ratio $S_{v,w}$ at $T=273K$.

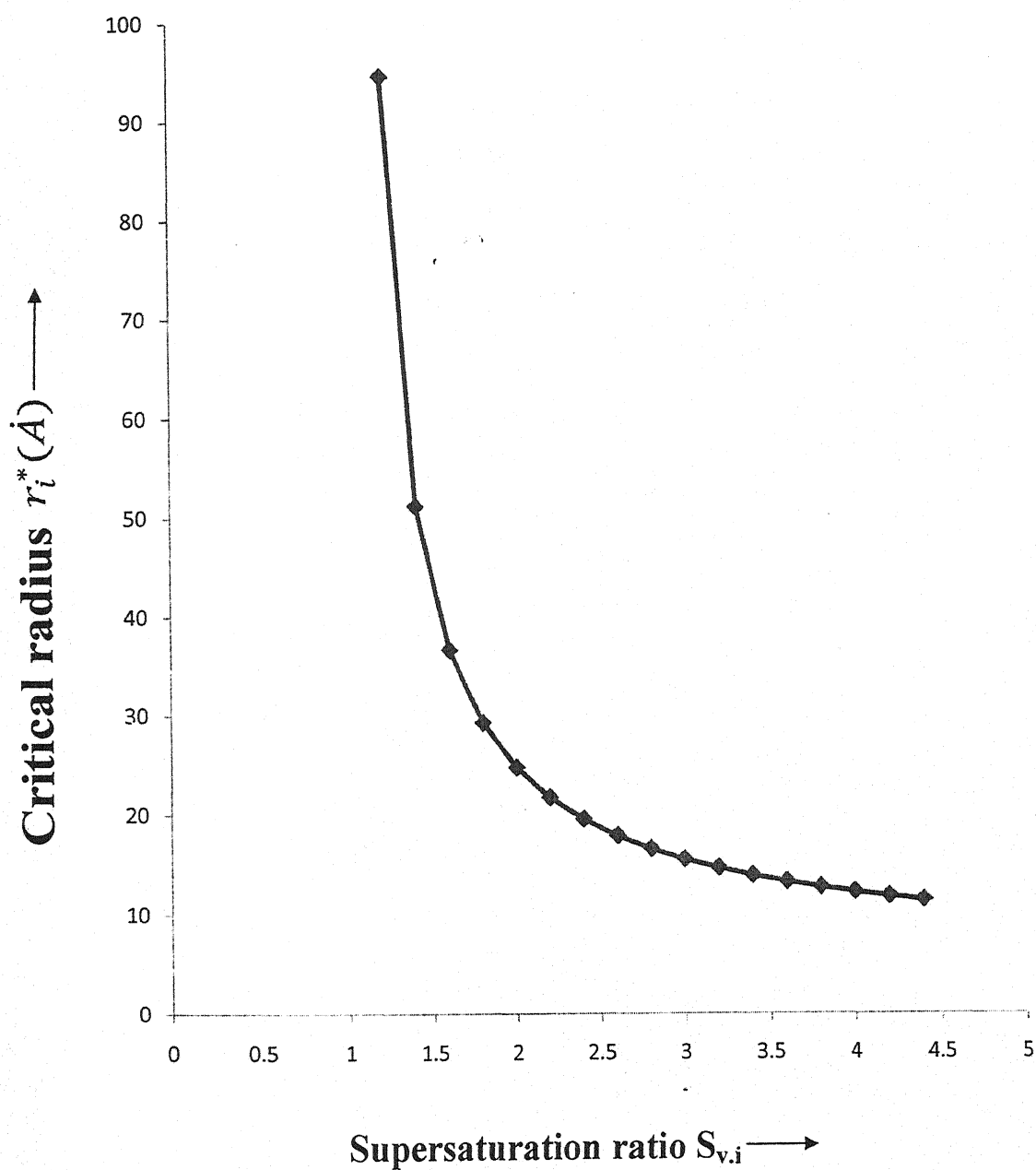


fig. 3.9 (a) Variation of Critical radius of ice molecules r_i^* (Å) with supersaturation ratio $S_{v,i}$ at $T=273K$.

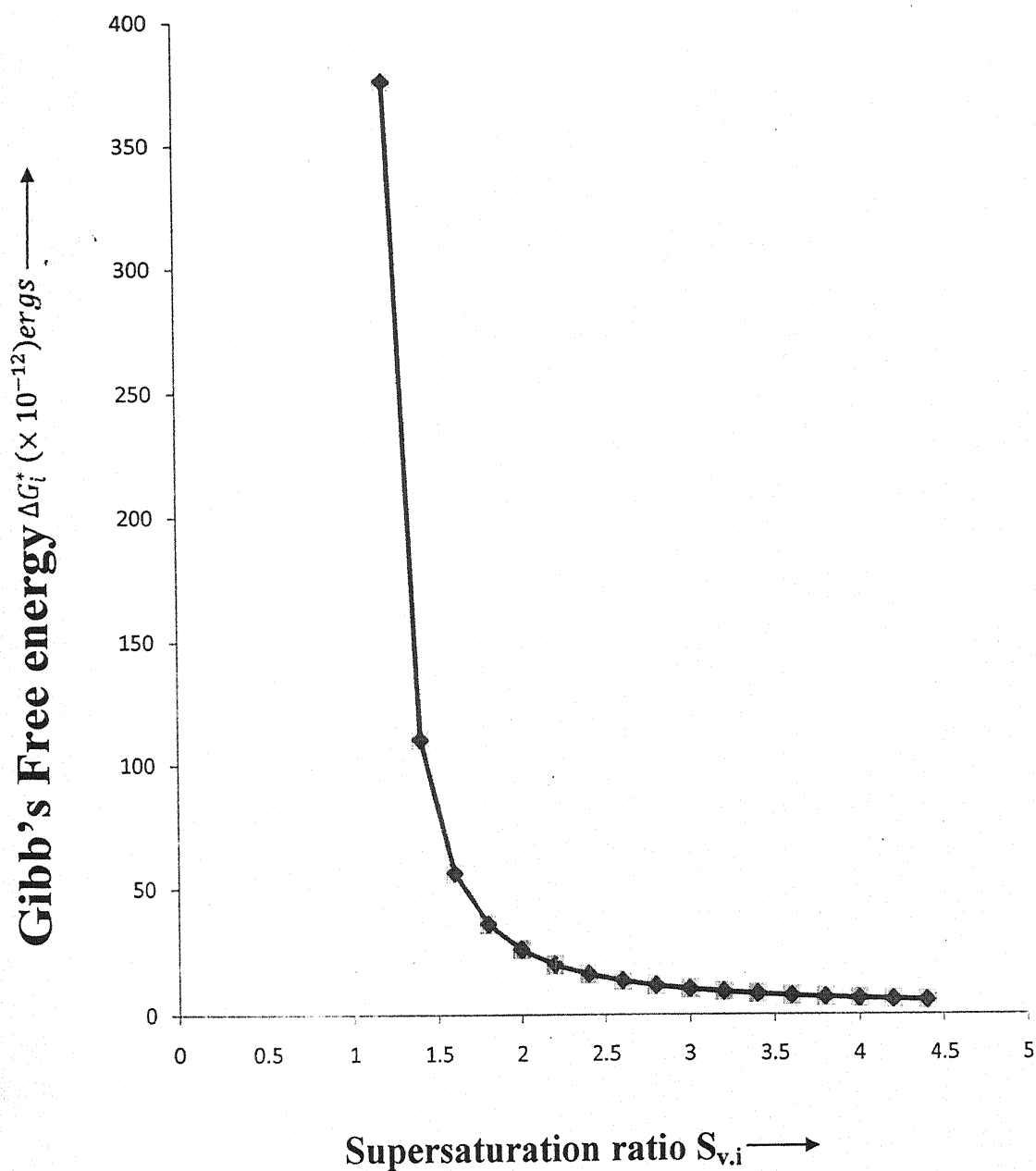


fig. 3.9 (b) Variation of Gibb's Free energy $\Delta G_i^* (\times 10^{-12})$ ergs with supersaturation ratio $S_{v,i}$ at $T=273K$.

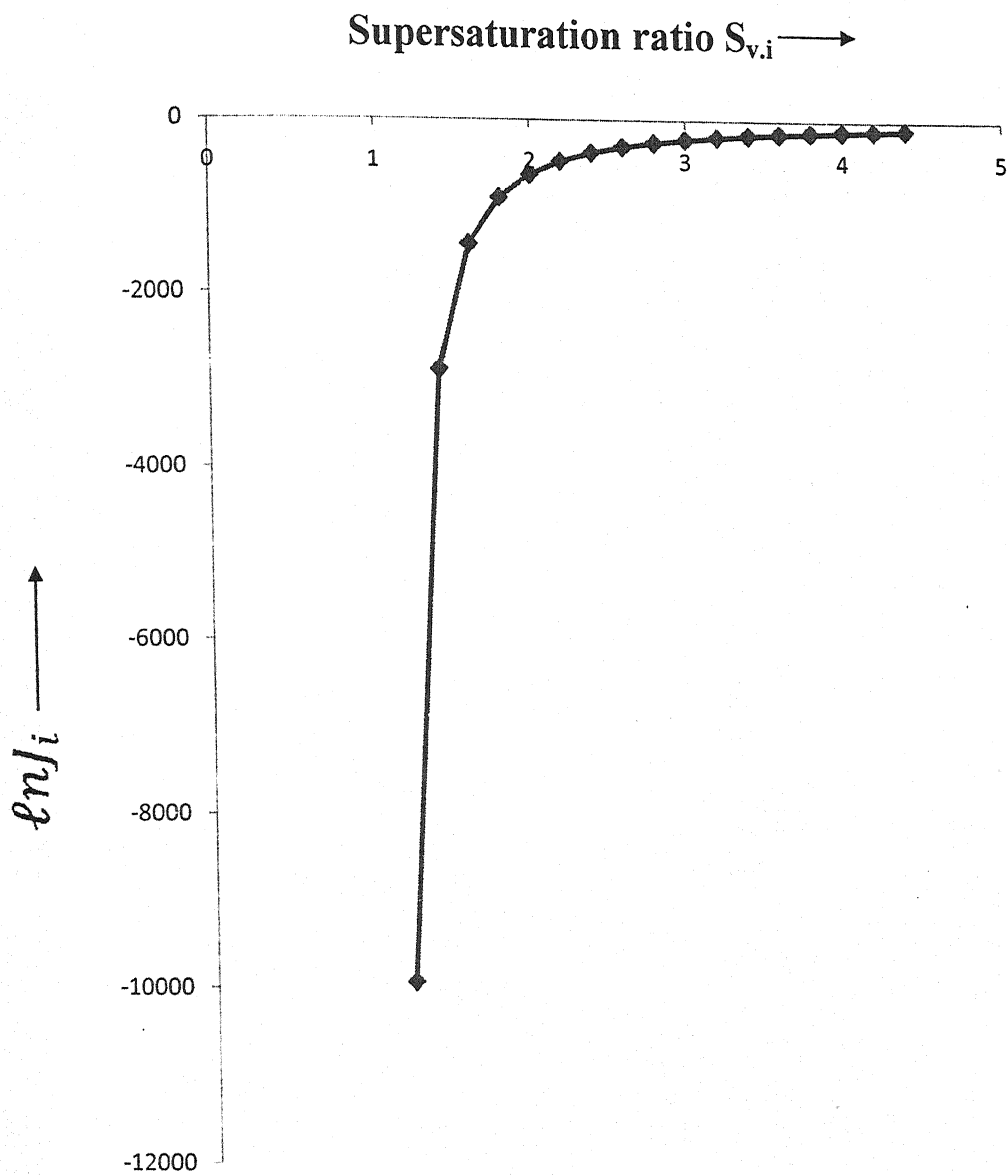


fig. 3.9 (c) Variation of natural log of rate of nucleation $\ln J_i$ with supersaturation ratio $S_{v,i}$ at $T=273K$.

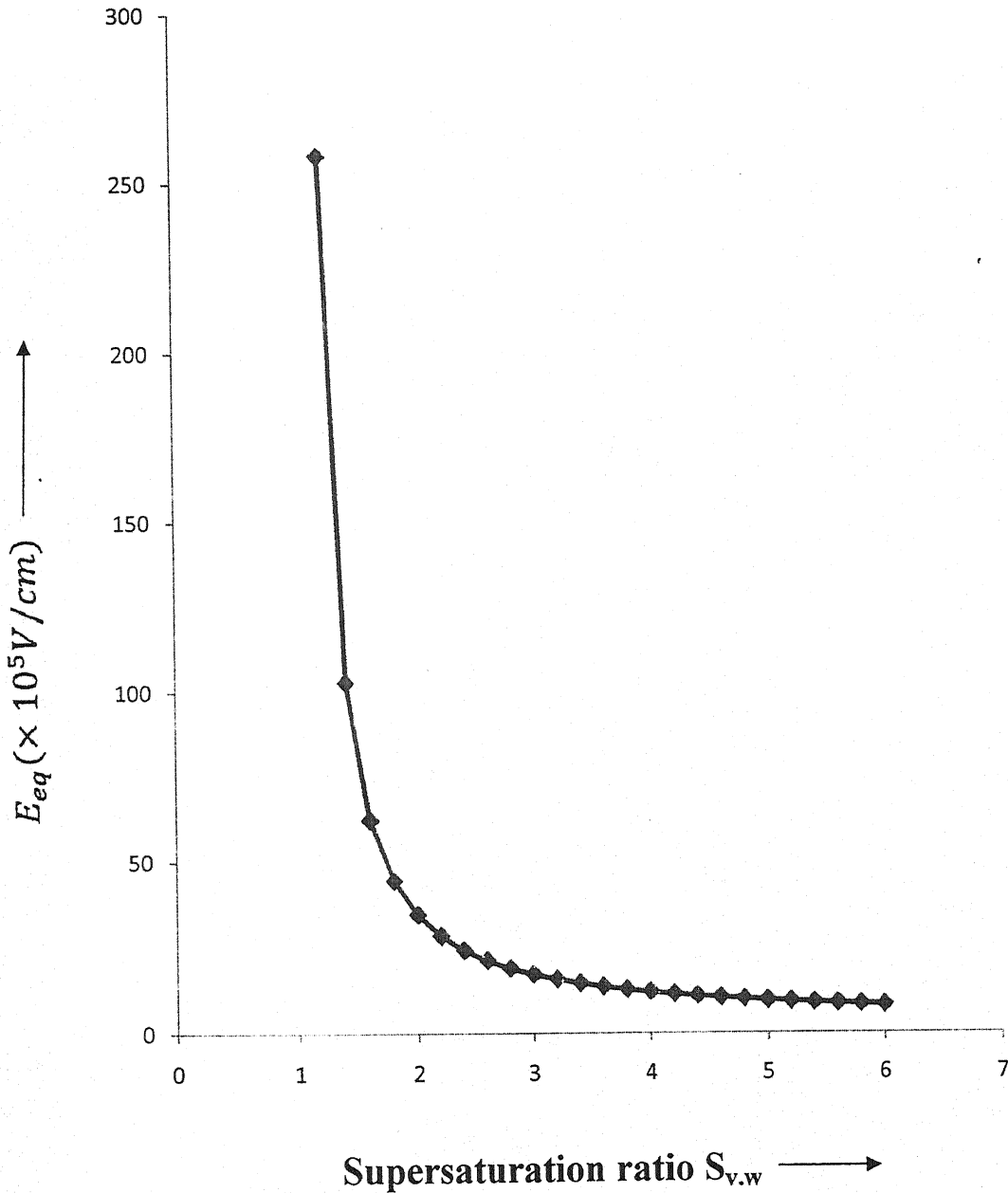


fig. 3.10 (a) Variation of supersaturation ratio $S_{v,w}$ with equivalent electric field $E_{eq} (\times 10^5 V/cm)$ at $T=278K$ and $\tau = 5 \times 10^{-6}$ sec.

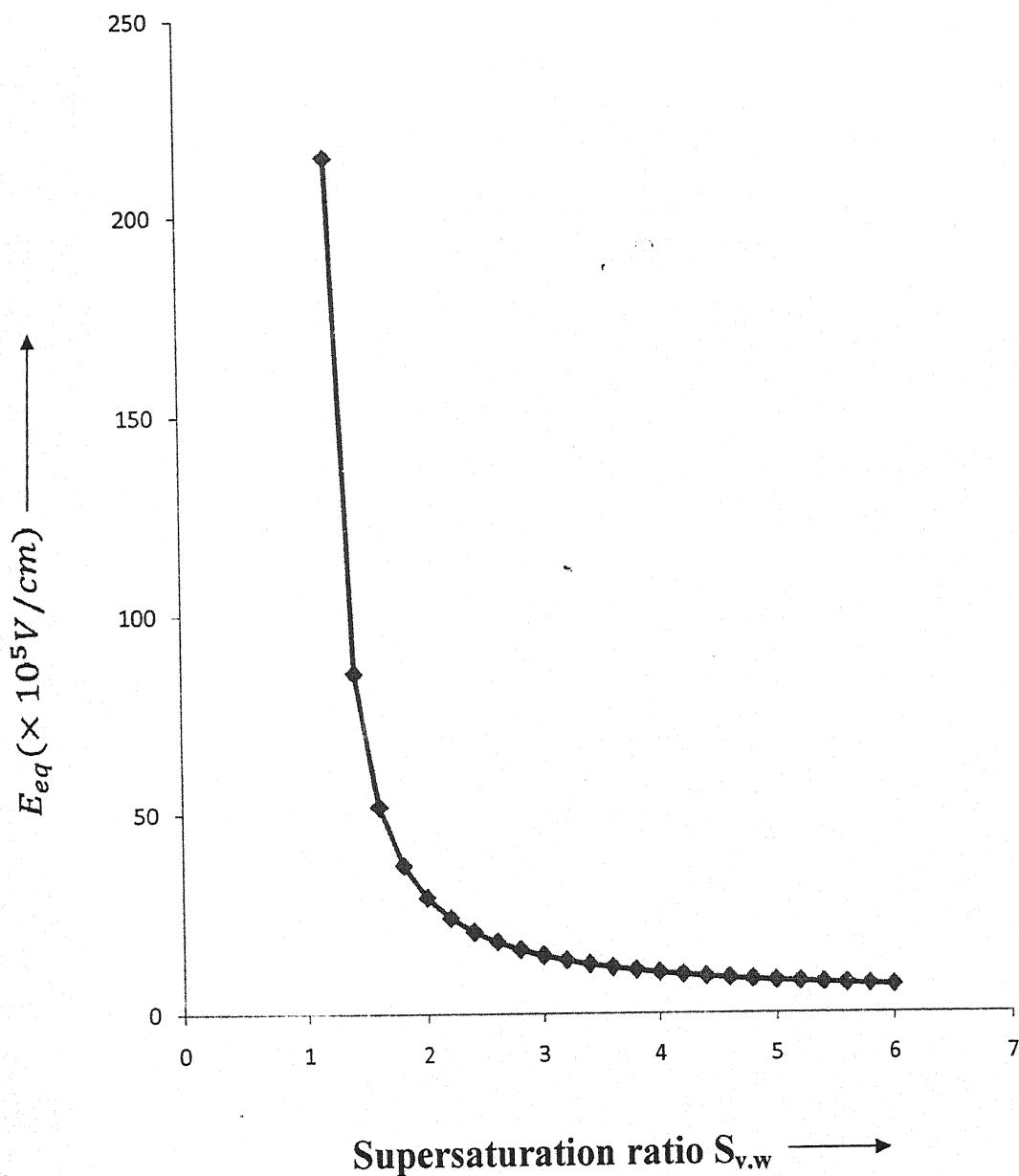


fig. 3.10 (b) Variation of supersaturation ratio $S_{v,w}$ with equivalent electric field $E_{eq} (\times 10^5 V/cm)$ at $T=278K$ and $\tau = 6 \times 10^{-6}$ sec.

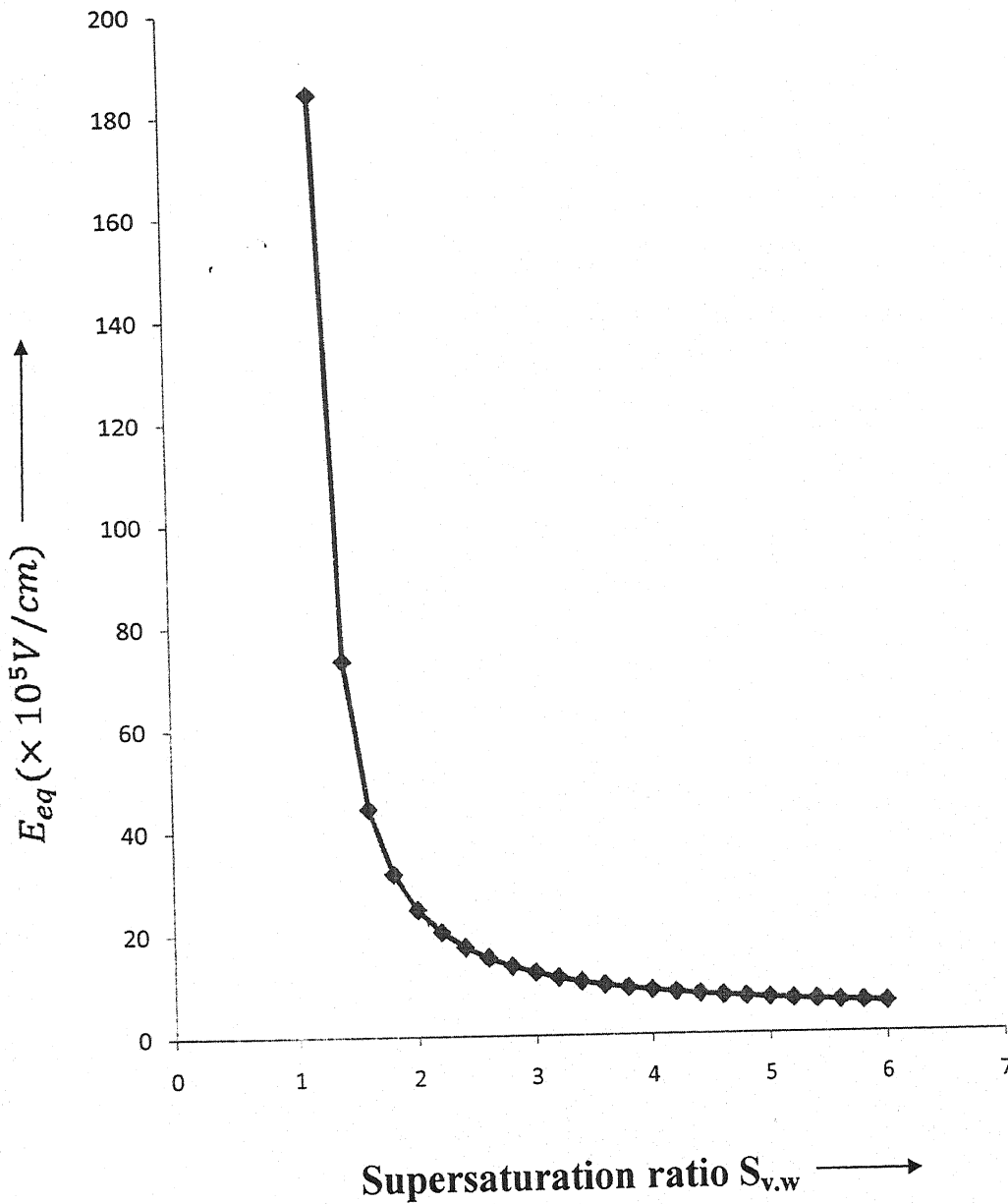


fig. 3.10 (c) Variation of supersaturation ratio $S_{v,w}$ with equivalent electric field $E_{eq} (\times 10^5 V/cm)$ at $T=278K$ and $\tau = 7 \times 10^{-6}$ sec.

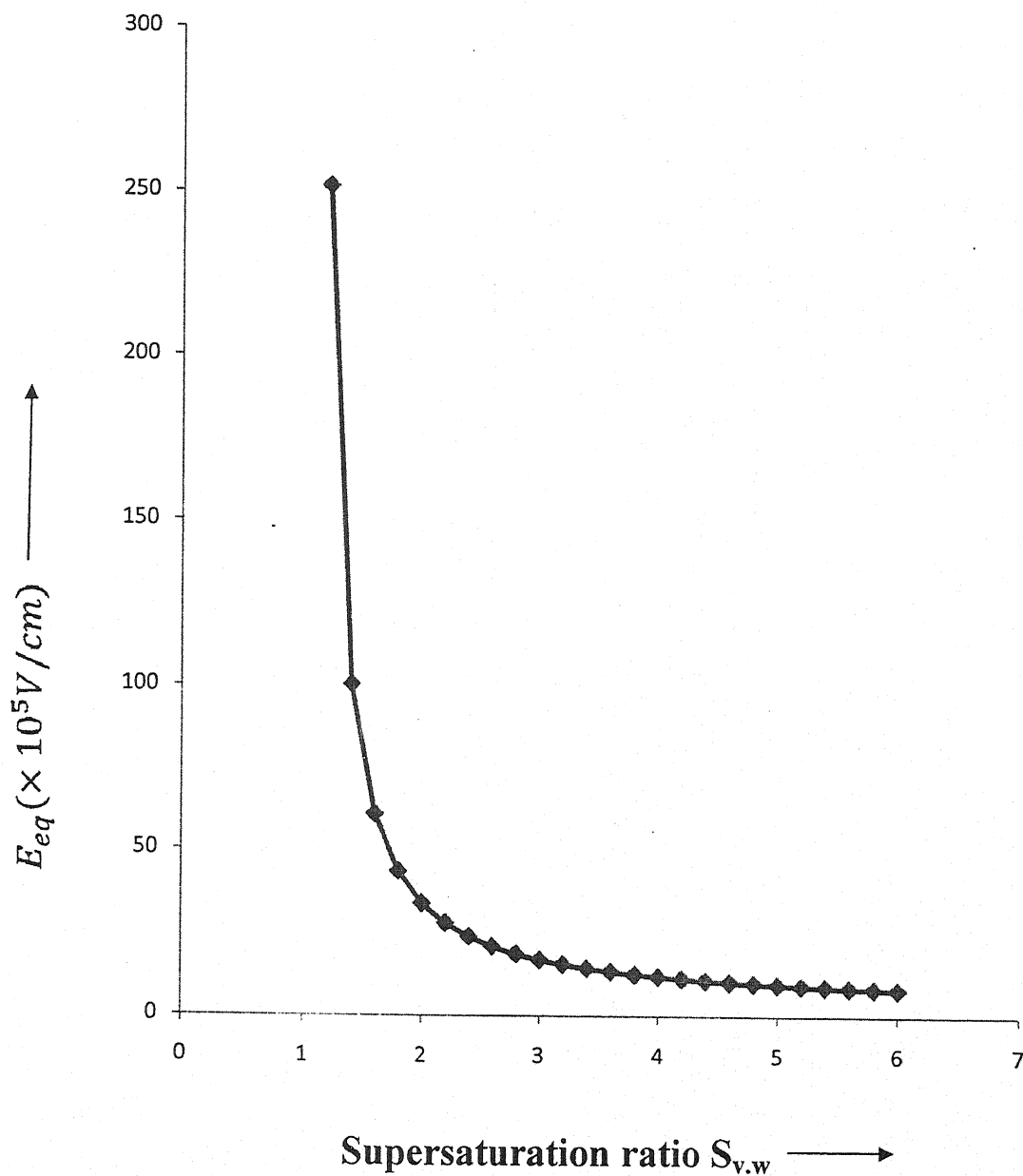


fig. 3.10 (d) Variation of supersaturation ratio $S_{v,w}$ with equivalent electric field $E_{eq} (\times 10^5 \text{ V/cm})$ at $T=288\text{K}$ and $\tau = 5 \times 10^{-6} \text{ sec}$.

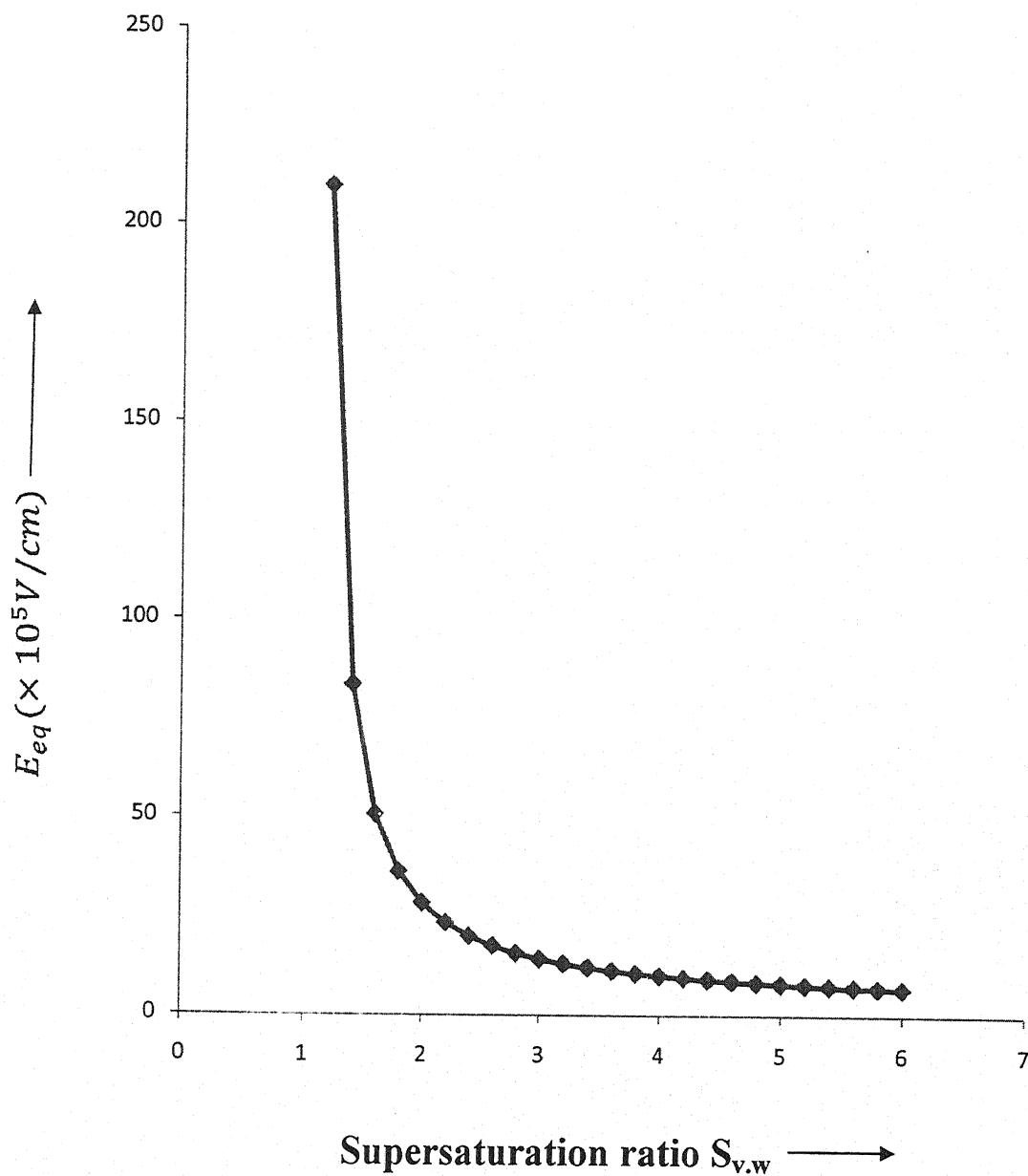


fig. 3.10 (e) Variation of supersaturation ratio $S_{v,w}$ with equivalent electric field $E_{eq} (\times 10^5 \text{ V/cm})$ at $T=288\text{K}$ and $\tau = 6 \times 10^{-6} \text{ sec}$.

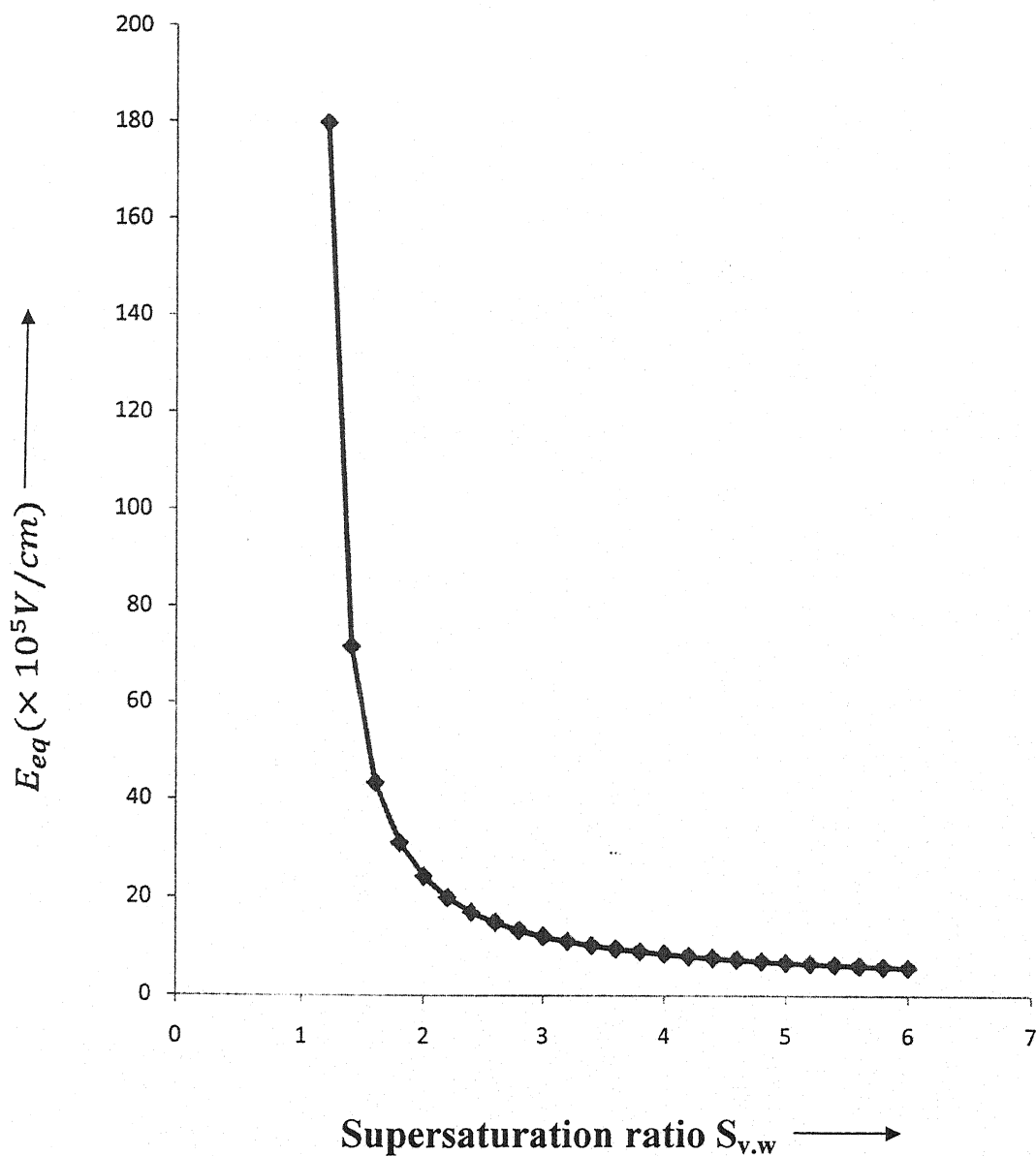


fig. 3.10 (f) Variation of supersaturation ratio $S_{v,w}$ with equivalent electric field $E_{eq} (\times 10^5 V/cm)$ at $T=288K$ and $\tau = 7 \times 10^{-6}$ sec.

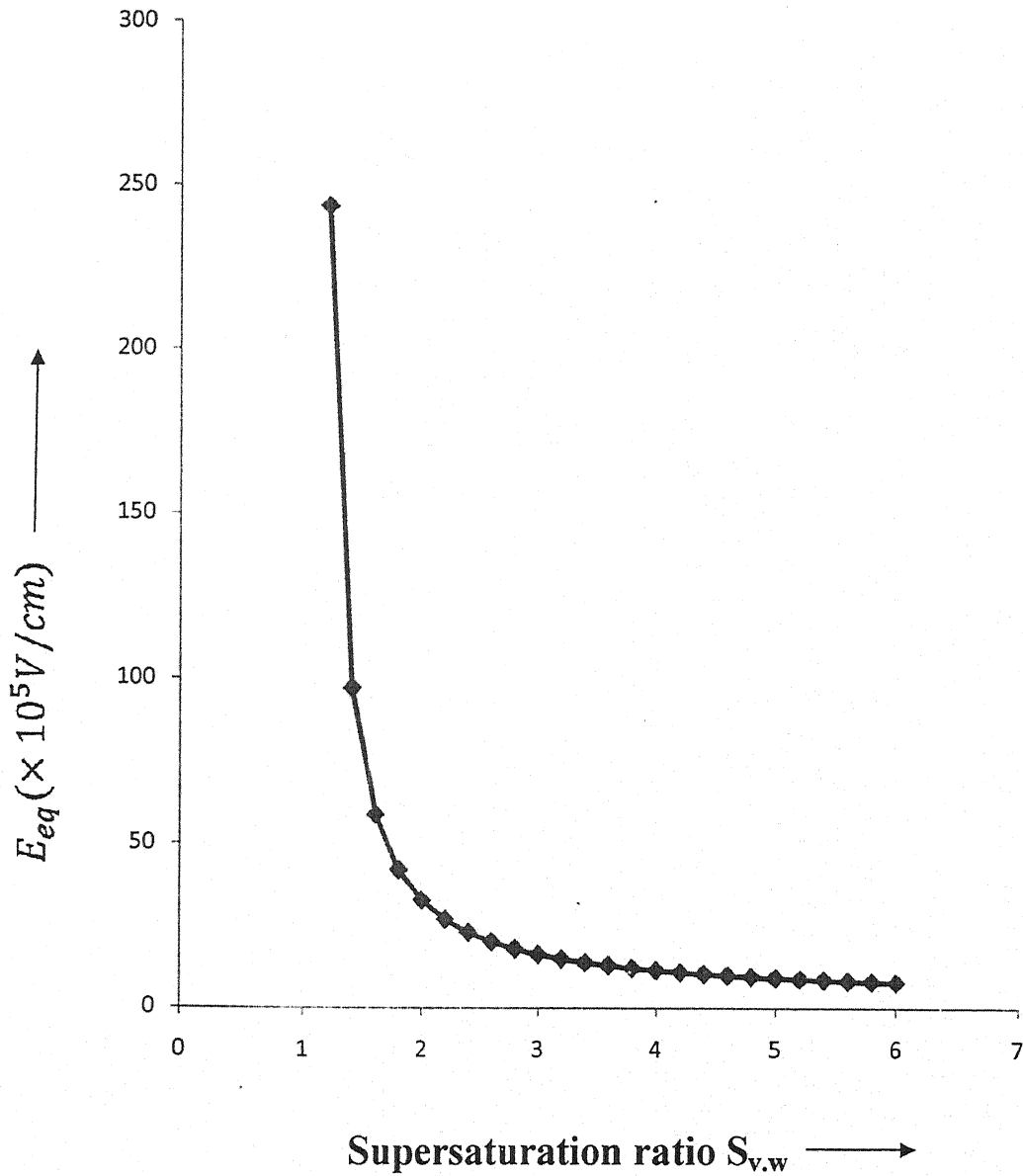


fig. 3.10 (g) Variation of supersaturation ratio $S_{v,w}$ with equivalent electric field $E_{eq} (\times 10^5 \text{ V/cm})$ at $T=298\text{K}$ and $\tau = 5 \times 10^{-6} \text{ sec}$.

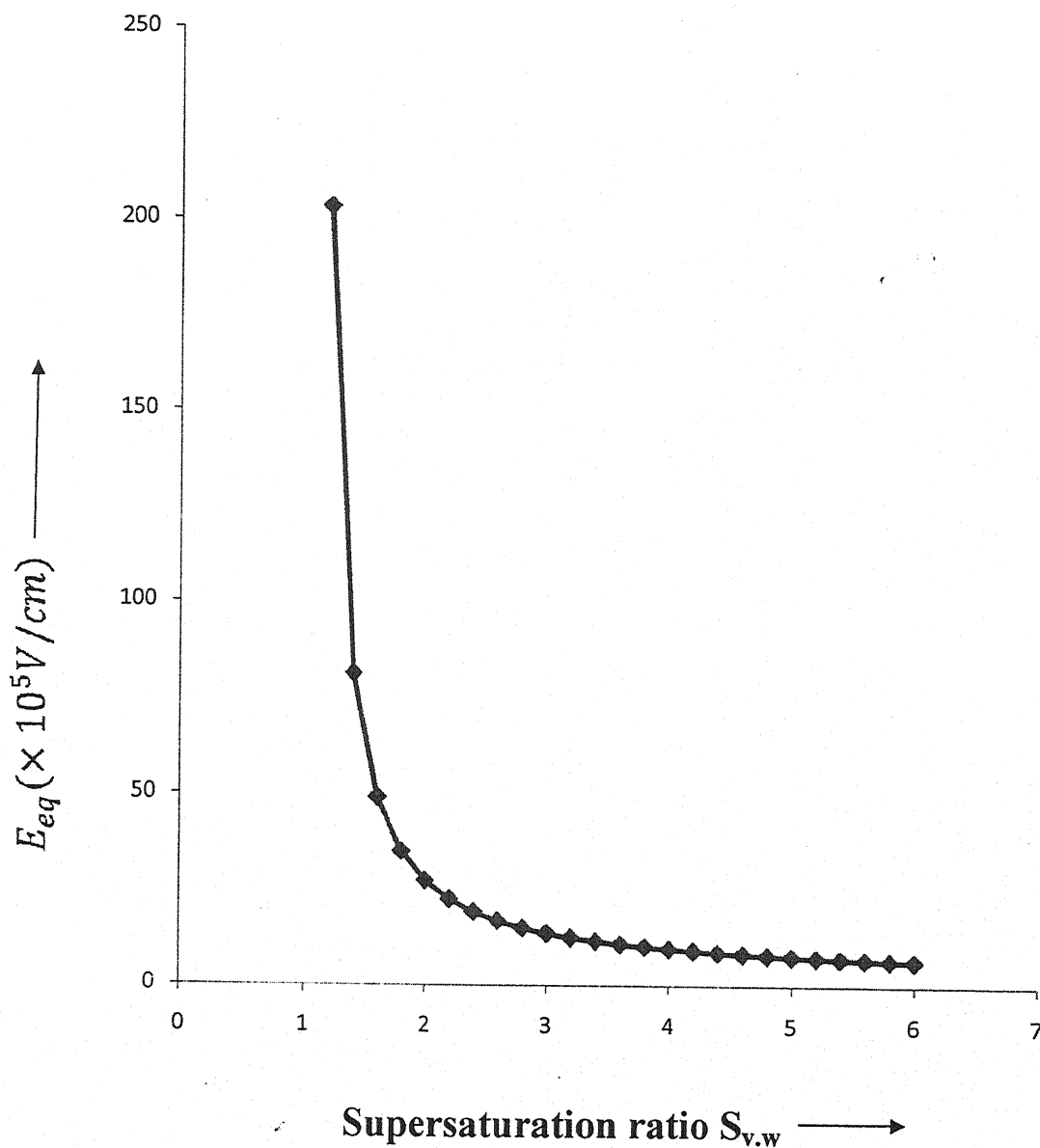


fig. 3.10 (h) Variation of supersaturation ratio $S_{v,w}$ with equivalent electric field $E_{eq} (\times 10^5 \text{ V/cm})$ at $T=298\text{K}$ and $\tau = 6 \times 10^{-6} \text{ sec}$.

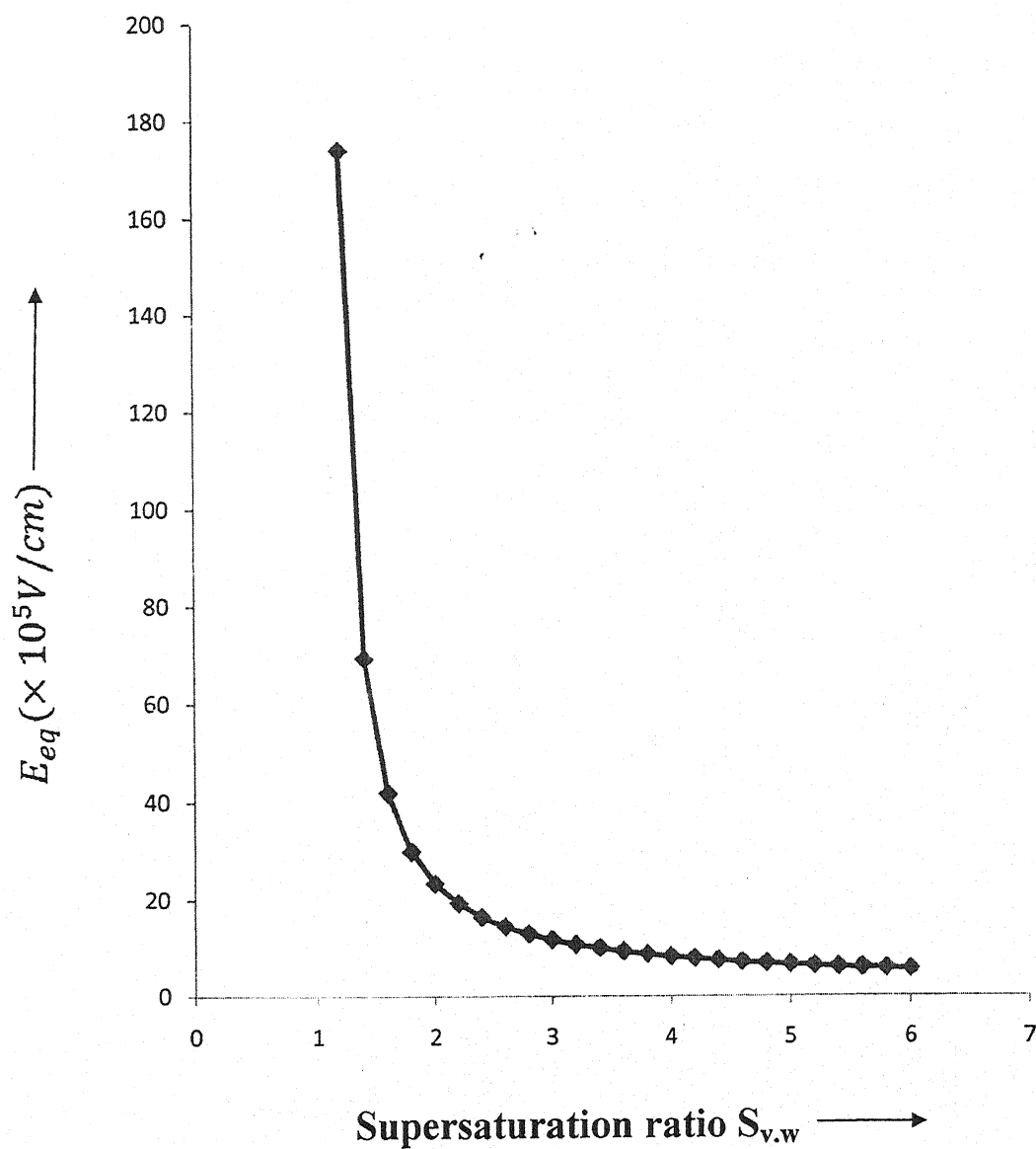


fig. 3.10 (i) Variation of supersaturation ratio $S_{v,w}$ with equivalent electric field $E_{eq} (\times 10^5 V/cm)$ at $T=298K$ and $\tau = 7 \times 10^{-6}$ sec.

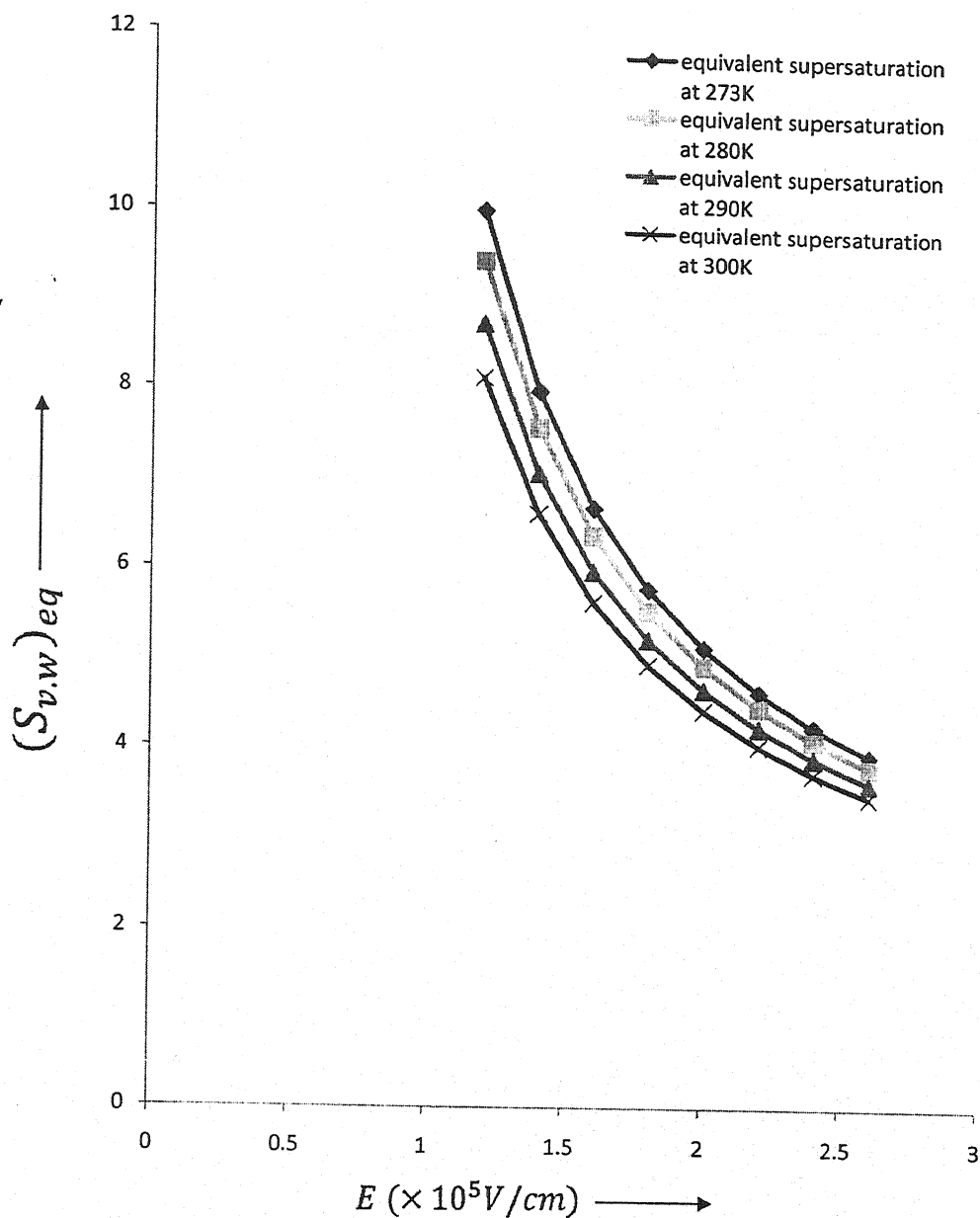


fig. 3.11(a) Variation of equivalent Supersaturation ratio $(S_{v,w})_{eq}$ Corresponding to E ($\times 10^5 \text{ V/cm}$) as the function of $\tau = 5 \times 10^{-6}$ sec. at various temperatures.

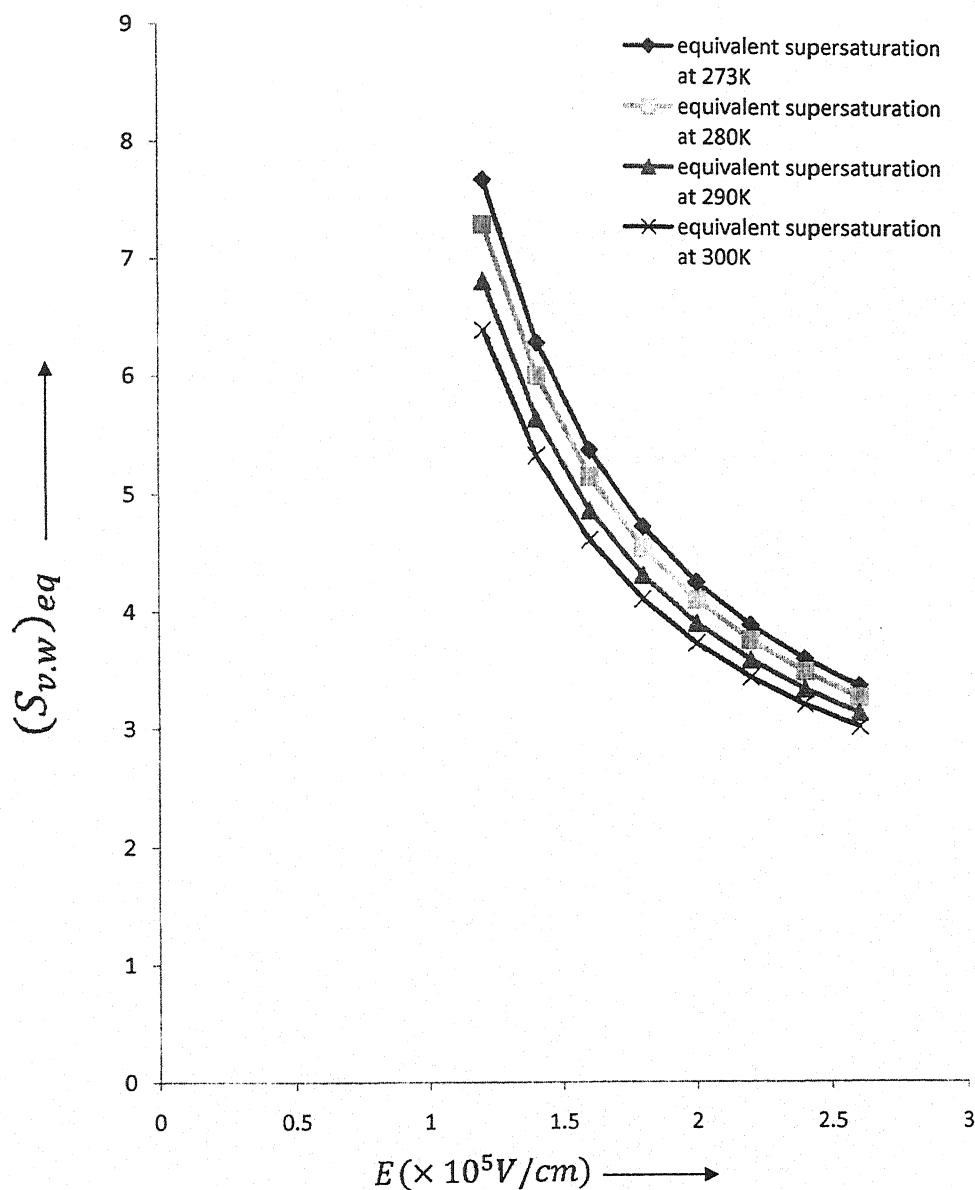


fig. 3.11(b) Variation of equivalent Supersaturation ratio $(S_{v.w})_{eq}$ Corresponding to $E (\times 10^5 V/cm)$ as the function of $\tau = 6 \times 10^{-6}$ sec. at various temperatures.

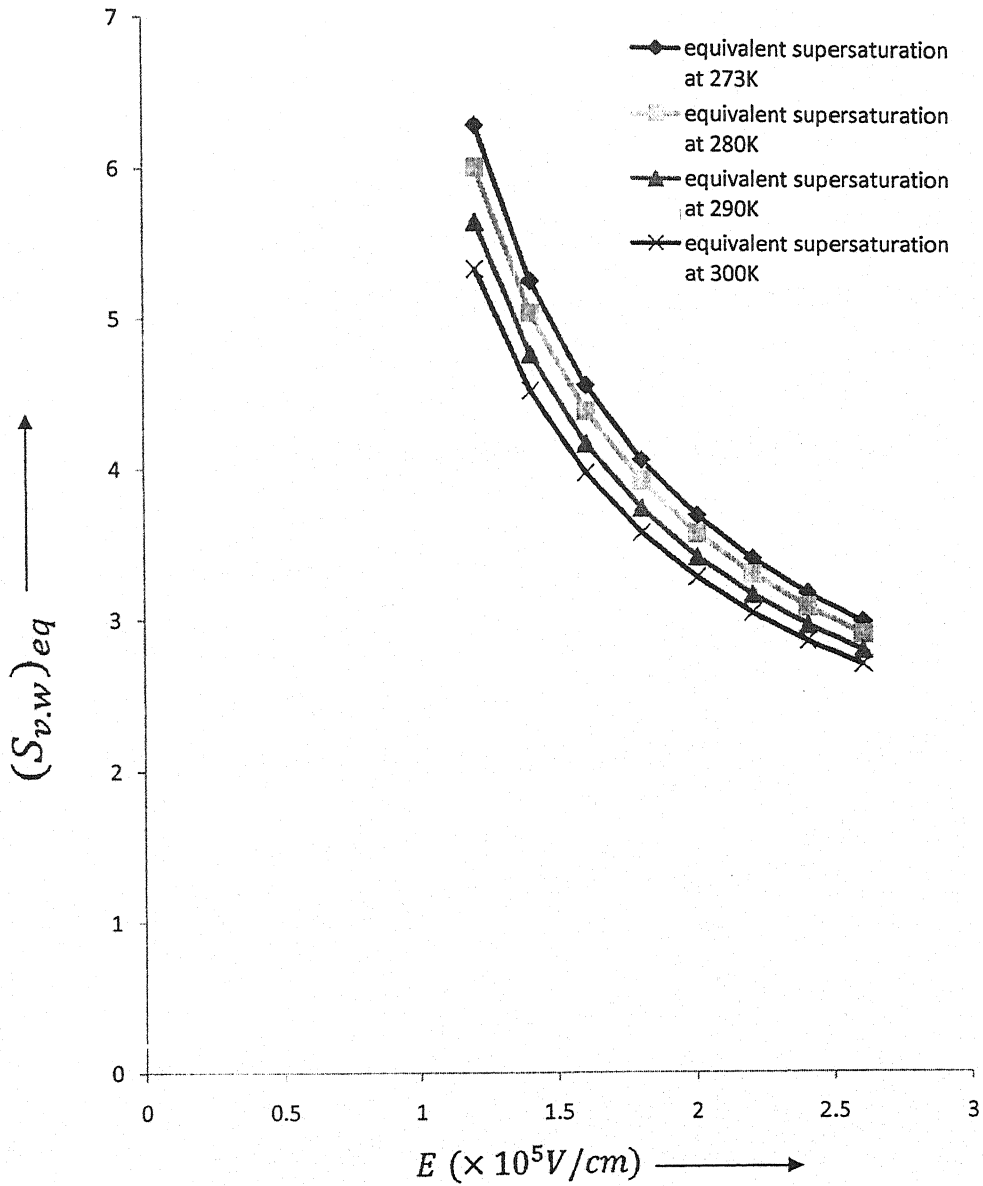


fig. 3.11(c) Variation of equivalent Supersaturation ratio $(S_{v,w})_{eq}$ Corresponding to E ($\times 10^5 V/cm$) as the function of $\tau = 7 \times 10^{-6}$ sec. at various temperatures.

CHAPTER-4

**EQUIVALENCE BETWEEN
TEMPERATURE AND THE ELECTRIC
FIELD DURING WATER VAPOUR
CONDENSATION AND GLACIATION**

CHAPTER-4

EQUIVALENCE BETWEEN TEMPERATURE AND THE ELECTRIC FIELD DURING WATER VAPOUR CONDENSATION AND GLACIATION

4.1 INTRODUCTION:

Atmosphere is filled with a large number of gases and water vapour. The amount of water vapour in an atmosphere is constrained by the restriction of partial pressures and temperature. On earth the condensing substance is typically water vapour, which forms small droplets or ice crystals, typically 0.1 mm in diameter. Above the earth surface the temperature varies with height due to thermal fluctuation at a certain supersaturation. The water vapour is nucleated to form water droplets or ice crystals under certain thermodynamical conditions. In this condition the necessary energy of formation of the droplet is provided by the phase change of vapour.

The same energy of formation of the droplet may be provided by some other external agency for example-ions, external electric field or some foreign material acting as clouds seeds. The phenomenon is called cloud seeding.

In the present study the equivalence between critical temperature corresponding to unit nucleation rate per unit volume has been studied with external electric field applied to the water vapour.

4.1.1 Water in the Atmosphere:

The amount of water vapour present in the atmosphere is a complicated function of (1) The amount, which enters the atmosphere through evaporation and sublimation, (2) Its transport by motions of

various scales throughout the troposphere and lower stratosphere, and (3) The amount which leaves the atmosphere intermittently and almost exclusively as a flux of rain, hail, and snow. The fact that all three phases of water contribute to this cycle of the prevailing terrestrial temperature and pressures is most fundamentally consequence of the molecular structure of water, which permits the strong association of water molecules through hydrogen bonding.

This is also the principal determinant for the relatively small amount of atmospheric water only about 1.3×10^{16} Kg. or about 10^{-5} of the total surface store inspite of the presence of extensive water surfaces for evaporation and sublimation.

Since the earth's surface is the primary source of water vapour, we expect a decrease in the water vapour mixing ratio W_v with height. From a slightly different point of view, one may also attribute this expectation to the observed decrease in temperature with height in the troposphere. Since the maximum possible (saturation) mixing ratio $W_{v, \text{sat}}$ decreases with decreasing temperature on the average water is squeezed out of air parcels during their ascent. Thus W_v is not a conservative quantity in the troposphere, but in fact decreases with height. An example of the observed vertical distribution of mixing ratio of water vapour in the lower troposphere is shown in fig. (4.1) and can be seen to be approximately exponential.

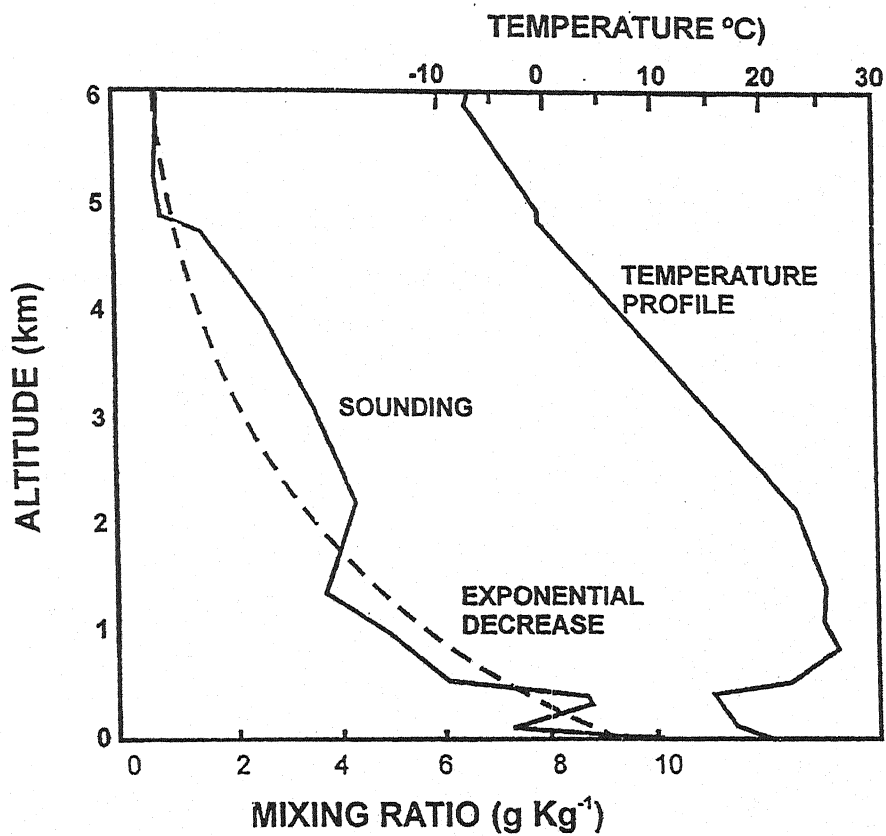


fig. 4.1 : Variation with height of the mixing ratio of water vapor in upper troposphere at lower stratosphere over Alaska on March 25, 1968.

4.1.2 The Standard Atmosphere:

The balloon surroundings have shown a wide scatter of temperatures at different pressures: warmer in summer than in winter, warmer near the equator than near the pole, and also changing from day to day with the passing weather systems. But it is possible and of much practical value to form some average of the temperature structure with height, or temperature lapse rate. Such averaging was first carried out in Europe and later the United States. One called the temperature structure so obtained the standard atmosphere (Table 4.1).

4.1.3 Thermal Layers of the Standard Atmosphere:

The entire temperature structure of the atmosphere has been approximately defined by the 1962 U.S. standard atmosphere. Our atmosphere is divided into five layers starting from the earth's surface fig. (4.2).

1. Troposphere
2. Stratosphere
3. Mesosphere
4. Thermosphere
5. Exosphere

1. **Troposphere:** This layer is the most important layer of atmosphere. Its average height is 13Km., the air we breathe exists here. Almost all the weather phenomenon like rainfall, fog and hailstorm occur in this layer.
2. **Stratosphere:** Above the troposphere lies the stratosphere. It extends up to a height of 50Km., this layer is almost free from clouds and associated weather phenomenon making conditions most ideal for flying aeroplanes. It contains a layer of ozone gas.

TABEL-4.1
Standard Atmosphere

Geometric Height (m)	Temperature °C	Pressure Millibars	Density Kg/m³
0	15.0	1013	1.23
1000	8.5	899	1.11
2000	2.0	795	1.01
3000	-4.5	701	0.99
4000	-11.0	617	0.82
5000	-17.5	541	0.74
6000	-24.0	472	0.66
7000	-23.5	411	0.59
8000	-36.9	357	0.53
9000	-43.4	308	0.57
10000	-50.0	265	0.41
11000	-56.4	227	0.36
12000	-56.5	194	0.31
13000	-56.5	166	0.27
14000	-56.5	142	0.23
15000	-56.5	121	0.20
16000	-56.5	104	0.17
17000	-56.5	89	0.14

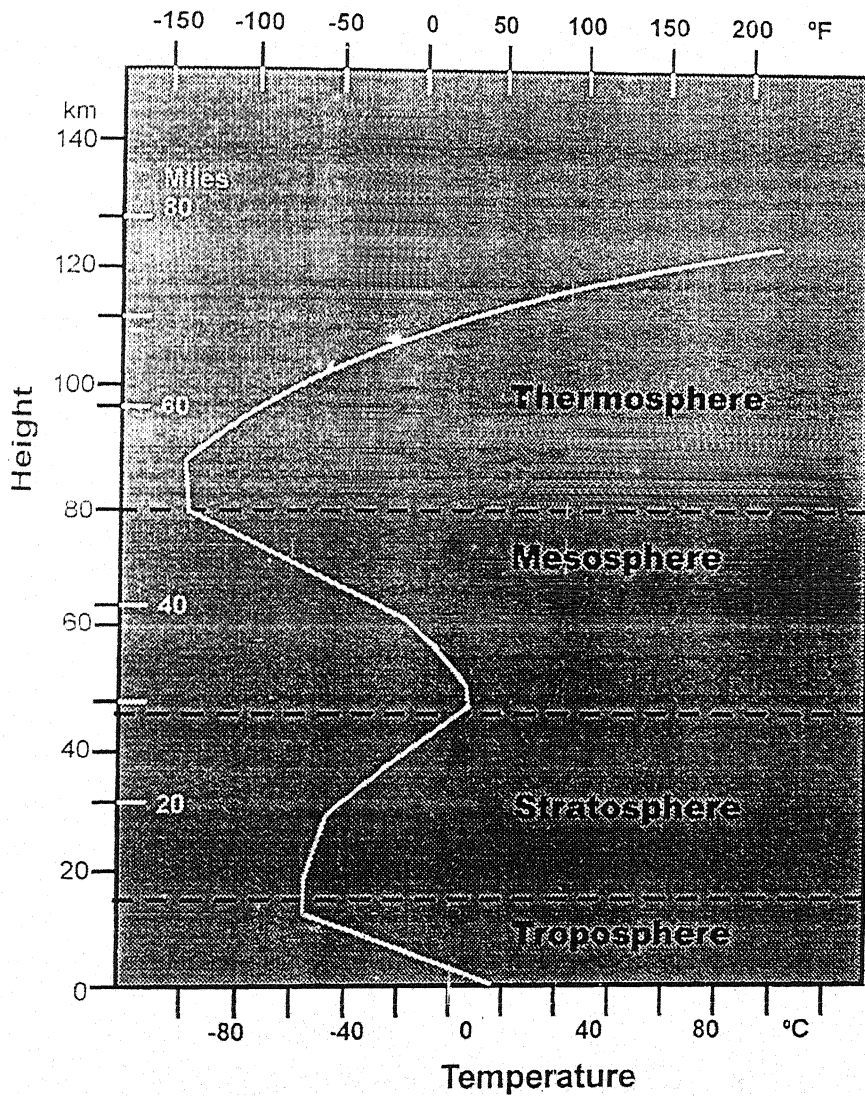


fig.4.2 : The four principal layers of the atmosphere, according to the 1962 U.S. Standard Atmosphere, Boundaries between the layers are approximate.

3. **Mesosphere:** It is the third layer. It lies above the stratosphere. It extends upto the height of 80Km., Meteorites burn up in this layer on entering from the space.
4. **Thermosphere:** Here temperature rises very rapidly with increasing height. Ionosphere is a part of this layer. It extends between 80-400 Km., this layer helps in radio transmission. In fact radio waves transmitted from the earth are reflected back to the earth by this layer.
5. **Exosphere:** This upper most layer of the atmosphere is known as exosphere. In this layer gases like He and H₂ float into the space from here.

4.1.4 Water Vapour:

In the atmosphere, water exists in all three phases, vapour, liquid and ice, at different temperature and supersaturation. Phase change takes place due to thermal fluctuations. In all phase changes at any temperature, a high supersaturation (several hundred percent) is required for homogeneous nucleation. In presence of foreign particles, heterogeneous nucleation takes place at much lower supersaturation ratio (about 1%) (Singh, N., et al., 1985).

Murino (1979) gave the theory of drop growth in external electric field has been extended to nucleation process in water condensation and ice glaciations (Singh, N. et al., 1986). In presence of external electric field water vapour molecules acquire much earlier the necessary Gibb's free energy for formation of critical nucleus. It has been shown that in electric field induced nucleation; nucleation rates have increased by several orders. Inamdar (1998) discussed the effective role of external

electric field on the relaxation time in nucleation process of water vapour condensation and ice glaciations. Pasko (1999) studied about electrical analogy applied to modeling dry deposition of particles, occurring soon after sunrise has been observed to be enhanced (Marshall, 1999).

The effect of electric field on water vapour condensation and also the polarizability of water vapour molecules have been discussed (Singh, N., et al., 2000, 2001). Singh, N. and Kumar (2002) and Sharma et al. (1992) have obtained equivalence between applied external electric field and the supersaturation ratio. But, to author's knowledge the equivalence between temperature and the external electric field has not been dealt so far.

It is a well-known fact that there exists a vertical electric field in free and undisturbed atmosphere. Also, intense electric fields are generated in thunderclouds (Sapkota, 1989). The intense electric fields in thunderclouds are not widespread and the charge and intense electric fields seem to be concentrated in relatively small volumes. Although, under actual cloud condition the electric field varies considerably, its rate of growth has been calculated by Winn (1974). Moore et al. (1962) and Levin and Ziv (1974) reported a raingush following lightning stroke. During a lightning discharge maximum electric field (about 10 e.s.u.) is produced near the channel.

Thus, the electric field plays an important role in cloud physics. This role could be effectively verified in absence of supersaturation. Murino (1979) has shown that a droplet acquires a particular size under very low supersaturation. Singh, N. et al. (1986) have shown that in the resultant effect on a droplet due to an external electric field and the field

induced due to the central dipole. The rate of nucleation in water vapour condensation and ice glaciation is about 100 times more near breakdown for dry air, as compared to that in absence of electric field.

In this chapter we have considered the resultant effect due to an external electric field and the electric field due to the central dipole. These theoretical considerations are applied to the nucleation process in water vapour condensation and ice glaciations in order to estimate the critical size of the nucleus.

Following kinetic theory, Collins (1955) inferred that the relaxation time is independent of the free energy of formation of the nucleus, but it varies as the square of the radius of the critical nucleus.

4.1.5 Structure of Water Vapour:

Experiments indicate that water molecules in water vapour tend to interact and form crystals, in contrast to ideal gas behaviour. Dimers as well as higher order polymers are considered to be present in water vapour, do in small concentration only. The experiments involving molecular beam techniques (Lin et al., 1973; Searcey, 1974) suggested that in oily supersaturated water vapour clusters of upto 180 water molecule may be present. Clusters of 21 water molecules seemed to exhibit particularly large stability. 21 water molecules can be arranged in the form of a pentagonal clode cahedron with a molecule at each corner and a single molecule in the center of the 'cage'.

Studies on the possible and more likely clusters types have been reviewed, by Rao (1972) and Kell (1972 a). Recent theoretical studies of the formation of water clusters have been carried out (Kistenmacher et

al., 1974a, 1974b; Abraham, 1974). Kistentenmacher et al. (1974a, 1974b) found two possible stable configuration for the dimmers, a cyclic form and an open form which was more stable. For the trimmers and tetramers the cyclic form seemed to be somewhat more stable than the open structures. For the large cluster the authors suggested not a single structure but a statistical distribution of different configurations, since many configurations with significantly different geometry were found to passes nearly the same energy.

The Potential energy of interaction, U , between a pair of water molecules has the general character of being strongly repulsive at very close separations and weekly attractive at longer range. One widely used and relatively simple expression for it is due to Stockmayer (1941).

$$U = -\frac{\mu^2 f}{r^3} - \frac{c}{r^6} + \frac{c\sigma^{18}}{r^{24}} \quad (4.1)$$

Where r is the separation of the molecules; μ , is the dipole moment of an isolated water molecule; σ , is the collision diameter (the molecular separation at which $U=0$ at $\mu = 0$); c is an adjustable constant and f is a known function of the mutual orientation of the two molecules.

The first term on the right side of eq. (4.1) is just the dipole-dipole contribution of the interaction energy, and may be attractive or repulsive, depending on the dipole orientations. The second term represents contribution from: (1) the interaction energy between a permanent dipole of one molecule and the dipole it induces in the other (dipole-polarization or induction interaction), (2) the net energy arising from momentary, fluctuating dipoles interacting with the corresponding induced dipoles (polarization- polarization or dispersion interaction). Even though the

time average of these dipole fluctuations may be zero, the energy contribution is proportional to their mean square, which is finite and positive. Both (1) and (2) are usually as Vander Wall's interaction, which by its nature can be seen to bring about an attractive force between the molecules. The third term in eq. (4.1) represents the short-range repulsive forces, which loosely may be ascribed to the overlap of electronic orbital, which are incompatible according to the Pauli Exclusion Principle.

There is a little doubt that the Stockmayer potential or similar ones, such as (Rowlinson, 1949, 1951) potential, portray with fair accuracy the interaction between pairs of water molecules at large separations in dilute water vapour (Singh, N. et al., 2002) . This is evidenced by the fact that values for the second virial coefficient computed via eq. (4.1) can be made to fit experimental values. On the other hand, the same potential functions yield values for the third virial coefficient of water vapour, which disagree substantially with experiment. Partly, this is due to the approximate nature of eq. (4.1), and partly because three-body interactions should be included also, since other molecules in the system can significantly modify the interaction of a given pair. In particular, the Stockmayer potential is insufficiently "directional" in character to account for the geometry of cluster formation in water vapour. A recent more complicated potential function, which has proven to be predictive value in this respect, is described briefly.

4.1.6 Vapour Pressure Over Pure Droplets:

It is found from measurement that the vapour tension of a concave surface of a liquid is lower than that of a flat surface. Convex surfaces show higher vapour tensions than flat surfaces. Droplets therefore require

a certain degree of supersaturation in the ambient space in order to remain in equilibrium. Physically, one might indeed expect the escaping tendency of molecules from a spherical droplet to be greater than the smaller droplet because the component of the binding force in the tangential direction is diminished. Lord Kelvin (Willam Thomson) first deduced the relation, which today can be presented in more modern thermodynamic from the point of view of the surface free energy.

In the supersaturated state the transition surface lies above that depicted in plate 2.1, each isotherm being at a higher pressure and therefore at a higher free energy. The elevation of the free energy above that for a plane surface of pure water depends on the saturation ratio and on the surface free energy.

The problem is approached by considering a system initially consisting of vapour at supersaturation, with saturation ratios, which changes of final state, and forming from the vapour a single embryonic droplet of radius r containing 'g' molecules. Note that

$$g = \frac{4}{3}\pi r^3 Z_L \quad (4.2)$$

Where Z_L is the number of molecules in a cubic centimeter at the liquid, and that $Z_L = N\rho_L/m_w$ where N is Avogadro's number (6.022×10^{23}). Its molecules are considered in place of moles, Nk is substituted for R , where k is Boltzmann's constant (1.381×10^{-16} erg K^{-1} molecule $^{-1}$, or effectively the gas constant per molecule). The free energy differential dG of equation becomes

$$dG = gkTd(\ln p) = \frac{4}{3}\pi r^3 Z_L kTd(\ln p) \quad (4.3)$$

As a molecules go from the vapour at pressure p to the liquid at tension p_0 the change in chemical potential or free energy of the system is given, after the manner of equation as,

$$\mu_{P_0} - \mu_P = \int_P^{P_0} gkTd(\ln p) = GkT \ln \frac{P_0}{P}$$

$$\mu_{P_0} - \mu_P = -\frac{4}{3}\pi r^3 Z_L kT \ln \frac{P}{P_0} = -\frac{4}{3}\pi r^3 Z_L kT d \ln S \quad (4.4)$$

Where S is now the saturation ratio. As the transition is made from vapour only to an embryo droplet of radius r , the surface free energy goes from zero to $4\pi r^2 \sigma$. The elevation of the total free energy of the system of g molecules in the presence of these two effects is therefore their sum, or

$$\Delta G = 4\pi r^2 \sigma - \frac{4}{3}\pi r^3 Z_L kT d \ln S \quad (4.5)$$

The significance of this expression may best be appreciated by plotting ΔG against ' r ' for several values of S at constant temperature, and therefore also, constant σ (fig.4.3).

4.1.7 Equation of State for Water Vapour:

Unlike other atmospheric constituents, water appears in all three phases, solid, liquid and vapour. In the vapour phase water in the atmosphere behaves as an ideal gas to a good approximation. Its equation of state is

$$e = \rho_v R_v T \quad (4.6)$$

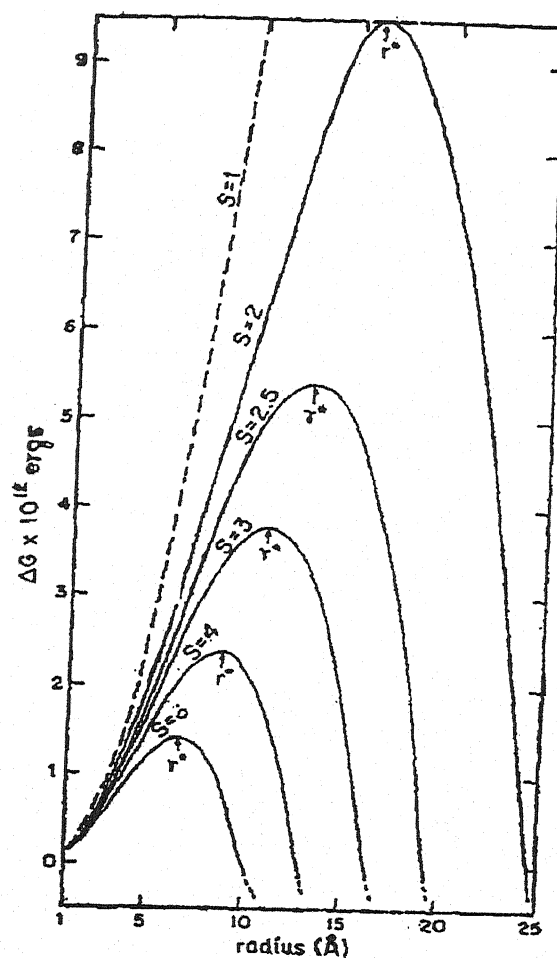


fig. 4.1 : Elevation of the free energy ΔG above equilibrium for a plane surface of pure water plotted against radius for various of the saturation ratio, S .

Where e , is vapour pressure; ρ_v , is vapour density; and R_v , is individual gas constant for water vapour ($461 \text{ JKg}^{-1}\text{K}^{-1}$). This equation sometimes appears in the form

$$e = \rho_v \frac{R'}{\varepsilon} T \quad (4.7)$$

$$\text{Where } \varepsilon = \frac{R'}{R_v} = \frac{m_v}{m} = 0.622$$

Water vapour has a specific heat at constant pressure equal to $1850 \text{ JKg}^{-1}\text{K}^{-1}$. The specific heat at constant volume equals to $1390 \text{ JKg}^{-1}\text{K}^{-1}$.

4.1.8 Equilibrium Vapur Pressure e_s and latent Heat L Over a range of Temperature:

Values of e_s and L over a range to temperature are given in Table 4.2. At temperature of 0°C and colder the latent heat of sublimation and the equilibrium vapour pressure e_i over ice are also tabulated.

4.2 THEORETICAL CONSIDERATIONS:

4.2.1 Equivalence between Electric Field and Temperature:

In presence of an external electric field, the rate of increase of radius with respect to time is given (Singh, N., 1986) as

$$\frac{dr_w}{dt} = \left(\frac{\rho_v}{\rho_w} \right) (9\alpha\lambda E^2 / m_w r_w)^{1/2} \quad (4.8)$$

Where ρ_v is the density of water vapour; ρ_w the density of water; α the polarizability; λ , the mean free path of water vapour molecules; E the applied external electric field; m_w , the mass of water molecule; r_w , the radius of water droplet.

TABEL- 4.2

**Latent heat of condensation (sublimation) and saturation vapour pressure for various temperatures
(Source, Smithsonian Meterological Tables)**

$T (^{\circ}\text{C})$	$e_s \text{ (mb)}$	$e_i \text{ (mb)}$	$L \text{ (calg}^{-1}\text{)}$	$L_s \text{ (calg}^{-1}\text{)}$
-40	0.189	0.128	621.7	678.0
-35	0.314	0.223		
-30	0.509	0.380	615.0	678.0
-25	0.807	0.632		
-20	1.254	1.032	608.9	677.9
-15	1.912	1.652		
-10	2.863	2.600	603.0	677.5
-5	4.215	4.015		
0	6.108	6.107	597.3	677.0
5	8.719			
10	12.272		591.7	
15	17.044			
20	23.373		586.0	
25	31.671			
30	42.430		584.4	
35	56.236			
40	73.777		574.7	

Integrating eq. (4.8) within limits $r_w = 0$ to r_w^* , the critical radius of nucleus and $t = 0$ to $t = \tau_N$ the relaxation time, we have

$$r_w^* = [3\rho_v(9\alpha\lambda E^2/m_w)^{1/2}\tau_N/2\rho_w]^{2/3} \quad (4.9)$$

Following liquid drop model, in homogeneous process of water condensation, the nucleation rate (Pruppacher, 1978) (i.e., number of critical nuclei per unit volume per sec.) is

$$J_w = \frac{\alpha_c}{\rho_w} \left[\frac{2N^3 M_w \sigma_{w/v}}{\pi} \right]^{1/2} \left(\frac{e_{sat,w}}{RT} \right)^2 S_{v,w} \exp \left[-\frac{\Delta G_w}{kT} \right] \quad (4.10)$$

Where α_c is condensation coefficient ; ρ_w , density of water; N , Avogadro's number; M_w , molecular weight of water; $\sigma_{w/v}$, surface energy of water-vapour interface; $e_{sat,w}$ the saturated vapour pressure over water; R , the universal gas constant; $S_{v,w}$ the supersaturation ratio of water vapour over liquid water; ΔG_w , the Gibb's free energy for formation of critical nucleus; k , Boltzmann constant and T , temperature of water vapour.

The pre-exponential factor has been calculated by Pruppacher (1978) for $\alpha_c=1$ is $9 \times 10^{21} \text{ cm}^{-3} \text{ sec}^{-1}$ and $3.7 \times 10^{25} \text{ cm}^{-3} \text{ sec}^{-1}$ at -30°C and 30°C , respectively. Although prefactor changes with temperature and supersaturation ratio, but it has been assumed constant for present calculations, because the nucleation rate is mainly dependent on the exponential term.

Hence, eq. (4.10) becomes

$$J_w = 9 \times 10^{21} \exp \left[-\frac{\Delta G_w}{kT} \right] \quad (4.11)$$

For critical nucleation rate, $J_w=1$, hence

$$1 = 9 \times 10^{21} \exp \left[-\frac{\Delta G_w}{kT} \right] \quad (4.12)$$

The value of ΔG_w in homogeneous nucleation process is

$$\Delta G_w = \frac{16\pi M_w^2 \sigma_{w/v}^3}{3[RT \rho_w \ell n S_{v,w}]^2} \quad (4.13)$$

Substituting eq. (4.13) in eq. (4.4), we have

$$(\ell n S_{v,w})^2 = \frac{16\pi M_w^2 \sigma_{w/v}^3}{R^2 T^2 \rho_w^2 \times 3k \ell n 9 \times 10^{21}} \quad (4.14)$$

For critical nucleation rate ($J = 1$) we use critical temperature $T = T_c$ hence

$$T_c = \left[\frac{16\pi M_w^2 \sigma_{w/v}}{(\ell n S_{v,w})^2 R^2 \rho_w^2 \times 3k \ell n 9 \times 10^{21}} \right]^{1/3} \quad (4.15)$$

Alternatively, radius of critical nucleus in homogeneous nucleation with supersaturation $S_{v,w}$ is

$$r_w^* = \frac{2M_w \sigma_{w/v}}{\rho_w RT \ell n S_{v,w}} \quad (4.16)$$

And in presence of external electric field, the same critical radius is obtained in electric field E and relaxation time τ_N , as

$$r_w'^* = \left[\frac{3\rho_v \tau_N}{2\rho_w} \left(\frac{2\alpha \lambda E^2}{m_w} \right)^{1/2} \right]^{2/3} \quad (4.17)$$

Equating eq. (4.16) and (4.17) at critical temperature $T=T_c$, we have

$$T_c = \frac{K}{\tau_N^{2/3} E^{2/3} \ln S_{v,w}} \quad (4.18)$$

$$\text{Where constant } K = \frac{2M_w \sigma_{w/v}}{\rho_w R} \left[\frac{2\rho_w}{3\rho_v} \left(\frac{m_w}{9\alpha\lambda} \right)^{1/2} \right]^{2/3}$$

Eq. (4.18) gives equivalence between critical temperature T_c and the applied external electric field.

4.3 RESULTS AND DISCUSSION:

From eq. (4.18), the values of critical temperature T_c have been computed at different values of supersaturation ratio for a given value of external electric field and relaxation time. At $E=2,3,4$ e.s.u. and $\tau_N = 2 \times 10^{-6}$ sec. The value of T_c at different values of supersaturation ratios are given in Table (4.3).

From the table, it is evident that at a given value of electric field, the values of critical temperature decrease with increase in supersaturation ratio. For example, at an external electric field of 4 e.s.u. and relaxation 2×10^{-6} sec., the critical temperatures are $2.0990 \times 10^4 K$, $0.814271 \times 10^4 K$, $0.552134538 \times 10^4 K$ corresponding to the supersaturation ratios 1.2, 1.6, 2. Similarly the values of critical temperatures have been calculated at $E=2,3$ e.s.u. also and are given in table (4.3).

TABEL- 4.3

Calculated values of critical temperatures for different supersaturation ratios at Relaxation time $\tau_N=2 \times 10^{-6}$ sec.

$S_{v,w}$	$T_c (\times 10^4) \text{ K}$		
	E=2 e.s.u.	E=3 e.s.u.	E=4 e.s.u.
1.2	3.332107614	2.542874029	2.099096262
1.4	1.805542870	1.377887092	1.137420734
1.6	1.292575227	0.986419515	0.814271368
1.8	1.033563849	0.788756839	0.651104425
2.0	0.876458947	0.668863359	0.552134538
2.2	0.770510973	0.588009923	0.485391497
2.4	0.693931173	0.529568598	0.437149246
2.6	0.635800911	0.485206906	0.400529476
2.8	0.590038453	0.450283614	0.371700933
3.0	0.552984027	0.422005795	0.348358108
3.2	0.522301186	0.398590405	0.329029129
3.4	0.496426903	0.378844631	0.312729352
3.6	0.474275116	0.361939653	0.298774601
3.8	0.455067088	0.347281185	0.286674302
4.0	0.438229473	0.33443168	0.276067269

4.4 CONCLUSION:

The study of equivalence between external electric field and the critical temperature suggests that in electric field induced nucleation process, the critical temperature required to critical nucleation ($J_w = 1$) decreases with increase in electric field as compared with homogeneous nucleation. Thus, the nucleations of water condensation increase very much due to applied external electric field. Hence, the electric field is very much effective in nucleation process. A small external electric field is equivalent to very large value of supersaturation ratio, which, otherwise, never exists in the clouds. In electric field induced nucleation, the critical nuclei of smaller sizes are formed having smaller number of water molecules and require less Gibb's free energy for their formation and equilibrium concentration of critical nuclei is enhanced as compared with the homogeneous nucleation. Also, from the equivalence of supersaturation ratio with external electric field, it appears that electric field is more efficient than supersaturation. Although, there are a number of mechanisms giving possible explanation for raingush after lightning. In present study, we may add possibility to explain the raingush phenomenon. A high electric field produces lightning discharge, creating ionization of the gaseous medium and a large number of ions are formed. Hence, for a given amount of liquid water a large number of droplets of smaller size are formed immediately following lightning. Hence, lightning seems to be cause of raingush and not the effect.

CHAPTER-5

**EFFECT OF IONS ON ELECTRIC
FIELD INDUCED NUCLEATION
PHENOMENON AND STUDY OF
THUNDERSTORMS**

CHAPTER-5

EFFECT OF IONS ON ELECTRIC FIELD INDUCED NUCLEATION PHENOMENON AND STUDY OF THUNDERSTORMS

5.1 INTRODUCTION:

Gagin (1972) and Huffman (1973) found that at any given temperature, the number concentration of ice nucleating (IN) particles increase with increasing relative humidity and co-relates with supersaturation over ice according to the relation

$$N_{IN} = CS_{v,i}^K \quad (5.1)$$

Where $S_{v,i}$ is the supersaturation ratio of water vapour over ice; C and K are arbitrary constant.

Considering that the aerosol particle (AP) concentration decreases with increasing height, one might expect the same from concentration of IN. However (Bigg, 1961, 1963), found that in air over Australia the concentration of IN was significantly higher at 13 to 27 km altitude than at the ground. Analogously (Rosinski, 1967), found over Colorado that on certain occasion the IN concentration was highest near the jet stream. If one compares the concentration of IN and cloud ice particles, it is found in many clouds, particularly at relatively warm temperatures, the concentration of ice particles may exceed by many orders of magnitude, the concentration of IN determined at the cloud top temperature (Pruppacher, 1978).

5.2 IONS, THE POTENTIAL CONDENSATION NUCLEATION CENTERS:

Studies of ion-induced nucleation were first made by Wilson (1897). Since the time of Wilson, numerous research papers have been devoted to the subject (Castleman, 1979a, 1979b, 1972; Suck, 1982; Varshneya, 1969, 1971) ion induced nucleation.

The ion provides a central force field, which is a simple form of attractive potential resulting in the formation of heterogeneous embryos. A basic understanding of ion induced nucleation therefore provides an important basis for further developments in the theory of heteromolecular nucleation, which is important in atmospheric processes (Allen, 1969; Doyle, 1961).

Below saturation the chemical bond energy of hydrated ions are too weak to permit the growth of critical embryos. The prominent forces resulting in the stabilization of small clusters about simple ions such as those isoelectronic with the noble gas structures are electrostatic in order to assess the importance of electronic structure on bounding investigation (Castleman, 1972) on metal ions (e.g. Pb^+) which have non-closed shell electronic configurations, were compared with alkali metal series (Dzidic, 1970).

Condensation of water vapour of ice germ formation in super cooled liquid, when ionizing radiations are passed (Vashneya, 1969), is a milestone in the understanding of ions as centers of condensation. This basis has been confirmed theoretically (Varshneya, 1971). The pioneer worker (Castleman, 1979; Mohnen, 1970, 1974; Chan, 1980a, 1980b) has placed the belief on a firm footing.

5.3 ION SPECIES IN TROPOSPHERE:

The sequence of chemical reactions that alters the ion species between their creating by cosmic rays or radioactive decays and their removal by either ion-ion recombination, attachment to a particle, or some other loss mechanism is quite complex.

Ion lifetimes in clean air are expected to be the order of 100 sec (Ferguson, 1979). However, during the first one-second interval after ionization, most of the ions in the troposphere have experienced enough collisions with neutral species, whose concentrations are in parts per billion (ppb) range or higher, to have established very stable core ions due to attachment.

Perkins and Eisele (1984) reported first mass spectrometric measurements of naturally occurring positive and negative ions at ground level under a variety of weather conditions. Positive ions were observed with masses 54, 60, 80 and 94 amu, mass 54 amu is believed to be $NH_4^+ \cdot 2(H_2O)$ the negative ions were observed to have the masses 60 and 125 amu and were believed to be NO_3^- and $NO_3^- (HNO_3)$. Several ions that appear to be H_2O cluster of the above ions were also observed.

Mohnen (1970) reported the terminal ions in troposphere as being hydrated, O_2^- and CO_4^- . The degree of hydration depends upon temperature and the mean number of water molecules attached to these ions. As soon as the water vapour concentration is less than the concentration of carbon dioxide (above 8km). The terminal ion is found to be hydrated CO_4^- .

Using an improved aircraft borne mass spectrometer with high mass resolution (Hauck, 1984), reported positive ion composition measurements in the lower stratosphere and upper troposphere (Table 5.1).

The ions 37 ± 1 , 55 ± 1 and 71 ± 1 may readily be identified as proton hydrates ($H^+(H_2O)_n$; $n = 2,3,4$) which are expected (Arnold, 1982) to form quickly at the tropopause from primary positive ions produced by galactic cosmic ray ionization.

Legrand and Delmass (1984) analyzed 100 snow samples representing a continuous sequence of 10 years of precipitation at South Pole. The results show that the ionic budget of deposited smoke at this central Antarctic location is satisfactorily balanced when the concentration of eight major ions ($H^+, Na^+, K^+, NH_4^+, Mg^{2+}, SO_4^{2-}, NO_3^-, Cl^-$) are taken into account. Na^+, K^+, Mg^{2+} and Cl^- are typical constituents of sea salt particles which form one part of atmospheric aerosol over Antarctica, but H^+, NO_3^+, NH_4^+ excess SO_4^{2-} and excess Cl^- are linked to an important acid aerosol fraction which is most probable gas derived.

Theory of ice formation charged particles has been supported indirectly by many workers. Bigg (1961) and Bigg et al., (1963) found experimentally that IN concentration is sufficiently higher ($\sim 10^5$) in upper and lower atmosphere than at ground. The number concentration of cloud ice particles have been observed in excess than the number concentration of IN at cloud top temperature. The above findings can be explained if we consider the effects of ions on condensation and ice nucleation.

Table- 5.1

Positive ion masses obtained from high-resolution spectra at

11.28 km altitude (Hauck, 1984)

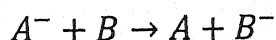
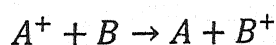
Mass	Tentative Ion Identification
28 ± 1	HCO^+ H^+HCN
32 ± 1	$\text{H}^+\text{CH}_3\text{OH}$
37 ± 1	$\text{H}^+(\text{H}_2\text{O})_2$
50 ± 1	$\text{H}^+\text{CH}_3\text{OH}.\text{H}_2\text{O}$
55 ± 1	$\text{H}^+(\text{H}_2\text{O})_3$
59 ± 1	$\text{H}^+(\text{CH}_3)_2\text{CO}$
64 ± 1	$\text{H}^+\text{CH}_3\text{COH}.\text{H}_2\text{O}$ $\text{H}^+\text{C}_2\text{H}_5\text{OH}.\text{H}_2\text{O}$ $\text{H}^+\text{CH}_3\text{OCH}_3.\text{H}_2\text{O}$ $\text{H}^+\text{HCOOH}.\text{H}_2\text{O}$
73 ± 1	$\text{H}^+(\text{H}_2\text{O})_4$
77 ± 1	$\text{H}^+(\text{CH}_3)_2\text{CO}.\text{H}_2\text{O}$
88 ± 1	$\text{H}^+\text{CH}_3\text{OH}.\text{(H}_2\text{O)}_2$
144 ± 1	$\text{H}^+(\text{CH}_3)_2\text{CO}.\text{(H}_2\text{O)}_3$
126 ± 1	$\text{H}^+(\text{H}_2\text{O})_7$

However, Detweiler and Vonnegut (1980) did not find any effect of ions on condensation process. Their estimate of the concentration of ice particles cannot be taken to be very reliable. Recently Dwivedi D. et al., (2009) studied the variation of relaxation time in water vapour condensation and ice glaciation as a function of supersaturation ratio in presence of ions.

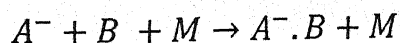
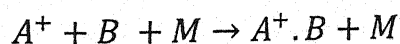
5.4 IONS IN THE ATMOSPHERE:

Near the ground α , β and γ radiations from Thoron and Radon decay and cosmic radiation are the principle ionizing agents causing charge separation initially into electrons and singly charged positive ions. At altitudes up to 60 km cosmic ray background is still the major ionization source; if we neglect disturbances known to occur after high solar activity.

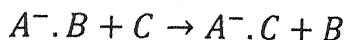
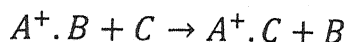
The free electrons will, after thermalization attach to neutral molecules. The positive and negative ions now undergo a series of so-called ion-molecule reactions covering simple charge transfer of the type (Mohnen, 1974).



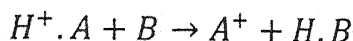
or attachment reactions (M=3rd body)



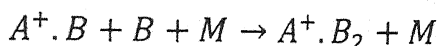
or switching reactions



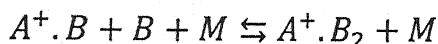
or proton transfer reactions



or clustering reactions



And



Each ion-molecule reaction is characterized by a rate constant.

5.5 DESTRUCTION OF SMALL IONS IN THE ATMOSPHERE:

Particles in the atmosphere may be formed through the coagulation of two or more particles. But this process does not produce any new particles. Infact it decreases the total number of particles. New particles are produced in the atmosphere through a number of mechanisms. The wind stresses and other natural or artificial mechanical stresses can detached the particle from the surface. For example, fragments can be detached from solids through abrasion cracking, weathering, etc. and from oceans through breaking of waves, bursting of bubbles. Supersaturated vapour can produce solid (i.e. ice) and liquid elements

directly from the water phase by nucleation. In addition, human activity is another effective producer of particles. (Table 5.2 gives a general picture of existing particles in the atmosphere.)

In general the concentration of large nuclei over oceans is one order less than that of over land. About half of the small condensation nuclei carry a net electrical charge.

The small ions (created by the atmospheric radioactivity and cosmic rays) will be destroyed by the attachment and uncharged large nuclei. When a small ion gets attached to uncharged large nuclei, it will become a large ion.

5.6 AN INTRODUCTION ON ATMOSPHERIC ELECTRICAL CONDUCTIVITY:

Deshpande and Kamra (2002) reported the atmospheric electrical conductivity measurements made over the Indian Ocean with a Gerdien's apparatus mounted MB polarbird during XVI Indian Scientific Expedition in 1996-1997. They also reported simultaneous three hourly measurements of aerosol concentrations of 13-1000 n.m. size and some meteorological parameters. Latitudinal variation of conductivity along the Cruise route show a minimum at $\sim 28^{\circ}$ S. Further, the variation in the conductivity in 10°N - 20°S and 60° - 70°S Latitudinal belts show opposite trends on the outward and return cruises, which fall near to the reset and withdrawal phases of the north-east monsoon season.

Table -5.2

(Ref ?)

Some Characteristic Features of Atmospheric Particles

Type	Concentration no/m ³	Range of Sizes Diameter in Meters	Approximate Terminal Velocity m/sec
Gas molecules	Almost 25×10^{24}	$(2.8-6.5) \times 10^{-10}$	
Small ions	$(1-7) \times 10^8$	$(1.5-1.0) \times 10^{-9}$	
Large ions	$(2-20) \times 10^8$	$(1-20) \times 10^{-8}$	
Small Aitken	(10^7-10^{11})	$(1-40) \times 10^{-8}$	$10^{-7}-10^{-5}$
Condensation Nuclei			
Large nuclei	(10^6-10^9)	$(4-20) \times 10^{-7}$	$10^{-5}-7 \times 10^{-5}$
Giant nuclei	(10^2-10^7)	$(20-1000) \times 10^{-7}$	$7 \times 10^{-4}-7 \times 10^{-3}$
Dry haze	(10^9-10^{11})	$(1-100) \times 10^{-7}$	$10^{-5}-10^{-4}$
Fog and cloud	$(25-600) \times 10^6$	$(1-200) \times 10^{-6}$	$10^{-4}-70 \times 10^{-2}$
Droplet	$25 \times 10^6-6 \times 10^8$		
Drizzle	$(1-10) \times 10^6$	$(2-40) \times 10^{-5}$	$(1-170) \times 10^{-2}$
Rain Drops	10^6-10^9	$(4-40) \times 10^{-4}$	$(17-90) \times 10^{-1}$

From these measurements in the free troposphere of the equatorial pacific, Clarke (1993) showed that nucleation in the upper troposphere and subsequent growth by coagulation and vapour diffusion could be a major source of new particles in that region. These measurements support the conclusions of a large scale model of aerosol nucleation and dynamics in the free troposphere and marine boundary layer developed by Raes (1995), which suggests that injection by mixing with the free troposphere is a major source of new sub-micron particles in the marine boundary layer. For interpreting their mid-pacific formation occur in outflow regions of the frontal or convective clouds in the free troposphere where conditions of new particle formation are met (Raes, 1993). These newly formed particles grow by coagulation and condensation. Transport of aerosols from the free troposphere to the marine boundary layer occurs by convective mixing in the vertical and general circulation in the horizontal. These particles grow by vapour deposition and therefore the growth is faster in the tropical marine boundary layer where gaseous precursor concentrations are large.

Their measurements of the atmospheric electric conductivity along the cruise track during the months of December and March do indicate a secular decrease in the conductivity which is most likely a consequence of an increase in the background air pollution.

5.6.1 Diurnal Variation of the Atmospheric Electric Field and Conductivity at Maitri, Antarctica:

Deshpande and Kamra (2002) made surface measurements of atmospheric electric conductivity at the Indian Station Maitri ($70^{\circ} 45'52''\text{S.}$, $11^{\circ} 44' 3''\text{E}$, 117 m above mean sea level), Antarctica from

January 10 to February 24, 1997. The total conductivity is $2.1 \times 10^{-14} \text{ S.m}^{-1}$ and does not show any significant diurnal variation fig.(5.1) shows the diurnal variation of hourly averaged values of conductivity of both polarities averaged for 20 fair weather days at Maitri. Where the convention was that the fair weather field pointing downward is negative. The electrical conductivity of both polarities does not show any significant variation except for somewhat higher values during the 1500 to 2400 UT period. The conductivity of positive polarity is generally always higher than that of negative polarity. The mean values of positive and negative conductivity are $+1.2$ and -0.9 Sm^{-1} , respectively. The difference may possibly be due to the manifestation of the electrode effect. Kandalgaonkar et al., (2003) analyzed the data of point discharge current (PDC) measurements during a total of 65 thunderstorm of Pune ($180^\circ 32' \text{N}$, 73° , $51' \text{E}$) to study the (PDC) local diurnal variation.

5.6.2 Variation in Atmospheric Electrical Conductivity Beneath A Thundercloud:

Singh et al. (1985) has developed an expression for atmospheric electrical conductivity on the assumption that thunderclouds produce intense electric field at the ground surface creating large scale ionization. Atmospheric electrical conductivity has been found to remain unchanged unless the ground electric field exceeds a certain threshold value to initiate corona near the ground surface. Effect of height of thunderclouds on the atmospheric conductivity has also been discussed.

Considering dimensions of thundercloud (Singh, N., 1984; Mathpal, 1983; Singh, N., 1985) $D=1.25 \text{ km.}$, $L=1.50 \text{ km.}$, $H=0.50 \text{ km.}$ the behaviour at atmospheric electrical conductivity beneath a

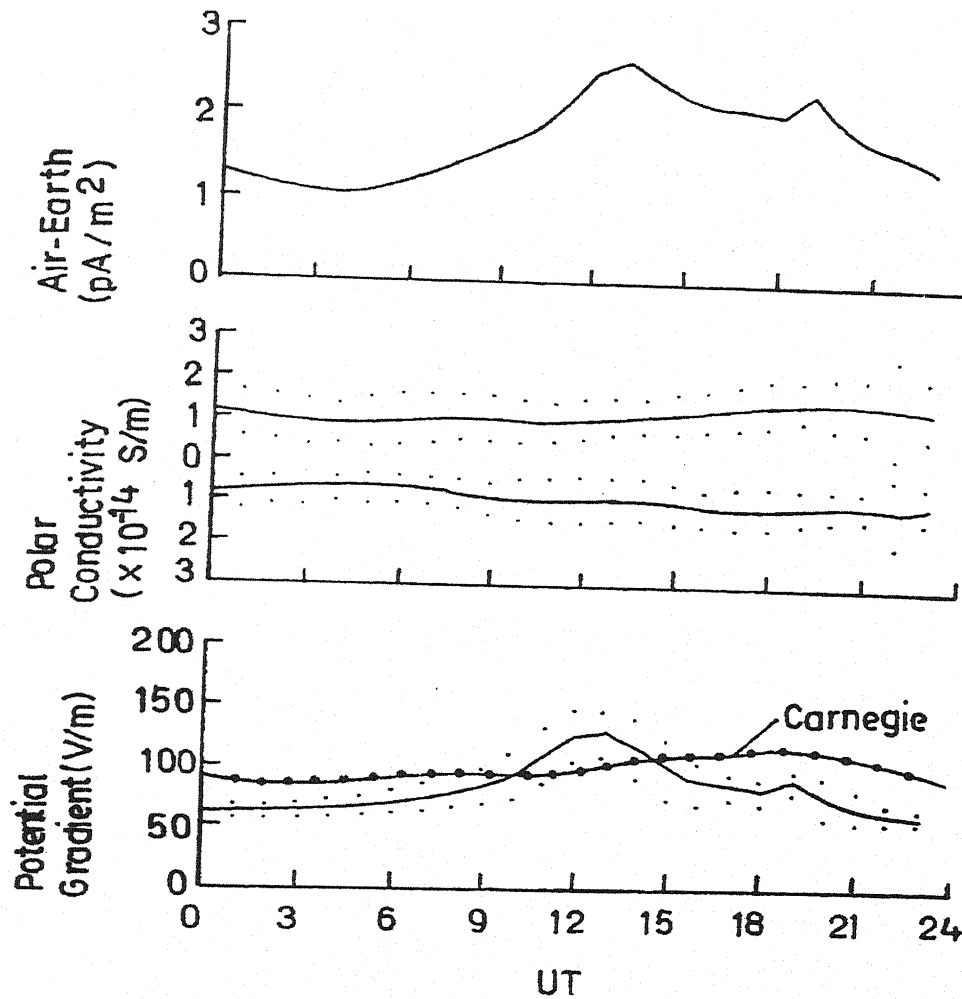


fig. 5.1 : Diurnal variations of the potential gradient, the conductivity of both polarities and the air-earth current averaged for 20 fair weather days at Maitri. Continuous curve with solid circles shows the Carnegie curve for the diurnal variation of potential gradient.

Ref ?

thundercloud have been determined. The calculations have been performed assuming $E_{in} = E_{out} = 100 \text{ Vm}^{-1}$, $q = 10 \times 10 \text{ Pl m}^3 \text{ sec}^{-1}$, $N = 1.5 \times 10^{-10} \text{ m}^{-3}$, $\eta = 4.6 \times 10^{-12} \text{ m}^{-3} \text{ sec}^{-1}$, $\eta_0 = 1.8 \times 10^{-12} \text{ m}^3 \text{ sec}^{-1}$ and $\alpha = 1.6 \times 10^{-12} \text{ m}^3 \text{ sec}^{-1}$. The results for various concentrations of large ions have been shown in fig. (5.2). This figure shows that atmospheric electrical conductivity remains unchanged unless ground electric field, E_{out} exceeds its threshold value to initiate corona near the ground surface. As ground electric field exceeds its threshold limit a sudden increase in the conductivity has been noted. Fig.(5.3) shows the nature of conductivity variation for different cloud base heights from the ground surface. A lower thundercloud produced electric field with higher growth rate at the ground surface, which involves into higher maximum value of ground electric field. The threshold value of ground electric field to produce corona ions also reaches earlier in case of lower clouds. Consequently lower base thunderclouds affect conductivity to the large extent fig. (5.3).

A thundercloud constitutes a rapid and widespread perturbation in the electric field at the ground surface. Anderson (1977) also pointed out that investigations of the atmospheric phenomenon near the ground must consider the electrode phenomenon (increased positive ions density) because almost all measurements near the ground will be affected by it to some degree therefore, taking this aspect into account efforts have been made to gain a physical insight into processes controlling the electrical state of the atmosphere near the ground.

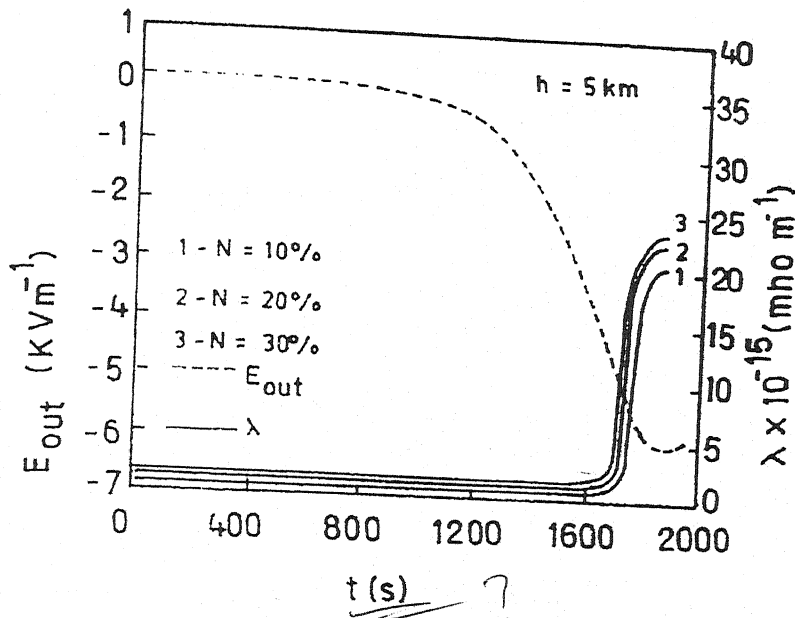


fig. 5.2 : Variation in conductivity for various concentration of large ions.

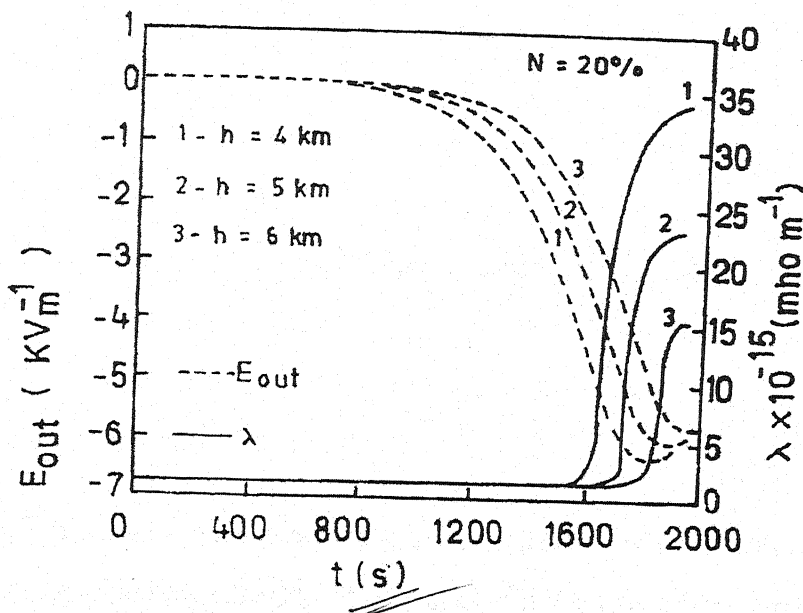


fig. 5.3 : Variation in conductivity by different cloud base heights

The electrical aspects of atmosphere near the ground surface are principally characterized by the different conditions of the ionization equilibrium existing near the ground. The general ionizing agencies, which are supposed to produce ions in the lower atmosphere, are: (1) the penetrating radiation from the radioactive substances in the earth crust, (2) radiation from the radioactive dust in the atmosphere and (3) cosmic rays.

The statistically inhomogeneous Markovian model and the stochastic radiative transfer equation have been used to derive equations for the mean radiance of solar radiation. It was demonstrated that in extreme cases the obtained equation agree with corresponding equation previously derived for (i) the statistically homogeneous broken clouds and (ii) the vertically inhomogeneous overcast clouds (Evgueni,2003).

5.7 CONTRIBUTION OF CLOUD AND PRECIPITATION PARTICLES TO THE ELECTRICAL CONDUCTIVITY AND THE RELAXATION TIME OF THE AIR IN THE THUNDERSTORMS:

Kamra (1979) calculated electrical conductivity caused by the charged cloud and precipitation particles in thunderstorms. It is found that the conductivity may be 1 or perhaps 2 orders of magnitude higher than the clear conductivity at the same altitude. Since the conductivity increases with the precipitation intensity, liquid water content, electric field and the electrical charge on the particles.

The value of electrical conductivity within thunderstorms is a matter of considerable dispute. Since small ions produce by cosmic rays should soon be captured by the cloud droplets. Gunn (1954), Phillips

(1967), and many others have suggested that the conductivity of cloudy air should be much less than that of clear air.

Incorporating polymerase chain reaction based identification, population characterization and quantification of microorganism into aerosol science is studied by Jordan Paccia et al. (2006).

There are many sources and types of charge carriers in thunderstorms. Small ions are produced by cosmic rays and are further supplemented by point discharge current flowing from the ground and the conduction currents flowing from outside the cloud. Hydrometeors themselves may produce small ions by corona in intense electric fields. Further, the cloud and precipitation particles may themselves become charged by capturing these small ions or various processes of charge generation in thunderstorms.

A unique feature of conductivity caused by cloud and precipitation particles is that in spite of its high values, the corresponding relaxation time of the cloudy air for the existence of space charges may not necessarily be small, this being specially so for small pockets of space charge and for the individual charged particles. Growth of large volumes of charge producing intense electric fields may, however, be significantly influenced by dissipation currents caused by this conductivity. This effect is now recognized and included in the calculations of the ambient electric field caused by the growth of the main charge centers of the thundercloud. (Kamra, 1970, 1971, 1975; Mason, 1972; Paluch, 1973; Ziv, 1974; Scott, 1975; Griffiths, 1975)

5.8 VARIATIONS IN ATMOSPHERIC AEROSOLS AND ELECTRICAL CONDUCTIVITY AT ROORKEE DURING THE TOTAL SOLAR ECLIPSE OF OCTOBER 1995

Singh et al. (1999) made measurements of some meteorological and electrical parameters with the total solar eclipse of October 24, 1995 continuously from October 22-27, 1995 at Roorkee (29° 52' N, 77° 53' 52" E, 275m above sea level). Roorkee observed (90-92%) maximum obscuration of eclipse, as it was close to the path of totality. The event lasted from 7.10 am to 9.30 am (IST; 0140-0400 hours GMT). Considerable increase of aerosol and positive and negative conductivities were recorded during the eclipse with respect to those made on any other day. Increase in relative humidity and decrease in temperature were also observed during the eclipse.

5.8.1 Measurement of Electrical Conductivity:

The technique for the measurement of atmospheric conductivities makes the use of the Gerdien condenser (Mukku, 1982). This instrument fig.(5.4), has been used widely for the measurement of electrical conductivity, ion mobility and density. It has been used for balloon-borne and ground-based measurements. The electrical conductivity of the air can be determined from current-voltage characteristics of the condenser.

A positive potential at the outer electrode makes electrons and negative ions move to the central electrode, thereby constituting a current. This gives the negative conductivity. The negative potential on the outer electrode similarly provides us the positive conductivity. The total conductivity σ , in terms of positive (σ_p) and negative (σ_n) conductivity, is given by

$$\sigma = \sigma_p + \sigma_n \quad (5.2)$$

From the measurement of output current of EMA fig. (5.4), the positive and negative conductivities can be obtained from (Mossop, 1955)

$$i_p = Men_p \frac{w_p}{w_c} \quad (5.3)$$

Where,

w_p - Mobility of positive ions

w_c - Critical mobility of ions

M - Aspiration rate

e - Electronic charge

n_p - Number of positive ions

σ_p - Conductivity of positive ions

Also,

$$W_c = \frac{M \ln(R_o/R_i)}{2\pi LV} \quad (5.4)$$

Where,

R_o - Radius of outer electrode

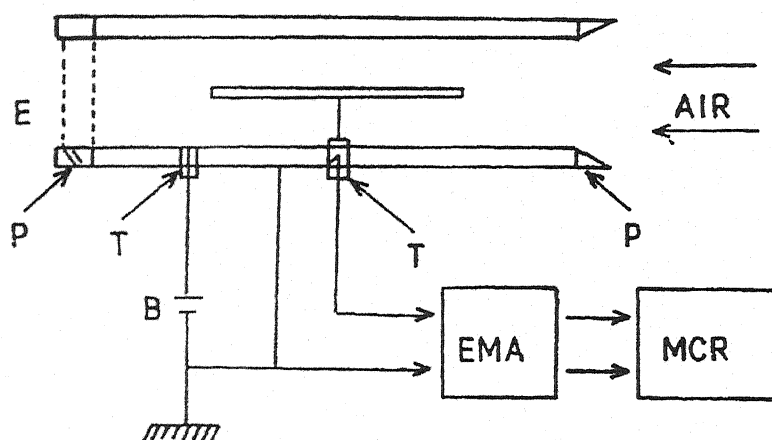
R_i - Radius of inner electrode

V - Voltage applied across the electrodes of the capacitor

L - Length of cylinder

Similarly, one may write

$$i_n = \frac{Me(n_n w_n + n_e w_e)}{w_e} = \frac{M\sigma_n}{w_e} \quad (5.5)$$



B = Battery

E = Electrostatic shield

EMA = Electrometer Amplifier

MCR = Multichannel Chart Recorder

P = Percepax

T = Taflon

fig. 5.4 : Experimental set-up for conductivity measurement.

Where i_n is the current due to negative ions and electrons, n_n the number of negative ions and n_e that of electrons, w_n and w_e are the mobilities of negative ions and electron, respectively.

In the present case, since the applied voltage was the same in each case ($\pm 30V$), the critical mobility is given by

$$w_c = 2.6624 \times 10^4 m^2 V^{-1} S^{-1} \quad (5.6)$$

5.8.2 The Observed Variation in Electrical Conductivity:

Singh et al. (1999) observed the variation in electrical conductivity of atmosphere fig. (5.5), at the time of eclipse. The variation in negative conductivity is found to be larger than for positive conductivity. The duration of peak negative conductivity is larger than for positive conductivity. Table 5.3 shows the measurements of atmospheric conductivities by other workers during various solar eclipses. The observed variations in positive and negative conductivity are in good agreement with the present results. During the solar eclipse, both the aerosol concentration and electrical in which the increase of aerosol concentration normally occurs with the decrease in atmospheric electrical conductivity.

Nitrogen budgets of agriculture fields of the Changjiang River basin from 1980 to 1990 (Xiang Bao, 2006). The increased ionization during the solar eclipse is responsible for the increase of both positive and negative conductivities. Singh et al. (1985) have shown that the atmospheric ions increase the cloud condensation nuclei (CCN) formation. Singh, N., Ph.D. Thesis, (1985) has shown that the atmospheric ionization plays an important role in aerosol formation.

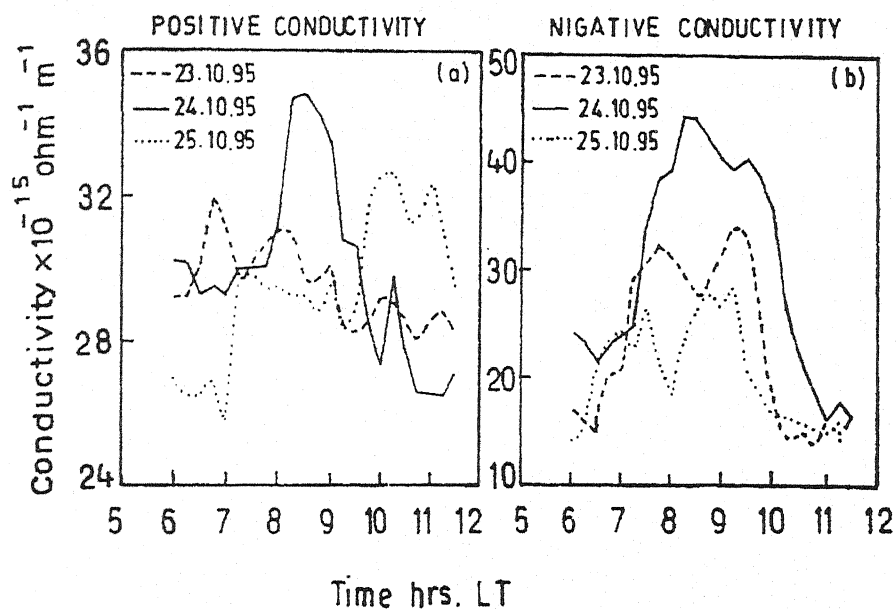


fig.5.5 : Time variation of atmospheric conductivity (a) for positive conductivity and (b) for negative conductivity.

Table-5.3

A Summary of Measurements of Electrical Conductivity by Various Investigators

Solar Eclipse period	Investigator (s)	Place	Remarks
7 March 1970	Anderson and Dolezalek (1972)	Waldor Annex of the Naval Research Lab., Washington DC (USA)	Clear decrease in negative conductivity
10 July 1972	Lane-Smith and Markson (1977)	Malignant Cove Nova Scotia (USA)	The negative conductivity began to rise up to High values about 5 min, after the totality
16 Feb 1980	Nizamuddin et al. (1981)	Nagarampalam Visakapatnam (India)	Both types of polar conductivities increase but increase in positive conductivity is more pronounced than negative conductivity
18 March 1988	Dhanokar Deshpande and Kamra (1989)	Pune (India)	Remarkable changes in atmosphere conductivity during the period of eclipse
24 Oct 1995	Singh et al. (1999)	Roorkee (India)	Increase in both positive and negative conductivity

The increased ionization would increase the concentration of aerosols. Thus, the atmospheric conductivity and aerosol both has been found to be increased during the total solar eclipse because of the excess atmospheric ions created by galactic cosmic rays. Forbush decrease enhanced by obstruction of solar wind particles by the moon.

5.9 USING ATMOSPHERIC ELECTRICAL CONDUCTIVITY AS AN URBAN AIR POLLUTION INDICATOR:

Guo et al. (1996) investigated the atmospheric electrical conductivity as an air, pollution indicator through correlation analysis based on two year of daily averaged observations of the atmospheric electrical conductivity; weather classification index, and the concentration of aerosol particles, carbon mono-oxide, sulfur dioxide and nitrogen dioxide at a single site in downtown Toronto from 1973-1974. The main findings are following: (1) The electrical conductivity was negatively and almost linearly correlated to the individual pollutant concentrations, (2) the effects of the individual gaseous pollutants (i.e. carbon monoxide, sulfur dioxide and nitrogen dioxide) on the electrical conductivity were superimposed with unequal weighting factors, (3) The multi-correlation of the electrical conductivity versus the superimposed concentration of the gaseous pollutants and the particulate pollutant concentration (i.e. aerosol particles was significant, suggesting that the atmospheric electrical conductivity can be used as a composite air pollution indicator for detecting total air pollution and (4) The weather conditions did not seem to have any significant impact on the above correlation, although they had influenced both electrical conductivity and pollutant concentrations.

In the Retezat Mountains concentrations of O₃, NO₂ and SO₂ in summer season 2000-2002 were low and below toxicity levels for forest trees. While NH₃ concentrations were low in 2000, the 2001 and 2002 concentrations were elevated indicating possibility for increased N deposition to forest stands. More than 90% of the rain events were acidic with pH values <5.5, contributing to increased acidity of soils. Crown condition of Norway spruce (*Picea abies*) and European beech (*Fagus sylvatica*) was good, however, defoliation described as > 25% of foliage injured increased from 9.1% in 2000 to 16.1% in 2002. Drought that occurred in the southern Carpathians between fall 2000 and 2002 and frequent acidic rainfalls could cause the observed decline of forest condition. Both Norway spruce and European beech with higher defoliation had lower annual radial increments compared to the trees with low defoliation. Ambient O₃ levels found in the Retezat did not affect crown condition of Norway spruce or European beech (Akula Venkatram, 2006).

Fundamentally, λ is related to concentrations of air pollutants through destruction processes for small air ions due to recombination (or neutralization) of small ions with opposite signs of charges and attachment (or adhesion) of the small ions to large particles, as described in the following ion budget equation (Mathpal, 1982):

$$\frac{dn}{dt} = q - \alpha n^2 - \beta nN \quad (5.7)$$

Where, q is the small ion formation rate by radioactive and cosmic sources, α the recombination coefficient, β the attachment coefficient, N the number density of large particles and t the time. In destroying small

air ions, both molecular (or gaseous) and aerosol (or particulate) air pollutants with various chemical characteristics and sizes are believed to be active contributors for reducing both and (Paoletti, 1989; Retalis, 1991; Sheftel, 1972).

The present study is intended for consideration of both individual and collective effects of important air pollutants based on experimental measurements at a single in Toronto for two consecutive years. Its investigation will cover (1) variation patterns of λ and air pollution, (2) statistical relationships between λ and concentrations of important air pollutants, and (3) influences of the weather on the relationships.

5.10 CONDUCTIVITY AND IONIC CONCENTRATION:

5.10.1 Sources of Ions in the Atmosphere:

Uranium and Thorium are distributed in the earth's crust. The Radon (Rn) and Thoron (Tn) gases, thus formed will diffuse through interstices or soil capillaries into the atmosphere where they decay. The decay products soon attach themselves to the fine particles (aerosols) in the atmosphere. Hence, the fine particles found in the atmosphere possess a small but measurable amount of natural radioactivity. Thus the chief ionizing agents in the lower atmosphere are the penetrating radiation from the radioactive substances in the earth's crust, radiation from the radioactive substances in the atmosphere and the cosmic rays.

The impact of urban street lay out on local atmospheric environment is studied by Xie Xiaomin (2006).

The β radiation from the earth's surface will give about 0.3×10^6 pairs of ions (PI) per m^3 per sec, with radiation about $3.2 \times 10^6 \text{ PI m}^{-3} \text{ sec}^{-1}$,

α activity of the air gives about 4.4×10^6 Pl m^{-3} sec^{-1} with β and γ radiations about 0.03×10^6 Pl m^{-3} sec^{-1} and 0.15×10^6 Pl m^{-3} sec^{-1} , respectively. Thus the total ionization rate from the radioactivity is about 8×10^6 Pl m^{-3} sec^{-1} (Bricard, 1965). Table 5.4 gives an average vertical distribution of soil radiation (Israel, 1971).

Contribution of radioactivity towards ionization over oceans is insignificant. The electric cosmic ray component at the ground level will give about 2×10^6 Pl m^{-3} sec^{-1} . The ionization due to solar cosmic rays is essentially a high altitude phenomenon and is important only at the time of solar disturbances. On the whole the ionization rate at the ground level is about 10×10^6 Pl m^{-3} sec^{-1} .

The characterization of atmospheric dry deposition particulates by Cobb (1970).

Table - 5.4

**RADIOACTIVE RADIATION FROM THE SOIL AS A
FUNCTION OF ALTITUDE**

Altitude above the ground (m)	Soil radiation in percentage
1	97
10	83
100	33
500	2
1000	0.1

5.10.2 Conductivity in Land and Sea Breeze:

Land and sea breeze is a consequence of simultaneous involvement of processes like heating expansion of air, development of pressure gradient, forces, accelerations and air motions. There are a number of studies on concentration of particulate matter and radioactive content in the land and sea winds (Misaki, 1977; Akula, 2006). Misaki et al. (1977) could notice drastic reduction in radioactive content in the sea air. Morita and Ishikawa (1971) recorded continuous increase in conductivities as their relationship, moved away from shore. Blanchard, (1966) had obtained high values P.G. and positive space charge in the sea wind opposite to the land wind.

5.10.3 Atmospheric Electric Conductivity:

In this section we describe how in our model we construct global values of the atmospheric electric conductivity. This includes taking cognizance of the distribution of aerosol particles at the earth's surface, its orography, the ionization by the cosmic rays and radioactivity and the corona ions beneath the active thunderclouds. The ionization rate by cosmic rays and radioactivity has been calculated from the empirical model of Makino and Ogawa (1985).

5.10.4 Electrical Conductivity in and Above the Thundercloud:

There is a considerable uncertainty with regard to an appropriate value for conductivity within the Thundercloud. Inside the cloud the ions may have extremely low mobility.

Size fractionated speciation of nitrate and sulfate aerosol in a subtropical industrial environment was found (Sudhir Kumar Pandey, 2006).

The regions of shielding charge that are observed at cloud boundaries are evidence to suggest these low conductivities. Supporting this are the measurements of Gish and Wait (1950) around the thunderstorm cells Freier (1962), Evans (1969) and Kamra (1979) on the other hand suggested that the conductivity within the thundercloud might be as high as 10 to 18 times that of the clear air conductivity. In this present study the conductivity has been calculated.

Atmospheric environmental protection was observed in China, current status, developmental trend and research emphasis (K. Madhavi Latha, 2006).

The effective attachment coefficient to the cloud particles $\bar{\beta}_c$ has calculated from (Volmer, 1939).

$$\bar{\beta}_c N_c = 4\pi R_c D N_c \quad (5.8)$$

Where R_c is the mean radius of the cloud particles; N_c , its number density and D , the diffusion coefficient of ions.

Variation of D with height is assumed as followed (Makino, 1985)

$$D = 4.2 \times 10^{-6} \exp[9.16 \times 10^{-5}(Z - Z_G)] m^2 S^{-3} \quad (5.9)$$

The altitude profile of atmospheric conductivity (λ_c) can be approximated by

$$\lambda_c(Z) = \lambda_{cN} \exp[-(Z - Z_G)/S_c] \quad (5.10)$$

Where,

$$S_c = -Z_N / \ell n(\lambda_G / \lambda_{cN}) \quad (5.11)$$

Z_N is height above the ground of negative charged region of thunderstorm; the ambient conductivity at the altitude Z_N .

The conductivity beneath the active thunderstorm at any time t is given by

$$\lambda(z, \theta_i, \Phi_j, t) = \lambda(z, \theta_i, \Phi_j) + \lambda_c(z, \theta_i, \Phi_j) f(t_{LT}) \quad (5.12)$$

Where, the conductivity, $\lambda(z, \theta_i, \Phi_j)$ at any grid ($i \times j$) has been calculated from

$$\lambda(z, \theta_i, \Phi_j) = 2n(z, \theta_i, \Phi_j) e \mu(z) \quad (5.13)$$

Where, z is the altitude; θ_i the co-latitude; Φ_j , the longitude; $\mu(z)$, the mobility of the ions and e , the electronic charge.

The conductivity is determined by the steady state ion balance equation:

$$q - \alpha n^2 - \beta N_0 n = 0 \quad (5.14)$$

$$\frac{1}{\tau_p} = \frac{1}{\tau_\alpha} + \frac{1}{\tau_\beta} \quad (5.15)$$

Where, the time constant associated with ion production (τ_p), ion recombination (τ_α) and ion attachment (τ_β) are given by:

$$\frac{1}{\tau_p} = \frac{q}{n}$$

$$\frac{1}{\tau_\alpha} = \alpha n. \quad (5.16)$$

$$\frac{1}{\tau_\beta} = \beta N_0$$

5.11 RESULTS AND DISCUSSION:

A conductivity above the thundercloud has been calculated. Fig. 5.6 (a) shows the vertical profile of ambient conductivity calculated at the equator, which has been compared with the observations of Gish and Wait (1950), Woessner et al., (1958), Morita et al., (1971), Widell et. al., (1976) and Rosen and Hofmann, (1981). The altitude profile of conductivity at the time when thundercloud is active has been shown in fig. (5.6 b). Value of $\lambda_c(Z)$ has been calculated from equation (5.10).

The LT variation of conductivity beneath the thundercloud due to coronal ions has been shown in fig.(5.6 c).

The monitoring for Pb and Cd pollution using feral pigeons in rural, urban and industrial environments of Korea was studied (Dong-Ha, 2006).

Our calculations show that increase in AP concentration to five time the average concentration over ocean decrease the conductivity by 48% as shown in fig. (5.7).

In calculating the effective attachment coefficient $\bar{\beta}_c$ we have used equations (5.8) and (5.9). Mason (1972) Chiu and Klett (1976) assumed the value of R_c and N_c as $10 \mu m$ and $2 \times 10^8 m^{-3}$, respectively.

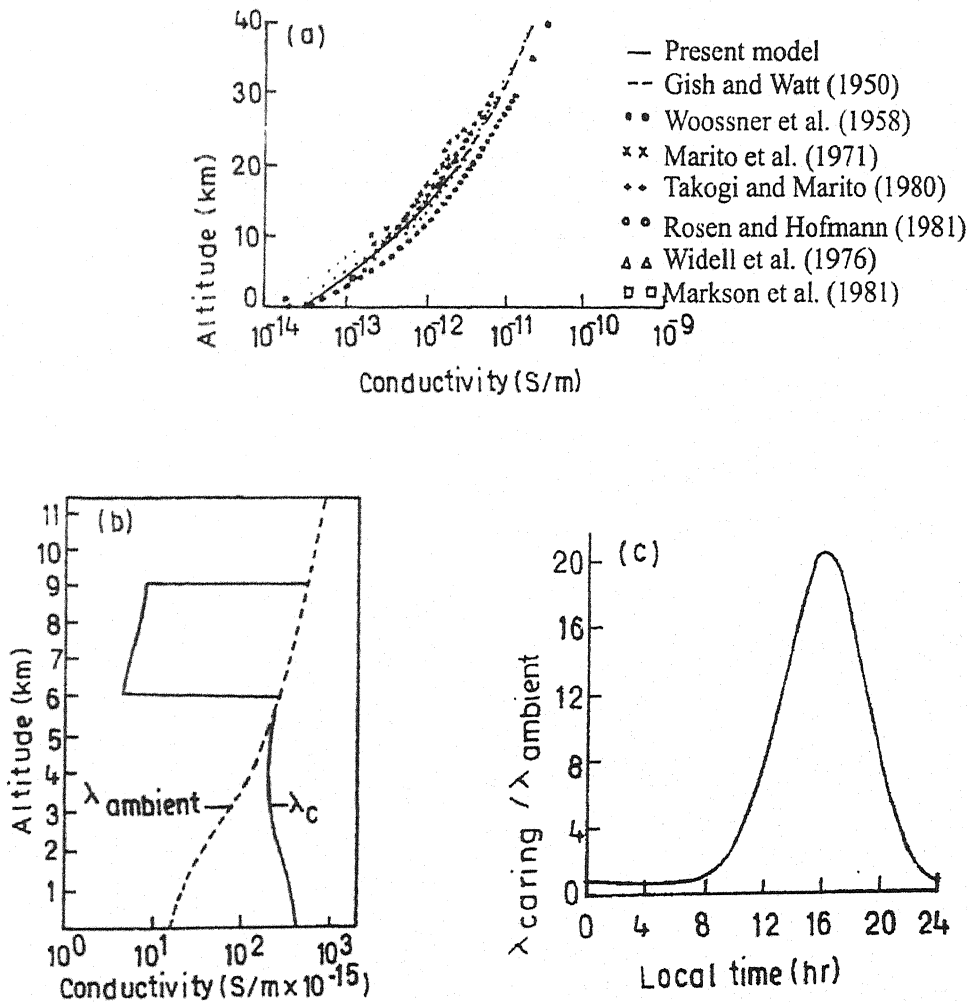


fig. 5.6 : (a) Vertical profile of ambient conductivity at the equator.
 (b) Effect of coronal ions on the conductivity.
 (c) Local time variation of conductivity beneath active thundercloud.

The calculated value $\bar{\beta}_c$ as the function of R_c are shown in Table 5.5 the graph between R_c (μm) and effective attachment coefficient $\bar{\beta}_c$ ($\times 10^{-10}$) $m^3 s^{-1}$ are plotted in fig. (5.7). The variation of $\bar{\beta}_c$ and D as the function of $(Z-Z_G)$ are given in Table 5.6. From these tables we note that the value of $\bar{\beta}_c$, and D vary exponentially with $(Z-Z_G)$ but $\bar{\beta}_c$ varies linearly with D . The altitude profile of atmospheric electric conductivity, $\lambda_c(Z)$ has calculated using eq. (5.10) and eq. (5.11) at the time when thundercloud is active. These calculations have shown in Table 5.7. We have taken conductivity near earth's surface $\lambda_c(Z)$ to be one order of magnitude higher than its ambient value ($\lambda_{cN} = 4.4 \times 10^{-1} Sm^{-1}$). We find that $\lambda_c(Z)$ decreases exponentially with increase in Z_N . At about $Z_N = 4.5$ km, $\lambda_c(Z)$ is minimum. At higher altitudes than $Z_N = 4.5$; $\lambda_c(Z)$ increases. Thus the values of $\lambda_c(Z)$ depend on ambient conductivity λ_G and $(Z - Z_G)$. Also at altitudes higher than 6 km both λ_G and $\lambda_c(Z)$ increase and remain the same at a given height. The calculated values of $\lambda_c(z)$ are in good agreement with the experimental work of Gish and Wait (1950), Woessner et al., (1958), Morita et al. (1971), Rosen and Hofmann (1981), Widell et al. (1976) and Markson et al. (1981).

CFD simulations of the wind environment around an airport terminal building was observed (P. Neofytou, 2006).

TABLE-5.5

CALCULATED VALUES OF EFFECTIVE ATTACHMENT
COEFFICIENT $\bar{\beta}_c$ AS THE FUNCTION OF MEAN RADIUS OF
CLOUD PARTICLES (R_c) AT $(Z-Z_G) = 1$ KM.

S.No.	$R_c(\mu m)$	$\bar{\beta}_c(\times 10^{-10})m^3s^{-1}$
1.	2	1.157
2.	6	3.471
3.	10	5.784
4.	14	8.098
5.	18	10.412
6.	22	12.725
7.	26	15.039
8.	30	17.353
9.	34	19.666
10.	38	21.980
11.	42	24.294
12.	46	26.607
13.	50	28.921

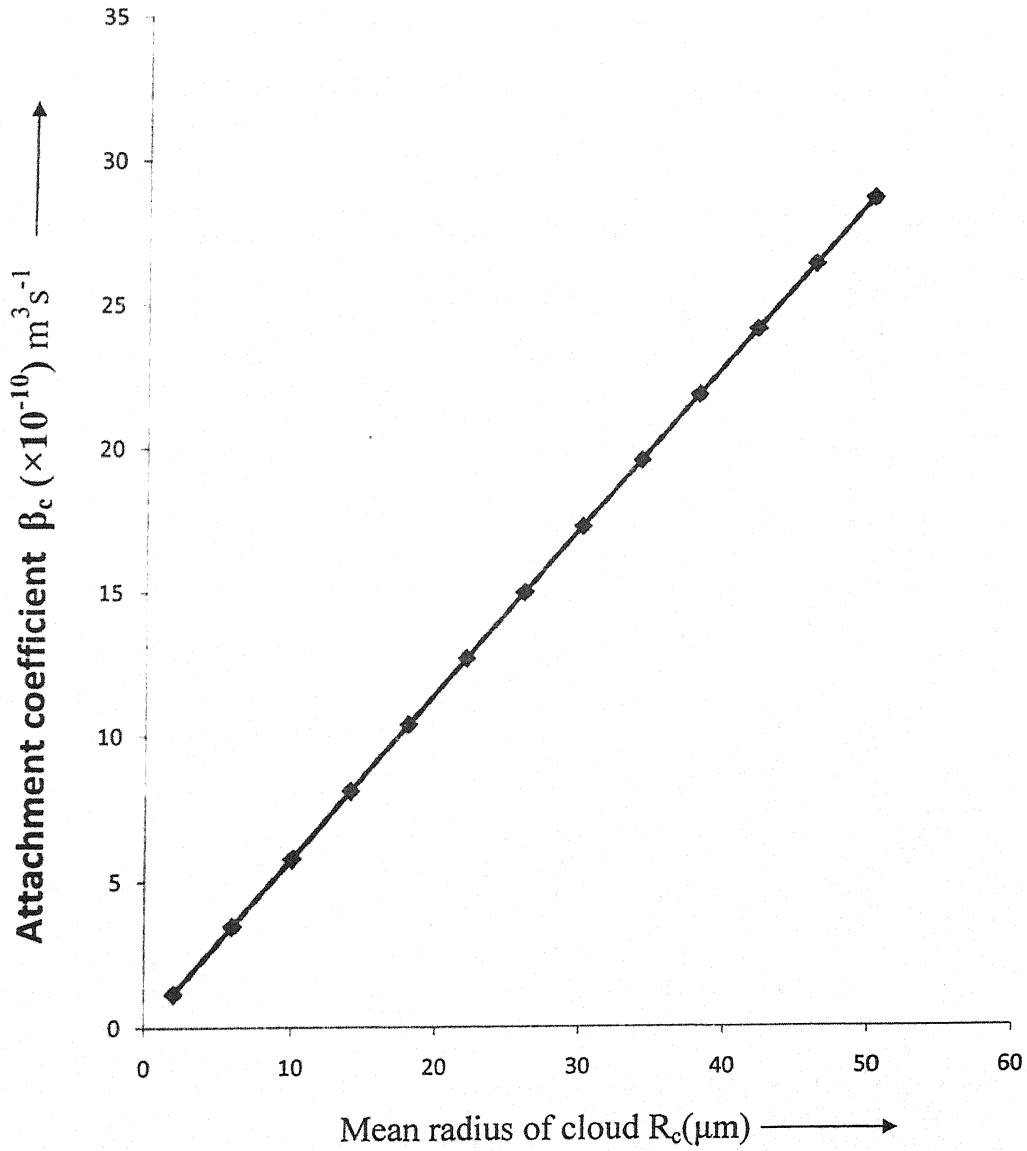


fig. 5.7 : Variation of attachment coefficient β_c ($\times 10^{-10} \text{ m}^3 \text{ s}^{-1}$) with mean radius of cloud particles at $(Z-Z_G) = 1 \text{ km}$.

TABLE-5.6

CALCULATED VALUES OF D, THE DIFFUSION COEFFICIENT OF IONS AND $\bar{\beta}_c$ THE EFFECTIVE ATTACHMENT COEFFICIENT AS THE FUNCTIONS OF $(Z-Z_G)$ AND $R_c = 20\mu m$ CONSTANT

S.No.	$(Z-Z_G)km$	$D (\times 10^{-6})m^2s^{-1}$	$\bar{\beta}_c (\times 10^{-10})m^3s^{-1}$
1.	2	4.2008	1.0558
2.	6	4.2023	1.0562
3.	10	4.2038	1.0565
4.	14	4.2054	1.0569
5.	18	4.2069	1.0573
6.	22	4.2085	1.0577
7.	26	4.2100	1.0581
8.	30	4.2116	1.0585
9.	34	4.2123	1.0586
10.	38	4.2146	1.0593
11.	42	4.2162	1.0596
12.	46	4.2177	1.0600
13.	50	4.2193	1.0604

TABLE-5.7

VARIATION OF ELECTRICAL CONDUCTIVITY $\lambda_c(Z)$ AS THE FUNCTION OF ALTITUDE (Z_N).

S.No.	Altitude Z_N (km)	λ_G ($\times 10^{-15}$) sm^{-1}	S_c	$\lambda_c(Z)$ ($\times 10^{-15}$) sm^{-1}
1.	1.0	37.50	32.075	500
2.	1.5	44.71	46.509	450
3.	2.0	57.50	61.530	400
4.	2.5	69.19	76.478	340
5.	3.0	83.70	91.242	300
6.	4.0	335.00	116.732	260
7.	4.5	376.00	130.885	260
8.	5.0	440.00	144.765	270
9.	5.5	530.00	158.389	300
10.	6.0	615.10	172.049	370

5.12 CONCLUSION:

From above study, we infer that there is a decrease in the electrical conductivity with altitude near the ground. It is minimum at about 4.5 km above the ground and it again increase above the height. The decrease in electrical conductivity may be attributed to the decrease in the concentration of ion because the ions get attached with aerosol particles or CCN and other particles. But at higher altitude, the concentration of ions increases due to ionization caused by galactic cosmic rays. This increase of ions increases the electric conductivity.

BIBLIOGRAPHY

BIBLIOGRAPHY

1. Abbas, M.A. and Latham, J., J. Meteorol Soc., Japan, 47, 67 (1969).
2. Abraham, F.F., Academic Press, N.Y. (1974).
3. Abraham, F.F., Homogeneous Nucleation Theory Supplement 1 to Advances in Theoretical Chemistry, Academic Press, New York (1974).
4. Abraham, F.F., J. Atmos. Sci. 25, 47 (1968).
5. Abraham, F.F., J. Chem. Phys., 61, 1221 (1974).
6. Akula Venkatram and T.W. Horst, J. Atmospheric Environment, 40, 2401 (2006).
7. Alexander Fladerer and Reinhard Strey, Atmos. Res. 65, issue 3-4, 161-187 (2003).
8. Allee, P.A., Proc. Conf. on Weather Mod., Santa Barbara, Calif., April 1970, Amer. Meteor. Soc., Boston, Mass, P-244 (1970).
9. Allen, J.B. and Kassner, J. L., Jr. J. Colloid Interface Sci., 30, 81 (1969).
10. Anderson, R.V. and Dolezalek, H., J. Atmos. & Terr. Phys., 34, 561 (1972).
11. Anderson, R.V., ed. Dolezalek, H. & Reiter, R., Germany, (1977).
12. Arnold, F., Nature, 299, 134 (1982).
13. Bader, R.F. and Jones, G.A., Canad. J. Chem. 41, 586 (1963)
14. Barker, J.A. and Watts, R.D., J.Chem. Phys. Lett., 3, 144 (1969).
15. Barlett, J.T., Vanden Heuvel, A.P. And Mason, B.J., Z. Angew Math. Phys., 14, 599 (1963).
16. Beared, K.V. and Ochs, H.T., The Earth's Electrical Environment studies in Geophys., National Academy press, 114-B (1986).

17. Beasley, W.H. and Eack, K.B., *Geophys. Res. Lett.* 27, 189 (2000).
18. Becker, R. and Doring, W., *Ann. Phys.*, 24, 719 (1935).
19. Ben-Naim, A. and Stillinger, F.H., *Water and Aqueous Solutions*, R.A. Horne, Ed., P. 295, Wiley-Interscience, New York (1972).
20. Ben-Naim, A., *Water*, F. Franks, Ed., Plenum Press, New York, P.413 (1972).
21. Benson, G.C. and Shuttleworth, R., *J. Chem. Phys.* 19, 130 (1951).
22. Bigg, E.K. and Hopwood, S.C., *J. Atmos. Sci.* 20, 185 (1963).
23. Bigg, E.K. and Mills, G.T., *Tellus*, 15, 162 (1963).
24. Bigg, E.K., Mills, G.T. and Hefferman, K.J., *J. Meteorol* 18, 804 (1961).
25. Bigg, E.K. and Stevenson, C., *J. de Rech. Atmos.* 4, 41 (1970).
26. Binder, K and Kalos, M.H., *J. Statist. Phys.*, 22, 363 (1980).
27. Bjerrum, N. and K. Danske Vielensk, Selsk., *SKr.* 27,1 (1951).
28. Blackman, M. and Lisgarten, N.D., *Proc. Roy. Soc. London*, A 239, 93 (1957).
29. Blanchard, D.C., *J. Atmos. Sci.*, 23, 507 (1966).
30. Bourdeau, C. and Chauzy, S., *Proceedings of Int. Conf. Atmospheric Electricity*, Uppsala, Sweden, June 13-16 (1988).
31. Brian A. Tinsleya, Limin Zhou a, b et al., *Atmospheric Res.* 79, 266-295 (2006).
32. Brian A. Tinsleya, Limin Zhoua, b and Abigail Plemmons, Chinese Academy of Sciences, Guiyang, Guizhou, China, June 10 (2005).
33. Bricard, J. Edited by S.C. Coroniti, pp. 82, Elsevier, New York (1965).

34. Bricard, J., Problems of Atmospheric and Space Electricity, S.C. Coronity, Ed., P-81, Elsevier, Amsterdam (1969).
35. Brill, R. and Tippe, A., Acta. Cryst., 23, 343 (1967).
36. Brook, M., Recent Advances in Thunderstorm Electricity, L.G. Smith, Ed., P-383, Pergamon Press, New York (1961).
37. Bucaro, J.A. and Litovitz, J.A., J. Chem. Phys. 54, 3846 (1971).
38. Cambell, E.S., J. Chem. Phys. 20, 1411 (1952).
39. Castleman, A.W. and Tang, I.N., J. Chem. Phys. 57, 3629 (1972).
40. Castleman, A.W., Jr., Adv. Colloid. and Interface Sci., Vol. 10, Academic Press, 73 (1979a).
41. Castleman, A.W., Jr., Edited by P. Ausloos, Plenum Press, New York, P. 295 (1979b).
42. Castleman, A.W., Jr., Holland, P.M. and Keese, R.G., J. Chem. Phys., 68, 1760 (1978).
43. Chan, L. Y. and Mohnen, V.A., J. Aerosol. Sci. 11, 35 (1980a).
44. Chan, L.Y. and Mohnen, V.A., J. Atmos. Sci. 37, 2323 (1980b).
45. Chiu, C.C. and Klett, J.D., J. Geophys. Res., 81, 1111 (1976).
46. Clarke, A.D., J. Geophys. Res., 98, 20, 633-647(1993).
47. Clementi, E., Kistenmacher, H. and Popkie, H., J. Chem.Phys., 58, 2460 (1973).
48. Cobb, W.E. and Wells, H.J., J. Atmos. Sci., 27, 814 (1970).
49. Cohen, N.V., Cotti, M., Iribarne, J.V. and weissmann, M., Trans. Farad. Soc. 58, 490 (1962).
50. Collins, F.C., Z. Elektsoenemic 59, 404 (1955).
51. Danford, M.D. and Levy, J. Am. Chem. Soc. 84, 3965 (1962).
52. Daniel Beysensa, B, J. Comptes Rendus Physique, 7, issue 9-10, 1082-1100 (2006).

53. Dawson, G.A. and Cardell, S.R., J. Geophys. Res., 75, 4589 (1973).
54. Dawson, P.B., Wilson, E.J., Hill, P.G. and Russell K.C., J. Chem. Phys., 51, 5389 (1969).
55. Defay, R., Prigogine, I., Bettermans, A and Everett, D.H., Wiley Inc., New York (1966).
56. Deshpande, C.G. and Kamra, A.K., J. Geophys. Res., 107, ACH 14-1 – ACH 14-9 (2002).
57. Detweiler, A. and Vonnegut, B., J. Atmos. Sci. 37,479 (1980).
58. Dhanorkar, S., Deshpande, C.G. and Kamra, A.K., J. Atmos. & Terr. Phys., 51, 1031 (1989).
59. Dolezalek, H., Proceedings of Int. Conf. Atmospheric electricity, Uppsala, Sweden, June 13-16 (1988).
60. Dong-Ha Nam and Doo-Pyo Lee, J. Science of Total Environment, 357, 288 (2006).
61. Doolittle, J.B. and Vali, G., J. Atmos. Sci., 32, 375 (1975).
62. Dorsch, R.G. and Hacker, P., NACA, Techn. Note, 2510 (1951).
63. Doyle, G.J., J. Chem. Phys. 35, 795 (1961).
64. Dufour, L. and Defay, R., Thermodynamic of Clouds, Academic Press, New York (1963).
65. Duncan, A.B. and Pople, J.A., Trans. Farad. Soc.49, 217 (1953).
66. Duning, W.J., Proc. Case Institute of Technology Symposium on Nucleation, Cleveland, Ohio (1965).
67. Dunning, W.J., P. 1-67, Edited by A.C. Zettlemoyer, Marcel Dekker, New York (1969).
68. Dwivedi, D. et al. J. Acta Ciencia Indica Vol. xxxv. P.No.2, 341-345 (2009).
69. Dwivedi, D., et al. SCITECH, vol-3, No.1, 56-58 (2008).

70. Dzidic, I. and Kebarle, P., J. Chem. Phys. 74, 1466 (1970).
71. E.J.Lund et al. Geophysical Res. Lett., Vol. 26, No.24, 3593-3596 (1999).
72. Edward, W.W. et al., International critical tables of numerical data, Physics, Chemistry, and technology; International Research Council; National Academy of Sciences (U.S.); Knovel (2003).
73. Eisenberg, D., Kauzmann, W., The structure and properties of water, Oxford Press, Oxford (1969).
74. Engel, A. Von, Ionized Gas, Geoffrey Cumberledge, Oxford (1955).
75. Ette, A.I.I. and Oladiran, E.O., Magnitudes and Variations, Pure Appl. Geophys. PAGEOPH 118, 753 (1980).
76. Evans, L.F., J. Atoms, Sci. 30, 1657 (1973).
77. Evans, W.H., J. Geophys. Res., 74, 939 (1969).
78. Evgueni Kassianov, J. Quantitative spectroscopy and radiative Transfer, 77, 373 (2003).
79. Feder, J., Russell, K.C., Lothe, J. and Pound G.M., Adv. Phys., 15, 111 (1966).
80. Ferguson, E.E., Fehsenfeld, F.C. and Albritton, D.L., Vol. 1, Edited by M.T. Bowers, Academic Press, New York (1979).
81. Fletcher, N. H., J. Meteor., 16, 173 (1959a).
82. Fletcher, N. H., The Chemical Physics of Ice, Cambridge University Press, London (1970a).
83. Fletcher, N.H., J. Chem. Phys., 29, 572 (1958).
84. Fletcher, N.H., The chemical physics of ice, Cambridge University Press, London (1970a).
85. Forslind, E., Acta. Polytechn. Scand. 3, No.5 (1952).
86. Franck, J.P. and Hertz, H.G., Z. Physik, 143, 559 (1956).

87. Frank, H.S. and Quist, A.S., J. Chem. Phys. 34, 604 (1961).
88. Frank, H.S. and Wen, W.Y., Disc. Farad. Soc. 24, 133 (1957).
89. Freier, G.D., J. Geophys. Res., 67, 4683 (1962).
90. Frenkel, J., Oxford University Press, London (1946).
91. Frenkel, J., P.378, Dover, New York (1955).
92. Fromm, J., Clementi, E. and Watts, R.D., J. Chem. Phys. 62, 1388 (1975).
93. G. Mandal and P. Pradeep Kumar, Atmos. Res., Vol. 61, Issue 2, 115-123, Feb. (2002).
94. Gabarashvili, T.G. and Gliki, N.V., Izv. Atmos and Oceanic Phys. 3, 570 (1967).
95. Gabarashvili, T.G. and Kartsivadze, A.I., Proc. Conf. Cloud Phys. Toronto, Aug. 1968, P. 188, Univ. of Toronto Press, Toronto (1968).
96. Gabarashvili, T.G. and Kartsivadze, A.I., Proc. Conf. on Condens and Ice Nuc., Praguevienna, Sept. 1969, P. 220 (Zechoslovak. Acad. Sci., Prague) (1969).
97. Gagin, A, J. de Rech. Atmos., 6,175 (1972).
98. Garraud, C., Role du givrage des electrodes dans electro congelation des brouillards surfondus. C.R. Acad, Sci. Paris, 268, 1042 (1969).
99. Gish, O.H. and Wait, G.R., J. Geophys. Res., 55, 473 (1950).
100. Glenn E. Shaw, Geophysical Res. Lett., Vol. 25, N. 23, 4317-4320, Dec. 1 (1998).
101. Goff, J.A., Humidity and Moisture, A Wexler, Ed., Rainhold Publ. Co., New York, Vol. 3, P. 289 (1965).
102. Gondot, P., Delannoy, A and Blanchet, P., Proceeding of Int. Conf. Atmospheric Electricity, Uppsala, Sweden, June 13-16 (1988).

103. Griffiths, R.F. and Latham, J., J. Atmos. Sci., 32, 958 (1975).
104. Guilder, L., Johnson, D.P. and Jones, F.E., Science 1991, 1261 (1975).
105. Gunn, R., J. Meteorol., 11, 130 (1954 b).
106. Guo, Y., Barthakur, N.N. and Bhartendu, S., J. Geophys. Res., 101, 9197 (1996).
107. Gupta, N. et al. SCITECH, 2, 75-80 (2007).
108. H. Hermann, R. Wolke, K. Muller, T. Gnauk, Atmos, Env. Vol.39, 4169-4183, July (2005).
109. Hagen D.E. and Kassner, J.L., Jr., J. Chem. Phys., 81, 1416 (1984).
110. Hagen, D.E., Bull, Amer. Phys. Soc., 18, 609 (1973).
111. Haggis, G.H., Hastd, J.B. and Buchanan, T.J., J. Chem. Phys. 20, 1452 (1952).
112. Hale, B. N. and Plummer, P.L.M., J. Chem. Phys., 61, 4012 (1974a.)
113. Hale, B. N. and Ward, R.C., J. Statist., Phys., 28, 487 (1982).
114. Hale, B.N. and Plummer, P.L. M., J. Atmos. Sci. 31, 1615 (1974b).
115. Hauck, F. and Arnold, F., Nature, 311, 547 (1984).
116. Heath, D.F. and Linnett, J., Trans. Farad. Soc. 44, 556 (1948).
117. Hirth, J.P. and Pound, G.M. Pergamon Press, Oxford (1963).
118. Hoare, M.R., Pal, P. and Wegener, P.P., J. Colloid Interface Sci., 75, 126 (1980).
119. Hobb's P.V. and Ketcham, W.M., Proc. Conf. Plenum Press, New York, P-95 (1969).
120. Hobb's, P.V., Ice physics, Oxford University Press, Oxford (1974).

121. Hobb's, P.V., Radke, L.F., Weiss, R.R., Biswas, K.R. Turner, F.M. and Robertson, C.E., Res. Rept. No. VIII, Cloud Physics Group, Dept. Atmospheric Sci., University of Washington, Seattle, Washington, Dec. (1974).
122. Holden, D.N., Holmes, C.R., Moore, C.B., Winn, W.P., Cobb, J.W., Cris wold, J.E. and Lytel, D.M., Proceeding in atmospheric electricity, Deepak Publishing, 179 (1983).
123. Hoppel, W.A., Dinger, J.E. and Ruskin, R.E., J. Atmos. Sci. 30, 1410 (1973).
124. Huffman, P., Res. Rept. No. AR108, Sept. 1973, Dept. of Atmospheric Resources, University of Wyoming, Laramie, Wyoming (1973).
125. Huffman, P.J., J. Appl. Meteor. 12, 1080 (1973a).
126. Huffman, P.J., Res. Rept. No. AR 108, Sept. 1973, Dept. of Atmospheric Resources, University of Wyoming, Laramie, Wyoming (1973b).
127. I.G. Usoskin et al., J. Atmos. and Solar Terri. Phy. 66, 1791-1796 (2004).
128. Inamdar, A.K . and Ramanathan, V., J. Geophys. Res. Atoms. 103, D-23 (1998).
129. Isaka, C., Ph.D, Thesis, Universite de Clermont-Ferrand, Dept. Nat. Sciences, Clermont Ferrand, France (1972).
130. Israel, H., Vol. I, U.S. Department of Commerce, NTIS AD-71-6359 (1971).
131. J.P.D. Abbatt, K. Brockhuizen and P. Pradeep Kumar; Dept. of chem., University of Toronto, ont. Canada, Accepted 25 April (2005).
132. Jaccard, C., Phys. D. Kondens, Materie, 2, 143 (1963).
133. Jacobi, W., Z.F. Naturforschung 10a, 332 (1955a).

134. Jalaluddin, A.K., Sinha, D.B., *Nuovo Cim. (Suppl.)*, 26, 234 (1962).
135. Jayaratne, E.R. and Saunders, C.P.R., *J. Geophys. Res.*, 90, 13063 (1985).
136. Jayaratne, E.R., Saunders, C.P.R. and J. Halle, *Quartz, J. Roy. Meteor. Soc.*, 109, 609 (1983).
137. Jiusto, J.E. and Kocmond, W.C., *J.de Rech. Atmos.* 3, 102 (1968).
138. John, M.S. Grosh, J., Rec., T. and Eyring, H., *J. Chem. Phys.* 44, 1465 (1966).
139. Jordan Peccia and Mark Hernandez, *J. Atmospheric Environment*, 40, 3941 (2006).
140. K.Madhavi Latha and K.V.S. Badarinath, *J. Quantitative Spectroscopy and Radiative Transfer*, 98, 180 (2006).
141. Kamra, A.K., *J. Atmos. Sci.*, 27, 1182 (1970).
142. Kamra, A.K., *J. Atmos. Sci.*, 28, 820 (1971).
143. Kamra, A.K., *J. Atmos. Sci.*, 32, 143 (1975).
144. Kamra, A.K., *J. Geophys. Res.*, 84, 5034 (1979).
145. Kandalgaonkar, S.S., Tinmaker; M.I.R., Kulkarni, M.K. and Asha Nath, *Ind. J. Radio and Space Phys.*, 32, 221 (2003).
146. Kantrowitz, A., *J. Chem. Phys.* 19, 1097 (1951).
147. Katz, J.L., *J. Chem. Phys.*, 52, 4733 (1970).
148. Keith, W.D. and Saunders, C.P.R., *Atmos. Res.* 25, 445 (1990).
149. Keith, W.D. and Sounders, C.P.R., *Nature*, 336, 362 (1988).
150. Kell, G.S., Water, Franks, Ed., *Plenum Press, New York*, Vol. 1, F.P. 363 (1972a).
151. Kern, C.W. and Karplus, M. and Water, F. Franks, Ed., *Plenum Press, New York*, P.21 (1972).
152. Ketcham, W.M. and Hobb's P.V., *Phil, Mag.*, 18, 659 (1968).

153. Ketcham, W.M. and Hobb's P.V., *Phil. Mag.* 19, 1161 (1969).
154. Khera, M.K. and Raina, B.N., *Ind. J. Radio and Space phys.*, 3, 232 (1994).
155. Kikuchi, K., *Antartica, J. Meteor. Soc. Japan* 49, 376 (1971).
156. Kikuchi, K., *J. Meteor. Soc., Japan*, 49, 20 (1971).
157. Kikuchi, R., *J. Statist. Phys.*, 1, 351 (1969).
158. Kikuchi, R., Vol. 7, P.67-102, *Adv. Colloid Interface Sci.*, Edited by A.C. Zettlemoyer Elsevier, N.Y. (1977).
159. Kistenmacher, H., Lie, G.C., Popkie, H. and Clementi, E., IBM Research Report, RJ 1334, IBM Res. Lab., San Jose, Calif., Jan. (1974a).
160. Kistenmacher, H., Popkie, H., Clementi, E. and Watts, R.O., IBM Research Report, RJ 1335, IBM Res. Lab., San Jose, Calif., Jan. (1974b).
161. Kittel, C., John Wiley and Sons, New York, P. 338 (1966).
162. Koutsky J.A., Walton, A.G. and Baer, *Surface Science* 3, 165 (1965).
163. Krehbiel, P.R., Thomas, R.J., Rison, W., Hamlin, T., Harlin, J., Davis, M. Gps-based mapping system reveals lightning inside storms. *EOS- Transactions* 81, 21-25 (2000).
164. Krestov, G.A., *Zh. Struct. Khim.* 5, 909 (1964).
165. Krishna Reddy, K., *Ind. J. Radio and Space Phys.*, 32, 198 (2003).
166. Kubelka, P. and Prokscha, R., *Koll. Z.* 109, 79 (1944).
167. Kumai, M., *J., Glacial.*, 7, 95 (1968).
168. Kumar, A., Rai, J., Nigam, M.J., Singh, A.K. and Shri Nivas, J. *Radio and Space Phys.* 27, 215 (1998).
169. La Placa, S. and Post, B., *Acta. Cryst.*, 13, 503 (1960).
170. Lane-Smith, D.R. and Markson, R., pp. 109 (1977).

171. Legrand, M.R. and Delmass, R.J., Atmos. Environ. 18, 1867 (1984).
172. Lev I. Dormana, b, and Irena V., Dormac, Advances in space research, Vol.35, Issue-3, 476-483 (2005).
173. Levin, Z. and Ziv. A., J. Geophys, Res. 79, 2699 (1974).
174. Lin, Sin-Shong, Rew. Sci. Instruments, 44, 516 (1973).
175. Loeb, L.B., J. Geophys Res. 68, 4475 (1963).
176. Lonsdale, K., Proc. Roy. Soc. London. A 247, 424 (1958).
177. Lothe, J. and Pound, G.M., edited by Zettlemoyer, P. 109, Marcel Dekker, New York (1969).
178. Lothe, J. and Pound, G.M., J. Chem. Phys. 36, 2080 (1962).
179. Lothe, J. and Pound, G.M., J. Chem. Phys. 45, 630 (1966).
180. Lothe, J. and Pound, G.M., J. Chem. Phys. 48, 1849 (1968).
181. Lothe, J.; Nishioka, K. and Pound G.M. Preprint 71-T86, Deptt. of Materials Research, Standford University (1971).
182. Lyons, W.A., Lightning, In: Pielke, R.J., Pielk, R. (Eds.) Storms. Vol.2. Routledge, London Chap-3, pg. 60-79 (1999).
183. Mac Gorman, D.R., Rust, W.D., The Electrical Nature of Storms, Oxford Press, Oxford (1998).
184. Mahata, P.C. and Alofs, D.J., J. Atoms. Sci. 32, 116 (1975).
185. Mahendra Fernando et al., J. Atmospheric and Solar Terrestrial Phy. 10, 1016 (2007).
186. Makino, M. and Ogawa, T., J. Geophys. Res., 90, 5961 (1985).
187. Manohar, G.K., Kandalgaonkar, S.S. and Tinmaker, M.I.R., J. Geophys. Res. 104 (D4), 4169 (1999).
188. Markson, R., Sedlacek, J. and Fairall, C.W., J. Geophys. Res., 86, 12115 (1981).

189. Marshall, T.C., Rust, W.D. and Stolzenberg, M., J. Geophys. Res. (Atmos), 104, 24455 (1999).
190. Marshall, T.C., Rust, W.D., Winn, W.P. and Gilbert, K.E., Int's Aerospace and ground conference on lightning and static electricity, Oklahoma City, Oklahoma, April (1988).
191. Mason, B.J., 2nd ed., Oxford Univ. Press, London (1971).
192. Mason, B.J., The Bakerian Lecture 1971: Proc. Roy. Soc. London, Ser. A, 327, 433 (1972).
193. Mason, B.J., The Physics of Cloud, Oxford University Press, London (1972).
194. Mathpal, K.C. and Varshneya, N.C., J. Met. Soc. Japan, 61, 909 (1983).
195. Mathpal, K.C., and Varshneya, N.C., Ann. Geophys. , 38, 383 (1982).
196. Mathpal, K.E., Varshneya, N.C. and Rai, J., Ann. Geophys., 38, 367 (1982).
197. Maybank, J. and Barthakur, N.N., Nature, 216, 50 (1967).
198. Mc Donald, J.E., J. Meteor, 10, 416 (1953b).
199. Miller, R.C., Anderson, R.J., Kassner, J.L., Jr. and Hagen, D.E., J. Chem. Phys., 78, 3204 (1983).
200. Misaki, M., Ikegami, M. and Kanazawa, I., In electric processes in atmospheres, edited by H. Dolezalek and R. Reiter, PP. 119, Steinkopff, Darmstadt, West Germany (1977).
201. Miyazaki, J., Pound, G.M., Abraham, F.F. and Barker, J.A., J. Chem. Phys., 67, 3851 (1977).
202. Mohnen, V.A, Formation, Nature and Mobility of Ions of Atmospheric Importance, Proceeding Fifth International Conference on Atmospheric Electricity, Garmisch Partenkirchen., Sept. 2-7 (1974).

203. Mohnen, V.A., J. Geophys. Res. 75, 1717(1970).
204. Moore, C.B., Vonnegut, B., Machado, J.A. and Sur vilas, H. J., J. Geophys. Res. 67, 207 (1962).
205. Moore, C.B., Vonnegut, B., Machado, J.A. and Survilas, H.J., J. Geophys. Res. 67, 207 (1962).
206. Morgan, G.M. and Langer, G., Quart. J. Roy. Meteor. Soc. 80, 583 (1973).
207. Morita, Y., Ishikawa, H. and Kanada, M., J. Geophys. Res., 76, 3431 (1971).
208. Mossop, S.C., Proc. Phys. Soc. B68, 193 (1955).
209. Mossop, S.C., Ruskin, R.E. and Haffernan, K.J., J. Atmos. Sci. 25, 889 (1968).
210. Mukku, V.N.R., Ph.D. thesis, University of Kashmir, Srinagar, India (1982).
211. Murino, G., Suidi, Afrik., Tydsker, Fis, 2, 113 (1979).
212. Murino, G., Suidi. Afrik., Tydsker. Fis., 2, 113 (1974).
213. Nickolay Yu. Sdobnyakov and Samsonov, M., Theoretical Physics, Dept. Tver State Uni, Sadovli Per., 35, 17002 Russia (2005).
214. Nishioka, K. and Pound, G.M., Vol. 7, P.205-278, Adv. Colloid Interface Sci., Edited by A.C. Zettlemoyer Elsevier, N.Y. (1977).
215. Nizamuddin, S., Ramanathan, R., Rao, A.M., Khera, M.K., Makhdomi, B.M., Raina, B.N., Rafiqui, A.R., Mukku, V.N.R., Geol, R.K., Pathak, P.P., Rai, J. and Varshneya, N.C., edited by H.V. Mohan Ram and S.E. Trehan, Indian Natl. Sci. Acad., New Delhi, pp. 35 (1981).
216. Odin Mendes. Jr., Margarete Oliveira Domingues, J., Atmos. And Soar-Terrestrial Physics 67, 1287-1297 (2005).

217. P. Neofytou, A.G. Venetsanos, D. Vlachogiannis, J.G. Gartzis and A. Scaperdas, J. Environmental Modelling and Software, 21, 520 (2006).
218. P.T. Tonev, a and P.I.Y. Velinova, Bulgarian academy of Sciences, Sofia, Bulgaria, Article in Press, accepted July 14 (2007).
219. Paluch, I.R. and Sartor, J.D., I. Particle Charges and Electric Fields, J. Atmos. Sci., 30, 1166 (1973).
220. Paoletti, D. and Schirripa, S.G., A Preliminary study, Atoms. Environ., 23, 1607 (1989).
221. Parmar, D.S. and Jalaluddin, A.K., J. Phys. D. Appl. Phys. 8, 971 (1975).
222. Parmar, D.S. and Jalaluddin, A.K., Phys. Lett., 42A, 497 (1973).
223. Pasko, V.P., Inan, U.S. and Bell, T.F., Geophys. Res. Lett. 25, 1247 (1999).
224. Pathak, P.P., Raj, J. and Varshneya, N.C., Ann. Geophys. 36, 613 (1980).
225. Pauling, L., Hydrogen Bonding, D. Hadzi, H.W. Thompson, Eds. Pergamon Press, New York (1959).
226. Pauling, L., The Nature of the Chemical Bond, 3rd ed. Cornell University Press, Ithaca, New York (1960).
227. Perkins, M.D. and Eisele, F.L., J. Geophys. Res. 89, 4649 (1984).
228. Phillips, B.B., Mon. Weather Rev., 95, 854 (1967).
229. Pinsky, M.B., Khan, A.P. and Levin, Z, Quart J. Roy. Meteorol. Soci. 125, 553 (1999).
230. Plummer, P.L.M. and Hale B.N., Eighth International Conference on Nucleation. Leningrad, 24-29, Sept. (1973).

231. Plummer, P.L.M. and Hale, B.N., J. Chem. Phys. 56, 4329 (1972).
232. Poc, M., J. Rech. Atoms, 3, 127 (1967).
233. Popkie, H., Kistenmacher, H. and Clementi, E., J. Chem. Phys. 59, 1325 (1973).
234. Pople, J.A., Proc. Roy. Soc., London A 205, 163 (1951).
235. Powell C.F., Proc. Roy. Soc. London, A 119, 553 (1928).
236. Probstein, R.F., J. Chem, Phy. 19, 619 (1951).
237. Pruppacher, H.R. & Klett, J.D., D. Reidal Publishing Company (DORDRECHT) (1978).
238. Pruppacher, H.R. Pure App. Geophys. 104, 623 (1973).
239. Pruppacher, H.R., J. chem. Phys. 39, 1586 (1963).
240. Pruppacher, H.R., J. Geophys. Res. 68, 4463 (1963).
241. Raes, F., J. Geophys. Res., 100, 2893 (1995).
242. Raes, F.; Van Dingenen, R.; Wilson, J. and Saltelli, A., vs in-situ production, in Dimethyl sulphide-Oceans, Atmosphere and climate Edited by G. Restelliand and Angeletti, PP. 311, Kluwer Acad., Norwell, Mass. (1993).
243. Rahman, A. and Stillinger, F.N., J. Phys. Chem. 55, 3336 (1971).
244. Rao, C.N.R., Water, F. Franks, Ed. Plenum Press, New York, P. 93 (1972).
245. Reiss, H. and Katz, J.L., J. Chem. Phys., 46, 2496 (1967).
246. Reiss, H. J. statist. Phvs., 2, 83 (1970).
247. Reiss, H., P. 1-66 in "Nucleation Phenomena", Adv. Colloid Interface Sci., Edited by A.C. Zettlemoyer, Elsevier, N.Y. (1977).
248. Reiss, H.; L, Katz, J.L. and Cohen, E.R., J. Chem.Phys., 48, 5553 (1968).

249. Retalis, D., Pitta, A. and Psallidas, P., Meteorol. Atmos. Phys., 46, 197 (1991).
250. Reuck, A.V.S., Nature, 179, 1119 (1957).
251. Reynolds, S.E., Brook, M. and Gaurley, M.F., J. Meteor. Soc., 14, 426 (1957).
252. Risto J. Pirijola, J. Atmos. And Solar-Terrestrial Physics, Vol. 60, 1139-1148 (1998).
253. Rodke, L.F. and Hobbs, P.V., J. Atmos. Sci. 26, 281 (1969).
254. Rosen, J.M. and Hofmann, D.J., J. Geophys. Res. 86, 7406 (1981).
255. Rosinski, J., J. Atmos. Terr. Phys. 29, 1201 (1967).
256. Roulleau, M., Evans, L.T. and Fukuta, N.J. Atmos. Sci. 28, 737 (1971).
257. Rowlinson, J.S., Trans. Farad. Soc. 45, 974 (1949).
258. Rowlinson, J.S., Trans. Farad. Soc. 47, 120 (1951).
259. Russell, K.C., J. Chem. Phys. 50, 1809 (1969).
260. Sahafer, V.J., J. Appl. Meteorol. 7, 452 (1968).
261. Salt, R.W., Science, 133, 458 (1961).
262. Sapkata, B.K. and Varshneya, N.C., Ind. J. Radio and space Phys. 18, 251 (1989).
263. Sapkota, B.K. and Varshneya, N.C., Meteorol. Atmos. Phys. 39, 213 (1988).
264. Sarkar, S.K., Dutta, H.N., Pasrich, P.K. and Reddy, B.M., National Physical Laboratory, New Delhi (1982).
265. Saunders, C.P.R., and J.S. Rimmer, Atmospheric Research, Vol-51, Issue 3-4, 337-343, July (1999).
266. Schaefer, V.J., Project Cirrus Part I Final, Port, R.I. 785, General Electric Res. Lab Schenectady, N.Y., 54 PP (1953).

267. Scott, W.D. and Levin, Z., J. Atmos. Sci., 32, 1814 (1975).
268. Searcey, J.Q. and Fenn, J.B., J. Chem. Phys. 61, 5282 (1974).
269. Sentman, D.D. Effects of Thunderstorm Activity on the upper Atmosphere and Ionosphere, Pergamon, Oxford, Ed. (1998).
270. Sharma, A.R., N. Singh and S.D. Pandey Ind. J. Radio and Space Phys. 21, 218 (1992).
271. Shaw, G.E., Geophys. Res. Lett. 25, 4317 (1998).
272. Sheftel, Y.H., Chernyshev, A.K. and Chernysheva, S.P., paper presented at the 9th International Conference of Atmospheric Electricity, Intl. Comm. on Atmos., Electr., Leningrad, Russia, June 15-19 (1992).
273. Shreve, E.L., J. Atmos. Sci., 27, 1186 (1970).
274. Singh, A.K., S. Nivas, Kumar, A., Rai, J. and Nigam, M.J., J. Radio & space Phys. 28, 1 (1999).
275. Singh, N. and Kumar, A., A Abstract Book 72nd Annual Session of Nat. Acad. Sci. India, NEHU, Shillong, Oct. 25-27 (2002).
276. Singh, N. Rai, J. and Varshneya, N.C., Ann. Geophys. 3, 343 (1985).
277. Singh, N., J. Rai and N.C. Varsheya, Ann. Geophys., 4B, 1, 37-44 (1986).
278. Singh, N., Kumar, A., Mohan, A. and Johri, G.K., Abstract Book, P. 180, Nat. Space Sci. Symp. (NSSS-2K), Toshalisands, Ethnic Village Resort, PURI, March 1-4 (2000).
279. Singh, N., Ph.D. Thesis, University of Roorkee, Roorkee, India, Dec. (1985).
280. Singh, N., Rai, J. and Varshneya, N.C., N.C., Nat. Acad. Sci. Lett., 7(12), 375 (1984).

281. Singh, N., Singh, D. and Kumar, A., Proceeding of National Workshop on Recent Development in Atmospheric and Space Science, Dept. of Physics, University of Roorkee, March 19-21 (2001).
282. Singh, N., Mathpal, K.C., Rai, J. and Vershneya, N.C., Nat. Acad. Sci. Lett., 8(2), 55 (1985).
283. Sjolander, A. and Turski, L.A., J. Phys. C., 11, 1973 (1978).
284. Smith, M.H., Griffiths, R.R. and Latham, J., Quart. J. Roy. Meteor. Soc. 97, 495 (1971).
285. Smitha R.P., Absolom D.R, Spelt J.K. and Neumann A.W., J., Colloid and Interface Science, vol. 110, Issue 2, 520-532 (1986).
286. Stillinger, F.H., J. Phys. Chem., 74, 3677 (1970).
287. Stillinger, F.N. and Rahman, A., J. Chem. Phys. 57, 1281 (1972).
288. Stockmayer, W.H., J. Chem. Phys. 9, 398 (1941).
289. Suck, S.H., Chen, T.S., Emmons, R.W., Hagen, D.E. and Kassner, J.L., Jr., Heterogeneous Atoms. Chem. Geophys. Mono. Sci. 26, 28 (1982).
290. Sudhir Kumar Pandey, B.D. Tripathi, V.K. Mishra and S.K. Prajapati, J. Chemosphere, 63, 49 (2006).
291. Thomas Ackermn and Pavlos Kollias, J. Spectroscopy Vol. 91, Issue 2, March 1 (2005).
292. Thorpe, A.J., Weather, 36, 4, 108 (1981).
293. Tolman, R.J. Chem. Phys. 17, 118 (1949a).
294. Tolman, R.J. Chem. Phys. 17, 333 (1949b).
295. Turnbull, D., J. Chem. Phys. 18, 769 (1950).
296. Turnbull, D., Liquids, Structure, Properties, Solid Interactions, Th. Hugel, Ed., P-15, Elsevier Publ. Co., New York (1965).
297. Twomey, S. and Davidson K.A., J. Atmos. Sci. 28, 1295 (1971).

298. Twomey, S. and Davidson, K.A., J. Atmos. Sci. 27, 1056 (1970).
299. Twomey, S. and Severynse, G.T., J. de Rech. Atmos., 1, 81 (1964).
300. Twomey, S. and Wojciechowski, T.A., J. Atmos. Sci. 26, 684 (1969).
301. Twomey, S., Geofys. Purae Appl. 43, 227 (1959a).
302. Van ECK, C.L.P., Mendel, H. and Fahrenfort, Proc. Roy. Soc., London, A 247, 472 (1958).
303. Van Eijk, A.M.J., and Tranchant, B., J. aerosol Science, 27, S61-S62 (1996).
304. Varshneya, N. C., Instruments and Methods, 92, 147 (1971).
305. Varshneya, N.C. Nature, 223, 826 (1969).
306. Venkatran, A., Atmos. Environ. 33, 3075 (1999).
307. Volmer, M., Dresden and Leipzing, Steinkopff (1939).
308. Vonnegut, B., Geophysical Research Paper No. 42, Proceeding Int. Conf. on Atmos. Electricity, AFCRC-TR-55-222, P-169 (1955).
309. Vonnegut, B., Proceedings of Int. Conf. Atmospheric Electricity, Uppsala, Sweden, June 13-16 (1988).
310. Wagner, P.G. and Telford, J.W., J. Rech. Atmos. Res. 15, 97 (1981).
311. Wahlin, L., Found of Phys. 3, 459 (1973).
312. Wakeshima, H., J. Chem. Phys. 22, 1614 (1954).
313. Walrafen, G.E., Hydrogen Bonded Solvent Systems, A.K. Covington and P. Jones, Eds., P.9, Taylor and Francis, London (1968b).
314. Walrafen, G.E., J. Chem. Phys., 44, 1546 (1966).
315. Walrafen, G.E., J. Chem. Phys., 47, 114 (1967).
316. Walrafen, G.E., J. Chem. Phys., 48, 244 (1968a).

317. Walrafen, G.E., Water, F. Franks, Ed., Plenum Press, New York, P. 151 (1972).
318. Ward, R.C., Holdman, J.M. and Hale, B.N., J. Chem. Phys., 77, 3198 (1982).
319. Wegner, P.P. and Wu, B.J.C., 325-in Nucleation Phenomena, Vol.7, Adv. Coloid Interface Sci., Ed. By A.C. Zettlemoyer, Elsevier, N.Y. (1977).
320. Whalley, E., Jones, S.J. and Gold, L.W., Physics and Chemistry of Ice, Roy. Soc. Of Canada, Ottawa, Eds. (1973).
321. Whipple, F.J.W. and Acrase, F.J., Geophys. Mem. Lond, (U.K.), 68, 1-20 (1936).
322. Whipple, F.J.W. and Chalmers, J.A., Quart, J. Roy. Meteor. Soc., 70, 103 (1944).
323. Widell, H.V., Rose, G. and Borchers, R., J. Geophys. Res, 81, 6217 (1976).
324. William H., Beasley et al., Geophy. Res. lett., Vol 27, No. 2, 189-192 (2000).
325. Williams, E.R., J. Geophys. Res., 90, 6013 (1985).
326. Wilson, C.T.R., J. Franklin Inst., 208, 1 (1929).
327. Wilson, C.T.R., Phil, Trans. Roy. Soc., London, A 189, 265 (1897).
328. Wilson, C.T.R., Phil. Trans Roy. Soc., A 193, 289 (1899).
329. Wilson, C.T.R., Phil. Trans. Roy. Soc., London, A 221, 73 (1920).
330. Winn, W.P., Schwede, G.W. and Moore, C.B., J. Geophys. Res. 79, 1761 (1974).
331. Woessner, R.11, Cobb, W.E. and Gunn, R., J. Geophys. Res. 63. 171 (1950).
332. Wood, G.R. and Walton, H.G., J. Appl. Phys. 41, 3027 (1970).

333. Worley, J.D. and Klotz, I.M., J. Chem. Phys. 45, 2868 (1966).
334. Xiang Bao, Masataka Watanabe, Qinxue Wang, Seiji Hayashi and Jiyuan Liu, J. Science of the Total Environment, 363, 136 (2006).
335. Xie Xiaomin, Huang Zhen and Wang Jiasong, J. Building and Environment 41, 1352 (2006).
336. Yuhang Wang, Russel, Earth and atmos. Sci. Atlanta Accepted (2005).
337. Ziv, A. and Levin, Z., J. Atmos. Sci., 31, 1652 (1974).

List of Publications

1. *"Effect of supersaturation ratio on the condensation of water vapour and ice glaciation", J. SCITECH; 2, No.2, 75-80 (2007).*
2. *"Equivalence between supersaturation ratio and the external electric field during water vapour condensation", J. SCITECH; 3, No. 1, 56-58 (2008).*
3. *"Variation of relaxation time in water vapour condensation as a function of supersaturation ratio in presence of ions", J. ACTA CIENCIA INDICA, Vol. XXXV, P. No. 2, 341-345 (2009).*
4. *"Effective role of Polarizability on nucleation phenomenon during ice glaciations considering the variation of surface free energy of ice with temperature", communicated to ACTA CIENCIA INDICA.*